

ABSTRACT

LUZIUS, DENNIS. Controlling Structure and Properties of High Surface Area Nonwoven Materials via Hydroentangling. (Under the direction of Dr. Behnam Pourdeyhimi and Dr. Eunkyong Shim).

Hydroentangling describes a technique using a series of high-velocity water jets to mechanically interlock and entangle fibers. Over the last decades researchers worked on a fundamental understanding of the process and the factors influencing the properties of the final nonwoven material. Recent studies discovered hydroentangling to be capable to create unique, knot-like structures characterized by high- and low density regions, which are believed to have interesting properties for filtration applications. However, just little is known about the impact of hydroentangling parameters on the properties of filtration media to this day.

In this study we report on the effect of various hydroentangling parameters, such as jet spacing, manifold pressure, number of manifolds but also specific energy on the structure and properties of high surface area nonwoven materials. Latter was achieved by different bicomponent fiber technologies and subsequent treatments removing the sacrificial compound from the structure. The highest BET surface area was measured to be $3.5 \text{ m}^2 \text{ g}^{-1}$ and the smallest mean fiber size about $0.5 \text{ }\mu\text{m}$.

Hydroentangling with large jet spacing was found to be a parameter significantly enhancing the filtration properties of caustic-treated island-in-the-sea nonwoven materials. Moreover, improved capture efficiencies and reduced pressure drops were achieved by reducing the manifold pressure and therefore specific energy during hydroentangling.

Jet spacing but not island count was found to be the dominant factor influencing the structure and properties of island-in-the-sea nonwovens. Contrary to our initial expectations

increasing the island count and thus decreasing the fiber size did not result in better filtration properties.

Mixed media nonwoven structures made from homocomponent and island-in-the-sea fibers were found to have lower densities, higher air permeabilities and better quality factors compared to island-in-the-sea structures hydroentangled under the exact same conditions.

Study showed the specific energy to not be an adequate measure for describing the process-structure relationship in hydroentangling. Hydroentangling with same specific energy but different manifold pressures revealed the structure and properties to be different and the peak manifold pressure to be the dominant parameter.

It was further shown that hydroentangling with multiple manifolds but same water pressure influences the structure and properties of mono- and bicomponent nonwoven materials. Hydroentangling with three manifolds having the same water pressure resulted in stronger, less permeable fabrics compared to two manifolds or one manifold with the same water pressure.

Necessary hydroentangling intensity for winged and island-in-the-sea nonwoven materials was found to be different. Winged fiber nonwovens required higher manifold pressures and a different energy ratio than island-in-in-the-sea nonwovens. Hydroentangling winged fiber webs with jet spacing larger than 600 μm resulted in materials too weak to withstand the caustic-treatment. Study indicated the charging potential of winged fiber nonwovens to be superior compared to island-in-the-sea-structures. In contrast to winged fiber nonwovens, island-in-the-sea structures showed higher pressure drops after corona discharge. Loading winged fiber nonwovens with potassium chloride revealed caustic-treated, IPA discharged materials to show the highest loading capacity.

© Copyright 2015 Dennis Luzius

All Rights Reserved

Controlling Structure and Properties of High Surface Area
Nonwoven Materials via Hydroentangling

by
Dennis Luzius

A dissertation submitted to the Graduate Faculty of
North Carolina State University
in partial fulfillment of the
requirements for the degree of
Doctor of Philosophy

Fiber and Polymer Science

Raleigh, North Carolina

2015

APPROVED BY:

Dr. Behnam Pourdeyhimi

Dr. Eunkyong Shim

Dr. Benoît Mazé

Dr. Saad Khan

DEDICATION

To my beloved family :o)

BIOGRAPHY

Dennis Luzius was born on December 7 1984 in Frankfurt a. M., Germany. In 2009, he graduated from Albstadt-Sigmaringen University with a Bachelor of Engineering degree. During his undergraduate studies he spent six months abroad in Mulhouse (France) as an ERASMUS student. In 2011, he graduated and received a Master of Science degree from Albstadt-Sigmaringen University. In the course of his studies, he spent 9 months as a Groz-Beckert scholar at The Nonwovens Institute (North Carolina State University) to prepare his Master's thesis. In 2011, he worked several months at São Paulo State University (UNESP - Universidade Estadual Paulista, Brazil) before returning to NC State in 2012. Supervised by Dr. Behnam Pourdeyhimi and Dr. Eunkyong Shim (The Nonwovens Institute) and financially supported by the Groz-Beckert KG, he received a Ph.D. degree in Fiber and Polymer Science in 2015.

ACKNOWLEDGMENTS

It's been a long journey and there are numerous, lovely people I'd like to express my deepest acknowledgement. After spending many years abroad and meeting many great and helpful people it's not easy to remember all of them (so forgive me if I did not mention you).

I'd like to start with my two mentors Dr. Behnam Pourdeyhimi and Dr. Eunkyong Shim, who put much effort in educating me. Dr. Pourdeyhimi not only helped me to pursue my doctorate degree but also shared his wisdom in many respects. Dr. Shim's relentless dedication to her work and students makes her the perfect mentor. I am deeply grateful for everything she did for me. Dr. Benoît Mazé not only served as one of my committee members but also pointed out problems and weaknesses with brutal honesty and provided many useful solutions. Many thanks to Dr. Saad Khan (Department of Chemical and Biomolecular Engineering), who served as my fourth committee member.

I'd like to express my deepest gratitude to many great people from NC State and The Nonwovens Institute, who helped me with many small and big problems. Jeff Krauss, Amy Minton, Bruce Anderson, Sherwood Wallace, Sue Pegram, William Barnes, Andy Batz, Angelo Corino, Alvin Fortner, John Fry, Ben Lambert, Stephen Sharp, Sharon Wright, Jimei Wang, Bradley Scroggins, Eric Lawrence and also Chuck Mooney from AIF. Also to the students of the NWI group, especially my former office mates Fatemeh and Wei.

I'd also like to express my acknowledgement to Groz-Beckert and FTA, especially to Dr. Andreas Tulke, Dr. Stefan Zamel and also Nicolai Wiedmann, for supporting and helping

me in many ways. Thanks to my German colleagues Fabian Stauss and Frank Endriss for being great teammates and many helpful discussions.

Special thanks to Dr. Dominique Adolphe from the Université de Haute Alsace (France), Dr. Maria Odila Hilário Cioffi from the Universidade Estadual Paulista (Brazil), Dr. Michael Ernst and my other former professors for helping me during the application process. Many thanks to Dr. Conny Bast for helping me so many times.

At this point I'd like to thank the most important people in my life, my mom and dad, my sister, my grandparents, friends, significant other and furry friends. Thanks for accepting my decision to leave my home for a long time and not being present for many important occasions. I am very grateful for your endless support and look forward to have you back with me! Anni, thanks for supporting me all the time and being so patient with me. I love you and I am proud to be with you.

TABLE OF CONTENTS

LIST OF TABLES	xi	
LIST OF FIGURES	xiii	
LIST OF SYMBOLS	xxiii	
CHAPTER 1		
Introduction.....	1	
1.1	Introductory Remarks	2
1.2	Problem Statement	4
1.3	Significance of the Study	4
1.4	Research Objectives and Approach.....	5
1.5	About the Dissertation.....	5
1.6	References.....	8
CHAPTER 2		
Background.....	9	
2.1	Nonwoven Structures	10
2.1.1	Historical Outline of Nonwoven Materials	10
2.1.2	Classification of Nonwoven Processes and Materials.....	11
2.1.3	Carding and Cross-Lapping Technology.....	13
2.1.4	Air-Lay Technology	14
2.1.5	Wet-Lay Technology.....	14
2.1.6	Spunbond Technology.....	15
2.1.7	Meltblown Technology.....	23
2.1.8	Flash-, Electro- and Solution-Blow Spinning.....	25
2.1.9	Nonwoven Applications, Market Situation and Prognosis.....	26
2.2	Hydroentangling Technology	27
2.2.1	Historical Development of the Hydroentangling Technology	29
2.2.2	Hydroentangling Process, Components and Parameters	30
2.2.3	Process-Structure-Property Relationship in Hydroentangling	37
2.2.4	Influence of Forming Belt	59
2.2.5	Hydroentangling Applications, Market and Future Prognosis	62
2.3	High Surface Area Nonwovens Structures.....	64
2.3.1	Bicomponent Fiber Technology	67
2.3.2	Island-in-the-Sea Technology.....	73
2.3.3	Winged Fiber Technology	78
2.3.4	Segmented Pie Technology	80
2.3.5	Further Technologies.....	82

2.4	Aerosol Filtration.....	84
2.4.1	Introduction to Aerosol Filtration.....	85
2.4.2	Filtration Theory.....	93
2.5	References.....	98

CHAPTER 3

Influence of Hydroentangling Parameters on Island-in-the-Sea Nonwoven Materials

Part I: Effect of Jet Spacing	114
-------------------------------------	-----

3.1	Abstract	115
3.2	Introduction	115
3.3	Methodology.....	118
3.3.1	Materials	118
3.3.2	Sample Preparation.....	121
3.3.3	Characterization Methods.....	121
3.4	Results and Discussion	125
3.4.1	Removal of Sea Polymer from the Bicomponent Structure	125
3.4.2	Jet Streak Analysis.....	127
3.4.3	Fiber Diameter	131
3.4.4	Influence of Jet Spacing on Thickness and Solidity.....	131
3.4.5	Influence of Jet Spacing on Air Permeability and Filtration Properties	133
3.5	Summary and Conclusion.....	136
3.6	References.....	138

CHAPTER 4

Influence of Hydroentangling on Island-in-the-Sea Nonwoven Materials

Part II: Effect of Hydroentangling Pressure.....	139
--	-----

4.1	Abstract	140
4.2	Introduction	140
4.3	Methodology.....	143
4.3.1	Materials	143
4.3.2	Sample Preparation.....	146
4.3.3	Characterization Methods.....	147
4.4	Results and Discussion	148
4.4.1	Removal of Sea Polymer from the Bicomponent Structure	148
4.4.2	Influence of Hydroentangling Pressure on Thickness and Solidity	150
4.4.3	Air Permeability and Filtration Properties.....	154
4.5	Conclusion	158
4.6	References.....	160

CHAPTER 5

Effect of Island Count of Island-in-the-sea Nonwoven Materials 161

5.1	Abstract	162
5.2	Introduction	162
5.3	Methodology	165
5.3.1	Materials	165
5.3.2	Sample Preparation.....	168
5.3.3	Characterization Methods.....	168
5.4	Results and Discussion	171
5.4.1	Removal of Sea Compound from the Bicomponent Structure	171
5.4.2	Influence of Island Count on Fiber Diameter	174
5.4.3	Influence of Island Count on Specific Surface Area	177
5.4.4	Effect of Island Count and Jet Spacing on Structure Properties.....	178
5.4.5	Influence of Island Count on Air Permeability and Filtration Properties.....	180
5.5	Summary and Conclusion	186
5.6	References	188

CHAPTER 6

High Surface Area Mixed Media Nonwovens Materials..... 189

6.1	Abstract	190
6.2	Introduction	191
6.3	Methodology	193
6.3.1	Materials	193
6.3.2	Sample Preparation.....	197
6.3.3	Characterization Methods.....	197
6.4	Results and Discussion	203
6.4.1	Part I: Comparison of 37 InS and 37 Mixed Media Alt. InS Structures.....	204
6.4.1.1	Removal of Sea Compound.....	204
6.4.1.2	Fiber Size and Specific Surface Area	206
6.4.1.3	Thickness and Solidity.....	210
6.4.1.4	Air Permeability and Filtration Performance	211
6.4.1.5	Summary (Part I)	214
6.4.2	Part II: Mixed Media Alt. 37 InS Hydroentangled with Higher Pressures....	215
6.4.2.1	Removal of Sea Compound.....	215
6.4.2.2	Influence on Structure and Properties	216
6.4.2.3	Summary (Part II).....	219
6.4.3	Part III: Mixed Media Alt. 37 and 108 Island-in-the-Sea Structures	220
6.4.3.1	Removal of Sea Polymer from Structures	220
6.4.3.2	Fiber Size and Specific Surface Area	221
6.4.3.3	Structure and Properties.....	225

6.5	Summary and Conclusion.....	229
6.6	References.....	231

CHAPTER 7

	Influence of Jet Intensity and Manifolds in Hydroentangling	
	Part I: Specific Energy and Force	233

7.1	Abstract	234
7.2	Introduction	235
7.3	Methodology.....	238
7.3.1	Materials	238
7.3.2	Sample Preparation.....	239
7.3.3	Structure Analysis.....	240
7.4	Results and Discussion	242
7.4.1	Part I: Mono- and Bicomponent Nonwovens	243
7.4.1.1	Fiber Diameter Distribution.....	243
7.4.1.2	Solid Volume Fraction and Air Permeability	244
7.4.1.3	Influence on Mechanical Properties	246
7.4.1.4	Summary (Part I)	250
7.4.2	Part II: Effect on Caustic-Treated 37 InS Nonwovens	251
7.4.2.1	Fiber Diameter Distribution.....	251
7.4.2.2	Influence on Structural Properties	251
7.4.2.3	Mechanical Properties	256
7.4.2.4	Summary (Part II).....	260
7.4.3	Part III: Changing Specific Energy	261
7.4.3.1	Solid Volume Fraction and Air Permeability	261
7.4.3.2	Tensile and Tear Strength.....	262
7.5	Overall Summary	265
7.6	References.....	266

CHAPTER 8

	Influence of Jet Intensity and Manifolds in Hydroentangling	
	Part II: Number of Manifolds	267

8.1	Abstract	268
8.2	Introduction	269
8.3	Methodology.....	271
8.3.1	Materials	271
8.3.2	Sample Preparation.....	272
8.3.3	Structure Analysis.....	273
8.4	Results and Discussion	275
8.4.1	Part I: Effect of Number of Manifolds on 37 InS Nonwoven Materials	275
8.4.1.1	Solid Volume Fraction and Air Permeability	275

8.4.1.2	Mechanical Properties	277
8.4.1.3	Summary (Part I)	282
8.4.2	Part II: Effect of Jet Spacing.....	282
8.4.2.1	Solid Volume Fraction and Air Permeability	282
8.4.2.2	Mechanical Properties	284
8.4.2.3	Summary (Part II)	286
8.4.3	Part III: Mono- and Bicomponent Nonwoven Structures.....	287
8.4.3.1	Solid Volume Fraction and Air Permeability	287
8.4.3.2	Mechanical Properties	288
8.4.3.3	Overall Conclusion	291
8.5	References.....	292

CHAPTER 9

	A Study on Winged Fiber Nonwoven Materials.....	293
--	---	-----

9.1	Abstract	294
9.2	Introduction	295
9.3	Methodology.....	298
9.3.1	Materials	298
9.3.2	Sample Preparation.....	299
9.3.3	Structure Analysis.....	299
9.4	Results and Discussion	303
9.4.1	Removal of Sea Compound.....	303
9.4.2	Solid Volume Fraction and Air Permeability	305
9.4.3	Effect of Specific Surface Area on Filtration Properties	306
9.4.4	Salt Loading Capacity	310
9.5	Conclusion	318
9.6	References.....	319

CHAPTER 10

	Overall Conclusion	320
--	--------------------------	-----

CHAPTER 11

	Future Recommendations	324
--	------------------------------	-----

	Appendix.....	327
--	---------------	-----

LIST OF TABLES

Chapter 3

Table 3- 1: Structures and hydroentangling parameters	119
Table 3- 2: Results of fiber diameter measurements (before caustic treatment)	131
Table 3- 3: Theoretical and measured island diameter (after caustic treatment)	131

Chapter 4

Table 4- 1: Structures and hydroentangling parameters	144
Table 4- 2: Results of fiber diameter measurements (before caustic treatment)	150
Table 4- 3: Results of fiber diameter measurements (after caustic treatment)	150

Chapter 5

Table 5- 1: Structures and hydroentangling parameters	165
Table 5- 2: Results of fiber diameter measurements (before caustic treatment)	175
Table 5- 3: Results of island diameter measurements (after caustic treatment)	176
Table 5- 4: Results of BET specific surface area measurements	178
Table 5- 5: 2-Way ANOVA (α : 0.05), Influence of island count and jet spacing on normalized thickness, after caustic treatment (performed with JMP Pro)	179
Table 5- 6: 2-Way ANOVA (α : 0.05), Influence of island count and jet spacing on SVF, before/after caustic treatment (performed with JMP Pro)	179
Table 5- 7: 2-Way ANOVA (α : 0.05), Influence of island count and jet spacing on air permeability, before/after caustic treatment (performed with JMP Pro)	181

Chapter 6

Table 6- 1: Structures and hydroentangling parameters	194
Table 6- 2: Results of fiber diameter measurements (before/after caustic treatment)	207
Table 6- 3: Calculated mass/volume fractions of the used mixed media structure	208
Table 6- 4: Results of fiber diameter measurements of MM 37/108 InS (before/after caustic treatment)	222
Table 6- 5: Calculated mass/volume fractions of the used mixed media structure	223

Chapter 7

Table 7- 1: Structures and hydroentangling parameters 239
Table 7- 2: Results of fiber diameter measurements 243
Table 7- 3: Results of fiber diameter measurements (before caustic treatment) 251
Table 7- 4: Results of fiber diameter measurements (after caustic treatment) 251
Table 7- 5: 2-Way ANOVA (α : **0.05**), Influence of pressure (P1/P2) and jet spacing on
solidity, after caustic treatment (JMP Pro) 253

Chapter 8

Table 8- 1: Structures and hydroentangling parameters 272
Table 8- 2: Quality factor of caustic-treated 37 InS structures hydroentangling with manifold
pressures P1-P3 and 600 μm jet spacing 281

Chapter 9

Table 9- 1: Structures and hydroentangling parameters 298
Table 9- 2: Comparison of BET specific surface area of intact/caustic-treated InS and winged
fiber nonwovens 307

LIST OF FIGURES

Chapter 2

Figure 2- 1: Illustration of an open spunbond process from polymer feed to material roll-up	18
Figure 2- 2: Schematic of a gear pump (Hutten, 2007, p. 212)	20
Figure 2- 3: Schematic of a Hills bicomponent spinpack (Hills, 1992).....	21
Figure 2- 4: Illustration of Fiber Attenuation in Meltblown Spinning	24
Figure 2- 5: Forecast of global nonwoven market (Transparency Market Research, 2014) ..	26
Figure 2- 6: Nonwoven disposable and raw materials share (Clean Indian Journal, 2011; Smithers Pira, n. d.).....	27
Figure 2- 7: Schematic of a five manifold hydroentangling unit.....	31
Figure 2- 8: Manifold and passing 0.5 meter web viewed from the side (NWI pilot facilities, North Carolina State University)	33
Figure 2- 9: Schematic of a single-row jet strip (plane view).....	34
Figure 2- 10: Schematic of the cross-section of a jet-strip in cone-down position (sectional view)	35
Figure 2- 11: Photography of Water-Jets (Mogul Tekstil Sanayi ve Ticaret Ltd.Sti., n.d.) ...	36
Figure 2- 12: Mechanisms during hydroentangling (Patanaik & Anandjiwala, 2010).....	38
Figure 2- 13: Mechanisms during hydroentangling (Mao & Russel, 2005).....	38
Figure 2- 14: 2-layered structure hydroentangled with 100 bar and 600 μm jet spacing (Suragani Venu, 2012, p. 187)	45
Figure 2- 15: 2-layered structure hydroentangled with 100 bar and 4800 μm jet spacing (Suragani Venu, 2012, p. 187)	45
Figure 2- 16: 2-layered structure hydroentangled with 200 bar and 600 μm jet spacing (Suragani Venu, 2012, p. 188)	46
Figure 2- 17: 2-layered structure hydroentangled with 200 bar and 4800 μm jet spacing (Suragani Venu, 2012, p. 188)	46
Figure 2- 18: Nozzle designs in hydroentangling	49
Figure 2- 19: Water Flow inside a Cone-Capillary Nozzle at different Re (Anantharamaiah, 2006, p. 61)	51
Figure 2- 20: Water jets from nozzles with different nozzle diameters (1,500 psi) (Anantharamaiah, 2006, pp. 21-22)	57
Figure 2- 21: Global production of hydroentangled materials (Butler, Medeiros et al., 2002, p. 3)	62
Figure 2- 22: Hydroentangling markets (Butler, Medeiros et al., 2002, p. 6)	63

Figure 2- 23: Global production of hydroentangled materials by region (Butler, Medeiros et al., 2002, p. 4)	63
Figure 2- 24: Specific surface area as a function of fiber linear density	65
Figure 2- 25: Illustration of different bicomponent fibers: concentric sheath/core, eccentric sheath/core, side-by-side, island-in-the-sea and mixed island-in-the-sea (from left to right) 70	
Figure 2- 26: Illustration of a 37 island-in-the-sea bicomponent fiber	73
Figure 2- 27: Cross-sectional images of a 37 island-in-the-sea (left) and 1120 island-in-the-sea fiber (Hills Inc., n.d.-a)	74
Figure 2- 28: Partially dissolved 600 island-in-the-sea fiber (Hagewood, n.d.).....	76
Figure 2- 29: Fiber diameter and specific surface area as a function of island count ($\rho_i = 0.9 \text{ g cm}^3, \rho_s = 1.24 \text{ g cm}^3, d_i = 15 \text{ micron}$), black symbols ($R_i/R_s=75/25$), red symbols ($R_i/R_s=50/50$), green symbols ($R_i/R_s=25/50$).....	77
Figure 2- 30: SEM Image taken from a 32 lobes winged fibers before and after removing the sheath polymer (Yeom & Pourdeyhimi, 2011b).....	78
Figure 2- 31: Illustration of an intact 16 segmented-pie fiber and intact and split 16 segmented-pie hollow fiber.....	80
Figure 2- 32: Fiber diameter as a function of segments (Pourdeyhimi, 2011b)	81
Figure 2- 33: Section view of a 4DG fiber (Deopura, Alagirusamy et al., 2008).....	82
Figure 2- 34: Section view of a segmented-pie fiber	83
Figure 2- 35: Illustration of a Tipped Trilobal, Modified Tipped Trilobal and Core Trilobal Fibers.....	83
Figure 2- 36: Typical Airborne Particles and their Corresponding Size (LTA Lufttechnik GmbH, n.d.)	86
Figure 2- 37: Surface filtration mechanism	87
Figure 2- 38: Depth filtration mechanism.....	88
Figure 2- 39: Particle deposition by inertial impaction	89
Figure 2- 40: Particle deposition by Brownian diffusion (Brownian motion).....	90
Figure 2- 41: Particle deposition by interception.....	90
Figure 2- 42: Particle deposition by electrostatic attraction	91
Figure 2- 43: Capture efficiency as a function of particle size for different deposition mechanisms (Hinds, 1999).....	92
Figure 2- 44: Principle of the single fiber theory.....	94

Chapter 3

Figure 3- 1: Calculated specific energy	120
Figure 3- 2: Schematic of a hydroentangling jet strip (\rightarrow not true to scale).....	120

Figure 3- 3: Cross-sectional image of a drawn poly (propylene)/poly (lactic acid) 37 InS fiber	121
Figure 3- 4: Schematic of dark-field illumination image capturing	124
Figure 3- 5: Basis weight before/after caustic treatment	126
Figure 3- 6: 37 InS structure before caustic treatment.....	127
Figure 3- 7: 37 InS structure after caustic treatment.....	127
Figure 3- 8: Dark-field illumination images showing the surface of unwashed (left) and caustic-treated (right) 37 InS nonwoven structures hydroentangled with 600 μm jet spacing	128
Figure 3- 9: Comparison co-occurrence results of unwashed/washed, 600 μm hydroentangled materials	128
Figure 3- 10: Dark-field illumination images showing the surface of unwashed (left) and caustic-treated (right) 37 InS nonwoven structures hydroentangled with 1800 μm jet spacing	129
Figure 3- 11: Comparison co-occurrence results of unwashed/washed, 1800 μm hydroentangled materials	129
Figure 3- 12: Dark-field illumination images showing the surface of unwashed (left) and caustic-treated (right) 37 InS nonwoven structures hydroentangled with 4800 μm jet spacing	130
Figure 3- 13: Comparison co-occurrence results of unwashed/washed, 4800 μm hydroentangled materials	130
Figure 3- 14: Thickness of 37 InS structures after caustic treatment	132
Figure 3- 15: Solidity of 37 InS structures after caustic treatment	133
Figure 3- 16: Air permeability of 37 InS structures after caustic treatment	134
Figure 3- 17: Filtration efficiency as a function of jet spacing ($dp: 0.3 \mu\text{m}, fv: 5.33 \text{ cm s}^{-1}, A: 100 \text{ cm}^2, DOP$).....	135
Figure 3- 18: Pressure drop as a function of jet spacing ($fv: 5.33 \text{ cm s}^{-1}$).....	135
Figure 3- 19: Quality factor of caustic washed samples	136

Chapter 4

Figure 4- 1: Cross-sectional image of 37 island-in-the-sea fibers	144
Figure 4- 2: Calculated specific energy of P1/P2 hydroentangled structures	146
Figure 4- 3: Basis weight of P1/P2 hydroentangled structures before/after caustic treatment	149
Figure 4- 4: 37 InS structure before caustic treatment.....	149
Figure 4- 5: 37 InS structure after caustic treatment.....	149
Figure 4- 6: Thickness of P1/P2 hydroentangled structures after caustic treatment.....	151

Figure 4- 7: Thickness of P1/P2 hydroentangled structures before/after caustic treatment .	152
Figure 4- 8: Solidity of P1/P2 hydroentangled structures after caustic treatment	153
Figure 4- 9: Air permeability of P1/P2 hydroentangled structures after caustic treatment ..	154
Figure 4- 10: Filtration efficiency of P1/P2 hydroentangled structures after caustic treatment ($dp: 0.3 \mu m, fv: 5.33 \text{ cm s}^{-1}, A: 100 \text{ cm}^2, DOP$)	155
Figure 4- 11: Pressure drop of P1/P2 hydroentangled structures after caustic treatment ($fv: 5.33 \text{ cm s}^{-1}$)	156
Figure 4- 12: Quality factor of P1/P2 hydroentangled structures after caustic treatment	157
Figure 4- 13: Quality factor of P1/P2 hydroentangled structures as a function of specific energy.....	158

Chapter 5

Figure 5- 1: Illustration of the structure of an island-in-the-sea fiber.....	163
Figure 5- 2: Cross-sectional microscopy image of 37 InS fibers.....	166
Figure 5- 3: Cross-sectional microscopy image of 108 InS fibers.....	166
Figure 5- 4: Cross-sectional microscopy image of 360 InS fibers.....	166
Figure 5- 5: Calculated specific energy during hydroentangling.....	168
Figure 5- 6: Basis weight before/after caustic treatment	172
Figure 5- 7: 37 InS structure before caustic treatment.....	173
Figure 5- 8: 37 InS structure after caustic treatment.....	173
Figure 5- 9: 108 InS structure before caustic treatment.....	173
Figure 5- 10: 108 InS structure after caustic treatment.....	173
Figure 5- 11: 360 InS structure before caustic treatment.....	174
Figure 5- 12: 360 InS structure after caustic treatment.....	174
Figure 5- 13: Fiber size distribution of intact island-in-the-sea fibers of structures with intact 37, 108 and 360 InS fibers	175
Figure 5- 14: Calculated theoretical accessible specific surface area based on fiber size measurements.....	177
Figure 5- 15: Influence of island count and jet spacing on normalized thickness after caustic treatment	178
Figure 5- 16: Influence of island count and jet spacing on solid volume fraction after caustic treatment	180
Figure 5- 17: Influence of island count and jet spacing air permeability after caustic treatment	181
Figure 5- 18: Filtration efficiency as a function of jet spacing ($dp: 0.3 \mu m, fv: 5.33 \text{ cm s}^{-1}, A: 100 \text{ cm}^2, DOP$).....	182
Figure 5- 19: Pressure drop as a function of jet spacing (5.33 cm s^{-1}).....	183

Figure 5- 20: Filtration as a function of jet spacing ($dp: 0.3 \mu m, fv: 5.33 cm s^{-1}, A: 100 cm^2, DOP$).....	184
Figure 5- 21: Pressure drop as a function of jet spacing ($fv: 5.33 cm s^{-1}$).....	185
Figure 5- 22: Quality factor as a function of jet spacing	186

Chapter 6

Figure 6- 1: Illustration of an alternating mixed media island-in-the-sea configuration	193
Figure 6- 2: Illustration of a layered mixed media island-in-the-sea configuration	193
Figure 6- 3: Illustration of a random mixed media island-in-the-sea configuration.....	193
Figure 6- 4: Microscopy image of cross-section of drawn fibers of MM 37 InS structure .	195
Figure 6- 5: Microscopy image of cross-section of drawn fibers of MM 108 InS structure	195
Figure 6- 6: Calculated specific energy during hydroentangling.....	196
Figure 6- 7: Abbreviations used for specific surface area calculation of MM InS structures	200
Figure 6- 8: Basis weight before/after caustic treatment	204
Figure 6- 9: SEM image of 37 InS structure before caustic treatment	205
Figure 6- 10: SEM image of 37 InS structure after caustic treatment	205
Figure 6- 11: SEM image of mixed media alt. 37. InS structure before caustic treatment....	206
Figure 6- 12: SEM image of mixed media alt. 37 InS structure after caustic treatment	206
Figure 6- 13: Fiber size distribution of 37 InS and MM alt. 37 InS structure	207
Figure 6- 14: Cross-sectional image of MM 37 InS structure, polymer distribution: 50/50 poly(propylene) homo/mono, 60/40 poly(propylene)/poly (lactic acid) island/sea.....	208
Figure 6- 15: Comparison of specific surface area of 37 InS & MM Alt. 37 InS Structures	209
Figure 6- 16: Normalized thickness as a function of jet spacing of caustic-treated 37 InS and MM 37 InS structures	210
Figure 6- 17: Solidity as a function of jet spacing of caustic-treated 37 InS and MM 37 InS structures	211
Figure 6- 18: Normalized air permeability as a function of jet spacing of caustic-treated 37 InS and MM 37 InS.....	212
Figure 6- 19: Filtration efficiency as a function of jet spacing ($dp: 0.3 \mu m, fv: 5.33 cm s^{-1}, A: 100 cm^2, DOP$).....	213
Figure 6- 20: Pressure drop as a function of jet spacing ($fv: 5.33 cm s^{-1}$).....	213
Figure 6- 21: Quality factor as a function of jet spacing	214
Figure 6- 22: Basis weight as a function of jet spacing of caustic-treated P1/P2 MM 37 InS structures	216
Figure 6- 23: Solidity as a function of jet spacing of caustic-treated P1/P2 MM 37 InS structures	217

Figure 6- 24: Air permeability as a function of jet spacing of caustic-treated P1/P2 MM 37 InS structures	217
Figure 6- 25: Filtration efficiency as a function of jet spacing ($dp: 0.3 \mu m, fv: 5.33 \text{ cm s}^{-1}, A: 100 \text{ cm}^2, DOP$).....	218
Figure 6- 26: Pressure drop as a function of jet spacing (5.33 cm s^{-1}).....	219
Figure 6- 27: Basis weight caustic-treated MM 37/108 InS structures hydroentangled with P2	220
Figure 6- 28: SEM image of MM alt. 108 InS structure before caustic treatment	221
Figure 6- 29: SEM image of MM alt. 108 InS structure after caustic treatment	221
Figure 6- 30: Fiber size distribution of MM alt. 108 InS structure.....	222
Figure 6- 31: Cross-sectional image of MM 108 InS structure, polymer distribution: 75/25 poly(propylene) homo/mono, 40/60 poly(propylene) / poly (lactic acid) island/sea.....	224
Figure 6- 32: Comparison of specific surface area of 37 InS, MM 37 InS, MM 108 InS structures	225
Figure 6- 33: Solidity as a function of jet spacing of caustic-treated, P2 hydroentangled MM 37 InS, MM 108 InS structures.....	226
Figure 6- 34: Air permeability as a function of jet spacing of caustic-treated, P2 hydroentangled MM 37 InS, MM 108 InS structures.....	227
Figure 6- 35: Filtration efficiency as a function of jet spacing ($dp: 0.3 \mu m, fv: 5.33 \text{ cm s}^{-1}, A: 100 \text{ cm}^2, DOP$).....	228
Figure 6- 36: Pressure drop as a function of jet spacing ($fv: 5.33 \text{ cm s}^{-1}$).....	228

Chapter 7

Figure 7- 1: Fiber size distribution of intact PP and PLA monocomponent and 37 InS fibers (PP, PLA, 37 InS)	243
Figure 7- 2: Solidity of 600 μm , P1/P2 hydroentangled mono- and bicomponent structures (before caustic treatment)	244
Figure 7- 3: Air permeability of 600 μm , P1/P2 hydroentangled mono- and bicomponent structures (before caustic treatment).....	245
Figure 7- 4: Strip tensile strength (MD) of 600 μm , P1/P2 hydroentangled mono- and bicomponent structures (before caustic treatment).....	246
Figure 7- 5: Strip tensile strength (CD) of 600 μm , P1/P2 hydroentangled mono- and bicomponent structures (before caustic treatment).....	247
Figure 7- 6: Tensile MD/CD ratio of 600 μm , P1/P2 hydroentangled mono- and bicomponent structures (before caustic treatment).....	248
Figure 7- 7: Tongue tear strength (MD) of 600 μm , P1/P2 hydroentangled mono- and bicomponent structures (before caustic treatment).....	249

Figure 7- 8: Tongue tear strength (CD) of 600 μm , P1/P2 hydroentangled mono- and bicomponent structures (before caustic treatment)	249
Figure 7- 9: Burst strength of 600 μm , P1/P2 hydroentangled mono- and bicomponent structures (before caustic treatment)	250
Figure 7- 10: Solidity of P1/P2 hydroentangled 37 island-in-the-sea structures (after caustic treatment)	252
Figure 7- 11: Illustration of high and low density regions.....	253
Figure 7- 12: Normalized air permeability of P1/P2 hydroentangled 37 InS structures (after caustic treatment)	254
Figure 7- 13: Solid volume fraction of P1/P2 hydroentangled 37 and 108 InS structures (after caustic treatment)	255
Figure 7- 14: Normalized air permeability of P1/P2 hydroentangled 37 and 108 InS structures (after caustic treatment)	255
Figure 7- 15: Tensile MD/CD ratio of 600 μm , P1/P2 hydroentangled 37 InS structures (before/after caustic treatment)	256
Figure 7- 16: Strip tensile strength (MD) of P1/P2 hydroentangled 37 island-in-the-sea structures (after caustic treatment).....	257
Figure 7- 17: Strip tensile strength (CD) of P1/P2 hydroentangled 37 island-in-the-sea structures (after caustic treatment).....	257
Figure 7- 18: Tensile MD/CD ratio of P1/P2 hydroentangled 37 island-in-the-sea structures (after caustic treatment)	258
Figure 7- 19: Tongue tear strength (MD) of P1/P2 hydroentangled 37 island-in-the-sea structures (after caustic treatment).....	259
Figure 7- 20: Tongue tear strength (CD) of P1/P2 hydroentangled 37 island-in-the-sea structures (after caustic treatment).....	259
Figure 7- 21: Burst strength of P1/P2 hydroentangled 37 island-in-the-sea structures (after caustic treatment)	260
Figure 7- 22: Influence of specific energy and jet spacing on the solidity of caustic-treated 37 island-in-the-sea nonwoven materials.....	261
Figure 7- 23: Influence of specific energy and jet spacing on the solidity of caustic-treated 37 island-in-the-sea nonwoven materials.....	262
Figure 7- 24: Tensile strength (MD) of caustic-treated 37 island-in-the-sea nonwoven materials hydroentangled with P1/P2 and P3/P4 with 600 μm and 4800 μm jet spacing	263
Figure 7- 25: Tensile strength (CD) of caustic-treated 37 island-in-the-sea nonwoven materials hydroentangled with P1/P2 and P3/P4 with 600 μm and 4800 μm jet spacing	263
Figure 7- 26: Tear strength (MD) of caustic-treated 37 island-in-the-sea nonwoven materials hydroentangled with P1/P2 and P3/P4 with 600 μm and 4800 μm jet spacing.....	264

Figure 7- 27: Tear strength (CD) of caustic-treated 37 island-in-the-sea nonwoven materials hydroentangled with P1/P2 and P3/P4 with 600 μm and 4800 μm jet spacing.....	264
--	-----

Chapter 8

Figure 8- 1: Solid volume fraction of caustic-treated 37 InS structures hydroentangled with P1-P3 and 600 μm jet spacing	276
Figure 8- 2: Air permeability of caustic-treated 37 InS structures hydroentangled with P1-P3 and 600 μm jet spacing	277
Figure 8- 3: Burst strength of caustic-treated 37 InS structures hydroentangled with P1-P3 and 600 μm jet spacing	278
Figure 8- 4: Tensile strength (MD) of caustic-treated 37 InS structures hydroentangled with P1-P3 and 600 μm jet spacing	279
Figure 8- 5: Tensile strength (CD) of caustic-treated 37 InS structures hydroentangled with P1-P3 and 600 μm jet spacing	279
Figure 8- 6: Tongue tear strength (MD) of caustic-treated 37 InS structures hydroentangled with P1-P3 and 600 μm jet spacing	280
Figure 8- 7: Tongue tear strength (CD) of caustic-treated 37 InS structures hydroentangled with P1-P3 and 600 μm jet spacing	280
Figure 8- 8: Pressure drop of caustic-treated 37 InS structures hydroentangling with manifold pressures P1-P3 and 600 μm jet spacing ($f_v: 5.33 \text{ cm s}^{-1}$)	281
Figure 8- 9: Solid volume fraction of caustic-treated 37 InS structures hydroentangled with P1-P3 and 600, 1800 and 4800 μm jet spacing.....	282
Figure 8- 10: Air permeability of caustic-treated 37 InS structures hydroentangled with P1-P3 and 600, 1800 and 4800 μm jet spacing	283
Figure 8- 11: Tensile strength (MD) of caustic-treated 37 InS structures hydroentangled with P1-P3 and 600, 1800 and 4800 μm jet spacing.....	284
Figure 8- 12: Tensile strength (CD) of caustic-treated 37 InS structures hydroentangled with P1-P3 and 600, 1800 and 4800 μm jet spacing.....	285
Figure 8- 13: Tear strength (MD) of caustic-treated 37 InS structures hydroentangled with P1-P3 and 600, 1800 and 4800 μm jet spacing.....	285
Figure 8- 14: Tear strength (CD) of caustic-treated 37 InS structures hydroentangled with P1-P3 and 600, 1800 and 4800 μm jet spacing.....	286
Figure 8- 15: Solidity of mono- and bicomponent nonwovens hydroentangled with P1-P3 and 600 μm jet spacing.....	287
Figure 8- 16: Air permeability of mono- and bicomponent nonwovens hydroentangled with manifold pressures P1-P3 and 600 μm jet spacing	288

Figure 8- 17: Tensile strength (MD) of mono- and bicomponent structures hydroentangled with P1-P3.....	289
Figure 8- 18: Tensile strength (CD) of mono- and bicomponent structures hydroentangled with P1-P3.....	289
Figure 8- 19: Tear strength (MD) of mono- and bicomponent structures hydroentangled with P1-P3.....	290
Figure 8- 20: Tear strength (CD) of mono- and bicomponent structures hydroentangled with P1-P3.....	290

Chapter 9

Figure 9- 1: Winged fiber before/after removing sheath polymer (Pourdeyhimi & Chappas, 2012b)	296
Figure 9- 2: Basis weight before/after caustic treatment (structure 9.-Winged.600-115-P4 to 9.-Winged.600-115-P5)	304
Figure 9- 3: Winged fiber nonwoven before caustic treatment	305
Figure 9- 4: Winged fiber nonwoven after caustic treatment	305
Figure 9- 5: Solid volume fraction of P4/P5 hydroentangled winged fiber nonwovens (after caustic treatment)	305
Figure 9- 6: Air permeability of P4/P5 hydroentangled winged fiber nonwovens (after caustic treatment)	306
Figure 9- 7: Filtration properties of IPA discharged/corona discharged 32 winged and 37 InS nonwovens	308
Figure 9- 8: Pressure drop of IPA and corona discharged InS and winged fiber nonwovens	309
Figure 9- 9: Mean pore size of IPA/corona discharged 37 InS and 32 winged fiber nonwovens	310
Figure 9- 10: Filtration efficiency as a function of salt load of unwashed/caustic-treated winged fiber nonwovens	311
Figure 9- 11: Pressure drop as a function of salt load of unwashed/caustic-treated winged fiber nonwovens	311
Figure 9- 12: SEM image taken from the surface of an unwashed winged fiber structure (IPA discharged)	312
Figure 9- 13: SEM image taken from the surface of a caustic-treated winged fiber structure (IPA discharged)	312
Figure 9- 14: Salt loading over time of unwashed/caustic-treated IPA discharged winged fiber materials	313

Figure 9- 15: Filtration efficiency as a function of salt load of IPA/Corona discharged caustic-treated winged fiber nonwovens.....	314
Figure 9- 16: Pressure drop as a function of salt load of IPA/Corona discharged caustic-treated winged fiber nonwovens	314
Figure 9- 17: Salt loading over time of unwashed/caustic-treated Corona discharged winged fiber materials	315
Figure 9- 18: SEM image taken from the cross-section of caustic-treated winged fiber nonwovens (IPA discharged).....	316
Figure 9- 19: SEM image taken from the cross-section of caustic-treated winged fiber nonwovens (corona discharged)	316
Figure 9- 20: SEM image taken from the surface of caustic-treated winged fiber nonwovens (IPA discharged)	317
Figure 9- 21: SEM image taken from the surface of caustic-treated winged fiber nonwovens (corona discharged).....	317

LIST OF SYMBOLS

Solid Volume Fraction	SVF, α
Filtration Efficiency [%]	E
Pressure Drop [Pa]	ΔP
Quality Factor [Pa^{-1}]	QF
Thickness [μm]	t
Basis Weight [g m^{-2}]	w
Single Jet Energy [J s^{-1}]	\dot{E}
Specific Energy [KJ s^{-1}]	SE
Fabric Mass Flow Rate [Kg s^{-1}]	\dot{M}
Fiber Polymer Density [g cm^{-3}]	ρ_f
Theoretical Island Diameter [μm]	$d_{f,s,t}$
Island Count	N
Volume Fraction Island/Sea	vol_i, vol_s
Up-/Downstream Particles	c_{up}, c_{down}
Jet Velocity [m s^{-1}]	v
Water Pressure [Pa]	P
Fluid Density [Kg m^{-3}]	ρ
Jet Diameter [m]	d_j
Structure Porosity	P

Mass Fraction of Island/Sea	R_i, R_s
Particle Diameter [μm]	d_p
Face Velocity [cm s^{-1}]	f_v
Filtration Testing Area [cm^2]	A
Discharge Coefficient	C_d
Nozzle Diameter	d_n
Belt Speed [m s^{-1}]	v_B
Specific Surface Area [$\text{m}^2 \text{g}^{-1}$]	A_s
Null Hypothesis	H_n
Fabric Width [m]	s

CHAPTER 1

- Introduction -

1.1 Introductory Remarks

Forecasts state the global nonwoven market to continue growing over the next years to meet increasing demands. Nonwoven webs can be produced by different means and most often require subsequent bonding to strengthen the structure. Bonding processes are usually classified into mechanical, thermal and chemical bonding techniques (Chapman, 2010, p. 11). Hydroentangling describes an acknowledged technique using fine, high-velocity water jets to entangle and interlock fibers. Annual growth rates of this technique are mentioned to be 5.7% describing the fastest growing sector of all nonwoven materials (EDANA, 2014). Recent studies demonstrated the versatility and also innovative potential of hydroentangling by creating novel, pocket-like structures with unique properties. Changing the jet density during hydroentangling to 4800 μm (600 μm is industrial standard) led to highly permeable structures comprising low and high density areas (Suragani Venu, 2012). Such structures could be advantageous for numerous applications, such as air filtration media or absorbent materials. Recent studies reported the global air filtration market to increase and surpass \$19 billion through 2020 (TechSci Research, 2015). Projected growth rates but also the market trends of the past years elucidate the importance and position of this industry.

Filtration efficiency and pressure drop are the two most important characteristics determining the performance of a medium engineered for air filtration. According to literature, filtration efficiency is mostly a function of basis weight and fiber diameter (Hinds, 1999, p. 196). Ironically, pressure drop of a filter is affected by the structure's solidity and also the fiber diameter. Thus, decreasing fiber diameters might enhance the capture efficiency of a filter but can also increase the resistance to flow (Gądor & Jankowska, 1999).

Well-known techniques to decrease fiber size are meltblowing, electrospinning or modified spunbond processes. Whereas electrospinning is capable to produce nonwoven materials with fiber sizes smaller than 50 nm and therefore tremendous specific surface areas, low output rates are a common drawback (Cao & Wang, 2011, p. 213). The meltblown process however is capable to produce submicron fibers but is limited in terms of suitable polymers. Furthermore, meltblown materials are usually very weak and require an additional layer or a scrim for pleatability. In contrast to that, polymer selection is far more flexible for the spunbond process. Webs are significantly stronger but the process is limited to produce submicron fibers (Yeom & Pourdeyhimi, 2011). Bicomponent fibers describe an interesting technique allowing manufacturing nonwoven materials with significantly smaller diameters or exotic fiber cross-sections at high throughput rates. However, bicomponent structures require subsequent processes to remove one polymer or separate both from each other. This can be done by fibrillating (e.g. island-in-the-sea structures combined with hydroentangling) or splitting (e.g. segmented pie fibers). Appropriate solvents can be used to dissolve one polymer leaving the second one (island polymer).

Looking at current literature, several interesting structures, structure modifications, bonding techniques and also fiber cross-sections for nonwoven materials can be found. Unfortunately, only little is known about their impact, benefits and usability as a filtrating or separating medium. In addition to that, interesting relationships as specific surface area and filtration performance are rarely mentioned. Moreover, a deeper understanding of the impact of various hydroentangling parameters on microfiber structures is from great interest.

1.2 Problem Statement

Small fiber sizes are claimed to be an important characteristic in terms of the aerosol filtration performance of fibrous structures. Put simply, a construct of small fibers enhances the probability of particles of getting trapped within the material. However, due to their torsional rigidity smaller fibers tend to collapse more easily resulting in denser structures having higher pressure drops. Moreover, fiber size affects the pore size of the structure and thus does not create open, permeable structures by itself. Obviously it is desired to keep the resistance of a filter as low as possible as the pressure drops is directly correlated to the energy necessary to push the contaminated air through the structure. Thus, having ability to create filtration media with small fiber sizes and also low densities would certainly reveal new opportunities.

Problem Statement: Can hydroentangling be used to control the structure and properties of high surface area nonwovens?

1.3 Significance of the Study

The findings of this study will contribute to the general understanding of structure and properties of high surface area nonwoven materials. Furthermore, it continues recent studies pursuing the target to better understand how and to which degree hydroentangling can be used to control the structure of nonwoven materials. In this context, both small and large fibers are part of the investigation contributing to a general understanding of this topic.

Furthermore, research provides information how high surface area nonwoven materials made from different fiber cross-sections differ in terms of their properties.

1.4 Research Objectives and Approach

The main objective of this research is to investigate how and in which way hydroentangling can be used to control the structure and properties of nonwovens with high specific surface areas. Objectives of this study can be subcategorized into the following:

- To understand the effect of various hydroentangling parameters on nonwoven materials after removing the sacrificial polymer (structures with high specific surface areas, e.g. micro-/nanofibers)
- Investigating various hydroentangled bicomponent structures in terms of their properties

1.5 About the Dissertation

This dissertation is grouped into different chapters examining different aspects of the subject. The following gives a brief overview about the topics investigated in each chapter.

Chapter 2: This chapter provides a wide-ranging, in-depth review of nonwoven materials in general along with current scientific knowledge. Moreover, chapter 2 serves as an introductory section explaining many concepts, principles and methods used later on.

Chapter 3: In this chapter we report on the influence of jet spacing (5 different jet spacing) on the structure (thickness, solidity etc.) and also properties (air permeability, aerosol filtration performance) of caustic-treated island-in-the-sea nonwoven materials.

Chapter 4: This chapter examines the influence of hydroentangling pressure on island-in-the-sea nonwovens. Structures were hydroentangled with reduced jet pressures and three different jet spacing and examined in terms of their structure and properties. Caustic-treated materials were examined and the impact of specific energy during hydroentangling discussed.

Chapter 5: This chapter reports on hydroentangled island-in-the-sea nonwovens with different island counts (37, 108 and 360). Webs were hydroentangled with same manifold pressures and 5 different jet spacing. We report on the structure, physical and aerosol filtration properties as well as the effect of fiber diameter and specific surface area.

Chapter 6: This chapter examines the effect of hydroentangled mixed media island-in-the-sea nonwovens in terms of structure and properties. Hybrid structures were spun in an alternating configuration with different island counts and hydroentangled with different manifold pressures and jet spacing.

Chapter 7: In the seventh chapter we report on the effect of specific energy and force on both mono- and bicomponent materials. Webs were hydroentangled with same specific energy but different manifold pressures and jet spacing. Structure and physical properties (air permeability, strip tensile, tongue tear and ball burst) are part of the discussion.

Chapter 8: This chapter discusses the influence of the number of manifolds on mono- and bicomponent nonwoven structures. Webs were bonded with 5 manifolds, whereas the last three manifolds had the same jet pressure. Subsequent webs were hydroentangled with 4 and 3 manifolds respectively. Materials were analyzed in terms of their structural and also physical properties (air permeability, strip tensile, tongue tear and ball burst).

Chapter 9: This chapter discusses the influence of hydroentangling on winged fiber materials. We report on structure, physical and aerosol filtration properties as well as the influence of fiber size and specific surface area. Moreover, unwashed and caustic-treated and also IPA and corona discharged winged fiber nonwovens were examined in terms of their salt loading capacity.

Chapter 10: Summary of the dissertation discussing the main findings and contributions of this research.

Chapter 11: Recommendations for future work regarding the continuation of the research topic.

1.6 References

- Cao, G. & Wang, Y. (2011). *Nanostructures and Nanomaterials: Synthesis, Properties, and Applications*: World Scientific.
- Chapman, R. (2010). *Applications of nonwovens in technical textiles*: Elsevier.
- EDANA. (2014). Nonwoven production exceeded 2 million tonnes in 2013 in Greater Europe. Retrieved Oct 13, 2014, from <http://www.edana.org/newsroom/news-announcements/2014/03/31/nonwoven-production-exceeded-2-million-tonnes-in-2013-in-greater-europe>
- Gądor, W. & Jankowska, E. (1999). Filtration properties of nonwovens. *International Journal of Occupational Safety and Ergonomics*, 5(3), 361-379.
- Hinds, W. C. (1999). *Aerosol Technology: Properties, Behavior, and Measurement of Airborne Particles* (Vol. 2nd Edition): John Wiley & Sons, Inc.
- Suragani Venu, L. B. (2012). *A Study on Hydroentangling Mechanisms and Structures*. (Ph.D. - Fiber and Polymer Science), North Carolina State University.
- TechSci Research. (2015). Global Air Filters Market to Surpass USD19 Billion by 2020. Retrieved May 21, 2015, from <http://www.techsciresearch.com/3333>
- Yeom, B. Y. & Pourdeyhimi, B. (2011). Aerosol filtration properties of PA6/PE islands-in-the-sea bicomponent spunbond web fibrillated by high-pressure water jets. *Journal of materials science*, 46(17), 5761-5767.

CHAPTER 2

- Background -

2.1 Nonwoven Structures

Many definitions describing a nonwoven structure can be found in today's literature, whereas INDA (former International Nonwovens and Disposables Association and now the Association of the Nonwoven Fabrics Industry) provides a precise and widely accepted explanation of what a nonwoven is. It is defined as a web structure consisting of finite fibers or filaments bonded together by mechanical, thermal or chemical means. Moreover, nonwoven structures are described as flat and porous sheets directly made from individual fibers. As a consequence, traditional spinning, which converts single fibers to yarns, is not necessary (INDA (Association of the Nonwoven Fabric Industry), n.d.-a).

2.1.1 Historical Outline of Nonwoven Materials

The very first attempts to fabricate textile goods from loose fibers can be traced back to the Neolithic era when people started felting woolen materials. According to literature, it is assumed that people from that period learned how to felt materials from observing the matting effect on sheep skin, which was used as clothing (Hagen, 2002, p. 8). Patents from the mid-19th century indicate the presence of early techniques using needles to strengthen loose fiber webs. These inventions mostly took place in the USA and Europe but especially England and Germany (Batra & Pourdeyhimi, 2012a, p. 88). The beginnings of fibrous structures resembling today's nonwovens are considered to be the late 1920's. This is mentioned to be the starting period and an impulse-giving time. In August 1928 the German company Kalff Vliesstoffe GmbH (former Weißweiler & Kalff) filed a patent (DRP 544324) claiming a product consisting of a nonwoven structure glued to a woven material. This

composite had the purpose to stiffen shoes and is still offered by the company (Lenzing AG, 1968). In those days nonwoven structures were mostly used as substrate materials for artificial leather. Production in larger, commercial scales is dated to the early 1940's (Batra & Pourdeyhimi, 2012b). Since then the nonwoven industry enjoyed phenomenal growth rates and generated many innovative products. Whereas the nonwoven market in Europe was more focused on creating re-usable high-end products it was the opposite in the US. Here, low-cost products (mostly disposable products) were from greater interest resulting in different markets and research priorities (Lenzing AG, 1968). Since then, the nonwoven market is a continuously growing and expanding field constantly creating new innovations and solutions. Nonwovens are highly-engineered materials demanding sophisticated research and expertise in the science of textiles, material science, chemistry but also physics (Batra & Pourdeyhimi, 2012a, p. XXII).

2.1.2 Classification of Nonwoven Processes and Materials

Nonwoven materials can be produced in many different ways depending on the desired performance and final application. It is impossible to generalize this kind of material as the versatility is almost infinite (Anand, Kennedy et al., 2010, p. 13; Kumar, 2013, p. 33). As previously mentioned, nonwoven materials can be found in many fields of application each having specific product demands. Selection of raw material, manufacturing process and specific treatments allow controlling the properties of the final product of which some are: Abrasion resistance, absorbency, antistatic features, pore size, bulk density etc. (EDANA, n.d.).

A typical nonwoven manufacturing process usually starts with the selection of the raw material, which not only defines many properties of the final product but also dictates the possibilities in terms of suitable web formation processes. The simplest distinction is to differentiate between staple fibers and filaments (Elias, 2013, p. 480; Scheirs & Long, 2005, p. 402). Whereas staple fibers have a defined, finite length, filament fibers are continuously spun fibers from various lengths. Staple fibers can be from natural or synthetic origin and staple length and fiber quality not only depends on the animal or plant but also the prevailing conditions. In contrast to that, man-made staple fibers either from a petroleum or plant base can be produced with a consistent quality and length. Pourdeyhimi et al. (Batra & Pourdeyhimi, 2012a, p. 29) classified raw materials used for nonwoven processing into five different categories: 1) staple fibers with an average length of ≥ 10 mm primarily used for carding or air-lay systems, 2) staple fibers with an average length of < 5 mm primarily used for pulp air-lay systems, 3) staple fibers with an average length of 10-25 mm primarily used for wet-lay systems, 4) polymer resin flakes primarily used for melt-spinning and 5) poly (ethylene) resins primarily used for flash spinning.

Albrecht et al. (Albrecht, Fuchs et al., 2006, p. 140) classified nonwoven web formation processes into three categories: 1) dry-laid systems, such as carding or air-lay, 2) wet-lay systems and 3) extrusion systems, such as spunbond, meltblown etc.. Further technologies are electro-spinning, blow-spinning and also precursor technologies in which fiber spinning and web formation are separated (e.g. early spunbond processes).

2.1.3 Carding and Cross-Lapping Technology

Carding describes one of the oldest technologies used in the production of textile materials known for thousands of years. Until the beginning of the Industrial Revolution in the 18th century textile goods were carded by hand (Batra & Pourdeyhimi, 2012a, p. 43). INDA (Association of the Nonwoven Fabric Industry), 2002) defined carding as a process used to make web structures consisting of fibers aligned in machine direction (MD) or randomly distributed. Traditionally, carding is known as a preliminary stage of yarn spinning where fiber tufts are disentangled to individual fibers and cleaned from impurities (e.g. twigs or straws in wool or cotton). Lawrence (Lawrence, 2003, p. 101) defined traditional carding as the process of converting tufts of entangled fibers into a web of individual fibers by using closely spaced surfaces equipped with opposing sharp points. Carding in nonwoven manufacturing uses the same principle and usually starts with the bale opening as fibers are delivered in a highly compressed form (Kumar, 2013, p. 36). During the carding process drums with differently equipped sharp points (stripper, worker and fancy roll) disentangle the fibers and align them in machine direction (e.g. roller top cards) (Batra & Pourdeyhimi, 2012a, pp. 50-51). After leaving the card webs are of relatively low weight and fibers are aligned in machine direction (which may not be desired for certain applications). One way to increase the basis weight of the webs is layering webs from multiple cards on top of each other (e.g. for heavy weight materials used as geotextiles).

Cross-lapping describes a subsequent process used to increase the basis weight of the web and/or change the ODF (orientation distribution function) from machine direction (MD) to a bimodal distribution by layering the structure in a specific angle. This angle is usually

controlled by the in-feed to output speed of the web (Russell, 2006, pp. 67, 495; van Dyk, 2008, p. 25). Carded webs can be bonded by mechanical bonding techniques, such as needle-punching or hydroentangling but also thermal or chemical bonding.

2.1.4 Air-Lay Technology

According to literature, air-lay technology has its roots in the mid-1930s when Fred Manning filed a patent about the process (Batra & Pourdeyhimi, 2012a, p. 71). The key element of this technology is the usage of air to distribute fibers. The process also requires pre-opening of the bales and the final basis weights can vary between 10 to 600 g m⁻² (Das & Pourdeyhimi, 2014, p. 93). Structures show a randomly orientated ODF and are primarily used for wipes but also napkins or in baby diapers (Anand, Kennedy et al., 2010, pp. 98-99; EAM Corporation, n.d.).

2.1.5 Wet-Lay Technology

The wet-lay process used for nonwoven manufacturing is mainly inspired by the papermaking industry, which can be traced back to 3,000 B.C. (Batra & Pourdeyhimi, 2012a, p. 189; Hunter, 1978, p. 464). According to Chapman (Chapman, 2010, p. 7), the wet-lay process used for nonwoven production was originally developed in the 1930s by Dexter (later Ahlstrom) and can be divided into three main steps: 1) the swelling and dispersion of the fibers in water, 2) web formation on a screen by filtration and 3) drying and bonding. Wet-lay structures can be bonded by hydroentangling but also bonding agents, such as poly (acrylates) or poly (styrene butadiene). Wet-laid nonwovens can be found in many

fields, such as filtration, backing materials and also diapers (Dahiya, Kamath et al., 2004b; Hutten, 2007, p. 22).

2.1.6 Spunbond Technology

The spunbond process describes a spun-laid technology, which is per definition a method of manufacturing nonwoven structures by melting and extruding polymer raw material into fibers and laying them to a web. Spun-laid processes are usually continuous processes resulting in high production speeds and therefore high productivity (Horrocks & Anand, 2000, p. 137). According to INDA (INDA (Association of the Nonwoven Fabric Industry), 2002, n.d.-b), three processes can be defined as spun-laid technologies: 1) spunbond, 2) meltblown and 3) flashspinning.

INDA (INDA (Association of the Nonwoven Fabric Industry), 2002) defines spunbond as a technology extruding and drawing filaments and collecting them on a moving screen to form a web. Spunbond webs require further stabilization as laid-down webs are usually weak and can't withstand applied forces. Webs can be strengthened by using chemical, thermal or mechanical bonding techniques adhering, melting or entangling fibers (Gupta & Kothari, 1997, p. 563; D. Zhang, 1995, p. 5).

Historically, the spunbond process seems to have its origin in the late 1930s to early 1940s when Lannan but also Slayter and Thomas patented a processes using steam or high pressured gas to attenuate glass fibers and a moving belt to collect them. All worked for the Owens Corning Fiberglass Cooperation, which is now the world's largest manufacturer of fiberglass materials. They claimed the process to deliver production rates higher than that of

previously known techniques (Lannan, 1939; Slayter & Thomas, 1940; D. Zhang, 1995, p. 5). Before that, most patents and papers dealt with the spinning process itself. According to Lewin (Lewin, 2006, p. 263), Carothers and Hill from DuPont can be seen as the pioneers of melt spinning. In 1932, they demonstrated meltspun, cold-drawn fibers from linear aliphatic polyester to have sufficient strength and good mechanical properties (Hill & Carothers, 1932). In the same year DuPont patented a process and apparatus to manufacture artificial filaments (Edmond, 1932). It was in the late 1950s when DuPont and 1965 when Freudenberg introduced their first spunbond lines. According to Russell (Russell, 2006, p. 150), it took several years until the potential of this technology was fully recognized and spunbond lines found broader acceptance. In the 1960s, research from DuPont led to the following products: Reemay[®], a polyester spunbond material, Typar[®], a spunbond structure made from poly (propylene) and Tyrek[®], a flash-spun poly (ethylene) material. Lutrivil[®], a spunbond process developed by Freudenberg, was used to produce Viledon[®] a nonwoven material made from polyamides used for heat-sealing and other purposes in the garment industry (Lenzing AG, 1968, p. 162; Russell, 2006, p. 150; D. Zhang, 1995). The Docan[®] process was introduced by the Lurgi Kohle & Mineraloeltechnik GmbH in 1970 and was the first commercial spunbond line. Docan[®] describes a single-step spunbond process forming random webs by spinning, drawing and laying down fibers on a conveyor belt (INDEX 11, 2010, p. 112; Russell, 2006, p. 150; Vasile, 2000, pp. 787-788; D. Zhang, 1995). In 1984 Reifenhäuser introduced the first Reicofil[®] spunbond line, which is still part of their product portfolio (D. Zhang, 1995). RFX[®] was introduced by Amoco Fibers and S-TEX[®] by Sodoca,

two processes able to produce structures with improved uniformity at relatively low weights (Russell, 2006, p. 150). Over the years the spunbond technology was further improved and led to systems capable to spin bicomponent fibers and webs with better uniformities. Bicomponent fibers are primarily used in the nonwovens industry and the spunbond technology describes the major platform used for manufacturing these types of fibers (D. Zhang, 2014, p. 60).

During the process polymeric raw material goes through a variety of steps before the fibrous material is wound up as roll good. Figure 2- 1 depicts an illustration of an open spunbond process. Prior processing, polymers with hygroscopic properties (e.g. polyesters or polyamides) need to be dried as moisture in the melt could result in air pockets causing defects or even hydrolytic degradation (e.g. polyesters) (Albrecht, Fuchs et al., 2006, p. 190; Lampman, 2003, p. 47) As a result, reduced molecular weight changes the rheological properties of the melt and therefore the spinnability of fibers. In contrast to that, polyolefins (e.g. poly (propylene), poly (ethylene)) are not able to hold moisture and do not require drying (Yarin, Pourdeyhimi et al., 2014, p. 19). However, transferring raw material between places with high temperature gradients could cause condensing and thus requires moisture abstraction (Giles, Wagner et al., 2013, p. 263). However, modern extruders consisting of so-called degassing zones have the ability to remove moisture but also air or other volatile components from the melt (Harburg-Freudenberger Maschinenbau GmbH, n.d.).

In a typical spunbond process raw material (most often in form of granulate chips) is transported through pipes (Figure 2- 1, No. 1) to the polymer hopper (Figure 2- 1, No. 2) and delivered to the extruder (Figure 2- 1, No. 4) (Elaissari, 2003, p. 1; Russell, 2006, p. 152).

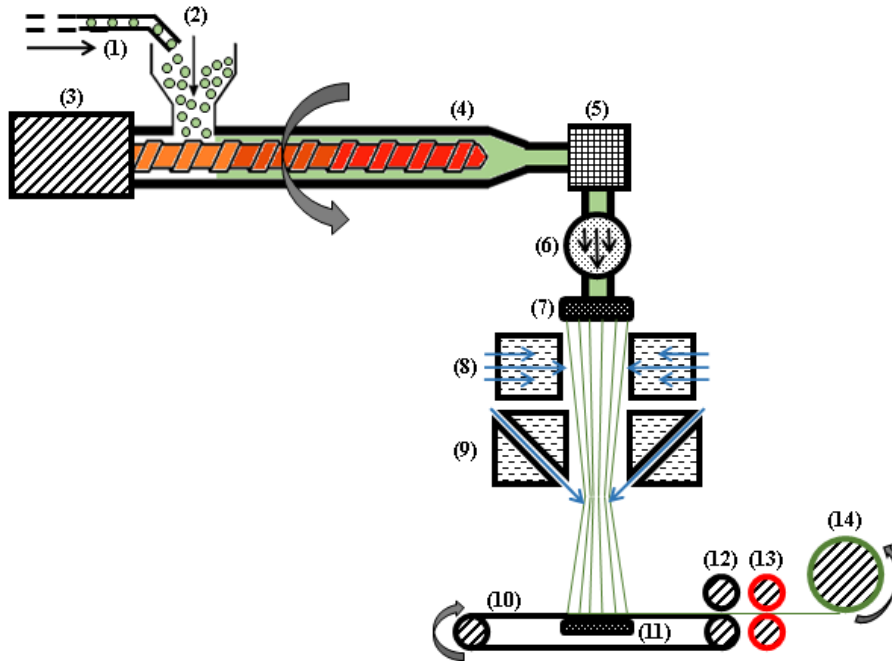


Figure 2- 1: Illustration of an open spunbond process from polymer feed to material roll-up

Polymers used for the spunbond process are characterized by melt flow rates (MFR) in the range between 12 to 70 g 600 s⁻¹ and a narrow molecular weight distribution (MWD). According to literature, polymers used in Europe tend to have slightly lower MFRs compared to the US (Maier & Calafut, 2008, p. 66; Russell, 2006, p. 161; Ugbolue, 2009, p. 170). Batra et al. (Batra & Pourdeyhimi, 2012a, p. 317) mentioned the desirable MFR of poly (ethylene) for spunbond processes to be 17 to 24. Depending on the machine and the desired fiber type, spunbond machines can consist of multiple extruders or extruders with multiple screws. Driven by a motor (Figure 2- 1, No. 3), the extruder has the purpose to heat up the polymeric material above its melting temperature (T_m) as well as to transport and pressurize it (Baird & Collias, 2014, p. 250). Specific extruders also offer the option to side-feed additives, which

are then blended with the polymer to a homogeneous mass. Single screw extruders are usually divided into three zones (feeding zone, compression zone and metering zone) each having its specific function. Another important characteristic of the extruder is the l/d (length-to-diameter) ratio, which not only depends on the desired production rate but also the polymer (e.g. PVC because of sensitivity to high shear rates) and required torque (R. J. Kent, 1998, pp. 6-7). According to literature, length-to-diameter ratio of extruders changed over the past decades. Whereas l/d ratios of 20:1 were typical in the early 1960s, today's industrial standard is 30:1. Extruders with even larger ratios (40:1) are somehow exotic and rather used for specific applications (Frankland 2011; Hills Inc., 2013). Temperatures in extruders can reach up to 350 °C high enough to process common polymer types, such as polyolefins or polyesters (Yarin, Pourdeyhimi et al., 2014, p. 19). Operating temperature is usually the highest temperature during the process and significantly greater than the melting temperature of the processed polymer (Batra & Pourdeyhimi, 2012a, p. 204). After leaving the extruder molten polymer is fed through a screen filter (Figure 2- 1, No.5) to remove contaminations from the melt (e.g. dust or dirt from transport containers or even larger particulates) (Yarin, Pourdeyhimi et al., 2014, p. 19). Screen packs usually consist of both fine and coarse mesh screen filters (mesh is defined as the number of openings per inch). According to Berins (Berins, 1991, p. 90), modest screen filter setups consist of a sequences of 14, 40 and 60 mesh screen filters. However, more restrictive filter packs are built from a 40, 60, 120, two 200 and another 14 mesh screen. Automatic screen changer can be used to minimize or even avoid downtimes of the machine. Sieved melt is then transported to the metering pump (synonyms are spin pump or gear pump, see Figure 2- 1, No. 6 and Figure 2- 2), which

precisely feeds the molten polymer to the die assembly ensuring a constant throughput (Berins, 1991, pp. 90-91; Hutten, 2007, p. 440; Kalinová, n. d.). Another function of the metering pump is to build up higher pressures in the spin beam (Batra & Pourdeyhimi, 2012a, p. 205).

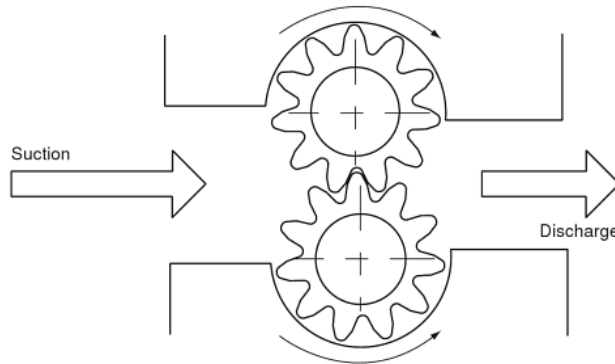


Figure 2- 2: Schematic of a gear pump (Hutten, 2007, p. 212)

The spin beam (Figure 2- 1, No. 7) is probably the most complex part of a spunbond line individually designed for the respective application. It can be described as a rectangular vessel consisting of a system of metal plates (spinpack) with numerous holes (up to 6,000 holes per meter) at its bottom. Function of these plates is to evenly distribute the melt along the width and to the individual holes. Orifices can have diameters in the range of 0.1 mm to 1 mm and also different cross-sections (Batra & Pourdeyhimi, 2012a, p. 205; Geus & Klunter, 2009; Han, 2007, pp. 265-266; Hills Inc., 2013; Yarin, Pourdeyhimi et al., 2014, p. 19). Figure 2- 3 depicts a schematic of a Hills bicomponent spinpack assembly. It can be divided into the top plate (Figure 2- 3, No. 11), support plate (Figure 2- 3, No. 12), metering

plate (Figure 2- 3, No. 13), distributor plate (Figure 2- 3, No. 14) and spinneret plate (Figure 2- 3, No. 15) (Hills, 1992).

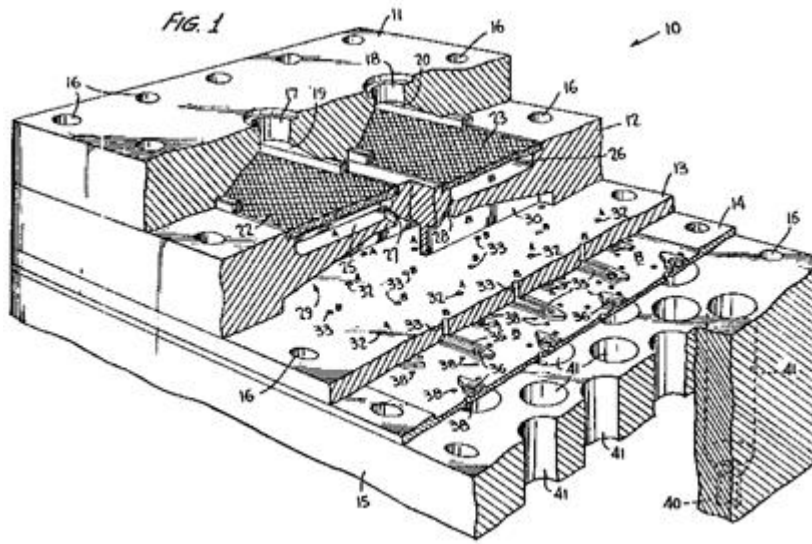


Figure 2- 3: Schematic of a Hills bicomponent spinpack (Hills, 1992)

Another filtration step takes place within the spinpack. Closely meshed screen filters separate the melt from small contaminations and prevent clogging of the small orifices of the assembly (D. Zhang, 2014, p. 56). Contaminations can either be hard particles, such as titanium oxide, degraded polymer but also color pigments or soft gels. Filters can be woven wire cloths, sintered wire cloths, sintered metal cloths, sintered metal powders, sintered fiber metal felts or shattered metal powders with openings ranging from a few micrometers to millimeters (Purolator, n. d.).

It was mentioned that spunbond systems have been further developed over the past decades. Whereas early systems consisted of about 500 holes in total, die density of state-of-

the-art spinpacks is typically in the range of 3,000 to 6,000 holes per meter (Batra & Pourdeyhimi, 2012a, p. 205; Gillespie, Kong et al., 2011). Most often in circular shape (depending on the desired cross-section), orifices have diameters between 0.3 to 0.8 mm and throughputs are in the range of 0.5 to 0.7 ghm (gram per hole per minute). During web formation fibers are spun with speeds between 2,000 and 6,000 m min⁻¹ (Albrecht, Fuchs et al., 2006, p. 206; Delucia, Hudson et al., 2003; Ortiz & Shambaugh, 2005; Ugbolue, 2009, p. 170).

Die swell and melt fracture describe two phenomena in polymer extrusion, which can deteriorate the properties of spun fibers. Die swell occurs right after the polymer is exiting the die and cause the diameter to increase. This can be explained by the pressure difference within and outside of the spinneret causing relaxation, i.e. polymer chains go back to their random coil configuration. Melt fracture, also known as shark-skin effect, can result in heavy surface distortions caused by high shear forces reaching a critical limit (Fleming, 1999; Ibeh, 2011, p. 249; Lampman, 2003, p. 47; Whelan, 1994, pp. 109, 243).

After leaving the spinneret spun fibers are still above melting temperature T_m and have to be quenched (Figure 2- 1, No. 8). Afterwards fibers are cold drawn (Figure 2- 1, No. 9) by using an aspirator inducing drag forces on the fibers to elongate them and induce molecular orientation. This allows the chains to pack closely together. High chain density is necessary to increase intermolecular forces (secondary bonds) between the chains but also to enhance the rate of crystallization by the order of 5 magnitudes (orientation-induced crystallization) (Cheng, 2008, p. 96; Van, Bansal et al., 2003). Drawing fibers causes the fiber diameter to significantly decrease and the ratio of initial to final diameter is defined as

draw ratio. Thus, increasing the draw ratio results in more oriented fibers enhancing the tensile strength and lowering the strain at break (Chanda, 2013, p. 28; Russell, 2006, p. 16). Fiber diameter of spunbond webs is usually in the range of 10 to 35 μm (Ibeh, 2011, p. 248). After spinning, fibers are collected on a moving belt (Figure 2- 1, No. 10) with a suction box installed underneath (Figure 2- 1, No. 11). Purpose of the suction is to remove aspirator air and also to fix fibers on the belt (Batra & Pourdeyhimi, 2012a, p. 220; Dahiya, Kamath et al., 2014). Moving belt causes fibers to show a bias in machine direction [24, p. 168]. At this stage of the process web is extremely weak and does not have sufficient structure integrity to withstand mechanical stress. Compaction rolls (Figure 2- 1, No. 12) are installed behind the fiber collection zone and slightly squeeze the web to consolidate and facilitate its transfer to subsequent bonding processes (e.g. needle-punching, calendering or hydroentangling) (K. L. Brown & Shelley, 2003). The example shown in Figure 2- 1 depicts a spunbond system with calendering (Figure 2- 1, No. 13) for subsequent bonding. In the last stage of the process nonwoven structure is wound up (Figure 2- 1, No. 14).

2.1.7 Meltblown Technology

According to INDA (INDA (Association of the Nonwoven Fabric Industry), n.d.-b), the meltblown process can be defined as a web forming technology used to form fine filaments. The idea of using hot, high speed air to stretch fibers was brought up by Wentz in 1956 (Batra & Pourdeyhimi, 2012a, p. 237). In contrast to the spunbond technology where fibers are first quenched and then drawn, meltblown technology uses hot, high velocity air to attenuate the molten polymer right after leaving the spinneret (see Figure 2- 4) (INDA

(Association of the Nonwoven Fabric Industry), n.d.-b). When collected on the belt, fibers are still tacky, stick to each other and form conjunction points. Therefore, additional bonding is not absolutely necessary. As fibers are still tacky when collected on the belt meltblown webs are imprinted by the structure of the belt (Chatterjee & Gupta, 2002, p. 369; Goddard III, Brenner et al., 2007, p. 215).

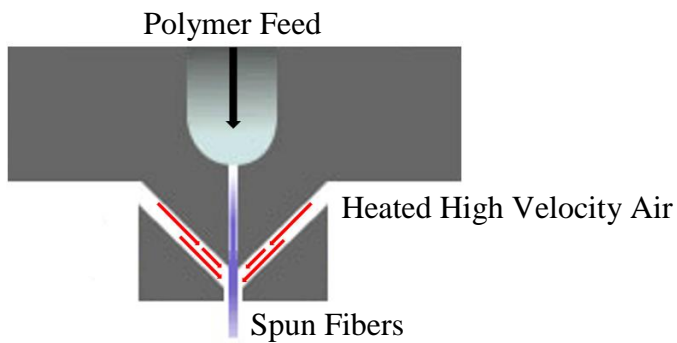


Figure 2- 4: Illustration of Fiber Attenuation in Meltblown Spinning

Diameters of meltblown fibers are usually in the range of 2 μm to 10 μm and can be controlled by both, process and also material parameters (Yarin, Pourdeyhimi et al., 2014, p. 93). Meltblowing has the capacity to produce webs with fiber sizes in the submicron range. Fiber sizes as small as 0.3 μm result in webs offering relatively large specific surface areas and also small pore sizes. Fabrics like this find great application as barrier materials but also in liquid filtration (Chapman, 2012, p. 60; Hassan, Yeom et al., 2013). Other technologies being capable to spin fibers of the mentioned or even smaller size are electrospinning or bicomponent spinning techniques (e.g. island-in-the-sea). However, in contrast to meltblown

or spunbond processes, electrospinning is limited by its low productivity (Hagewood & Wilkie, n. d.; Ramakrishna, Fujihara et al., 2005, p. 130).

Compared to spunbond, polymer selection is limited for the meltblown process as polymers of relatively low viscosity (e.g. LMWPP, LMWPE) are required. Necessary MFRs (melt flow rate) are usually in the range of 1000-1500 g 600 s⁻¹, whereas more viscous polymers (MFRs of 20-25) can be used in the spunbond process. Thus, the spunbond process offers more flexibility in terms of polymer selection (Russell, 2006, p. 161).

2.1.8 Flash-, Electro- and Solution-Blow Spinning

Other technologies capable to produce fibers from small diameters and structures having relatively high specific surface areas are flash-, electro but also solution blow-spinning. Ward (Ward, 1987, p. 45) mentioned flash-spinning to use a pressurized poly (ethylene) solution, high extrusion speeds and temperatures. Fibers are collected after slight drawing and fast solvent evaporation. Flash-spinning has the capability to create microporous nonwoven structures (Scott, 2005, p. 161). Contrary to that, solution-blow systems use a syringe and high-velocity gas to elongate fibers. Literature mentions systems being capable to produce poly (lactic acid) webs consisting fibers with diameters as small as 40 nm (Lagarón, 2011, p. 113; Medeiros, Glenn et al., 2009). Electrospinning setups are contactless systems using an electric field to draw polymer solutions to fibers in the nanometer range (Eichhorn, Hearle et al., 2009, p. 460; Shukla, 2010, p. 49).

2.1.9 Nonwoven Applications, Market Situation and Prognosis

There are many reasons why the nonwoven market was and still is a success story and growth can be expected in the following years. Low material costs, high productivity but also the versatility of process and materials are just a few of many examples (Gregor, 2003). Nonwovens find application in markets, such as hygiene, medical, automotive but also filtration (Batra & Pourdeyhimi, 2012a, pp. xxiii-xxvi). Disposable nonwoven products describe the dominant market, whereas the filtration sector shows the highest profit. Further growth in terms of sale and volume can be expected from the medical but also filtration industry. Spun-melt technologies continue to be the largest segment followed by carded materials (Freedonia, 2013; Smithers Apex, 2014). Development of the global nonwoven market in terms of volume and revenue can be seen in Figure 2- 5 and market data about the disposable and raw material share of 2010 in Figure 2- 6.

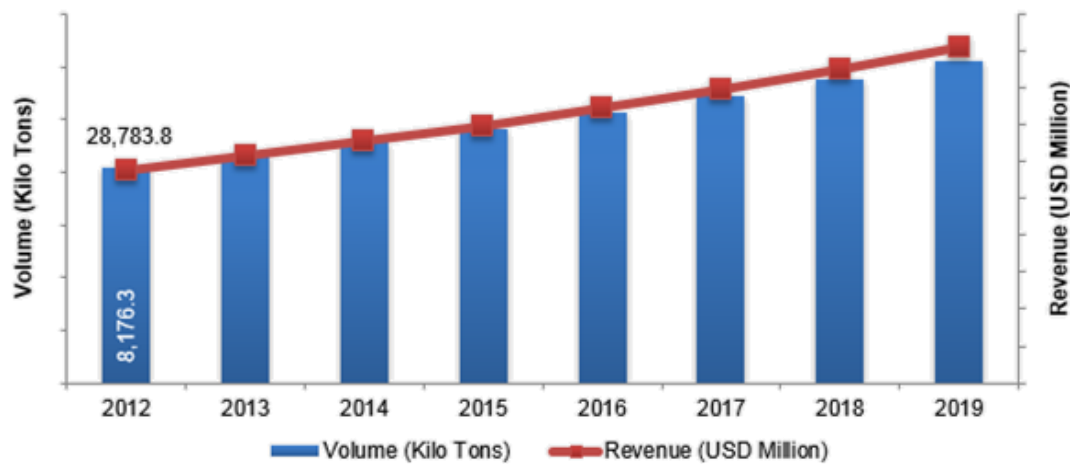


Figure 2- 5: Forecast of global nonwoven market (Transparency Market Research, 2014)

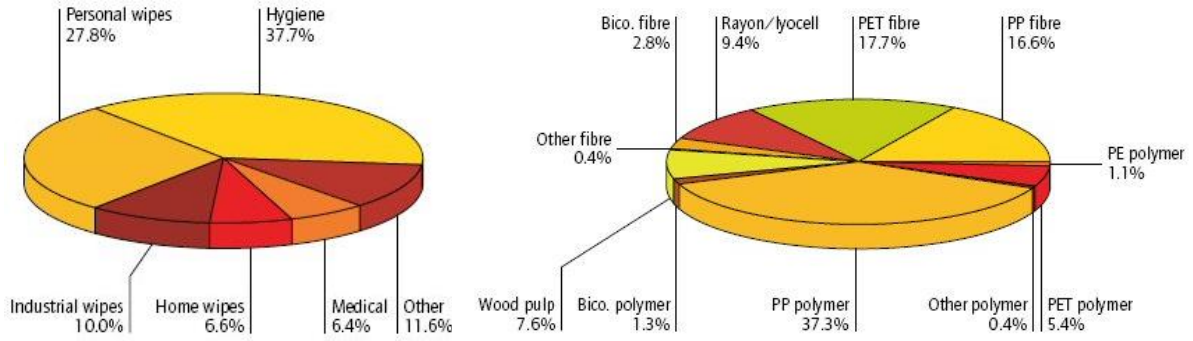


Figure 2- 6: Nonwoven disposable and raw materials share (Clean Indian Journal, 2011; Smithers Pira, n. d.)

2.2 Hydroentangling Technology

Nonwoven webs require a specific quantity of strength to withstand forces applied during application. Bonding techniques in nonwovens science are usually divided into three categories: mechanical, thermal and chemical bonding. Hydroentangling and needle-punching are classified as mechanical bonding techniques, whereas the following discussion is focused on the former (Gordon & Hsieh, 2006, p. 508). In hydroentangling, also known as spunlacing, water-jet entangling, water or hydraulic needling, a web is exposed to a curtain of high-velocity water jets to interlock and entangle fibers (Batra & Pourdeyhimi, 2012a, p. 113; INDA (Association of the Nonwoven Fabric Industry), n.d.-c; Vuillaume, 1991). Hydroentangling can be seen as an energy transfer process using kinetic energy stored in high-velocity water jets used for fiber reorientation. Energy necessary to sufficiently entangle fibers depend on several factors, such as fiber size, bending rigidity, fiber movement et cetera (Majumdar, Das et al., 2012, p. 286). Hydroentangled nonwovens are characterized by their smooth, textile-like hand as well as their brilliant drapeability and also high strength. Because of high forces and concentrated appliance of energy so-called jet streaks (or distinct

ridges, jet marks) are typical marks of hydroentangled nonwovens (Shim & Pourdeyhimi, 2005). Hydroentangled nonwovens find application in the wipe but also hygiene and medical (medical gowns etc.) sector (Dahiya, Kamath et al., 2004a; Das & Pourdeyhimi, 2014, p. 96). With recent growth rates of 5.7% p.a., hydroentangled nonwovens showed the highest increase rates compared to other nonwoven products demonstrating the importance of this technology (EDANA, 2014). This can be explained by a plurality of advantages, such as process versatility and also production speed. However, increasing energy costs and the necessity of a complex filtration system describe known downsides of the technology (Batra & Pourdeyhimi, 2012a, p. 121).

Hydroentangling can also be used to bond and simultaneously split bicomponent fibers nonwoven webs. Bicomponent fibers (e.g. segmented pie, segmented ribbon, tipped trilobal) made from incompatible polymers can be separated by the force of water jets (Hagewood, n. d.). Evolon[®] from Freudenberg is well-known example made from a split 16-segmented pie poly (ethylene terephthalate)/poly (amide-6) nonwoven structure (Das & Pourdeyhimi, 2014, p. 95). Another application of hydroentangling is to pattern structures, which depends on the conveyor belt and also water jet intensity during the process (Dahiya, Kamath et al., 2004a; Ndaro, Xiangyu et al., 2007) Hydroentangling can also be combined with other bonding techniques, such as thermal or chemical bonding to either increase the degree of bonding or reduce the energy during hydroentangling (Xiang, 2007, p. 91).

2.2.1 Historical Development of the Hydroentangling Technology

The hydroentangling process, as we understand it today, was first mentioned in 1961 when Joseph A. Guerin submitted a patent describing a method to hydraulically form fiber mats (Batra & Pourdeyhimi, 2012a, p. 113; Tanchis, 2008, p. 127). According to Hutten (Hutten, 2007, p. 73), both the hydroentangling process and products were first developed and patented by DuPont in the 1960s and 1970s. The initial idea of hydroentangling was to use water jets to strengthen Corfam, a needle-punched poromeric synthetic leather replacement, and to avoid needle-breaking during bonding. DuPont realized the process's enormous potential and named it hydraulic needling (Kanigel, 2011; Mansfield, 2004; White, 1990b). Sontara[®], DuPont's first product line of hydroentangled fabrics (notably wipes), was introduced in the early 1970s (Hutten, 2007, p. 73; Russell, 2006, p. 256; White, 1990b). Chicopee, a former division of Johnson & Johnson and today part of PGI, but also Kendall contributed remarkable inventions during this time. Chicopee's work can even be traced back to the mid-1950s but was more concentrated on rearranging fibers by using water pressures as low as 100 psi. The company's efforts were concentrated on Keybak[®], a process used to imprint nonwovens with water jets coming out of perforated drums. Both Chicopee and DuPont are mentioned to be the original inventors of hydroentangling as both companies used unbonded webs for hydroentangling (Batra & Pourdeyhimi, 2012a, pp. 113-114; Hutten, 2007, p. 73; White, 1990b). According to White (White, 1990b), numerous patents filed by DuPont from 1963 on built the foundation of the commercial entry in the early 1970s. White further refers to five key patents (US3485706, US3486168, US3493462, US3494821 and US3508308), which were filed by DuPont in 1976. Asahi Chemical

Company, a Japanese company, used water jets to entangle fibers made from splittable bicomponent fibers for the production of synthetic suede leather. Uni-Charm Corporation looked at the possibilities of using the energy reflected by impervious conveyor belts for fiber entanglement (White, 1990a). Many hydroentangling lines, especially for consumer goods, such as wipes, were brought to market in the 1990s and early 2000s. From this time, equipment was further developed allowing the operation to be more efficient and profitable (Russell, 2006, p. 256).

2.2.2 Hydroentangling Process, Components and Parameters

It was previously discussed that hydroentangling can be classified as an energy transfer process using high-velocity water jets to interlock and entangle fibers of a fibrous web. The complexity of the process, uniqueness and also diversity can be explained by the various manipulable parameters offering the freedom for new innovations and alternative applications (White, 1990b). White (White, 1990b) classified the process chain in hydroentangling into five categories: 1) the web-forming process, 2) the web support system, 3) the entanglement system, 4) the water circulation system and 5) the drying system. Materials used for hydroentangling are, among many others, air-laid, wet-laid, carded, spunbond or meltblown webs (Anantharamaiah, 2006, p. 4; Dahiya, Kamath et al., 2004a). With production speeds between 300 and 500 m min⁻¹ hydroentangling is significantly faster than other bonding techniques used in the nonwoven industry (Anantharamaiah, 2006, p. 4; Groz-Beckert KG, 2011). Maximum production speed is limited by both the capacity of the machine and also the energy necessary to sufficiently entangle the structure for its later

application. As a comparison, state-of-the-art needle-punching looms allow production speeds of up to 150 m min^{-1} (N. Sun, 2014, p. 2). Width of commercial hydroentangling units can vary between 4.5 to 5.5 meters allowing very high productivity. Bartles (Bartels, 2011, p. 112) mentioned the width of hydroentangling units used for wipe production to be 3.6 to 4.5 meters and 1.8 to 2.6 meters for cotton wipes or pads.

The jet velocity or stored kinetic energy within the water jets is a function of the applied water pressure. Pressures of up to 300 bar are often used in industry, whereas systems using pressures as high as 1000 bar are mentioned in literature. However, such high pressures are rarely used (Pourdeyhimi, 2005; Pourdeyhimi, Suragani Venu et al., 2013; Russell, 2006, p. 278). As discussed, hydroentangling is a very cost intensive process not only because of energy consumption but also filtration and maintenance. For instance, water consumption for wipes is mentioned to be as high as $100 \text{ m}^3 \text{ h}^{-1}$, whereas 96% of water can be reclaimed without and 99% with backwashing (Bartels, 2011, p. 112). Figure 2- 7 depicts a schematic of a five manifold hydroentangling setup with subsequent drying and winding.

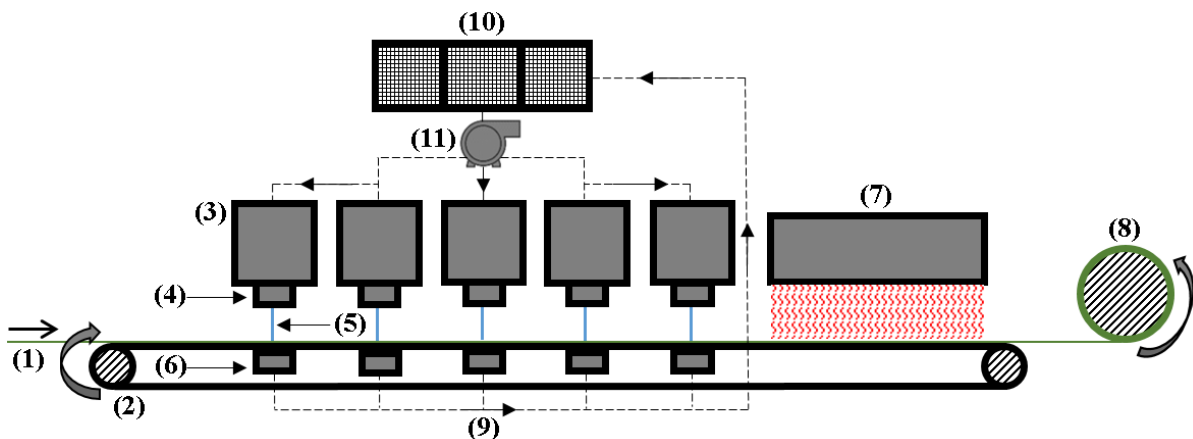


Figure 2- 7: Schematic of a five manifold hydroentangling unit

In the first stage (Figure 2- 7, No.1) material is either fed in-line from another process (e.g. spun-lay, carding or cross-lapping, air- or wet-lay etc.) or a pre-manufactured structure. Lying flat on a permeable, endless forming belt (Figure 2- 7, No.2) (synonyms are conveyor, support or transfer belt) or a perforated drum, material is exposed to stages of preparation, bonding and drying. The belt's main function is to carry the fabric through the process but beside that it also influences the water suction underneath, the energy transfer from the jet to the fabric as well as the final winding. Specific patterns allow influencing the material's appearance and haptic (Dahiya, Kamath et al., 2004a). The porous belt but also an adequate suction are important to prevent water accumulation on the surface of the material as this would drastically reduce the effectiveness of water jets. Instead of reorienting fibers kinetic energy would be used and lost for splashing accumulated water.

The heart of the process are manifolds (Figure 2- 7, No.3 and Figure 2- 8), i.e. injectors or jet heads equipped with so-called jet strips, which are thin plates made from wear-resistant metal materials with a quantity of holes (~40-50 per inch) (Figure 2- 7, No.4, Figure 2- 9 and Figure 2- 10). Batra et al. (Batra & Pourdeyhimi, 2012a, p. 120) describe the manifold as an engineered pressure vessel of highest precision withstanding very high forces during operation. It has the purpose to hold the jet strip but also to evenly distribute the water along its width (Fleissner GmbH, 2008). In hydroentangling the first manifold is usually used for pre-wetting the structure at relatively low jet pressures. One purpose of that is to remove air pockets sitting inside the web (Vuillaume, 1991, p. 151).

Jet strips (or nozzle strips) describe another important part of a hydroentangling unit as their design and also condition strongly influence the process but also the properties of the

bonded structure. Jet strips are high-precision elements built with tightest tolerances allowing them to generate constricted water jets with laminar flow. To support laminar flow and reduce the risk of imperfect jets most hydroentangling units are equipped with pulsation dampeners to minimize vibrations.

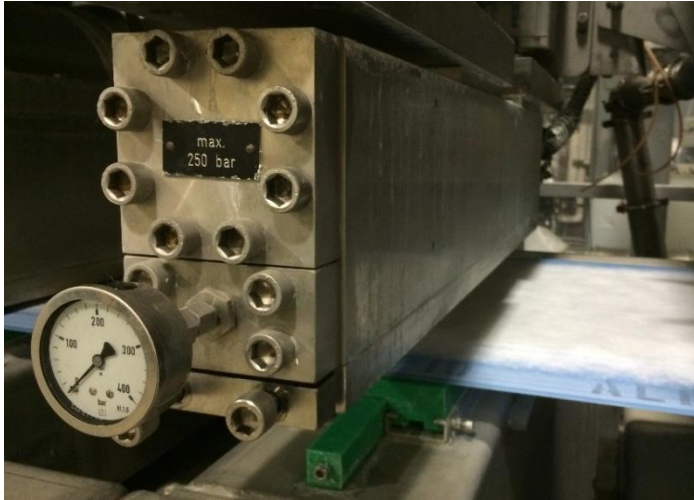


Figure 2- 8: Manifold and passing 0.5 meter web viewed from the side (NWI pilot facilities, North Carolina State University)

Figure 2- 9 and Figure 2- 10 depict a top- and cross-view schematic of a conventional single-row jet strip. A crucial characteristic of jet strips is the jet spacing (nozzle-to-nozzle or orifice-to-orifice spacing), which defines the distance between the holes from which water, i.e. the water jets, leaves the component. This spacing can vary from 600 μm to several millimeters influencing the final properties of the hydroentangled fabric (Suragani Venu, 2012). The nozzle diameter (Figure 2- 9, b) (or capillary or inlet diameter) defines the opening at the upper part of the cone. According to Anantharamaiah et al. (Anantharamaiah, Tafreshi et al., 2007), the nozzle diameter of hydroentangling jet strips is usually in the range

of 80-140 μm (typical industrial standard is 128 μm), whereas even smaller or larger versions are available. Width of jet strips (Figure 2- 9, c) is usually about 25 mm (e.g. Groz-Beckert HyTec[®] 25.4 mm). The length of the jet strip (Figure 2- 9, d) is predetermined by the width of the unit (Groz-Beckert KG, 2012). Commercial hydroentangling units are mentioned to have widths of up to 5.5 meters (Bartels, 2011, p. 112; Das & Pourdeyhimi, 2014, p. 101). Anantharamaiah (Anantharamaiah, 2006, pp. 20-21) mentioned the outlet diameter of the cone (Figure 2- 10, e) to be 0.34 mm, whereas the cylindrical region (or capillary region) (Figure 2- 10, f) usually has the same size as the nozzle diameter (aspect ratio, AR: 1). Angle between capillary and cone region (Figure 2- 9, g) is mentioned to be about 15° , whereas other sources mentioned it to be about 18 degrees (Tafreshi & Pourdeyhimi, 2004). Batra et al. (Batra & Pourdeyhimi, 2012a, p. 120) stated the thickness (Figure 2- 10, g) of conventional jet strips to be between 0.6 to 1 mm. Distance between nozzle outlet and web is reported to be typically less than 5 cm (Anantharamaiah, 2006, p. 162).

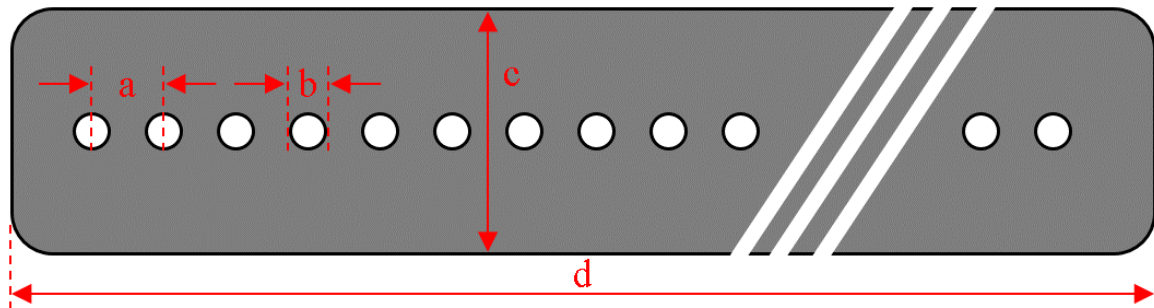


Figure 2- 9: Schematic of a single-row jet strip (plane view)

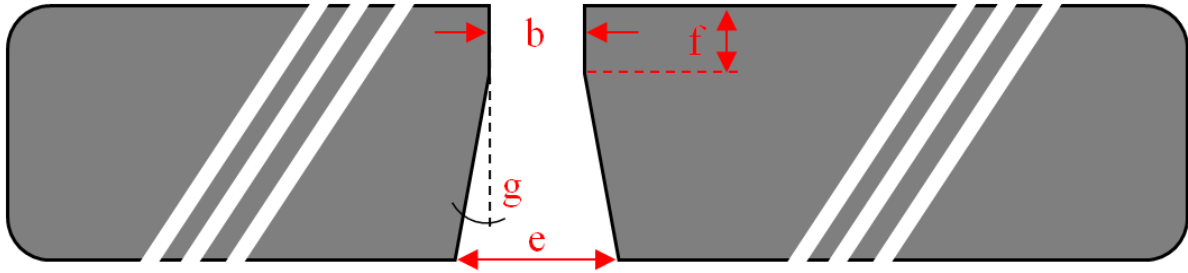


Figure 2- 10: Schematic of the cross-section of a jet-strip in cone-down position (sectional view)

After leaving the orifices collimated water jets (Figure 2- 7, No.5) can have speeds of more than 200 m s^{-1} (200 m s^{-1} jet velocity corresponds to a water pressure of about 200 bar). In order to make use of that tremendous amount of kinetic energy jets need to be in columnar shape. Early break-up of jets is a critical factor and a common problem often addressed in research papers. As soon as a jet breaks up the water is dispersed in many small droplets (spraying) followed by a massive loss of kinetic energy and thus bonding intensity (Begenir, Tafreshi et al., 2004; Tafreshi & Pourdeyhimi, 2004).

Cavitation is a phenomenon known to be crucial for the formation of constricted jets with reduced break-up lengths. It describes the formation of vapor bubbles in a liquid initiated when the local pressure is lower than the vapor pressure of the liquid. After entering the sharp-edged nozzles pressurized water detaches from the nozzle wall causing the formation of a hollow space between water and nozzle wall, which is immediately filled with liquid or air. Jet detachment requires the horizontal momentum of the flow to be high enough. In case that the pressure in that region is lower than the vapor pressure of the liquid cavitation can occur and formed vapor bubbles move from the nozzle inlet towards the exit. Intense cavitation builds an air pocket big enough to reach the nozzle exit, which causes the

region to be filled with air and the jet to be separated from the capillary wall and to be transformed into a constricted shape. This phenomenon is called hydraulic flip. Continuous cavitation without hydraulic flip is mentioned to increase material wear and erosion and to reduce the break-up length of the jet (Anantharamaiah, 2006, pp. 24, 56-62, 90, 104-105; Dabiri, Sirignano et al., 2007; Tafreshi & Pourdeyhimi, 2004).

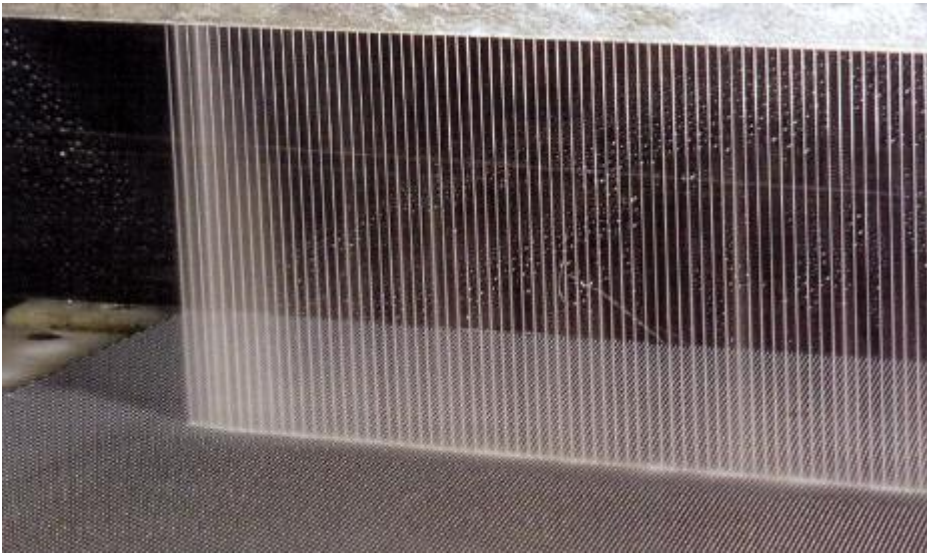


Figure 2- 11: Photography of Water-Jets (Mogul Tekstil Sanayi ve Ticaret Ltd.Sti., n.d.)

After being removed by a vacuum (Figure 2- 7, No.6), piped back (Figure 2- 7, No.9) and cleaned by a series of filters (Figure 2- 7, No.10) majority of process water can be recovered. Afterwards, water is pumped (Figure 2- 7, No.11) back to the system. The filtration system used to recycle the process water is mentioned to be one of the major cost drivers in hydroentangling. Russell (Russell, 2006) noted the water quality to be a critical factor greatly influencing the efficiency of the process. To achieve the required purity, water undergoes a

series of filtration steps (sand filters, bag filters) before being pumped back to the system (Figure 2- 7, No.11). Even before reentering the manifolds another filter is used to remove coarse particles and prevent the nozzles from being clogged. After bonding fabric is carried through a drying zone (Figure 2- 7, No.7) and winded up as roll good (Figure 2- 7, No.8).

2.2.3 Process-Structure-Property Relationship in Hydroentangling

Before hitting the web and reorienting fibers high-velocity water jets are in columnar shape and most often perpendicular aligned to the structure (Dahiya, Kamath et al., 2004a). When the water jets impinge the structure but also short time thereafter, nonwoven web undergoes phases of structure change, deformation and consolidation. Patanaik et al. (Patanaik & Anandjiwala, 2010) introduced a representation of the ongoing mechanisms, which is depicted in Figure 2- 12. In the first stage nonwoven webs are condensed, whereas fibers in machine direction (MD) shift and fibers in cross direction (CD) bend. Patanaik also distinguished between jet forces acting parallel or perpendicular to the fiber axis. Whereas parallel forces were stated to support the folding and wrapping around neighboring fibers, forces acting perpendicular to the fiber axis initiate fiber bending.

In another work Mao et al. (Mao & Russel, 2005) investigated the structural changes during hydroentangling and reported three different stages (Figure 2- 13). First stage is the compression of the web in response to the impinging jet followed by the actual fiber entanglement and a phase of recovery. Möschler and his co-workers (Möschler, Meyer et al., 1995, pp. 26-28) reported on the changes within the structure during the bonding process and sub-divided them into four different categories. First the parallelization and longitudinal

reorientation of fibers about 2 cm before the impact point of the jet, second the crescent-shaped backward movement of fibers, third the deflection in horizontal direction and web compression and fourth a potential decline of compression.

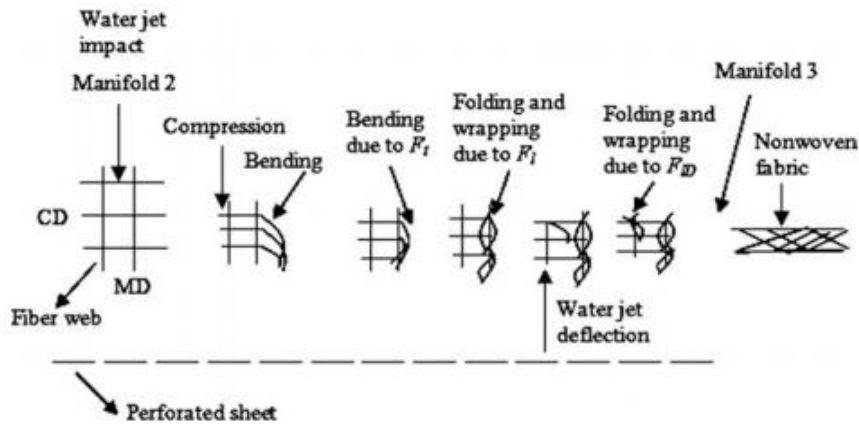


Figure 2- 12: Mechanisms during hydroentangling (Patanaik & Anandjiwala, 2010)

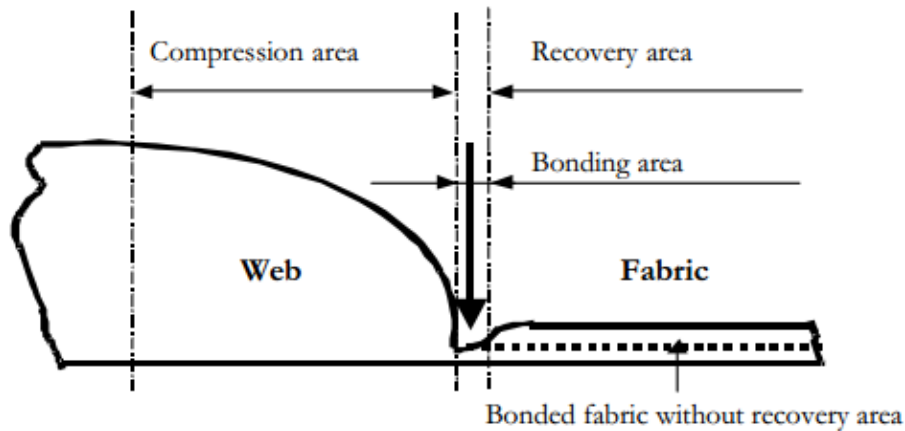


Figure 2- 13: Mechanisms during hydroentangling (Mao & Russel, 2005)

According to Albrecht et al. (Albrecht, Fuchs et al., 2006, p. 327), factors influencing the transfer of kinetic energy to the web and therefore the properties of hydroentangled nonwovens can be divided into three categories: 1) fiber properties, 2) water jet characteristics and 3) process-related parameters, such as production speed, striking angle of jets, conveyor belt etc.. This list could be further extended by the web properties itself, e.g. fiber mobility within the material, basis weight, packing density and many others. Parameters affecting the ability to bond a web could also be categorized as fiber-related influences, such as polymer, fiber geometry or fiber additives, wettability etc., process-related influences, such as web structure, process speed and the properties of the jet (Möschler, Meyer et al., 1995, p. 26). The fact that all parameters are not acting independently further complicates the process. Efforts to investigate the influence of these factors helped building a fundamental understanding of the hydroentangling process but also to make it more efficient (Ghassemieh, Acar et al., 2001).

The following discusses factors influencing the transfer of kinetic energy to the web as well as how the properties of hydroentangled materials are affected by that.

Influence of Nonwoven Web

Nonwoven materials before being bonded are designated as web structures and the simplest way to categorize them is to differentiate between a staple fiber or filament based material or a mixture thereof. Over the past decades scientists investigated how the web properties influence the transfer of specific energy, affect the fiber entanglement and reorientation and the properties of the final material. These impact factors can be, among others, fiber size,

fiber length, fiber cross-section, fiber crimp, fiber bending or flexural rigidity, fiber surface, fiber wettability, solid volume fraction, fiber orientation (ODF: orientation distribution function), basis weight and fiber mobility (Dahiya, Kamath et al., 2004a; Mao & Russel, 2005).

According to Kamath et al. (Dahiya, Kamath et al., 2004a), fibers with larger diameters of the same polymer type are harder to entangle as their fiber bending rigidity is higher. This is in agreement with Mao et al. (Mao & Russell, 2006), who reported the intensity of hydroentangling to be a function of the fiber bending rigidity. The equation to calculate fiber bending rigidity (or fiber flexural rigidity, fiber stiffness) is given in the following.

$$F_{fiber} = 1\eta ET^2(4\pi\rho)^{-1} \quad \text{Eq. 2-1}$$

where η is the shape factor, E is the specific bending modulus (in Nm Kg^{-1}), T is the fiber linear density (in Kg m^{-1}) and ρ is the fiber density (in Kg m^{-3}) (Fan & Hunter, 2009, p. 108). The maximum fiber size suitable for hydroentangling is mentioned to be 4 to 6 dtex. Fibers larger than that are restricted due to their stiffness and relatively low surface area (Albrecht, Fuchs et al., 2006, p. 335). According to literature, fibers with low bending rigidities can be deformed easier facilitating the formation of loops or curved shapes and higher manifold pressures increase the number of loops within the material (Mao & Russel, 2005). Möschler and his co-workers (Möschler, Meyer et al., 1995, p. 28) demonstrated the fiber entanglement to be a function of fiber size but also water pressure. Hydroentangling webs with coarser fibers but same manifold pressure, fiber length etc. resulted in lower mechanical properties.

Comparable breaking strengths for structures with coarser fibers were achieved by increasing the jet pressure.

In contrast to that, hydroentangling is less influenced by fiber length. Both, relatively short fibers (e.g. carded-airlaid wood pulp for wipes, which usually in the range of 1 to 3 mm) but also filaments can be hydroentangled (Albrecht, Fuchs et al., 2006, p. 335; Bouchette, 2000; Das & Pourdeyhimi, 2014, p. 104). Limits exist as very short fibers could be released from the structure and pass through the porous belt. Due to restricted immobility, long fibers could be pushed aside or even cut resulting in inadequate bonding (Gahide, 1999). Kamath et al. (Dahiya, Kamath et al., 2004a) mentioned shorter fibers to have a higher mobility and ability to produce more anchor points.

The influence of fiber cross-section in hydroentangling depends on multiple factors. Russell (Russell, 2006, p. 265) commented triangular-shaped fibers to require more energy to be hydroentangled than round fibers. In contrast to that, flat and elliptical fibers can be hydroentangled more efficiently. Same can be read from Kamath et al. (Dahiya, Kamath et al., 2004a), who attributed this to the higher bending rigidity of triangular-shaped fibers (~1.4 times higher). Gordon et al. (Gordon & Hsieh, 2006) argued non-round fiber cross-sections to cause additional friction and thus to be favorable for hydroentangling.

Crimp, which can be defined as the waviness of a fiber, is known to be an essential property of staple fibers intended to be carded (Gupta, 2008, p. 301; Rosato, Rosato et al., 2000, p. 272). In hydroentangling crimp is not necessarily required, whereby too much crimp can actually lower degree of entanglement (Dahiya, Kamath et al., 2004a). In another work researchers investigated the effect of three different crimp densities on the mechanical

properties of hydroentangled webs. According to the work, effect of crimp is more important for lower manifold pressures, whereas high hydroentangling pressures led to comparable mechanical properties (Möschler, Meyer et al., 1995). Fibers without crimp and too much stiffness (e.g. glass fibers) can be mixed with other fibers (e.g. PET) before being hydroentangled (Vaidya, 2002).

Another important aspect in hydroentangling is the wettability of fibers as the process requires uniform and rapid wetting (Russell, 2006, p. 265). Due to the fact that most nonwoven structures are made from synthetic and therefore relatively hydrophobic materials, wetting can be challenging. Hong et al. (Hong, Lianshun et al., 2010) investigated the effect of wetting agents on the hydroentangling process. It was reported that enhancing the wettability of poly (ethylene terephthalate) fibers resulted in a higher degree of entanglement and remarkably better mechanical properties. Kamath (Dahiya, Kamath et al., 2004a) mentioned hydrophilic fibers to show a higher degree of entanglement because of higher drag forces. In contrast to that, application of hydrophobic fibers, such as poly (propylene), can increase the risk of water accumulation and ineffective bonding. Thus, rapid water removal and therefore sufficient suction is required for proper operation.

To date it seems nothing to be published about the influence of packing density of a web prior hydroentangling. Prior discussion noted nonwoven webs to be compressed by the force of jets. Möschler et al. (Möschler, Meyer et al., 1995) mentioned the web to be compressed 10 to 20 times of its initial thickness and that a portion of energy is used for that. Thus, it can be assumed that rate of initial compression is different for dense and open structures. Suragani (Suragani Venu, 2012, pp. 143-144) reported better fiber penetration for

pre-wetted structures (up to 40%) and assumed fiber softening and consequential decrease in bending rigidity to be responsible for that. This could be related to the mentioned compression phenomena as pre-wetted and therefore “pre-compressed” structures require less energy to reach maximum compression and more energy can be used for the actual fiber transport.

Another factor greatly influencing hydroentangling is the basis weight of the web. According to Mao et al. (Mao & Russel, 2005), Ijaiya and Qiao demonstrated that most fiber bending and reorientation to take place at the surface or in the upper layer of the structure. Fibers in lower regions were not uniformly distributed and the operating pressure was reported to play a crucial role to reach them. Suragani (Suragani Venu, 2012, p. 189) reported the fiber penetration to not only depend on the hydroentangling pressure but also on the jet spacing (topic is addressed later on).

Influence of Jet Strip Design

A number of studies investigated the impact of jet strip design on water jet formation as well and the jets' ability to receive, store and deliver energy to the fibrous web. These studies examined the influence of nozzle diameter and shape, jet spacing but also the effect of flipped or worn jet strips. Jet spacing in hydroentangling was mentioned to be in the range between 600 to 4800 μm (~40 to 5 holes per inch) and one characteristic defining the specific energy during the process (Pourdeyhimi, Suragani Venu et al., 2013).

Batra et al. (Batra & Pourdeyhimi, 2012a, p. 126) defines the specific energy as the energy applied per unit mass of material. In fluid dynamics Bernoulli equation can be used to

calculate the jet velocity assuming the flow to be incompressible, inviscid and steady (Madihally, 2010, p. 133). Corresponding equation is given in the following.

$$P_1 + 0.5\rho v_1^2 = P_2 + 0.5\rho v_2^2 \quad \text{Eq. 2- 2}$$

where P_1 is the pressure at the nozzle inlet [Pa], P_2 at the nozzle outlet [Pa], ρ the specific gravity of the fluid [$\rho_{water} = 998.2 \text{ Kg m}^{-3}$ at room temperature], v_1 the speed at the nozzle inlet [m s^{-1}] and v_2 the speed at the nozzle outlet [m s^{-1}]. Thus, jet velocity v can be obtained as follows.

$$v = \sqrt{\frac{2P}{\rho}} \text{ [m s}^{-1}\text{]} \quad \text{Eq. 2- 3}$$

where P is the water pressure within the manifold [Pa] and ρ the specific gravity of water [998.2 Kg m^{-3} at room temperature]. The energy of a single water jet \dot{E} can be estimated by using the following equation.

$$\dot{E} = \frac{\pi}{8} \rho d_n^2 C_d v^3 \text{ [J s}^{-1}\text{]} \quad \text{Eq. 2- 4}$$

where ρ is the specific density of the fluid [Kg m^{-3}], d_n the nozzle diameter [m], C_d the discharge coefficient and v the jet velocity [m s^{-1}].

Total energy of all jets can be calculated by multiplying the single jet energy \dot{E} with the number of jets having the same manifold pressure. Specific energy SE can be obtained by using the following equation.

$$SE = \frac{\dot{E}_{Total}}{\dot{M}_{fabric}} \text{ [KJ Kg}^{-1}\text{]} \quad \text{Eq. 2- 5}$$

where \dot{M}_{fabric} is the mass flow rate of fabric [Kg s^{-1}], which is determined by the following term.

$$\dot{M}_{fabric} = s \times w \times v_B \text{ [Kg s}^{-1}\text{]} \quad \text{Eq. 2- 6}$$

where s is the fabric width [m], w is the basis weight of the material [g m^{-2}] and v_B is the operating speed [m s^{-1}] (Pourdeyhimi, Minton et al., 2004).

As can be seen from the equations specific energy is also a function of the jet density (number of jets operating during the process). Suragani (Suragani Venu, 2012) investigated the influence of jet spacing and manifold pressure on carded, 2-layered cross-lapped webs (upper layer: blue-dyed 40 g m^{-2} nylon material, backing layer: 160 g m^{-2} polyester material). Study revealed jet spacing to play an important role during hydroentangling leading to completely different structures. Whereas webs hydroentangled with narrow jet spacing resulted in flat and relatively stiff structures, bulky, knot-like structures were obtained by using low jet densities (see Figure 2- 14 to Figure 2- 17).

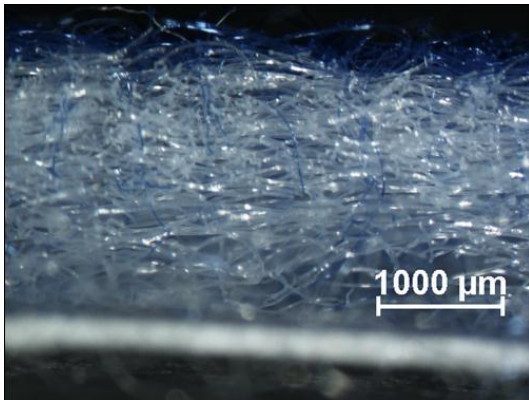


Figure 2- 14: 2-layered structure hydroentangled with 100 bar and $600 \mu\text{m}$ jet spacing (Suragani Venu, 2012, p. 187)

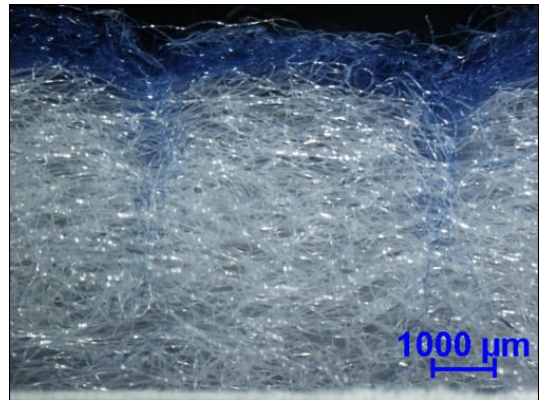


Figure 2- 15: 2-layered structure hydroentangled with 100 bar and $4800 \mu\text{m}$ jet spacing (Suragani Venu, 2012, p. 187)

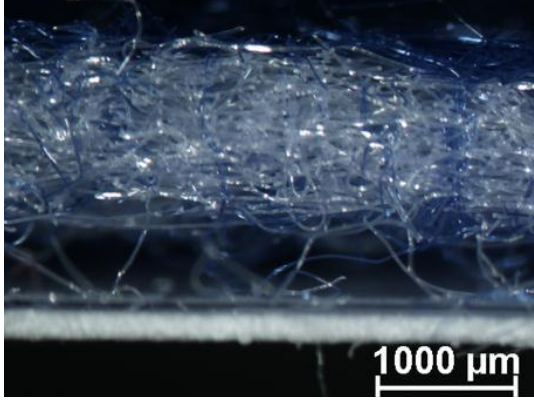


Figure 2- 16: 2-layered structure hydroentangled with 200 bar and 600 μm jet spacing (Suragani Venu, 2012, p. 188)

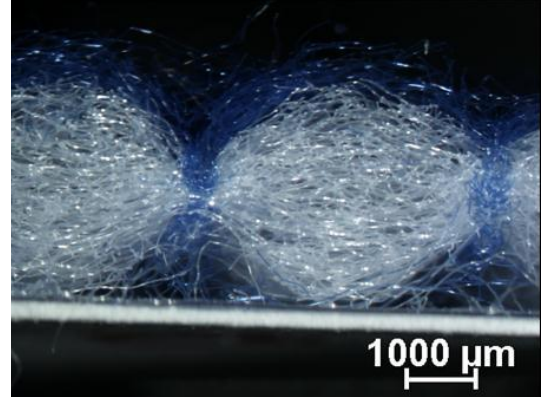


Figure 2- 17: 2-layered structure hydroentangled with 200 bar and 4800 μm jet spacing (Suragani Venu, 2012, p. 188)

It was shown that hydroentangling with high jet densities and moderate manifold pressures did not result in deep fiber penetration as reorienting fibers interacted with adjacent fibers, which are also in a phase of movement and prevented them to penetrate into the material. In contrast to that, low jet densities showed deeper fiber penetration as distance between jets is larger and adjacent fibers no longer prevent others to penetrate into the structure. Materials hydroentangled with large jet spacing showed higher air permeabilities and absorbencies but lower mechanical properties compared to structures hydroentangled with higher jet densities. Increasing the manifold pressures resulted in comparable fiber penetration, whereas the influence of jet spacing was still measurable (Suragani Venu, 2012).

In another experiment Suragani (Suragani Venu, 2012) used a combination of narrow and large jet spacing. Control sample was bonded with two manifolds at 600 μm jet spacing, whereas the second material with 600 μm for the first and 4800 μm for the second manifold. Surprisingly second material turned out to have better mechanical properties even though less energy was used during bonding. Combination of deep fiber penetration (because of large jet

spacing) and fiber interlocking on the surface (because of narrow jet spacing) led to this kind of structure.

According to Hwang (Hwang, 1985), hydroentangling with low jet densities results in structures with relatively poor mechanical properties compared to structures hydroentangled with more jets.

In another work Kirayoglu et al. (Kirayoglu & Zafiroglu, 1984) claimed the hydrostatic head of hydroentangled nonwovens to be a function of jet density. Using lower jet densities resulted in structures having better liquid barrier properties. This could be related to the higher degree of surface entanglement obtained with higher jet densities.

Jet strips with multiple rows of orifices describe another practice in hydroentangling (Groz-Beckert KG, n.d.). Anantharamaiah et al. (Anantharamaiah, 2006, p. 185; Anantharamaiah, Römpert et al., 2007; Pourdeyhimi & Tafreshi, 2007b) reported on a two row design with different nozzle diameters to minimize jet defects and therefore low tear behavior in machine direction (MD). The setup comprised of a jet strip with 130 μm nozzles in the first and 110 μm nozzles in the second row.

Jet strips with more than one row of nozzles can also be used to enhance the specific energy used during the process and to apply more force on the material. Contractor et al. (Contractor & Kirayoglu, 1978) claimed a process using multiple nozzle rows to enhance the tensile strength of nonwoven materials. In this particular example distance between the rows was mentioned to be 10 to 80 mils.

The nozzle diameters of jet strips, which is usually in the range of 80-140 μm , not only influences the size of the water jet and the final properties of the fibrous structure but

also the specific energy during hydroentangling (Anantharamaiah, Tafreshi et al., 2007). Several patents mention different nozzle diameters to have advantages in terms of the properties of hydroentangled nonwovens (Greenway, Schortmann et al., 1990; Pourdeyhimi & Tafreshi, 2007b; Takai & Konishi, 2004).

Suragani (Suragani Venu, 2012, pp. 142-147) investigated the fiber penetration, web compression but also penetration area as a function of nozzle size. According to the study, larger nozzle diameters result in larger penetration areas but also a higher degree of fiber penetration. Nozzle diameters larger than 300 μm showed little or no change in terms of fiber penetration even for different manifold pressures (100 and 200 bar). Compared to 128 μm , nozzle diameters of 300 μm resulted in fiber penetrations about 40% higher. Web compression with nozzle sizes of 300 μm or even larger was found to be 60%, whereas conventional 128 μm nozzles led to a web compression of less than 10%. Fiber penetration of multiple jets was found to be a function of nozzle diameter and manifold pressure. Interestingly fiber penetration of structures impinged with 100 bar indicated less dependency on the actual nozzle diameters, whereas hydroentangling with 200 bar resulted in more fiber penetration and showed a higher dependency on the nozzle diameter. Hydroentangling with 100 or 200 bar and a nozzle diameter of 32 μm showed no fiber penetration, whereas 130 μm nozzles at 200 bar resulted in a fiber penetration of almost 100%.

Tausif et al. (Tausif & Russell, 2012) reported hydroentangling with relatively low production speeds of 5 m min^{-1} and nozzle diameters of 90 and 140 μm to have no significant influence on the tensile strength in machine direction. The opposite was found for faster production speeds of 15 m min^{-1} .

The shape of the nozzle plays another crucial role in hydroentangling dictating the properties of jet and structure. Cone-capillary-shaped nozzles are typically used in hydroentangling and are characterized by a cylindrical region connected to cone-shaped area. Depending on the application, these jet strips can be flipped to have the cone up- or downwards. Later dramatically changes the water flow as cone-up nozzles do not undergo hydraulic flip (Anantharamaiah, 2006, p. 88). Figure 2- 18 depicts different nozzles designs whose impact on the water jets and structure is discussed in the following.

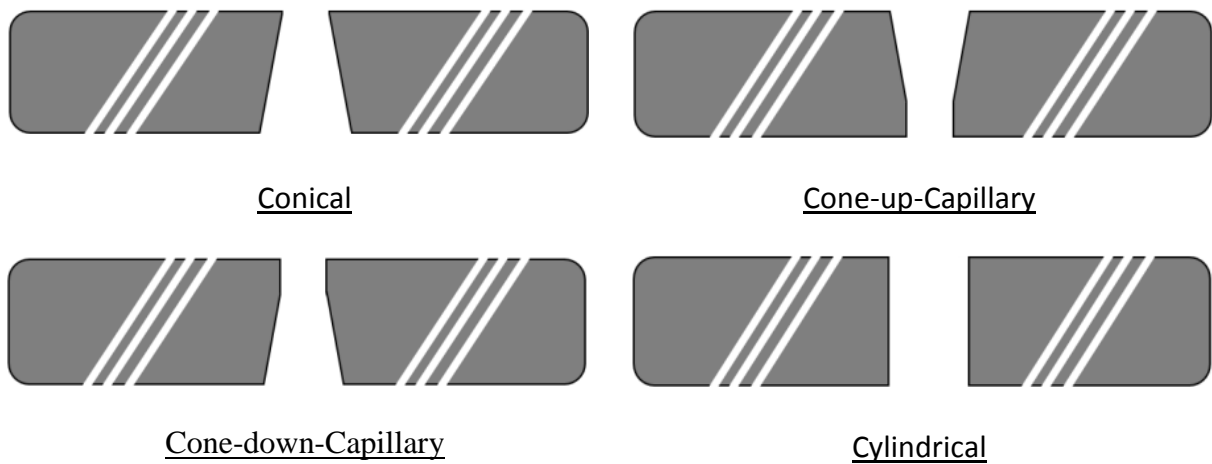


Figure 2- 18: Nozzle designs in hydroentangling

There exist many different patents about systems using nozzles to create high velocity water jets (Fleissner, 2000; Norman, 1973; Wands & Scott, 1998). Industrial hydroentangling nozzles typically consist of a sharp-edged entrance significantly affecting the water flow inside the orifice (Nagendra Anantharamaiah, Hooman Vahedi Tafreshi et al., 2006; Pourdeyhimi & Tafreshi, 2007a; Tafreshi & Pourdeyhimi, 2004). Cone-capillary nozzles are most often used in industry as they are easier to manufacture (Anantharamaiah, Tafreshi et

al., 2007). Nozzles are usually punched or drilled into the jet strip (Russell, 2006, p. 281). Even though conical nozzles are not causing cavitation, sharp-edges of this type of nozzle are known to last considerably shorter (Anantharamaiah, 2006, pp. 60, 104). According to Dixon et al. (Dixon, Lowder et al., 2005), cavitation free nozzles can be produced by having an impeccable inlet roundness at the entrance of the nozzle. It is further mentioned that the accurate production of this kind of nozzle is very challenging and the manufacturing of cone-capillary nozzles to be easier. Even though nozzles with perfect inlet roundness are preventing the jet to detach from the nozzle wall, they cause friction-induced turbulences (as water is always attached to the nozzle wall) or even unexpected cavitation. Nozzles, which are neither round nor sharp (intermediate) can cause cavitation but no hydraulic flip (Anantharamaiah, 2006, pp. 89, 106).

It was mentioned that a combination of high horizontal jet momentum and sharp edged nozzles can cause the water to separate from the inner wall. Whether the water jet can or cannot follow the sharp inlet of a nozzle depends on the water pressure and therefore the jet velocity and Reynolds number (Anantharamaiah, 2006, p. 62). According to Begenir et al. (Begenir, Tafreshi et al., 2004), Reynolds number Re is a function of nozzle size and jet velocity and can be calculated as follows.

$$Re = \frac{\rho v L}{\mu} \quad \text{Eq. 2- 7}$$

where ρ the specific gravity of the fluid [998.2 Kg m⁻³ for water at room temperature], v the velocity [m s⁻¹], L the characteristic length [m] and μ the dynamic viscosity of the fluid [1.002 mPa s⁻¹ for water at room temperature].

As previously discussed, Bernoulli equation can be used to predict jet velocity v and inserting Eq. 2- 3 in Eq. 2- 7 and defining the nozzle diameter d_n as the characteristic length L gives the following.

$$Re = \frac{d_n \sqrt{2\rho\Delta P}}{\mu} \quad \text{Eq. 2- 8}$$

where d_n is the nozzle diameter [m], ρ the specific gravity of the fluid [998.2 Kg m⁻³ for water at room temperature], ΔP the pressure difference [Pa] and μ the dynamic viscosity of the fluid [1.002 MPa s⁻¹ for water at room temperature].

Anantharamaiah (Anantharamaiah, 2006, pp. 61-64) investigated the influence of Reynolds number on the detach and attachment behavior inside hydroentangling nozzles.

It was observed that jets with Reynold numbers lower than 3,150 did not detach from the nozzle wall and jets with Reynold numbers in the range of 3,150 to 10,000 first detached before reattaching at the capillary region of the nozzle. For Reynolds numbers higher than 10,000 reattachment length was not changing. An aspect ratio (l/d ratio) <0.7 was mentioned to be suitable to prevent reattachment at high Reynold numbers (Figure 2- 19).

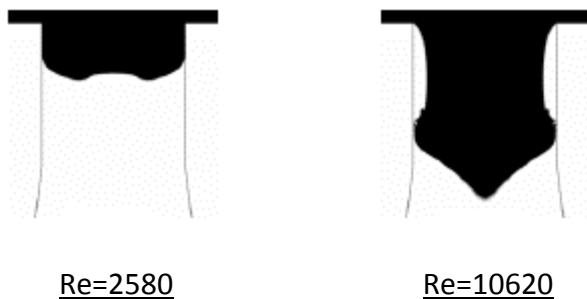


Figure 2- 19: Water Flow inside a Cone-Capillary Nozzle at different Re (Anantharamaiah, 2006, p. 61)

Begenir (Begenir, 2003, p. 23) reported the break-up length in hydroentangling to be a function of the l/d ratio of the nozzle. The higher the l/d ratio and therefore the longer the capillary wall the more likely reattachment occurs. Begenir et al. (Begenir, Tafreshi et al., 2004) also investigated the break-up behavior of cone-up-capillary, cone-down-capillary as well as cylindrical nozzles at different Reynold numbers. According to the paper, both cone-up-capillary and cylindrical nozzles showed shorter break-up lengths compared to cone-down-capillary nozzles. In addition, intact length was mentioned to be a function of the Reynolds number and therefore jet velocity. Whereas intact length at relatively low Reynold numbers was found to be comparable, experiments with high jet velocities demonstrated cone-down-capillary nozzles to be more efficient.

Another research project examined the influence of nozzle diameter and jet velocity of sharp-edged nozzles on the break-up length. Nozzle diameters ranging from 0.1 mm to 3 mm were used for this particular research and showed increasing break-up lengths with increasing nozzle diameters. Furthermore, break-up length was reported to increase with jet velocity before decreasing after reaching a critical jet velocity (Begenir, 2003, pp. 22-23).

Mass flow rate \dot{m} during hydroentangling is another factor affected by the shape of the nozzle. Flow rate of different nozzle shapes with identical inlet diameter is different and thus differ from the ideal value. Ratio of the actual mass flow rate \dot{m}_{actual} to the ideal mass flow rate \dot{m}_{ideal} is defined as the discharge coefficient C_d and can be calculated as follows.

$$C_d = \frac{\dot{m}_{actual}}{\dot{m}_{ideal}} \quad \text{Eq. 2- 9}$$

where \dot{m}_{actual} is the measured mass flow rate [Kg s⁻¹] and \dot{m}_{ideal} is the theoretical mass flow rate [Kg s⁻¹]. The ideal mass flow rate \dot{m}_{ideal} can be estimated as follows.

$$\dot{m}_{ideal} = \rho v A = \rho \dot{V} \quad \text{Eq. 2- 10}$$

where ρ is the specific gravity of the fluid [998.2 Kg m⁻³ for water at room temperature), v the flow velocity [m s⁻¹], A the area [m²] and \dot{V} the volumetric flow rate [m³ s⁻¹] (Baukal, 2001, p. 152; Begenir, Tafreshi et al., 2004). The mentioned is derived from the following equations.

$$C_d = \frac{v_{actual} A_{actual}}{v_{ideal} A_{ideal}} \quad \text{Eq. 2- 11}$$

$$C_v = \frac{v_{actual}}{v_{ideal}} \quad \text{Eq. 2- 12}$$

$$C_c = \frac{A_{actual}}{A_{ideal}} \quad \text{Eq. 2- 13}$$

where v_{actual} is the measured jet velocity [m s⁻¹], v_{ideal} the theoretical jet velocity [m s⁻¹], A_{actual} the cross-sectional area at the vena contracta of the jet [m²] and A_{ideal} the cross-sectional area of the nozzle [m²] (Moyo & Anandjiwala, 2013; Zheng, 2003, pp. 19-20).

Anantharamaiah (Anantharamaiah, 2006, p. 87) investigated the discharge coefficient for cone-up and cone-down positioned cone-capillary nozzles. As expected, cone-down-capillary nozzles delivered lower discharge coefficients because of constricted water jets. Also, there seems only little relation between the discharge coefficient and the water pressure. Discharge coefficient for cone-down-capillary nozzles was reported to be about 0.6 and about 0.9 for cone-up-capillary nozzles.

Begenir et al. also reported the discharge coefficient to be affected by the nozzle design. Furthermore, discharge coefficient did not remarkably change for Reynold numbers between ~6,000 and 30,000. Discharge coefficient of cone-down-capillary and cylindrical nozzles was reported to be around 0.6.

Moyo et al. (Moyo & Anandjiwala, 2013) investigated the coefficient of discharge and also C_v for different manifold pressures (30 to 180 bar). Both C_d and C_v were reported to increase with increasing hydroentangling pressure.

High manifold pressures during hydroentangling cause material wear, which influences the process and therefore the properties of the nonwoven materials (Anantharamaiah, 2006, p. 72; N Anantharamaiah, H Vahedi Tafreshi et al., 2006; NCRC - Nonwovens Cooperative Research Center, 2005, p. 8). Stress-induced corrosion, water-borne particles but also cavitation phenomena are assumed to be responsible for nozzle wear (Anantharamaiah, 2006, p. 96). US patent 7237308 B2 (Dixon, Lowder et al., 2005) claims on composite hydroentangling nozzles made from more wear resistant materials.

Influence of Water Jet Properties

It was discussed that the properties of water jets not only depend on process parameters, e.g. the manifold pressure, but also on the nozzle design. Water jets store and deliver energy and the break-up length is a crucial factor immensely influencing the degree of bonding. Water jets in hydroentangling can have velocities as fast as 280 m s^{-1} making them perfect not only for bonding but also applications, such as fiber splitting, pattern and others (Groz-Beckert KG, 2012). The water jet in hydroentangling is characterized by properties, such as the jet

diameter, jet velocity but also the intact length. Mass flow rate in hydroentangling was mentioned to be different from the theoretical, ideal value. The ratio defining the actual and ideal mass flow rate was discussed to be the discharge coefficient. Following equation allows predicting the jet diameter d_j .

$$d_j = d_n \sqrt{C_d} \text{ [m]} \quad \text{Eq. 2- 14}$$

where d_n the nozzle diameter [m] and C_d the discharge coefficient (Anantharamaiah, 2006, p. 26). Discharge coefficient was discussed to be 0.62 for sharp-edged cone-down-capillary nozzles. Thus, assuming a typical nozzle diameter of 128 μm would result in a jet diameter of about 100 μm .

Impact force f_i (fluid momentum) of the water jet is responsible for reorienting and interlocking fibers of the web and can be calculated by using Newton's second law.

$$f_i = \frac{\pi}{4} \rho v^2 d_j^2 \text{ [Kg m s}^{-2}\text{]} \quad \text{Eq. 2- 15}$$

where ρ is the specific gravity [998.2 Kg m⁻³ for water at room temperature], v the jet velocity [m s⁻¹], d_j the jet diameter [m] and C_d the discharge coefficient (Anantharamaiah, 2006, pp. 18, 134; Patanaik & Anandjiwala, 2010).

According to Patanaik (Patanaik & Anandjiwala, 2010), forces act perpendicular but also parallel to the fiber axis. Whereas transverse drag forces f_t are responsible for bending fibers, longitudinal drag forces f_l are important for wrapping fibers around neighboring fibers. Equations to for calculating transverse drag forces f_t and longitudinal drag forces f_l are given in the following.

$$f_t = 0.5 \rho v^2 A_t C_{drag} \text{ [Kg m s}^{-2}\text{]} \quad \text{Eq. 2- 16}$$

$$f_l = 0.5\rho v^2 A_t C_{drag} \text{ [Kg m s}^{-2}\text{]} \quad \text{Eq. 2- 17}$$

where ρ is the specific gravity [998.2 Kg m⁻³ for water at room temperature], v the jet velocity [m s⁻¹], A_t the area of the fiber on which the fluid acts perpendicular [m²], A_l the area of the fiber on which the fluid acts parallel [m²] and C_{drag} the drag coefficient.

Anantharamaiah (Anantharamaiah, 2006, pp. 21-22) investigated the influence of nozzle diameter on the jet force and reported the force to increase with increasing jet diameter. Furthermore, measured values were reported to be in accordance with the calculated force. Figure 2- 20 shows water jets for different nozzle diameters but constant manifold pressure (1,500 psi).

The specific energy is a common term used in hydroentangling science and can be defined as the energy applied per unit mass of material (Batra & Pourdeyhimi, 2012a, p. 126). According to Mao et al. (Mao & Russel, 2005, p. 60), specific energy during hydroentangling is not only used for fiber entanglement. In fact, portions of specific energy are absorbed by standing water, used and dissipated for web compression, fiber deformation, temporary deformation, fluid drag forces and fiber-fiber friction (Majumdar, Das et al., 2012, pp. 285-286; Mao & Russel, 2005; Russell, 2006, p. 258).

According to Ghassemieh et al. (Ghassemieh, Acar et al., 2001), amount of energy necessary for sufficient bonding is mainly determined by the web and fiber properties. Ghassemieh and his group changed the amount of specific energy by varying the water pressure, the number of passes and the belt speed. Results indicated the tensile strength of fabrics to decrease beyond a critical water pressure $P_{critical}$. Furthermore, $P_{critical}$ was reported to increase with increasing solid volume fractions.

Ndaro et al. (Ndaro, Xiangyu et al., 2007) investigated the impact of manifold pressure (3, 5, 7, 10 bar) and inclination angle (+20° to -20°) on the mechanical properties of island-in-the-sea structures (PA6/PET, PA6/CoPET, PET/Co-PET). It was reported that increasing jet pressures and inclination angles improved the tensile properties. According to the results, low forces resulted in partial fibrillation, whereas PET/Co-PET fibers did not separate (similarities in the molecular structure were assumed to be the reason).

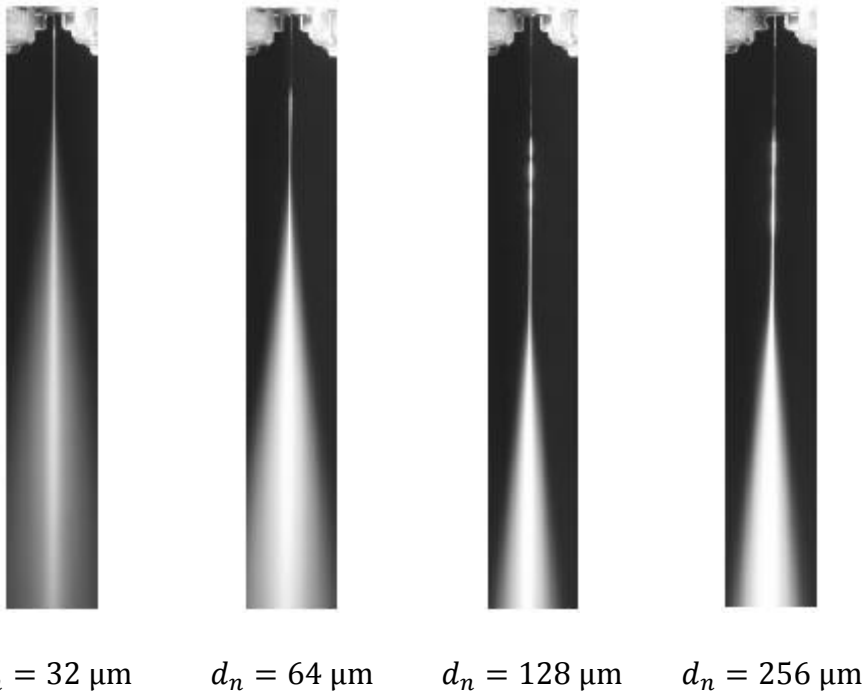


Figure 2- 20: Water jets from nozzles with different nozzle diameters (1,500 psi) (Anantharamaiah, 2006, pp. 21-22)

Connolly et al. (Connolly & Parent, 1993) examined the influence of specific energy and energy ratio (defined as the energy delivered to first side to the energy delivered to the other side of the structure) on carded, cross-lapped nonwoven webs. Strength, stiffness, thickness

and also fiber loss were investigated. According to the paper, higher energy levels delivered stronger fabrics but strength flattened after applying a critical amount of energy. Interestingly a specific energy ratio of 50% (applying energy equally on both sides) was reported to be not ideal. In contrast to that, fiber loss was reported to be less for structures bonded from both sides.

Möschler (Möschler, Meyer et al., 1995, p. 30) noted the MD:CD breaking strength ratio to increase with increasing hydroentangling intensity. Increasing hydroentangling forces are reported to increase the fiber oriented in machine direction (MD). Latter is reported and confirmed by others (Moyo, Patnaik et al., 2014).

Pourmohammadi et al. (Pourmohammadi, Russell et al., 2003) investigated the effect of water jet profile (arrangement of manifold pressure) and initial web geometry. Water jet profile was reported to have no influence on the air permeability. In other words, hydroentangling with one manifold with 70 bar or two with 30 and 40 bar results in comparable results. Initial web structure was mentioned to be crucial. However, hydroentangling from both sides (30 bar and 40 bar) was mentioned to result in better tensile strengths than bonding from just one side (70 bar). That indicates the strength to not only depend on the total energy delivered to the web but also the arrangement of manifolds.

Ghassemieh (Ghassemieh, Acar et al., 2001) reported the entanglement to be limited by a maximum pressure when hydroentangling from one side. However, a higher degree of entanglement can be achieved when continuing bonding on the other side.

Another work pointed out the relationship of manifold pressure and tensile strength to be linear. Specific energy was mentioned to be an independent factor influencing the tensile

strength, elongation and also pore size. It was stated that increasing the energy beyond a critical value has only little effects on the tensile properties (Moyo, Patnaik et al., 2014).

Patanaik et al. (Patanaik & Anandjiwala, 2010) reported the mean pore size to decrease with increasing hydroentangling pressures.

Pourdeyhimi et al. (Pourdeyhimi & Zapletalova, 2004) investigated the influence of specific energy on nonwoven fabrics made from hollow 16-segmented pie fibers. Results indicated the tensile properties (in MD) to stay constant, whereas the air permeability decreased as a function of specific energy.

Suragani (Suragani Venu, 2012) reported deeper fiber penetration and a higher degree of fiber interlocking with increasing jet pressures. Suragani also investigated the effect of multiple manifolds with same jet pressures (100 bar) on the structure properties and fiber transfer. According to the results, tensile strength first increased with the number of active manifolds but then decreased. Whereas the jet first impact resulted in deep fiber penetration subsequent impacts did not.

Tausif and his colleagues (Tausif & Russell, 2012) reported hydroentangling with multiple manifolds at high pressures (140 bar) to not enhance the tensile strength in machine direction (MD), whereas using the same setup with lower jet pressures (90 bar) led to better mechanical properties.

2.2.4 Influence of Forming Belt

In the language of nonwovens many terms are used for the forming belt. Some of them are forming surface, conveyor-, support-, transfer-, moving-, sieve- and porous belt or wire. The

main purpose of the belt is to transport the material through the process but also to give the web sufficient support for an efficient energy transfer. Water removal from the bonding zone is another factor influenced by the properties of the belt.

Stagnant water on the surface of the web was discussed to be critical in hydroentangling. Published information about the influence of the belt on the process is very limited but looking at the individual characteristics, such as mesh size, material and pattern is a good starting point.

Mesh size used for non-apertured applications typically varies from about 60 to 150, whereas patents also mention mesh sizes from 20 to 200 (Ishiyama & Yamada, 2000; Simpson & Smith, 2001).

Widen (Widen, 1991) mentioned fine mesh sizes in the range of 70 to 100 to be preferable for non-apertured applications.

Jaganathan et al. (Jaganathan, Tafreshi et al., 2008) reported the vacuum pressure to be a function of the belt's porosity, the fiber diameter but also the solid volume fraction of the web.

Seyam et al. (Seyam, Shiffler et al., 2005) reported the tensile strength of fabrics hydroentangled with different mesh sizes. Data indicated the tensile strength to decrease with decreasing mesh size. It was further reported that the mesh size seems to influence the mechanisms responsible for the actual fiber transfer. Similar results are reported by Kamath et al. (Dahiya, Kamath et al., 2004a).

Stahl (Stahl, 2010, pp. 56-60) investigated the mechanical properties of nonwovens hydroentangled with mesh sizes between 61 and 100 at different energy levels. Data

indicated that hydroentangling with low specific energies gives higher tensile strengths when using a 61 mesh forming belt. In contrast to that, hydroentangling with a 100 mesh forming belt required higher specific energies to achieve peak strength.

Widen (Widen, 1991) pointed out forming belts with fine meshes to increase web support. Wires with open structures, at high manifold pressures, tend to pinch fibers from the web. Latter is reported to also influence the final winding of the material (Russell, 2006, p. 260). Uni-Charm's efforts to use impervious conveyor belts to use reflected energy for bonding were mentioned earlier.

According to Widen (Widen, 1991), metal wires can still be found in industry even though plastic wires (e.g. from poly (ethylene terephthalate)) provide beneficial advantages. Even though the papermaking industry changed from metal to plastic wires this is far more complicated for nonwovens. Material properties obtained from metal belts are not the same as from plastic wires making a direct substitution far more difficult. This might explain the slow transition and rethinking in the hydroentangling industry.

In another study Kamath (Dahiya, Kamath et al., 2004a) noted the tensile strength to be a function of belt speed and the strength to decrease with increasing belt velocity.

2.2.5 Hydroentangling Applications, Market and Future Prognosis

Hydroentangled materials were mentioned to be the fastest growing sector for nonwoven materials with annual growth rates of about 5.7% (EDANA, 2014). INDA (Butler, Medeiros et al., 2002, p. 3) estimated the growth rate of hydroentangling as follows.

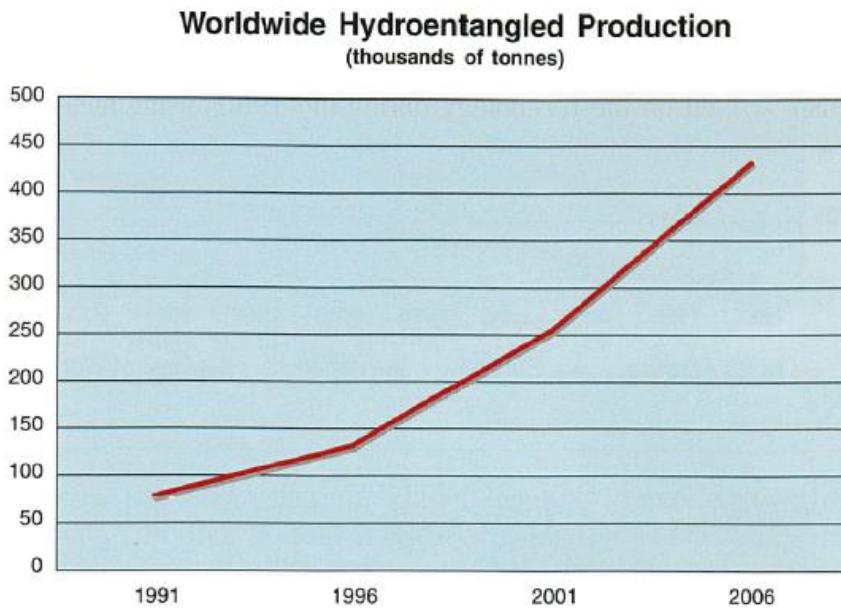


Figure 2- 21: Global production of hydroentangled materials (Butler, Medeiros et al., 2002, p. 3)

Hydroentangled nonwoven materials find application in fields as wipes and hygiene products but also surgical gowns or fabrics for medical protection (Das & Pourdeyhimi, 2014, p. 96; Russell, 2006, p. 292). Figure 2- 22 and Figure 2- 23 provide information about the hydroentangling market and segmentation.

World Hydroentangled Markets
(based upon tonnes)

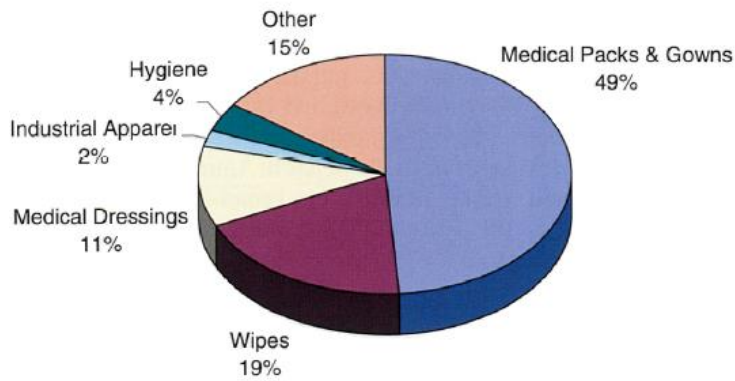


Figure 2- 22: Hydroentangling markets (Butler, Medeiros et al., 2002, p. 6)

Hydroentangled Production by Region
(thousands of tonnes)

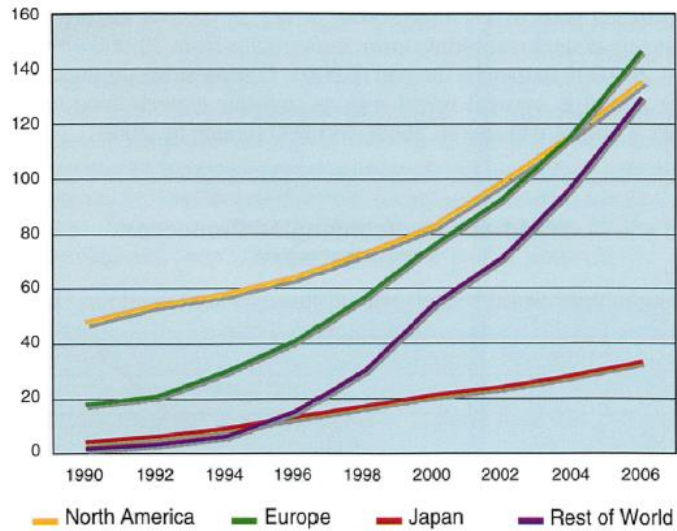


Figure 2- 23: Global production of hydroentangled materials by region (Butler, Medeiros et al., 2002, p. 4)

2.3 High Surface Area Nonwovens Structures

The specific surface area of a fibrous structure can be defined as the total fiber surface per unit mass of material (Hequet, Abidi et al., 1998). Accessible surface area A_S can be estimated by using the following equation.

$$A_S = \alpha \sqrt{\frac{4\pi \times 10^6}{\rho D}} [\text{m}^2 \text{g}^{-1}] \quad \text{Eq. 2- 18}$$

where α is the shape factor, ρ is the specific density of the material [g cm^{-3}] and D the fiber denier [g 9000 m^{-1}] (Anantharamaiah, Durany et al., 2009).

Equation to calculate the shape of a fiber is given in the following.

$$\alpha = \frac{P^2}{4\pi A} \quad \text{Eq. 2- 19}$$

where P is the perimeter [m] and A is the cross-sectional area of the fiber [m^2].

Calculation of specific surface area assumes the fiber to have a perfect circular shape, to have the same size and in case of bicomponent fibers a perfect splitting, fibrillation or dissolved/removed sheath polymer.

Fiber diameter in spunbond processing was discussed to be in the range of 10 to 35 μm . Electrospinning techniques are capable to produce nanofibers from different base materials (synthetic or natural polymers) and therefore nonwovens with significantly larger specific surface areas. For instance, producing webs with fibers of about 40 nm, which is reported to be the lower bound, would result in a specific surface area of $\sim 105 \text{ m}^2 \text{g}^{-1}$ (for $\rho = 0.9 \text{ g cm}^{-3}$). Smallest electrospun fibers are reported to be $\sim 3 \text{ nm}$ and based on a styrene-butadiene-styrene co-polymer. Fibers were built from just six atoms across the diameter (Cramariuc, Cramariuc et al., 2013; Goddard III, Brenner et al., 2007, p. 212;

Reneker & Chun, 1996; Skotheim & Reynolds, 2006, p. 255). Well known drawbacks of electrospinning are its low productivity (about 0.3 g per hour per needle), low mechanical properties and limited process control (Hamrang, 2014, p. 31; Wei, 2012, p. 255). Solution blow spinning was mentioned to be capable to produce nonwoven webs consisting fibers in the nanometer range (Medeiros, Glenn et al., 2009). Meltblown nonwovens can be produced with fiber sizes as small as 0.3 μm (Hassan, Yeom et al., 2013). Figure 2- 22 depicts the specific surface of structures with circular-shaped fibers as a function of fiber denier.

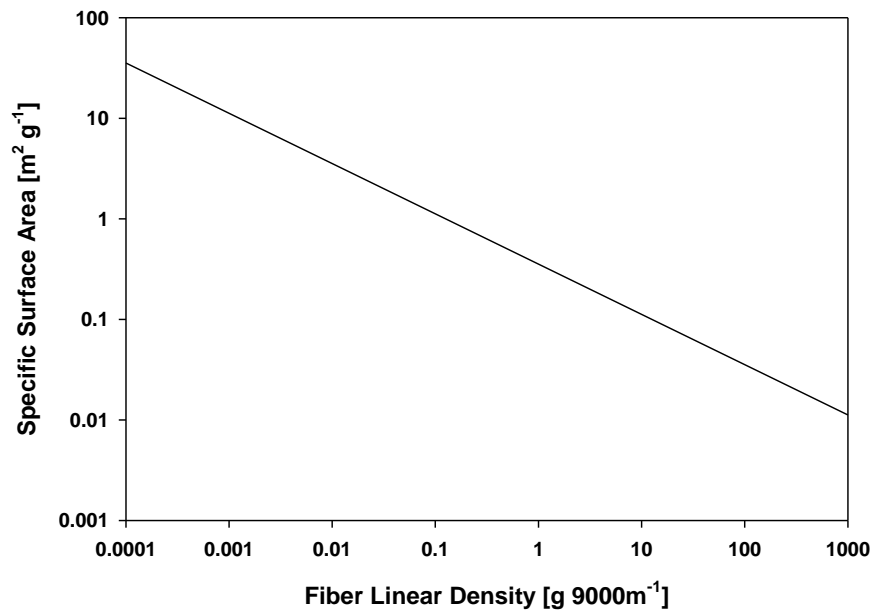


Figure 2- 24: Specific surface area as a function of fiber linear density

Bicomponent fiber technology describes another way to decrease fiber size and achieve nonwovens with high specific surface areas. Bicomponent fiber spinning allows higher production speeds but often requires subsequent processes.

High specific surface area materials are mentioned to be superior for filtration applications as the probability of particles to get trapped within the material is significantly higher (Anantharamaiah, Durany et al., 2009; Chapman, 2010, p. 15; J. A. Kent, 2010, p. 494; Wei, 2009, p. 260). Yeom et al. (Yeom & Pourdeyhimi, 2011b) mentioned the specific surface area to be one of the most important characteristics for nonwoven materials. Higher surface area can improve properties of materials, such as filtration media or wipes and influence properties, such as insulation, fluid retention, adsorption, drapeability or durability (M Tascan, Vaughn et al., 2011; Mevlut Tascan & Vaughn, 2008b). Shim et al. (Shim, Pourdeyhimi et al., 2010) noted materials with reduced fiber sizes and thus higher specific surface areas to offer a softer hand, higher absorption and enhanced filtration properties. Burton et al. (Burton, Carbonell et al., 2012) patented a method using high surface area nonwoven for bioseparation.

Specific surface area of materials can be experimentally determined by Brunauer-Emmet-Teller (BET) method. Named after their inventors, BET theory is simply spoken an extension of the Langmuir theory. Whereas Langmuir theory is based on the adsorption of a single layer, BET theory extends that theory and looks at the physisorption of multiple layers. BET theory assumes the following to be true, 1) more than one layer can be formed on the surface, 2) adsorption forces (van der Waals forces) are stronger for the first than for all subsequent layers, 3) sticking coefficient and attempt frequency of second layer is valid for all subsequent layers (different between surface and first layer) , 4) each adsorbed layer has the same volume, 5) at saturation pressure amount of layers is infinite, 5) molecules are not

moving laterally (ad- and desorption only happens between surface and surrounding vapor) (Butt, Graf et al., 2006, p. 189; Gates & Jentoft, 2013, p. 18).

2.3.1 Bicomponent Fiber Technology

Bicomponent fiber spinning, also known as multicomponent-, conjugate-, composite- or hetero fiber spinning, can be defined as the co-extrusion of two immiscible polymers with different chemical and or physical structure from a single spinneret, whereas both polymers are part of the same fiber (Dasdemir, 2011, p. 11; Pohl, 2010, p. 17).

According to Lewin (Lewin & Preston, 1996, p. 262), meltspinning is most often used for bicomponent fiber spinning, except acrylics, which are produced by either dry- or wet spinning. Numerous patents can be found about bicomponent fiber spinning techniques and products taking advantage of so called bico-fibers. Companies frequently filing patents are Nordson Corp., Hills Inc. and Reifenhäuser GmbH & Co. Maschinenfabrik.

The beginnings of the technology can be traced back to the late 1930s when the former German company IG Farben AG filed a patent about side-by-side viscose fibers having increased crimp to imitate wool (Koslowski, 2009). Sisson and Moorhead also worked on side-by-side viscose fibers and suitable spinning techniques back in 1953. According to literature, a septum was used to separate both polymers right before extrusion (Lewin & Preston, 1996, p. 250). According to literature, most development took place in the 1950s and early 1960s when Alvin Breen from DuPont worked on bicomponent fibers and filed several patents in that area (Baker, 1998; Breen, 1958). Since then bicomponent technology developed further providing a wide spectrum of possible fiber cross-sections.

Example are sheath/core, side-by-side, tipped trilobal, modified tipped trilobal, core trilobal, segmented ribbon, solid and hollow segmented pie, winged and island-in-the- sea fibers (Baker, 1998). Bicomponent fibers can be used for many purposes, such as reducing fiber size, implementation of additives within the structure, binder fibers or self-crimping fibers (Fedorova, 2006, p. 99; Houck, 2009, pp. 124-125; Lewin & Preston, 1996, p. 268)

Bicomponent fiber nonwovens most often require subsequent processes to separate or remove one polymer compound. Bicomponent fiber technologies are used in filament spinning for the production of staple fibers but also in spunbond and meltblown lines. Yarin et al. (Yarin, Pourdeyhimi et al., 2014, p. 93) mentioned meltblown bicomponent technologies to be mostly unexplored and somehow exotic. One reason is the limitation in polymer selection as low molecular weight polymers are required in meltblown processing. However, die assemblies being capable to spin cross-sectional shapes as side-by-side, sheath/core, tipped trilobal, tipped cross etc. are commercially available (Hagewood, 2004; Hills Inc., n.d.-b; Zhao, Wadsworth et al., 2002). Zhao et al. (Zhao & Wadsworth, 2003) investigated the fiber diameter of meltblown side-by-side fibers as a function of DCD (die-to-collector distance). According to the results, attenuation of side-by-side fibers increased with increasing DCD, which is similar to monocomponent fibers. Also, fiber diameter distribution of bicomponent fibers was reported to be broader compared to poly(propylene) monocomponent fibers and increasing the airflow led to narrower distributions. This topic was also investigated by others (D. Zhang, Sun et al., 2002; Zhao, Wadsworth et al., 2002).

Typically there are three methods to combine polymers in bicomponent fiber spinning: 1) co-extrusion melt spinning, where both polymers are molten and pressurized in separate extruders and meet right before the exit of the spinneret, 2) molten polymers are mixed at the same place with a static mixer before spinning and 3) coating a polymer to a monocomponent fiber after leaving the spinneret (Dasdemir, 2011, p. 18; Hedge, Dahiya et al., 2004). Examples for co-extrusion spinning are bilateral methods for side-by-side configurations and pipe-in-pipe spinning for sheath/core fibers. In bilateral spinning a knife or septum divides both polymer streams before they are brought together at the exit of the spinneret. In pipe-in-pipe however, core polymer is transported through a pipe surrounded by another pipe carrying the sheath polymer (Lewin & Preston, 1996, p. 261). These methods describe just a small fraction of processes available for bicomponent fiber spinning.

Island-in-the-sea fibers describe another type of sheath/core configuration and are characterized by multiple cores (islands) embedded in a matrix (sea). Lewin (Lewin & Preston, 1996, pp. 252-258, 261) mentioned several ways how island-in-the-sea fibers can be manufactured: 1) using a so-called combining chamber (conical chamber), which combines and narrows multiple sheath/core fibers below the spinneret hole (pipe-in-pipe method), 2) side-injecting streams of core polymer into the sheath polymer, 3) mixing of island and sea polymer with a static mixer, whereas mixing forms multiple cores within the sea polymer, 4) using numerous small pipes within the sheath pipe to inject core polymer (limited at some point because pipe diameter is getting too small) and 5) a method patented by Hills Inc. using etching instead of drilling, milling or reaming for the formation of small distribution channels inside the distribution plates of the spinpack (see also Figure 2- 3). In the final stage

of this process, island and sea polymer meet in the counterbore and built the final fiber at its bottom (Dasdemir, 2011, p. 20). Whereas the mixed island-in-the-sea process generates fibers with random diameters and island counts, process from Hills allows controlling that.

Despite the fact that there is a large variety of available polymers not all of them can be combined to spin bicomponent fibers. Lewin (Lewin & Preston, 1996, p. 261) mentioned the physical properties, i.e. rheology of polymers to be most important for bicomponent fiber spinning. It was stated that the melt viscosity of both polymers has to be: 1) high enough to avoid turbulences right after the spinneret and 2) to be in the same range.



Figure 2- 25: Illustration of different bicomponent fibers: concentric sheath/core, eccentric sheath/core, side-by-side, island-in-the-sea and mixed island-in-the-sea (from left to right)

In case that melt viscosities but also cooling rates of both polymers are too different distortion of cross-section but also spinline stress concentration at, or fracturing of, the more viscous polymer can occur. Lewin (Lewin & Preston, 1996, p. 261) further mentioned the adhesion between the polymers to be a critical factor. Draw ratios beyond a certain limit could cause premature fiber splitting during the actual drawing step (Dasdemir, 2011, pp. 22-23; Fedorova, 2006, p. 29).

As mentioned, bicomponent structures most often require subsequent steps to reveal their full functionality. Examples for that are: 1) splitting/fibrillation of bicomponent fibers by exerting mechanical force, 2) thermal treatment and 3) dissolving one of the polymers. Splitting and fibrillation requires poor interfacial adhesion between the two compounds and can be obtained by using incompatible polymers, i.e. polymers having dissimilarities in their chemical structure (e.g. polyolefin/polyesters, polyolefin/polyamides, polyamides/polyesters) (Fedorova, 2006, p. 21; Hagewood, n. d.). A well-known example is Evolon[®] from Freudenberg, which is a 16-segmented pie poly (ethylene terephthalate)/poly (amide-6) structure split by means of hydroentangling. Shim et al. (Shim, Pourdeyhimi et al., 2010) mentioned ultrasonic energy, steam but also laundering to be alternative ways to split bicomponent fibers. Other techniques are reported to be carding, twisting, beating, needlepunching or drawing (Fedorova, 2006, p. 21). Hagewood (Hagewood, n. d.) mentioned sanding or brushing to be alternative ways to split bicomponent fibers. According to Batra et al. (Batra & Pourdeyhimi, 2012a, p. 283), shear forces at the polymer interface but also swelling or shrinking under heat, humidity, steam or chemical influences can split fibers.

Sun et al. (C. Q. Sun, Zhang et al., 2004) investigated different methods to separate side-by-side meltblown bicomponent fibers made from incompatible polymers. Hydroentangling with manifold pressures between 80 to 120 bar was used to split fibers. However, combination of impact force and poor molecular orientation in meltblown fibers led to fiber breakage instead of splitting. Anantharamaiah et al. (Anantharamaiah, Verenich et al., 2008) successfully used hydroentangling with jet pressures of up to 200 bar to fibrillate modified island-in-the-sea structures of various island counts. It was shown that beyond a

certain amount of energy mechanical properties were not further improved. Hydroentangling being a suitable technique for fiber splitting was also confirmed by Yeom et al. (Yeom & Pourdeyhimi, 2011a), who fibrillated island-in-the-sea bicomponent structures with island counts between 1 and 108. Pourdeyhimi et al. (Pourdeyhimi & Zapletalova, 2004) split hollow segmented pie fibers by using hydroentangling and reported them to be easier to split compared to solid segmented pie fibers. Besides that, calendering could be considered as a method to “pre-crack” bicomponent fibers facilitating subsequent splitting/fibrillating. Furthermore, ability to split fibers also depends on the density and also basis weight of the material. Shim et al. (Shim, Pourdeyhimi et al., 2010) used hydroentangling to penetrate nonwoven materials consisting of 8-segmented pie fibers. It was found that most of the splitting took place on the surface/upper layer of the material.

For other applications bicomponent fibers are heat-treated, e.g. sheath/core binder fibers with polymers having different melting temperatures. Schenk (Schenk, 2014, pp. 20-21) mentioned side-by-side but also sheath/core fibers with eccentric shape to be suitable for self-crimping applications. Dissolving (e.g. with acids or caustics) describes another common way to remove one polymer compound of a bicomponent fiber. Polymers, such as polyamides or polyester's (e.g. poly (lactic acid), co-polyester) are often used as sacrificing polymer in bicomponent structures. Zhang et al. (D. Zhang, Sun et al., 2004) dissolved Eastman's water-soluble polymer AQ35 from a side-by-side bicomponent meltblown nonwovens.

2.3.2 Island-in-the-Sea Technology

Island-in-the-sea fibers can be defined as a type of sheath/core fiber having multiple cores of same or varying diameter at defined or random positions. Batra et al. (Batra & Pourdeyhimi, 2012a, p. 282) mentioned the beginnings of island-in-the-sea fibers to be in the 1970s when the Japanese company Toray developed a suede-like structure built from polyester fibers embedded in a soluble polymer. Fibers are mentioned to have linear densities as low as 0.1 denier. Early approaches by Okamoto, who was a former employee of Toray, are even dated in the mid-1960s (Schenk, 2014, p. 16). As from 1966, Toray filed several patents about a technique being capable to produce 37 island-in-the-sea structures. Their apparatus used separate pipes to inject the island polymer into the sea stream before leaving the spinneret (Keiichi, Miyoshi et al., 1972; Okamoto, Watanabe et al., 1970). Following depicts a three-dimensional schematic of a 37 island-in-the-sea fiber.



Figure 2- 26: Illustration of a 37 island-in-the-sea bicomponent fiber

As discussed in the previous section, there exist different spinning techniques for island-in-the-sea fibers. However, state-of-the-art technologies allow precise control of the spinning process, spin more uniform fibers and are capable to produce island counts higher than 1000. Hagewood from Hills Inc. (Hagewood, n.d.) mentioned 1 denier island-in-the-sea

fibers with a total of 1120 embedded islands. Island counts in the range of 37 to 49 are often used for suede materials, whereas sea polymer for this kind of application is most often removed by using appropriate solvents (Anantharamaiah, Durany et al., 2009; Anantharamaiah, Verenich et al., 2008). As mentioned, island-in-the-sea fibers require subsequent treatment to release island fibers. Depending on the used polymer this can be done by either fibrillation or dissolving.

Fibrillation takes advantage of the weak interface between incompatible polymers and contrary to dissolving, both island fibers and sea fragments are part of the final structure. Cross-Sectional microscopy images showing a 37 and 1120 island-in-the-sea structure can be seen in the following.

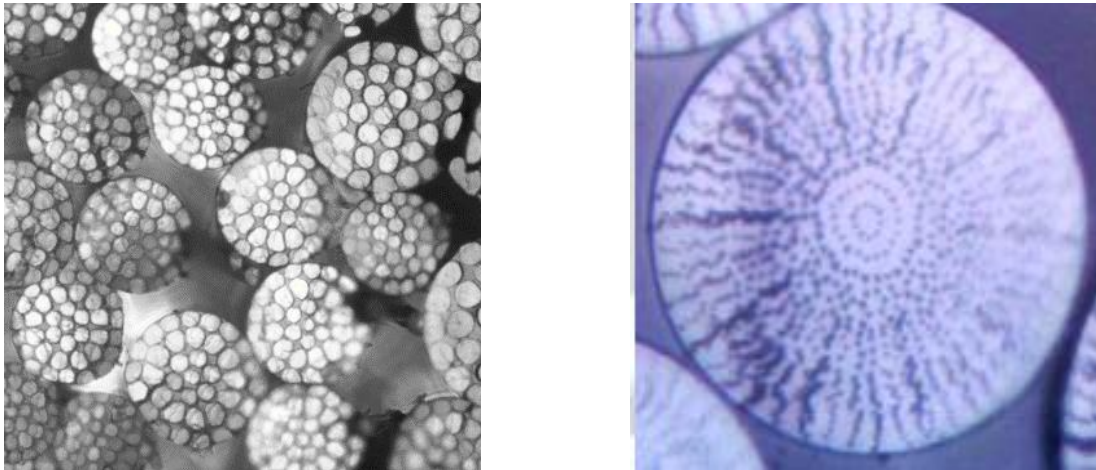


Figure 2- 27: Cross-sectional images of a 37 island-in-the-sea (left) and 1120 island-in-the-sea fiber (Hills Inc., n.d.-a)

Anantharamaiah (Anantharamaiah, Verenich et al., 2008) but also Fedorova (Fedorova, 2006) demonstrated that island-in-the-sea structures can have mechanical properties much

better than commercial microfiber fabrics, such as Evolon[®]. Yeom et al. (Yeom & Pourdeyhimi, 2011a) investigated the filtration performance of nonwoven materials with island counts of 1, 7, 19, 37 and 108. According to the results, filtration efficiency first increases with increasing island count before reaching a plateau and not changing anymore. Quality factor of monocomponent fibers was noted to be higher than for island-in-the-sea fibers. Also, solidity was reported to increase with increasing island count. It was reported that 108 island-in-the-sea nonwovens were not fully fibrillated. Anantharamaiah et al. (Anantharamaiah, Durany et al., 2009) reported optimum hydroentangling energies for fibrillating island-in-the-sea structures. Beyond that point mechanical properties of structures declined. Anantharamaiah further mentioned the air permeability and pore size to decrease with increasing island count.

It was discussed that polymers used in bicomponent spinning should have similarities in terms of their viscosities and cooling rates. Fedorova (Fedorova, 2006, p. 140) mentioned the importance of having similar solidification rates and elongational viscosities when spinning island-in-the-sea fibers. In case of faster solidification of the island polymer, higher spinline stresses and therefore higher molecular orientation can be expected. Furthermore, hydroentangled structures were reported to be suitable for subsequent sea removal treatments, whereas thermal bonded structures failed. It was further mentioned that calendered island-in-the-sea structures led to stronger fabrics compared to point-bonded monocomponent structures. Sea polymers with lower melting temperature acted as a matrix transferring stress to the strong and still intact island fibers (Fedorova, 2006, pp. 195-197).

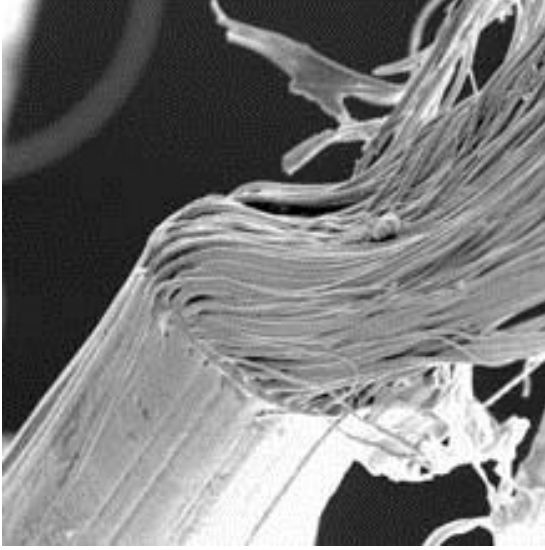


Figure 2- 28: Partially dissolved 600 island-in-the-sea fiber (Hagewood, n.d.)

Following section discusses an approach to theoretically calculate the diameter of island fibers. At first, mass fraction of island polymer ratio needs to be converted to the volume fraction vol_i .

$$vol_i = \frac{\frac{R_i}{\rho_i}}{(R_i\rho_i)+(R_s\rho_s)} \quad \text{Eq. 2- 20}$$

where R_i is the mass fraction of island polymer, ρ_i is the specific density of the island polymer [g cm^{-3}], R_s is the mass fraction of the sea polymer and ρ_s is the specific density of the sea polymer [g cm^{-3}]. The mass fraction of island and sea polymer can be calculated from the extruders' throughputs.

From this we can assume that vol_i is the total volume covered by island fibers and can be correlated to the total cross-sectional area of island fibers. This assumes the following to be true: 1) cross-section of all fibers is circular, 2) diameter of spun fibers is constant and 3) specific density of island and sea polymer is not changing along the fiber axis. In reality,

cross-sectional area of island fibers might vary along the fiber axis as the diameter of island fibers might not be the same at every point. Thus, island diameter predicted with this approach is the average island diameter $d_{f,s,t}$ and can be calculated as followed.

$$d_{f,s,t} = d_f \sqrt{\frac{vol_i}{N}} \text{ [}\mu\text{m]} \quad \text{Eq. 2- 21}$$

where d_f is the initial fiber diameter [μm], vol_i is the volume fraction of island polymer and N the island count. Relation between fiber diameter, specific surface area and island count is depicted in Figure 2- 29.

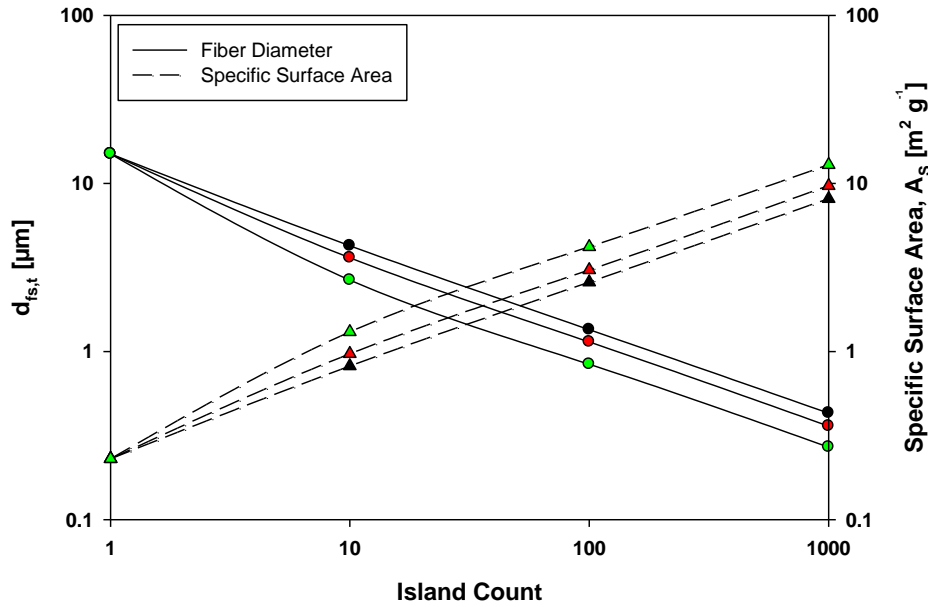


Figure 2- 29: Fiber diameter and specific surface area as a function of island count ($p_i = 0.9 \text{ g cm}^3$, $p_s = 1.24 \text{ g cm}^3$, $d_i = 15 \text{ micron}$), black symbols ($R_i/R_s=75/25$), red symbols ($R_i/R_s=50/50$), green symbols ($R_i/R_s=25/50$)

2.3.3 Winged Fiber Technology

Winged fibers describe a relatively new technology invented by Allasso Industries Inc. and The Nonwovens Institute (North Carolina State University). Winged fibers can be defined as oval-shaped fibers consisting of multiple wings connected to a center part. This lamella-like structure is mentioned to have a length of about 10 to 20 μm offering many different applications. According to Rodie (Rodie, 2012), winged fibers are intended to be used in areas, such as filtration, insulation, battery separators but also for tissue scaffolds. Further applications are reported to be wipes, composite structures (e.g. for artificial leather) but also outerwear due to the fast moisture transport through channels (similar effect as Coolmax[®] fibers) (Pourdeyhimi, 2011a; Pourdeyhimi, Chappas et al., 2013). SEM images from unwashed and treated winged fibers can be seen in the following.

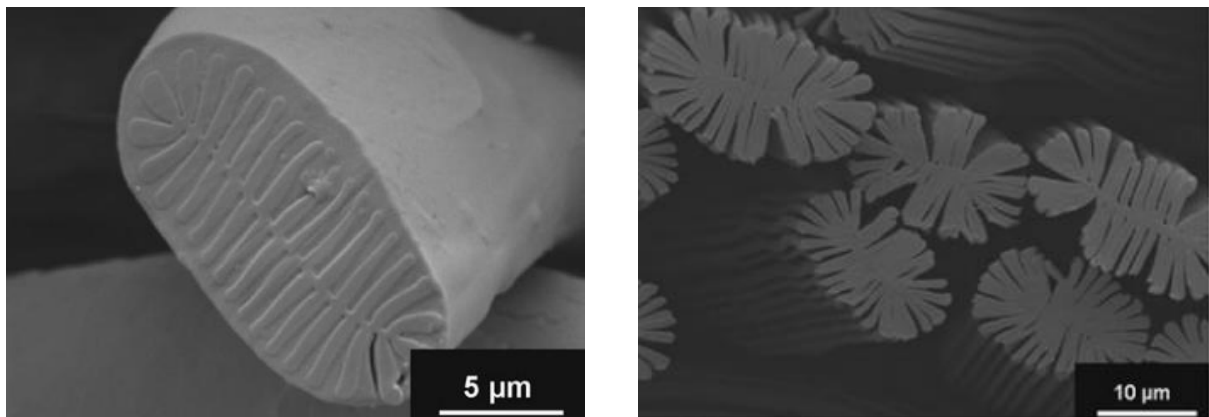


Figure 2- 30: SEM Image taken from a 32 lobes winged fibers before and after removing the sheath polymer (Yeom & Pourdeyhimi, 2011b)

The cross-section of winged fibers is formed by a specific spinpack design and not the spinneret itself. Pourdeyhimi (Pourdeyhimi, 2011a) mentioned winged fibers with linear densities of 1 denier to be possible. In contrast to bicomponent fibers, which can be split or fibrillated, sheath polymer of winged fibers has to be removed. Suitable polymers can be poly (amide-6), poly (ethylene terephthalate), poly (butylene terephthalate) or poly (lactic acid) for the core and poly (lactic acid) or water-soluble polymers, such as EastOne for the sheath (Pourdeyhimi, Chappas et al., 2013; Yeom & Pourdeyhimi, 2011b).

One of the main advantages of winged fibers is their extraordinary large specific surface area. To achieve that it requires the flawless formation of wings but also the perfect removal of the sacrificing polymer from the structure. Realistic specific surface areas are reported are as high as $20 \text{ m}^2 \text{ g}^{-1}$ compared to $0.3 \text{ m}^2 \text{ g}^{-1}$ of a circular-shaped fiber with similar denier (Pourdeyhimi, 2011a). A comparison of the specific surface area of different fiber types can be seen in the following.

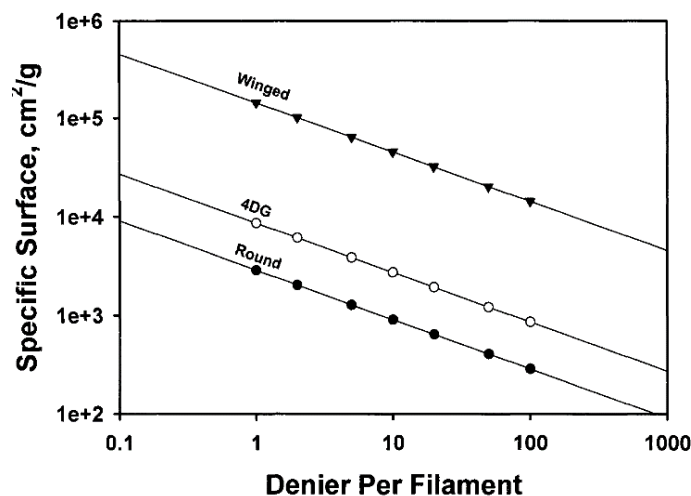


Figure 12- 1: Specific surface areas as a function of fiber denier for different fiber types (Chappas & Pourdeyhimi, 2013)

2.3.4 Segmented Pie Technology

Segmented pie or wedge fibers describe another type of bicomponent fibers, which are mostly known because of a poly (ethylene terephthalate)/poly (amide-6) 16-segmented pie structure called Evolon[®]. Segmented pie fibers can be classified as splittable fibers and are usually built from 2 immiscible polymers. This means that the polymers do not share similarities in terms of their chemical structure and can be separated. It was discussed that exerting mechanical force, e.g. by using hydroentangling, calendaring but also methods like twisting, beating et cetera, can split segmented pie fibers into their individual parts. In contrast to dissolving and therefore sacrificing one polymer, splitting can be seen as a more “environmental and economically friendly” process (Anantharamaiah, Verenich et al., 2008). Hollow segmented pie fibers describe a modification, which is mentioned to be easier to spin and split (Deopura, Alagirusamy et al., 2008, p. 206; Hagewood, n. d.). Figure 2- 31 depicts an illustration of intact 16-segmented pie fibers, 16-segmented pie hollow fibers and split 16-segmented pie hollow fibers

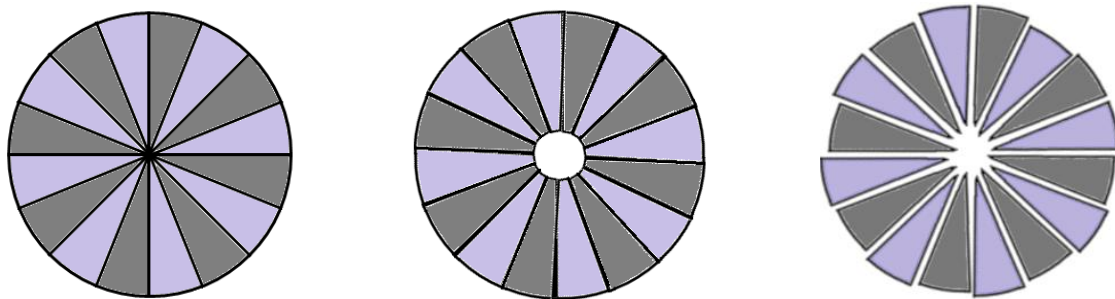


Figure 2- 31: Illustration of an intact 16 segmented-pie fiber and intact and split 16 segmented-pie hollow fiber

Because of their wedge-like shape, split segmented pie fibers pack tightly together, which not only results in low permeabilities but also makes it harder to control the structure in terms of consolidation and mechanical properties. The limit of wedges is mentioned to be 24 (Pourdeyhimi, 2011a; The Nonwovens Institute, n.d.). Figure 2- 32 shows the influence of the number of wedges on the fiber diameter.

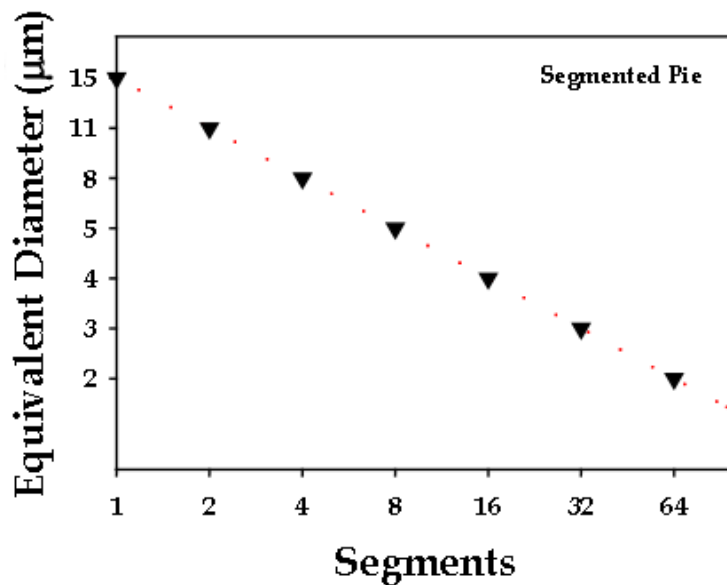


Figure 2- 32: Fiber diameter as a function of segments (Pourdeyhimi, 2011b)

As mentioned, Shim et al. (Shim, Pourdeyhimi et al., 2010) investigated the feasibility of using hydroentangling to split 8-segmented pie nonwoven structures. According to the results, splitting was rather found on the surface than in the bulk of the structure. Furthermore, high-density regions were not found at the jet streaks but the neighboring hill regions. Moreover, solid volume fraction was found to be higher in the inner part of the structure than on the surfaces.

2.3.5 Further Technologies

Other common bicomponent fibers used for nonwovens are segmented ribbon, tipped trilobal and also modified tipped trilobal. Contrary to that, 4DG fibers (see Figure 2- 33) are not defined as bicomponent fibers per se. This type of fiber is directly spun from spinnerets with castellated holes and thus, do not require subsequent treatments. According to Mogahzy (Mogahzy, 2008, p. 377), this fiber type was invented by Eastman Chemical and can be described as a fiber having deep grooves along its center. It is further mentioned that the specific surface area of 4DG fiber is roughly three times larger compared to a conventional round-shaped fiber. 4DG fibers look are similar to winged fibers and show similarities in their properties (e.g. moisture transport, enhanced filtration properties) (Mevlut Tascan & Vaughn, 2008a).



Figure 2- 33: Section view of a 4DG fiber (Deopura, Alagirusamy et al., 2008)

Similar to winged fibers, 4DG fibers are capable to hold particles, such as dust inside of the grooves making them interesting for filtration applications (Deopura, Alagirusamy et al., 2008, p. 208). Due to limitations of the spinneret, 6 denier is reported to be smallest linear density possible for 4DG fibers (The Nonwovens Institute, n.d.).

Segmented ribbon fibers are categorized as splittable bicomponent fibers. As splittable segmented pie, segmented ribbon fibers are usually built from two incompatible polymers. Literature mentions them to be the most readily splittable fiber from all bicomponent fibers (Deopura, Alagirusamy et al., 2008, p. 206).

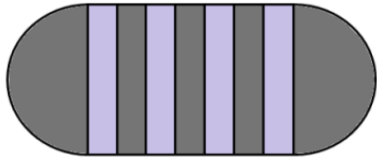


Figure 2- 34: Section view of a segmented-pie fiber

Tipped trilobal fibers also belong to the family of splittable bicomponent fibers. This type of fiber can be defined as a triangular shaped fiber having tips at their edges. Modified tip trilobal describe a modified version of this fiber having extended tips. The third version is known as core trilobal fibers, which are characterized by extended tips and a second, embedded trilobal fiber (Pourdeyhimi, 2011a).

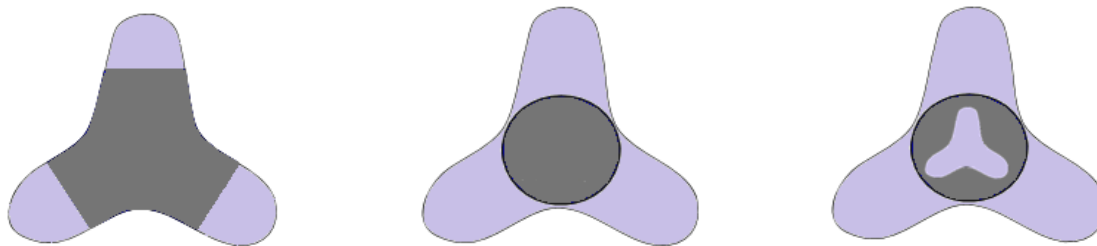


Figure 2- 35: Illustration of a Tipped Trilobal, Modified Tipped Trilobal and Core Trilobal Fibers

Tipped trilobal are generally easy to split as all parts are directly exposed to the surface, whereas the core of modified tipped trilobal fibers is surrounded by the tips. Pourdeyhimi (Pourdeyhimi, 2011b) mentioned spinning of modified tipped trilobal fibers to be more difficult but the materials to have a smooth hand, excellent dyeability and durability and no “velcro” (not readily sticking) effect.

2.4 Aerosol Filtration

Defining the science of filtration is certainly not easy and literature provides many different approaches for that. In the following some examples, 1) filtration can be defined as the separation of two or more components from a fluid stream, 2) filtration refers to the act of separation of one or more distinct phases from another using the physical differences of the phases, 3) the separation of an insoluble solid from a fluid by means of a porous medium that retains the solid but allows the fluid to pass or 4) the process of the removal of solid particles from a suspension by passaging the suspension through a porous medium (Aulton & Taylor, 2013, p. 407; Cheryan, 1998, p. 1; Crittenden, Trussell et al., 2012, p. 730; Sutherland & Chase, 2011, p. 1). Brown (R. C. Brown, 1993, p. 2) categorized filter types as follows: fibrous filters (nonwovens), fabric filters (woven or knitted materials), membrane- and granular filters, whereas the particle-carrying suspension can be either gaseous (air or gas) or liquid (water, blood etc.).

The following discussion will focus on aerosol filtration (or air filtration), which represents a cornerstone for many industries demanding clean air in the workplace to either protect either their staff or the product itself. Well-known examples are cleanrooms as to find

in the microchip industry but also hospitals, where a clean, pollute-free environments stand for quality, purity or even safety. Air filtration media can also be found in the automotive sector, facemasks and not to forget millions of households around the world.

The question why nonwoven and not woven or knitted materials are preferred materials for filtration can be answered by many reasons. Woven and in some cases knitted fabrics they can be considered as two-dimensional fabrics with a pre-defined structure and pore size. Density of weft and warp yarn determines the opening of a woven material. Nonwovens however are three-dimensional structures with properties less predictable but in many aspects advantageous. Woven materials can be excellent filtration materials but they would also have high resistances to the airflow. The three-dimensional structure of nonwovens forces particles to travel long distances through the medium enhancing the probability of being trapped (Adanur, 1995, p. 291; R. C. Brown, 1993, p. 4; Crowe, 2014, pp. 7.48-49).

2.4.1 Introduction to Aerosol Filtration

Even though most particles around us are not noticeable or visible they could be from hazardous nature causing serious health problems or interfere with sensible manufacturing processes. Particles can be emitted from various sources either man-made or natural. Examples are combustion processes or stone crushing, whereas natural sources could be eruptions and particles from outer space or living beings itself (Department of the Environment and Heritage, 2005). The following figure shows typical airborne particles along with their corresponding particle size.

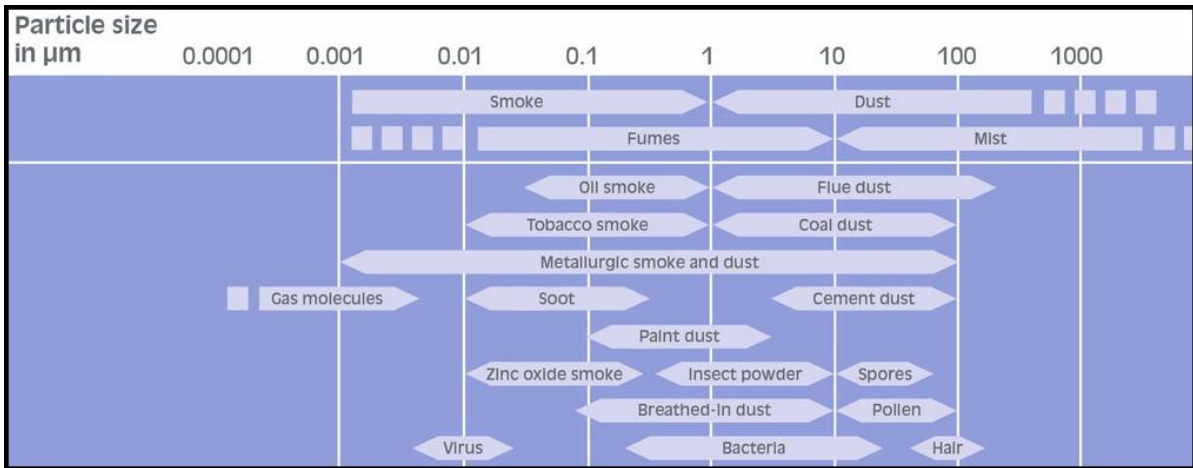


Figure 2- 36: Typical Airborne Particles and their Corresponding Size (LTA Lufttechnik GmbH, n.d.)

Depending on the particle size, filtration mechanisms can be classified into different categories, which are: 1) reverse osmosis (particles sizes $<0.007 \mu\text{m}$), 2) nanofiltration (particles size $<0.01 \mu\text{m}$), 3) microfiltration (particle sizes $<10 \mu\text{m}$) and 4) macrofiltration or particle filtration (particles sizes $<900 \mu\text{m}$) (Chapman, 2010, p. 166). One way to classify filtration mechanisms is to distinguish between surface and depth filtration. Chapman (Chapman, 2010, p. 164) mentioned surface and depth filtration to most often take place simultaneously. The simplest version of a surface filter is a net having a certain pore size and collecting particles larger than the openings. Accumulation of particles happens at the surface and due to the formation of a particle cake, pressure drop but also total efficiency increase over time. As a consequence, particles even smaller than the pore size of the filter are captured after some time (R. C. Brown, 1993, p. 1).

The following figure depicts an illustration of the principle of surface filtration.

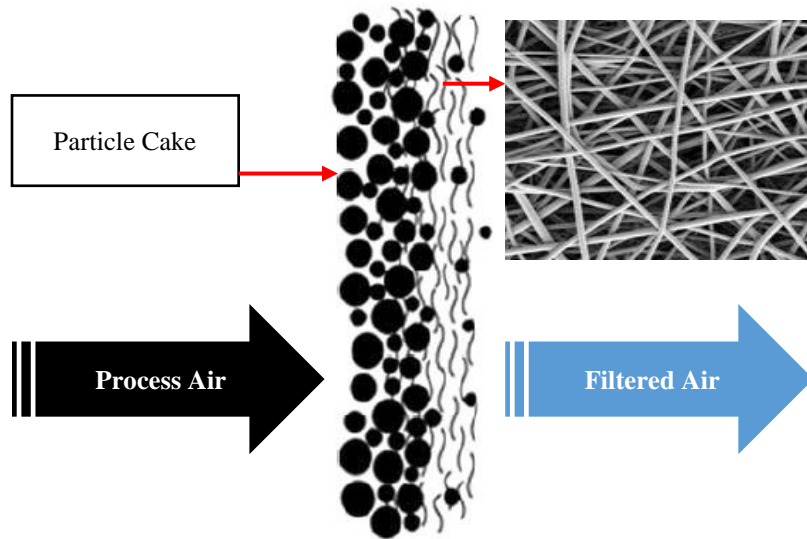


Figure 2- 37: Surface filtration mechanism

In contrast to depth filters, most surface filters can be cleaned after the pressure drop reached a certain limit. Removing of dust particle cakes can either be done by pulsation (pulse jet cleaning), an air pulse reverse to the direction of airflow during operation, reverse air or shaking. All induce the cake to partly or fully dislodge from the surface before being removed. However, cleaning also requires a certain degree of dimensional stability of the structure as forces acting on the filter could cause damages (Das & Pourdeyhimi, 2014, p. 167; Hutten, 2007, p. 326; Liu & Liptak, 1999, p. 124; Ortega-Rivas, 2012, p. 161; Purchas & Sutherland, 2002, p. 181). Due to limitations of the cleaning process but also because of particles being trapped in the inner part of the structure, filters cannot be completely cleaned and fully restored to obtain initial pressure drop. Pressure drop after cleaning still increases

until the filter is completely changed (Das & Pourdeyhimi, 2014, p. 136; Ewsuk, 2007, p. 310).

In contrast to that, depth filtration mostly takes place in the inner part of the fibrous structure. Other than for surface filtration, particle capturing is not based on pore size but different deposition mechanisms, which are discussed later on. Figure 2- 38 illustrates the basic principle of a composite filter used for depth filtration.

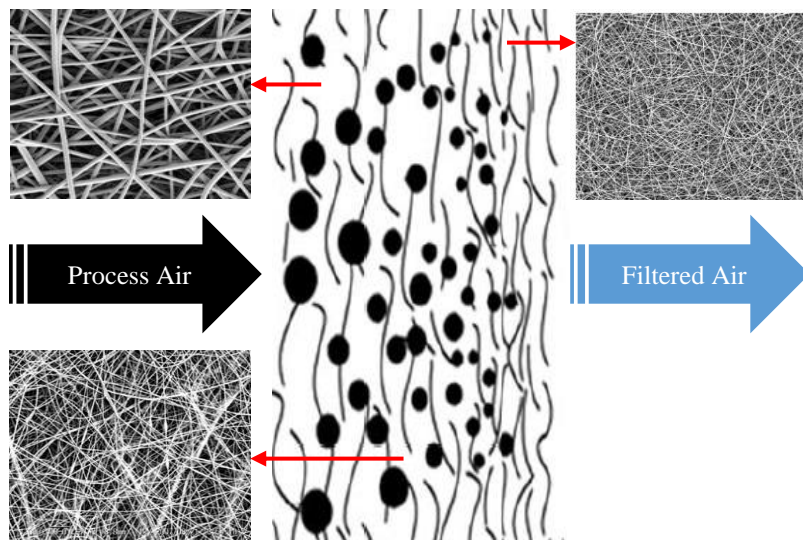


Figure 2- 38: Depth filtration mechanism

Particle deposition in the fibrous material is a consequence of different physical mechanisms, which are interception, inertial impaction, Brownian diffusion, electrostatic attraction and gravitational settling (Chapman, 2010, p. 167; Godish, 1989, p. 248; Tan, 2014, p. 173). Inertial Impaction describes the deposition of a particle due to its inertia. Because of its weight or size particle is no longer following the streamlines around the fiber and collides

with the fiber. Inertial impaction also depends on the velocity of the stream and increasing the air speed enhances the deposition by inertial impaction (Chapman, 2010, pp. 167-168). In physical terms, inertial impaction depends on the Stokes and Reynolds number and below a critical value of $St_{critical}$ inertial impaction does not occur (Ruzer & Harley, 2012, p. 442). An illustration of the particle deposition by inertial impaction can be seen in the following.

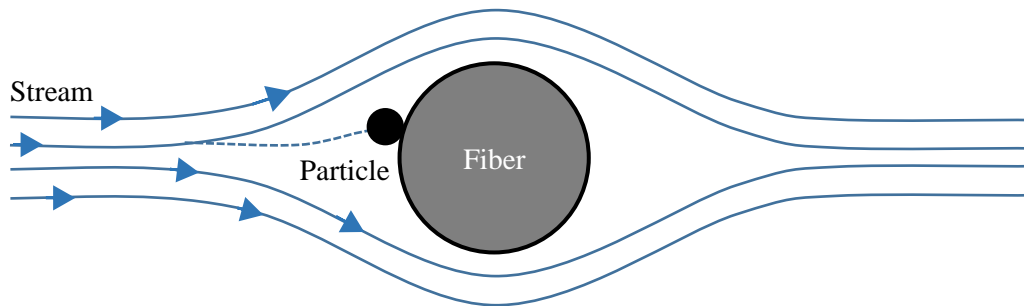


Figure 2- 39: Particle deposition by inertial impaction

In contrast to that, Brownian diffusion occurs at lower stream velocities and smaller particle sizes. Diffusion describes a random zig-zag motion, the so-called Brownian motion, of particles caused by collision with other molecules (Chapman, 2010, p. 168). Depending on the velocity of the flow, particles can move independently from the stream and, like gases, tend moving from high to low concentration areas (Ruzer & Harley, 2012, p. 443). Figure 2-40 depicts a schematic of the principle of Brownian diffusion.

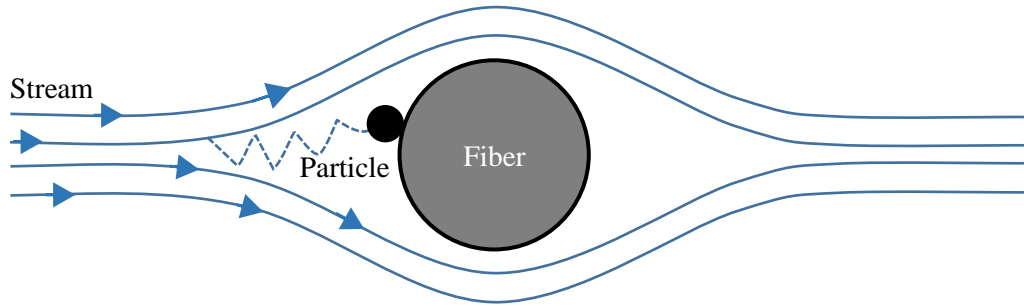


Figure 2- 40: Particle deposition by Brownian diffusion (Brownian motion)

The third deposition mechanism is described by interception, which occurs if the streamline carrying the particle has a distance of at least half of the diameter of the particle. Interception assumes the particles to perfectly follow the path of the streamlines (Chapman, 2010, p. 167; Tan, 2014, p. 173). Deposition by interception also depends on the size of particles and is more dominant for smaller particles. According to Schiffner (Schiffner, 2013, p. 87), interception is relevant for particle sizes in the range of 1 to 3 μm . Particles with reduced mass and low momentum are more likely to follow the streamlines around the fiber. Figure 2- 41 shows the general principle of deposition by interception.

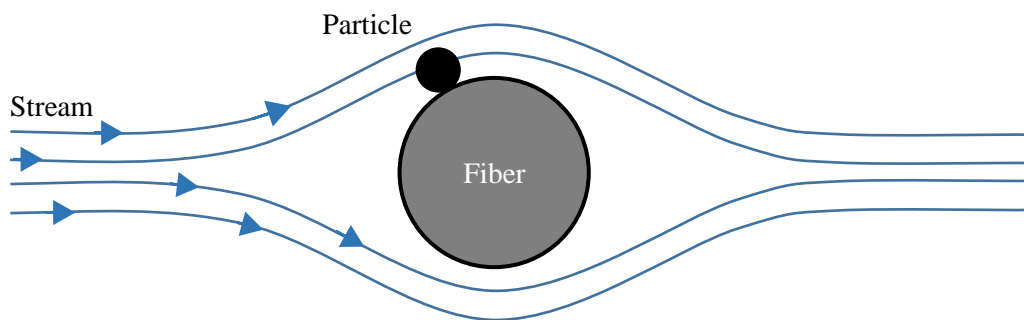


Figure 2- 41: Particle deposition by interception

In contrast to the described mechanical deposition mechanisms, electrostatic attraction occurs due to the static charge of fibers (Tan, 2014, p. 173). Material can either receive charge during the manufacturing process or in a subsequent process. According to Davey et al. (Davey & Diba, 2012, p. 276), electrostatic attraction of particles can occur in three different ways: 1) particles have the opposite charge than fibers, 2) charged fibers induce a dipole in neutral particles and 3) charged particles induce image forces on neutral fibers. Charging filters can immensely increase the filtration efficiency of filters without enhancing its pressure drop (Kulkarni, Baron et al., 2011, p. 117). Figure 2- 42 depicts an illustration of the general principle of electrostatic particle deposition.

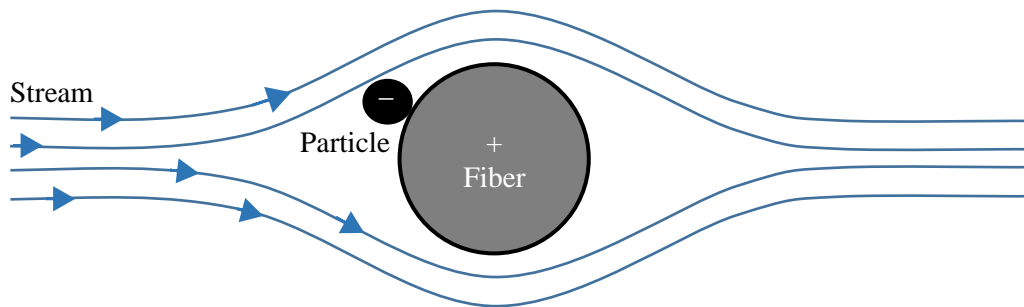


Figure 2- 42: Particle deposition by electrostatic attraction

As mentioned, intensity of deposition mechanism depends on factors, such as particle size, fiber diameter, temperature, face velocity et cetera. A filtration curve showing the different deposition mechanisms as a function of particle size can be seen in Figure 2- 43. Most penetrating particle size (MPPS) is the particle diameter at which the filter shows lowest efficiency. At this point none of the deposition mechanisms is dominant (Shaffer & Rengasamy, 2009).

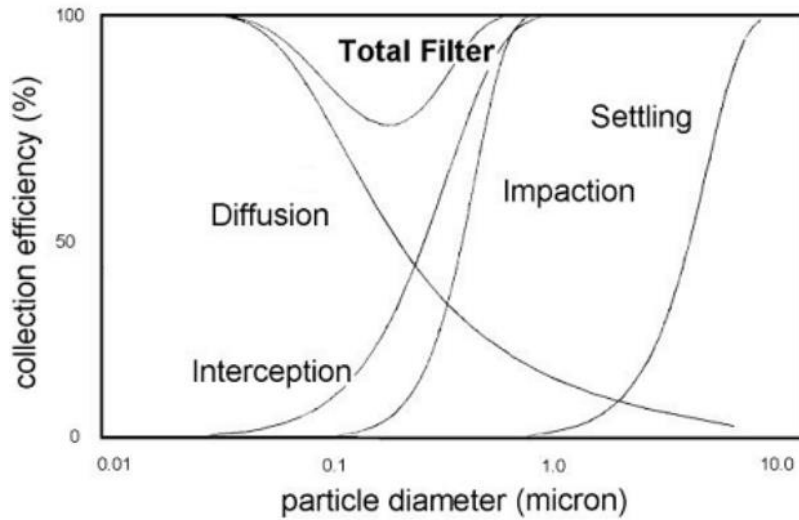


Figure 2- 43: Capture efficiency as a function of particle size for different deposition mechanisms (Hinds, 1999)

Important terms for filtration are: 1) filtration efficiency, 2) particle penetration and 3) pressure drop. The general function for measuring the filtration efficiency E is shown in the following.

$$E = \frac{N_{upstream} - N_{downstream}}{N_{upstream}} \quad \text{Eq. 2- 22}$$

where $N_{upstream}$ is the number of particles measured at the upstream (before the filter) and $N_{downstream}$ the number of particles measured at the downstream (after the filter). Particle Penetration P is defined as follows.

$$P = \frac{N_{downstream}}{N_{upstream}} = 1 - E \quad \text{Eq. 2- 23}$$

According to Brown (R. C. Brown, 1993, p. 5), penetration is the correct measure for quantifying the performance of high efficiency filtration media.

The pressure drop ΔP describes the resistance to the airflow because of frictional forces (Wakeman & Tarleton, 1999, p. 88; Y. Zhang, 2004, p. 290). The higher the resistance of the filter the more force and therefore energy is required to push the suspension through the filter. The general expression for the pressure drop ΔP of a structure can be seen in the following.

$$\Delta P = P_1 - P_2 \text{ [Pa]} \quad \text{Eq. 2- 24}$$

where P_1 is the pressure [Pa] before and P_2 the pressure [Pa] after the medium.

The quality factor (or q-factor) is a dimensionless number describing the performance of a filter by taking both particle penetration and pressure drop into consideration. The equation for calculating the quality factor QF of a filter can be seen in the following.

$$QF = \frac{-\ln(P)}{\Delta p} [Pa^{-1}] \quad \text{Eq. 2- 25}$$

where P the particle penetration and Δp the pressure drop [Pa] (R. C. Brown, 1993, p. 9).

2.4.2 Filtration Theory

The so-called single fiber theory is one way to explain, estimate and theoretically calculate the efficiency of filters. The theory allows calculation of the different deposition mechanisms for a single fiber perpendicular positioned to the flow field (Hinds, 1999, p. 190). It further assumes particles to be deposited after touching the fiber.

Per definition, single fiber efficiency is the ratio of the number of particles collected by the fiber to the number of particles that would have been collected with straight

streamlines. If all particles of a diameter y are captured by a fiber having the diameter d_f then the single fiber efficiency η_{fiber} is the following.

$$\eta_{fiber} = \frac{y}{d_f} \quad \text{Eq. 2- 26}$$

where y is the width of the stream at a certain distance [m] and d_f is the diameter of the fiber [m] (Liu & Liptak, 1997, p. 344; Ramachandran, 2005).

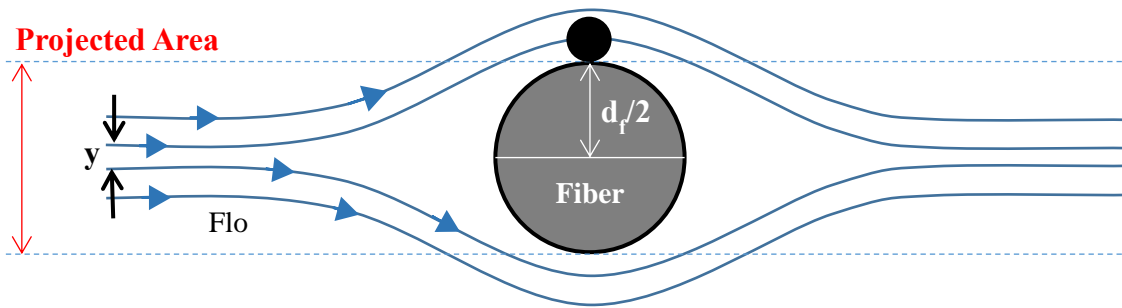


Figure 2- 44: Principle of the single fiber theory

The Reynolds number gives information about the flow around fibers, i.e. if the flow is turbulent (inertial forces are dominant) or laminar (viscous forces are dominant). Reynolds number Re can be calculated as follows.

$$Re = \frac{\rho v L}{\mu} \quad \text{Eq. 2- 27}$$

where ρ is the specific density of the fluid [kg m^{-3}], v the velocity of the fluid [m s^{-1}], L the characteristic length [m] and μ is the dynamic viscosity of the fluid [Kg m s^{-1}].

Assuming a process at $T = 20^\circ\text{C}$, specific density of air ρ_{air} would be 1.2 kg m^{-3} and the dynamic viscosity μ_{air} $1.84 \times 10^{-5} \text{ Kg ms}^{-1}$ kg. Assuming the velocity to be

$f_v = 0.0533 \text{ m s}^{-1}$ and the characteristic length L to be the diameter of the fiber $d_f = 15 \text{ }\mu\text{m}$, Re of ~ 0.05 indicates the flow around the fiber to be laminar.

In single fiber theory total efficiency $E_{Theoretical}$ of the filter can be predicted as follows.

$$E_{Theoretical} = 1 - \exp\left(\frac{-4\alpha\eta_{fiber}t}{\pi d_f}\right) \quad \text{Eq. 2- 28}$$

where α is the solid volume fraction of the material, η_{fiber} is the single fiber efficiency, t is the thickness [μm] and d_f is the fiber diameter [μm].

Equation assumes the flow to be uniform and the particles to be well-mixed (Liu & Liptak, 1999, p. 121). Total single fiber efficiency η_{fiber} assumes all mechanisms to act independently and can be calculated by using the following equation.

$$\eta_{fiber} = 1 - (1 - \eta_I)(1 - \eta_D)(1 - \eta_R) \quad \text{Eq. 2- 29}$$

where η_I is the single fiber efficiency due to inertial impaction, η_D is the single fiber efficiency due to Brownian Diffusion and η_R is the single fiber efficiency due to interception (Hinds, 1999, p. 196; Liu & Liptak, 1997, p. 344).

As fibrous structures contain numerous fibers flow can't be considered as ideal as adjacent fibers are influencing the stream. Kuwabara's cell model, which is a solution of the Navier-Stokes equation for viscous flow, considers that by assuming the filter to be a construct of parallel aligned fibers perpendicular to the flow. It also assumes the flow to be continuous, which is explained by the Knudsen number (Raber & Johnston, 1986, p. 84; Spurny, 1998, p. 55). The fiber Knudsen number Kn allows predicting the gas flow region and can be calculated as follows.

$$Kn = \frac{2\lambda}{d_f} \quad \text{Eq. 2- 30}$$

where λ is the mean free path [nm], which describes the average distance a molecule can travel between collisions, and d_f is the fiber diameter d_f [nm].

Four different regimes can prevail depending on λ and d_f , which are: 1) free molecular regime ($Kn > 10$), transient regime ($10 > Kn > 0.25$), slip flow regime ($0.25 > Kn > 0.001$) and the continuum flow regime ($Kn < 0.001$) (Tipler & Mosca, 2008, p. 578; Wang, 2007, p. 32).

Darcy's law can be used to estimate the dimensionless pressure drop ΔP of a filter with continuous flow by using following equation.

$$\frac{\Delta P}{v} = \frac{\mu t f(\alpha)}{d_f^2} \quad \text{Eq. 2- 31}$$

where μ is the dynamic viscosity of the fluid [Kg ms^{-1}], t is the thickness [m], $f(\alpha)$ is a dimensionless function relating the pressure drop to the material's density and d_f the fiber diameter [m] (R. C. Brown, 1993, p. 33; Mercer, 2012, p. 125; Wang, 2007, p. 33).

As can be seen from the equation, pressure drop is a function of the face velocity and also the fiber diameter. Literature provides different estimations for the dimensionless function $f(\alpha)$, depending on the flow regime and density of the medium. For fibrous materials with a solid volume fraction $\alpha < 0.3$ Davies introduced the following.

$$f(\alpha) = 64\alpha^{1.5}(1 + 56\alpha^3) \quad \text{Eq. 2- 32}$$

and thus,

$$\Delta P = \frac{\mu t v (64^{1.5} (1 + 56 \alpha^3))}{d_f^2}$$

Eq. 2- 33

where α is the solid volume fraction of the medium (Gervais, Bardin-Monnier et al., 2012; Wang, 2007, p. 34).

2.5 References

- Adanur, S. (1995). *Wellington Sears handbook of industrial textiles*: CRC Press.
- Albrecht, W., Fuchs, H. & Kittelmann, W. (2006). *Nonwoven fabrics: raw materials, manufacture, applications, characteristics, testing processes*: John Wiley & Sons.
- Anand, S. C., Kennedy, J. F., Miraftab, M. & Rajendran, S. (2010). *Medical and healthcare textiles*: Elsevier.
- Anantharamaiah, N. (2006). *An investigation of the influence of nozzle geometry in the hydroentangling process*.
- Anantharamaiah, N., Durany, A. & Pourdeyhimi, B. (2009). High surface area nonwovens via fibrillating spunbonded nonwovens comprising Islands-in-the-Sea bicomponent filaments: structure–process–property relationships. *Journal of materials science*, 44(21), 5926-5934.
- Anantharamaiah, N., Römpert, K., Tafreshi, H. V. & Pourdeyhimi, B. (2007). A novel nozzle design for producing hydroentangled nonwoven materials with minimum jet-mark defects. *Journal of materials science*, 42(15), 6161-6170.
- Anantharamaiah, N., Tafreshi, H. V. & Pourdeyhimi, B. (2006). Numerical simulation of the formation of constricted waterjets in hydroentangling nozzles: effects of nozzle geometry. *Chemical Engineering Research and Design*, 84(3), 231-238.
- Anantharamaiah, N., Tafreshi, H. V. & Pourdeyhimi, B. (2006). A study on flow through hydroentangling nozzles and their degradation. *Chemical Engineering Science*, 61(14), 4582-4594.
- Anantharamaiah, N., Tafreshi, H. V. & Pourdeyhimi, B. (2007). A simple expression for predicting the inlet roundness of micro-nozzles. *Journal of Micromechanics and Microengineering*, 17(5), N31.
- Anantharamaiah, N., Verenich, S. & Pourdeyhimi, B. (2008). Durable nonwoven fabrics via fracturing bicomponent islands-in-the-sea filaments. *Journal of Engineered Fibers and Fabrics*, 3(3), 1-9.
- Aulton, M. E. & Taylor, K. M. (2013). *Aulton's pharmaceuticals: the design and manufacture of medicines*: Elsevier Health Sciences.
- Baird, D. G. & Collias, D. I. (2014). *Polymer processing: principles and design*: John Wiley & Sons.

- Baker, B. (1998). Bicomponent fibers: a personal perspective. *International Fiber Journal*, 13(3), 26-35.
- Bartels, V. (2011). *Handbook of medical textiles*: Elsevier.
- Batra, S. K. & Pourdeyhimi, B. (2012a). *Introduction to nonwovens technology*: DEStech Publications, Inc.
- Batra, S. K. & Pourdeyhimi, B. (2012b). Introduction to nonwovens technology. Retrieved September 24, 2014, from http://www.textileworld.com/Issues/2012/May-June/Nonwovens-Technical_Textiles/Introduction_To_Nonwovens_Technology
- Baukal, C. E. (2001). *The John Zink Combustion Handbook*: Taylor & Francis.
- Begenir, A. (2003). *The role of orifice design in hydroentanglement*. (MS - Textile and Apparel, Technology and Management), North Carolina State University.
- Begenir, A., Tafreshi, H. V. & Pourdeyhimi, B. (2004). Effect of nozzle geometry on hydroentangling water jets: Experimental observations. *Textile Research Journal*, 74(2), 178-184.
- Berins, M. (1991). *Plastics engineering handbook of the society of the plastics industry*: Springer Science & Business Media.
- Bouchette, M. P. (2000). US Patent No. US6110848 A.
- Breen, A. L. (1958). US Patent No. US2861319 A.
- Brown, K. L. & Shelley, J. D. (2003). Multilayer approach to producing homofilament crimp spunbond: Google Patents.
- Brown, R. C. (1993). *Air filtration: an integrated approach to the theory and applications of fibrous filters*: Pergamon.
- Burton, S. J., Carbonell, R. G., Gurgel, P. V. & Zheng, Y. (2012). High-surface area fibers and nonwoven membranes for use in bioseparations: Google Patents.
- Butler, I., Medeiros, F. J. & Turi, M. (2002). *Hydroentangling technology primer: capabilities and end-uses, market outlook, manufacturing process*: INDA, Association of the Nonwoven Fabrics Industry.
- Butt, H.-J., Graf, K. & Kappl, M. (2006). *Physics and chemistry of interfaces*: John Wiley & Sons.

- Chanda, M. (2013). *Introduction to Polymer Science and Chemistry: A Problem-Solving Approach*: CRC Press.
- Chapman, R. (2010). *Applications of nonwovens in technical textiles*: Elsevier.
- Chapman, R. (2012). *Smart textiles for protection*: Elsevier.
- Chappas, W. & Pourdeyhimi, B. (2013). US Patent No. US8410006 B2.
- Chatterjee, P. K. & Gupta, B. S. (2002). *Absorbent technology* (Vol. 13): Elsevier.
- Cheng, S. Z. (2008). *Phase transitions in polymers: the role of metastable states: the role of metastable states*: Elsevier.
- Cheryan, M. (1998). *Ultrafiltration and Microfiltration Handbook*: Taylor & Francis.
- Clean Indian Journal. (2011). Sustainable non-woven market. Retrieved Nov 01, 2014, from <http://www.cleanindiajournal.com/monsoon-mats-maintenance/>
- Connolly, T. & Parent, L. (1993). Influence of specific energy on the properties of hydroentangled nonwoven fabrics. *Tappi journal*, 76(8), 135-141.
- Contractor, R. M. & Kirayoglu, B. (1978). US Patent No. US4069563 A.
- Cramariuc, B., Cramariuc, R., Scarlet, R., Manea, L. R., Lupu, I. G. & Cramariuc, O. (2013). Fiber diameter in electrospinning process. *Journal of Electrostatics*, 71(3), 189-198.
- Crittenden, J. C., Trussell, R. R., Hand, D. W., Howe, K. J. & Tchobanoglous, G. (2012). *MWH's Water Treatment: Principles and Design: Principles and Design*: John Wiley & Sons.
- Crowe, C. T. (2014). *Multiphase flow handbook*: CRC press.
- Dabiri, S., Sirignano, W. & Joseph, D. (2007). Cavitation in an orifice flow. *Physics of Fluids (1994-present)*, 19(7), 072112.
- Dahiya, A., Kamath, M. G. & Hedge, R. R. (2004a). Spunlace (Hydroentanglement). Retrieved Oct 10, 2014, from <http://www.engr.utk.edu/mse/Textiles/Spunlace.htm>
- Dahiya, A., Kamath, M. G. & Hedge, R. R. (2004b). Wet-Laid Nonwovens. Retrieved from: <http://www.engr.utk.edu/mse/Textiles/Wet%20Laid%20Nonwovens.htm>
- Dahiya, A., Kamath, M. G. & Hedge, R. R. (2014). Spunbond Technology. Retrieved Oct 31, 2014, from <http://www.engr.utk.edu/mse/Textiles/Spunbond%20Technology.htm>

- Das, D. & Pourdeyhimi, B. (2014). *Composite Nonwoven Materials: Structure, Properties and Applications*: Elsevier Science.
- Dasdemir, M. (2011). *Investigating Polymer Interface and Its Influence on Bicomponent Nonwoven Structures for Thermoplastic Composites*. (Ph.D. - Fiber and Polymer Science), North Carolina State University.
- Davey, A. J. & Diba, A. (2012). *Ward's Anaesthetic Equipment*: Elsevier Health Sciences UK.
- Delucia, M. L., Hudson, R. L., Kobylivker, P. M., Ofosu, S. K. & Sayovitz, J. J. (2003). High strength spunbond fabric from high melt flow rate polymers: Google Patents.
- Deopura, B., Alagirusamy, R., Joshi, M. & Gupta, B. (2008). *Polyesters and polyamides*: Elsevier.
- Department of the Environment and Heritage. (2005). What are particles? Retrieved November 22, 2014, from <http://www.environment.gov.au/resource/particles>
- Dixon, M. D., Lowder, J. T., Behnam, P. & Tafreshi, H. V. (2005). US Patent No. US7237308 B2.
- EAM Corporation. (n.d.). Airlaid Nonwoven Technology. Retrieved from: <http://www.eam-corp.com/news/AirlaidNonwovenTechnologyOverview.pdf>
- EDANA. (2014). Nonwoven production exceeded 2 million tonnes in 2013 in Greater Europe. Retrieved Oct 13, 2014, from <http://www.edana.org/newsroom/news-announcements/2014/03/31/nonwoven-production-exceeded-2-million-tonnes-in-2013-in-greater-europe>
- EDANA. (n.d.). What are Nonwovens? Retrieved September 25, 2014, from <http://www.edana.org/discover-nonwovens/what-are-nonwovens-/>
- Edmond, P. (1932). US Patent No. US1856401 A.
- Eichhorn, S., Hearle, J. W. S., Jaffe, M. & Kikutani, T. (2009). *Handbook of Textile Fibre Structure: Fundamentals and Manufactured Polymer Fibres*: Elsevier Science.
- Elaissari, A. (2003). *Colloidal polymers: synthesis and characterization* (Vol. 115): CRC Press.
- Elias, H. G. (2013). *Macromolecules: Volume 1 · Structure and Properties / Volume 2 · Synthesis and Materials*: Springer US.

- Ewsuk, K. (2007). *Characterization and Control of Interfaces for High Quality Advanced Materials II* (Vol. 2): John Wiley & Sons.
- Fan, J. & Hunter, L. (2009). *Engineering apparel fabrics and garments*: Elsevier.
- Fedorova, N. (2006). *Investigation of the utility of islands-in-the-sea bicomponent fiber technology in the spunbond process, 2006*. (Ph.D. - Fiber and Polymer Science), North Carolina State University.
- Fleissner, G. (2000). US Patent No. US6012654 A.
- Fleissner GmbH. (2008). Hydroentanglement Systems. Retrieved Oct 20, 2014, from http://www.manichylla.com/Documentos/FLEISSNER_Instalaciones%20de%20hidroligado%20AquaJet_E.pdf
- Fleming, J. D. (1999). *Capillary Rheometry*. Paper presented at the Polymer Rheology '99, Shawbury, Shrewsbury, Shropshire, UK.
- Frankland, J. (2011). How Much L/D Do You Really Need? Retrieved October 7, 2014, from <http://www.ptonline.com/columns/how-much-ld-do-you-really-need>
- Freedonia. (2013). Nonwovens to 2016 - Demand and Sales Forecasts, Market Share, Market Size, Market Leaders. Retrieved Sep 25, 2014, from <http://www.freedoniagroup.com/Nonwovens.html>
- Gahide, S. F. (1999). Combination of hydroentanglement and foam bonding technologies for wood pulp and polyester fibers in wet lay nonwoven fabrics.
- Gates, B. C. & Jentoft, F. C. (2013). *Advances in Catalysis*: Elsevier Science.
- Gervais, P.-C., Bardin-Monnier, N. & Thomas, D. (2012). Permeability modeling of fibrous media with bimodal fiber size distribution. *Chemical Engineering Science*, 73, 239-248.
- Geus, H. G. & Klunier, H. B. (2009). US Patent No. US20090026647 A1.
- Ghassemieh, E., Acar, M. & Versteeg, H. (2001). Improvement of the efficiency of energy transfer in the hydro-entanglement process. *Composites Science and Technology*, 61(12), 1681-1694.
- Giles, H. F., Wagner, J. R. & Mount, E. M. (2013). *Extrusion: The Definitive Processing Guide and Handbook*: Elsevier Science.

- Gillespie, J. D., Kong, D. D. & Alexander, R. C. (2011). Spunbond nonwoven fabrics from reclaimed polymer and the manufacture thereof: Google Patents.
- Goddard III, W. A., Brenner, D., Lyshevski, S. E. & Iafrate, G. J. (2007). *Handbook of nanoscience, engineering, and technology*: CRC press.
- Godish, T. (1989). *Indoor air pollution control*: CRC Press.
- Gordon, S. & Hsieh, Y.-I. (2006). *Cotton: science and technology*: Woodhead Publishing.
- Greenway, J. M., Schortmann, W. E., Mancini, P., Metrick, D. & Connolly, T. (1990). Apparatus for producing symmetrical fluid entangled non-woven fabrics and related method: Google Patents.
- Gregor, E. C. (2003). Primer on nonwoven fabric filtration media. *Edward C. Gregor & Associates*.
- Groz-Beckert KG. (2011). Hydroentangling with Jetstrips - The full Power of Water. Retrieved Oct 13, 2014, from https://www.groz-beckert.com/cms/en/news/newsletter/last_issue/getPrm/letter/n1_hydroentanglement_with_jetstrips/
- Groz-Beckert KG. (2012). HyTec® The jet strip from Groz-Beckert for hydroentanglement systems Retrieved Oct 20, 2014, from <http://www.groz-beckert.de/home/getFileCh.php?chbid=36&lang=en&file=content&download=true>
- Groz-Beckert KG. (n.d.). Jet Strips. Retrieved Oct 26, 2014, from https://www.groz-beckert.com/cms/en/products_services/felting/product_range/jet_strips/
- Gupta, B. (2008). *Friction in textile materials*: Elsevier.
- Gupta, B. & Kothari, V. (1997). *Manufactured fibre technology*: Springer Science & Business Media.
- Hagen, C. A. (2002). *Feltmaking: Fabulous Wearables, Jewelry & Home Accents*: Lark Books.
- Hagewood, J. (2004, September 20-23, 2004). *Properties study of new bico spunbond and meltblown barrier fabrics*. Paper presented at the INTC 2004, Toronto.
- Hagewood, J. (n. d.). Splitting Bicomponent Fibers in Spunbond Fabrics Retrieved Oct 13, 2014, from <http://www.hillsinc.net/assets/pdfs/splitting-bicomponent-fibers-spunbond-fabrics.pdf>

- Hagewood, J. (n.d.). Ultra microfibers: beyond evolution. Retrieved Nov 14, 2014, from <http://www.hillsinc.net/assets/pdfs/ultra-microfibers.pdf>
- Hagewood, J. & Wilkie, A. (n. d.). Production of Sub-micron Fibers in Non-Woven Fabrics. Retrieved Oct 10, 2014, from <http://www.hillsinc.net/assets/pdfs/production-submicron.pdf>
- Hamrang, A. (2014). *Advanced Non-Classical Materials with Complex Behavior: Modeling and Applications*: Apple Academic Press.
- Han, C. D. (2007). *Rheology and processing of polymeric materials* (Vol. 2): Oxford University Press New York.
- Harburg-Freudenberger Maschinenbau GmbH. (n.d.). Compact Rubber Extruder - Degassing Screw Design. Retrieved from: <http://www.hf-tiretechgroup.com/downloads/docs/defa96106f1e0f25d6ef746f5e0a167a>
- Hassan, M. A., Yeom, B. Y., Wilkie, A., Pourdeyhimi, B. & Khan, S. A. (2013). Fabrication of nanofiber meltblown membranes and their filtration properties. *Journal of Membrane Science*, 427, 336-344.
- Hedge, R. R., Dahiya, A. & Kamath, M. G. (2004). Bicomponent fibers. Retrieved November 8, 2014, from <http://www.engr.utk.edu/mse/Textiles/Bicomponent%20fibers.htm>
- Hequet, E., Abidi, N. & Gourolot, J. (1998). Application of methylene blue adsorption to cotton fiber specific surface area measurement: Part 1 methodology. *J. of Cotton Science*, 2, 164-173.
- Hill, J. W. & Carothers, W. H. (1932). Studies of polymerization and ring formation. XIV. A linear superpolyanhydride and a cyclic dimeric anhydride from sebacic acid. *Journal of the American Chemical Society*, 54(4), 1569-1579.
- Hills Inc. (2013). Lab Scale Bicomponent Extruder Fed Spinning Machine Model LBS. Retrieved from: <http://www.hillsinc.net/brochures/lbs-brochure.pdf>
- Hills Inc. (n.d.-a). Hills nano-technology. Retrieved Nov 14, 2014, from <http://www.hillsinc.net/assets/pdfs/nano-fibers.pdf>
- Hills Inc. (n.d.-b). An introduction to bicomponent fibers. Retrieved November 7, 2014, from <http://www.hillsinc.net/assets/pdfs/introduction-bicomponent-fiber.pdf>
- Hills, W. H. (1992). US Patent No. US5162074 A.

- Hinds, W. C. (1999). *Aerosol Technology: Properties, Behavior, and Measurement of Airborne Particles* (Vol. 2nd Edition): John Wiley & Sons, Inc.
- Hong, W., Lianshun, P., Xiangyu, J., Baopu, Y. & Haibo, W. (2010). The Influences of Hydrophilic Finishing of PET Fibers on the Properties of Hydroentangled Nonwoven Fabrics. *Measurements*, 3, 60.
- Horrocks, A. R. & Anand, S. C. (2000). *Handbook of technical textiles*: Elsevier.
- Houck, M. M. (2009). *Identification of textile fibers*: Elsevier.
- Hunter, D. (1978). *Papermaking: the history and technique of an ancient craft*: Courier Corporation.
- Hutten, I. M. (2007). *Handbook of nonwoven filter media*: Elsevier.
- Hwang, S. H. (1985). US Patent No. US4514455 A.
- Ibeh, C. C. (2011). *Thermoplastic Materials: Properties, Manufacturing Methods, and Applications*: Taylor & Francis.
- INDA (Association of the Nonwoven Fabric Industry). (2002). INDA Nonwovens Glossary. Retrieved from: <http://www.inda.org/Glossary.pdf>
- INDA (Association of the Nonwoven Fabric Industry). (n.d.-a). About Nonwovens - What is Nonwoven Fabric. Retrieved September 24, 2014, from <http://www.inda.org/about-nonwovens/>
- INDA (Association of the Nonwoven Fabric Industry). (n.d.-b). Spunbond and Melt Blown Technology. Retrieved October 1, 2014, from <http://www.inda.org/spunbond-melt-blown.html>
- INDA (Association of the Nonwoven Fabric Industry). (n.d.-c). Spunlace Bonded Nonwovens (Hydroentangling). Retrieved Oct 10, 2014, from <http://www.inda.org/hydroentangling.html>
- INDEX 11. (2010). INDEX 11 - We have the Technology.... Retrieved October 7, 2014, from <http://www.index11.ch/en/news/id-0-219>
- Ishiyama, S. & Yamada, J. (2000). US Patent No. US6063717 A.
- Jaganathan, S., Tafreshi, H. V. & Pourdeyhimi, B. (2008). The influence of forming surface on the vacuum pressure in hydroentangling process. *Journal of the Textile Institute*, 99(5), 407-414.

- Kalinová, K. (n. d.,). Thermal and Chemical Technologies of Nonwoven Production 1/2. Retrieved October 7, 2014, from https://nanoed.tul.cz/pluginfile.php/1016/mod_resource/content/1/tct%201.pdf
- Kanigel, R. (2011). *Faux real: genuine leather and 200 years of inspired fakes*: University of Pennsylvania Press.
- Keiichi, A., Miyoshi, O., Shinzo, T. & Koji, W. (1972). US Patent No. US3692423 A.
- Kent, J. A. (2010). *Kent and Riegel's Handbook of Industrial Chemistry and Biotechnology: Vol. 1*: Springer Science & Business Media.
- Kent, R. J. (1998). *Plastics Profile Extrusion* (Vol. 104): iSmithers Rapra Publishing.
- Kirayoglu, B. & Zafiroglu, D. P. (1984). US Patent No. US4442161 A. U.S. Patent and Trademark Office.
- Koslowski, H. (2009). Man-Made Fibres Congress: Dornbirn Austria:16-18th Sept 2009. Retrieved September 9th, 2014
- Kulkarni, P., Baron, P. A. & Willeke, K. (2011). *Aerosol measurement: principles, techniques, and applications*: John Wiley & Sons.
- Kumar, R. S. (2013). *Textiles for industrial applications*: CRC Press.
- Lagarón, J. M. (2011). *Multifunctional and Nanoreinforced Polymers for Food Packaging*: Elsevier Science.
- Lampman, S. (2003). *Characterization and failure analysis of plastics*: ASM International.
- Lannan, G. M. (1939). US Patent No. US2165280 A.
- Lawrence, C. A. (2003). *Fundamentals of spun yarn technology*: CRC Press.
- Lenzing AG. (1968). Lenzinger Berichte - Folge 26. Retrieved September 24, 2014, from http://www.lenzing.com/fileadmin/template/pdf/konzern/lenzinger_berichte/ausgabe_26_1968/LB-0261968150.pdf
- Lewin, M. (2006). *Handbook of fiber chemistry*: Crc Press.
- Lewin, M. & Preston, J. (1996). *Handbook of fiber science and technology volume 3: high technology fibers*: Taylor & Francis.
- Liu, D. H. F. & Liptak, B. G. (1997). *Environmental engineers' handbook*: CRC Press.
- Liu, D. H. F. & Liptak, B. G. (1999). *Air Pollution*: Taylor & Francis.

- LTA Lufttechnik GmbH. (n.d.). Air purification basics. Retrieved November 22, 2014, from <http://www.lta.de/en/luftfilter/filtertechnik/grundlagen-der-luftreinigung.php>
- Madihally, S. V. (2010). *Principles of Biomedical Engineering*: Artech House.
- Maier, C. & Calafut, T. (2008). *Polypropylene: the definitive user's guide and databook*: Taylor & Francis.
- Majumdar, A., Das, A., Alagirusamy, R. & Kothari, V. (2012). *Process control in textile manufacturing*: Elsevier.
- Mansfield, R. G. (2004). H2O Tricks. Retrieved Oct 15, 2014, from <http://www.textileworld.com/Issues/2004/February/Nonwovens-Technical Textiles/H2O Tricks>
- Mao, N. & Russel, S. (2005). Structure–process–property relationships of hydroentangled nonwovens. *Lenzinger Berichte*, 84, 50-61.
- Mao, N. & Russell, S. (2006). A framework for determining the bonding intensity in hydroentangled nonwoven fabrics. *Composites Science and Technology*, 66(1), 80-91.
- Medeiros, E. S., Glenn, G. M., Klamczynski, A. P., Orts, W. J. & Mattoso, L. H. (2009). Solution blow spinning: A new method to produce micro-and nanofibers from polymer solutions. *Journal of Applied Polymer Science*, 113(4), 2322-2330.
- Mercer, T. (2012). *Aerosol technology in hazard evaluation*: Elsevier.
- Mogahzy, E. Y. (2008). *Engineering textiles: integrating the design and manufacture of textile products*: Elsevier.
- Mogul Tekstil Sanayi ve Ticaret Ltd.Sti. (n.d.). Production Processes. Retrieved Oct 20, 2014, from <http://www.mogulsb.com/production-processes-22-4.html>
- Möschler, W., Meyer, A. & Brodtka, M. (1995). Influences of fibre and process on the properties of spunlaced fabrics. *Int Tetx Bull Nonwovens Ind Text*, 41(2), 4.
- Moyo, D. & Anandjiwala, R. D. (2013). Studies on waterjet impact forces in the hydroentanglement process. *Textile Research Journal*, 0040517513478452.
- Moyo, D., Patnaik, A. & Anandjiwala, R. D. (2014). Optimization of energy usage in the hydroentanglement process. *Textile Research Journal*, 84(9), 913-923.
- NCRC - Nonwovens Cooperative Research Center. (2005). NCRC Newsletter. Retrieved Oct 28, 2014, from http://www.thenonwovensinstitute.com/ncrc/acrobatfiles/newsletters/may_2005.pdf.

- Ndaro, M. S., Xiangyu, J., Ting, C. & Yu, C. (2007). Effect of impact force on tensile properties and fiber splitting of splittable bicomponent hydroentangled fabrics. *Fibers and Polymers*, 8(4), 421-426.
- Norman, F. (1973). US Patent No. US3750961 A.
- Okamoto, M., Watanabe, K., Nukushina, Y. & Aizawa, T. (1970). US Patent No. US3531368 A.
- Ortega-Rivas, E. (2012). *Non-thermal food engineering operations*: Springer Science & Business Media.
- Ortiz, D. L. & Shambaugh, R. L. (2005). Melt-spun polybutylene fibers and nonwovens. *Int Nonwovens J*, 36-54.
- Patanaik, A. & Anandjiwala, R. D. (2010). Hydroentanglement nonwoven filters for air filtration and its performance evaluation. *Journal of Applied Polymer Science*, 117(3), 1325-1331.
- Pohl, G. (2010). *Textiles, polymers and composites for buildings*: Elsevier.
- Pourdeyhimi, B. (2005). US Patent No. US20050125908 A1.
- Pourdeyhimi, B. (2011a). Durable Nonwovens. Retrieved November 18, 20[4], from [http://www.textileworld.com/Issues/2011/May-June/Nonwovens-Technical Textiles/Durable Nonwovens](http://www.textileworld.com/Issues/2011/May-June/Nonwovens-Technical%20Textiles/Durable%20Nonwovens)
- Pourdeyhimi, B. (2011b). *A new generation of micro-denier fabrics*. Paper presented at the Innovative Nonwovens Conference, Atlanta.
- Pourdeyhimi, B., Chappas, W. & Barnes, H. M. (2013). US Patent No. US20130133980 A1.
- Pourdeyhimi, B., Minton, A. & Putnam, M. (2004). Structure-process-property relationships in hydroentangled nonwovens-part 1: preliminary experimental observations. *International Nonwovens Journal*, 13, 15-21.
- Pourdeyhimi, B., Suragani Venu, L. B., Anantharamaiah, N. & Shim, E. (2013). US Patent No. WO2013103844 A1.
- Pourdeyhimi, B. & Tafreshi, H. V. (2007a). US Patent No. US7303465 B2.
- Pourdeyhimi, B. & Tafreshi, H. V. (2007b). US Patent No. US20070226970 A1.
- Pourdeyhimi, B. & Zapletalova, T. (2004). *Wipes produced by in-line splitting of segmented pie spunbonds*. Paper presented at the INTC 2004, Toronto.

- Pourmohammadi, A., Russell, S. J. & Höffele, S. (2003). Effect of water jet pressure profile and initial web geometry on the physical properties of composite hydroentangled fabrics. *Textile Research Journal*, 73(6), 503-508.
- Purchas, D. & Sutherland, K. (2002). *Handbook of filter media*: Elsevier.
- Purolator. (n. d.). Selecting the perfect filter media for each spin pack application. Retrieved September 09, 2014, from <http://www.purolator-efp.com/Resources/Tools/Selecting-Filter-Media>
- Raber, R. R. & Johnston, P. R. (1986). *Fluid Filtration: Gas*: ASTM.
- Ramachandran, G. (2005). *Occupational Exposure Assessment for Air Contaminants*: Taylor & Francis.
- Ramakrishna, S., Fujihara, K., Teo, W.-E., Lim, T.-C. & Ma, Z. (2005). *An introduction to electrospinning and nanofibers* (Vol. 90): World Scientific.
- Reneker, D. H. & Chun, I. (1996). Nanometre diameter fibres of polymer, produced by electrospinning. *Nanotechnology*, 7(3), 216.
- Rodie, J. B. (2012). Featherweight filtration. Retrieved November 18, 2014, from www.textileworld.com/Issues/2012/September-October/Quality Fabric Of The Month/Featherweight Filtration
- Rosato, D. V., Rosato, M. G. & Rosato, D. V. (2000). *Concise encyclopedia of plastics*: Springer Science & Business Media.
- Russell, S. (2006). *Handbook of nonwovens*: Woodhead Publishing.
- Ruzer, L. S. & Harley, N. H. (2012). *Aerosols handbook: measurement, dosimetry, and health effects*: CRC press.
- Scheirs, J. & Long, T. E. (2005). *Modern polyesters: chemistry and technology of polyesters and copolyesters*: John Wiley & Sons.
- Schenk, A. K. (2014). *Study of the Impact of the Nonwoven Substrate Formation on Artificial Leather*. (MS - Textile Engineering), North Carolina State University.
- Schiffner, K. C. (2013). *Air Pollution Control Equipment Selection Guide*: CRC Press.
- Scott, R. A. (2005). *Textiles for Protection*: Elsevier Science.
- Seyam, A., Shiffler, D. & Zheng, H. (2005). An examination of the hydroentangling process variables. *International Nonwoven Journal*, 14(1), 25-33.

- Shaffer, R. E. & Rengasamy, S. (2009). Respiratory protection against airborne nanoparticles: a review. *Journal of nanoparticle research*, 11(7), 1661-1672.
- Shim, E. & Pourdeyhimi, B. (2005). A note on jet streaks in hydroentangled nonwovens. *Textile Research Journal*, 75(7), 569-577.
- Shim, E., Pourdeyhimi, B. & Latifi, M. (2010). Three-dimensional analysis of segmented pie bicomponent nonwovens. *The Journal of The Textile Institute*, 101(9), 773-787.
- Shukla, A. (2010). *Intelligent Medical Technologies and Biomedical Engineering: Tools and Applications: Tools and Applications*: Igi Global.
- Simpson, P. C. & Smith, L. M. (2001). US Patent No. US5023130 A.
- Skotheim, T. A. & Reynolds, J. (2006). *Conjugated polymers: processing and applications*. CRC, Boca Raton, 101.
- Slayter, G. & Thomas, J. H. (1940). US Patent No. US2206058 A.
- Smithers Apex. (2014). Nonwovens for Filtration Market to Grow to \$4.6 Billion by 2019. Retrieved Sep 25, 2014, from <https://www.smithersapex.com/news/2014/september/nonwovens-for-filtration-market-to-grow-to-2019>
- Smithers Pira. (n. d.). Smithers Pira News. Retrieved Nov 01, 2014, from <https://www.smitherspira.com/news>
- Spurny, K. R. (1998). *Advances in Aerosol Gas Filtration*: CRC Press.
- Stahl, J. (2010). Study of Hydroentangling of Un-bonded Tyvek Nonwoven Fabric.
- Sun, C. Q., Zhang, D., Liu, Y. & Xiao, J. (2004). Bicomponent meltblown nonwovens and fibre splitting. *Journal of industrial textiles*, 34(1), 17-26.
- Sun, N. (2014). *Structures of Needle-punched Fabrics and Needling Mechanism*. (Ph.D. - Fiber and Polymer Science), North Carolina State University.
- Suragani Venu, L. B. (2012). *A Study on Hydroentangling Mechanisms and Structures*. (Ph.D. - Fiber and Polymer Science), North Carolina State University.
- Sutherland, K. S. & Chase, G. (2011). *Filters and Filtration Handbook*: Elsevier Science.
- Tafreshi, H. V. & Pourdeyhimi, B. (2004). Simulating cavitation and hydraulic flip inside hydroentangling nozzles. *Textile Research Journal*, 74(4), 359-364.

- Takai, H. & Konishi, T. (2004). Water-disintegratable sheet and manufacturing method thereof: Google Patents.
- Tan, Z. (2014). *Air Pollution and Greenhouse Gases: From Basic Concepts to Engineering Applications for Air Emission Control*: Springer Singapore.
- Tanchis, G. (2008). *Textile Reference Book Of Nonwovens*.
- Tascan, M., Vaughn, E., Stevens, K. & Brown, P. (2011). Effects of total surface area and fabric density on the acoustical behavior of traditional thermal-bonded highloft nonwoven fabrics. *Journal of the Textile Institute*, 102(9), 746-751.
- Tascan, M. & Vaughn, E. A. (2008a). Effects of fiber denier, fiber cross-sectional shape and fabric density on acoustical behavior of vertically lapped nonwoven fabrics. *Journal of Engineered Fibers and Fabrics*, 3(2), 32-38.
- Tascan, M. & Vaughn, E. A. (2008b). Effects of total surface area and fabric density on the acoustical behavior of needlepunched nonwoven fabrics. *Textile Research Journal*, 78(4), 289-296.
- Tausif, M. & Russell, S. J. (2012). Influence of hydroentangling variables on the properties of bi-layer polyethylene terephthalate–glass fabrics. *Textile Research Journal*, 82(16), 1677-1688.
- The Nonwovens Institute. (n.d.). Non-conventionanl nonwovens. Retrieved November 18, 2014, from http://www.innovationtakesroot.com/~media/ITR2014/2014/presentations/fibers/01/Nonconventionanl-Nonwovens_Pourdeyhimi_pdf
- Tipler, P. A. & Mosca, G. (2008). *Physics for scientists and engineers*: Macmillan.
- Transparency Market Research. (2014). Nonwoven Materials & Products (Polypropylene, Polyester, Nylon and Others) Market For Disposable and Durable Applications - Global Industry Analysis, Size, Share, Growth, Trends and Forecast, 2013 - 2019. Retrieved Oct 10, 2014, from <http://www.transparencymarketresearch.com/nonwoven-materials-and-products.html>
- Ugbolue, S. C. O. (2009). *Polyolefin Fibres: Industrial and Medical Applications*: CRC.
- Vaidya, N. (2002). The Manufacturing of Wet-laid Hydroentangled Glass Fiber Composites For Industrial Applications.
- van Dyk, H. (2008). *Development of a Wood Fiber Composite using Nonwoven Textile Technology*: ProQuest.

- Van, T. J. E., Bansal, V. & Davis, M. C. (2003). Stretchable multiple component spunbond webs and a process for making: Google Patents.
- Vasile, C. (2000). *Handbook of Polyolefins, Second Edition*: Taylor & Francis.
- Vuillaume, A. M. (1991). A global approach to the economics and end-product quality of spunlace nonwovens. *Tappi journal*, 74(8), 149-152.
- Wakeman, R. J. & Tarleton, E. (1999). *Filtration: equipment selection, modelling and process simulation*: Elsevier.
- Wands, D. C. & Scott, J. L. (1998). US Patent No. US5848753 A.
- Wang, Q. (2007). *An Investigation of Aerosol Filtration via Fibrous Filters*: ProQuest.
- Ward, I. M. (1987). *Developments in Oriented Polymers—2* (Vol. 2): Springer Science & Business Media.
- Wei, Q. (2009). *Surface modification of textiles*: Elsevier.
- Wei, Q. (2012). *Functional nanofibers and their applications*: Elsevier.
- Whelan, T. (1994). *Polymer technology dictionary*: Springer Science & Business Media.
- White, C. (1990a). Hydroentanglement technology applied to wet-formed and other precursor webs. *Tappi journal*, 73(6), 187-192.
- White, C. (1990b). Hydroentanglement technology: a review and projection of markets. Retrieved from:
<http://www.thefreelibrary.com/Hydroentanglement+technology%3A+a+review+and+projection+of+markets.-a09083786>
- Widen, C. B. (1991). Forming fabrics for spunlace applications. *Tappi journal*.
- Xiang, P. (2007). *Numerical Modeling and Experimental Investigation of the Hydroentanglement Process*: ProQuest.
- Yarin, A. L., Pourdeyhimi, B. & Ramakrishna, S. (2014). *Fundamentals and Applications of Micro and Nanofibers*: Cambridge University Press.
- Yeom, B. Y. & Pourdeyhimi, B. (2011a). Aerosol filtration properties of PA6/PE islands-in-the-sea bicomponent spunbond web fibrillated by high-pressure water jets. *Journal of materials science*, 46(17), 5761-5767.

- Yeom, B. Y. & Pourdeyhimi, B. (2011b). Web fabrication and characterization of unique winged shaped, area-enhanced fibers via a bicomponent spunbond process. *Journal of materials science*, 46(10), 3252-3257.
- Zhang, D. (1995). *Fundamental investigation of the spunbonding process*. University of Tennessee, Knoxville.
- Zhang, D. (2014). *Advances in Filament Yarn Spinning of Textiles and Polymers*: Elsevier Science.
- Zhang, D., Sun, C., Beard, J., Brown, H., Carson, I. & Hwo, C. (2002). Development and characterization of poly (trimethylene terephthalate)-based bicomponent meltblown nonwovens. *Journal of Applied Polymer Science*, 83(6), 1280-1287.
- Zhang, D., Sun, C. Q. & Song, H. (2004). An investigation of fiber splitting of bicomponent meltblown/microfiber nonwovens by water treatment. *Journal of Applied Polymer Science*, 94(3), 1218-1226.
- Zhang, Y. (2004). *Indoor air quality engineering*: CRC press.
- Zhao, R. R. & Wadsworth, L. C. (2003). Attenuating PP/PET bicomponent melt blown microfibers. *Polymer Engineering & Science*, 43(2), 463-469.
- Zhao, R. R., Wadsworth, L. C., Zhang, D. & Sun, C. (2002). Polymer distribution during bicomponent melt blowing of poly (propylene)/poly (ethylene terephthalate) and its improvement. *Journal of Applied Polymer Science*, 85(14), 2885-2889.
- Zheng, H. (2003). *The impact of input energy, fiber properties, and forming wires on the performance of hydroentangled fabrics*. (Ph.D. - Fiber and Polymer Science), North Carolina State University.

CHAPTER 3

- Influence of Hydroentangling Parameters on Island-in-the-Sea Nonwoven Materials -

Part I: Effect of Jet Spacing

Sections of this chapter will be submitted for publication in a peer-reviewed journal

3.1 Abstract

Hydroentangling provides an effective way to bond nonwoven webs by means of high-pressure water jets interlocking and entangling fibers. The properties of water jet and bonding intensity depend on various parameters including jet spacing. It is defined as the distance between the nozzles and thus the water jets. In this study we investigate the effect of jet spacing on the structure and properties of spunbond poly (propylene)/poly (lactic) acid 37 island-in-the-sea (InS) nonwoven materials. Structures with identical island count, polymer ratio and basis weight were hydroentangled under the exact same conditions except jet spacing. Materials underwent a caustic soda washing to remove the sea polymer before being discharged and tested for aerosol filtration performance. Structure characteristics and properties were analyzed prior and after the caustic washing. With larger jet spacing and therefore less energy applied onto the structure materials showed lower solidities and higher air permeabilities. Filtration efficiency first decreased with larger jet spacing but then increased for jet spacing larger than 1800 μm . Thus, materials hydroentangled with less specific energy showed better filtration properties compared to structures bonded with narrow jet spacing and higher energy expenditure.

3.2 Introduction

Hydroentangling (or spunlacing, water-jet entangling, hydraulic needling) describes a mechanical bonding process using a curtain of high-velocity water jets initiating fiber-fiber interlocking and loop formation (INDA (Association of the Nonwoven Fabric Industry), n.d.; Russell, 2006, p. 255). Hydroentangling can be seen as an energy transfer process delivering

energy by the means of water jets to a fibrous material (Majumdar, Das et al., 2012, p. 286). Latter can be made from short fibers having a defined, finite length (staple fibers) or infinite length (filaments).

During hydroentangling web passes multiple stages from pre-wetting, bonding to drying. Resulting structures are characterized by their strength, soft hand as well as drapeability (Shim & Pourdeyhimi, 2005). Hydroentangling parameters influencing the final properties of the material include, among others, water pressure, belt speed, jet spacing (or nozzle-to-nozzle spacing) but also the shape and number of jets impinging the structure. In hydroentangling jets are formed in a pre-defined order by using metal plates called jet strips having holes in the micrometer range. Water jet constitution (jet constriction, break-up length etc.) depends on various conditions, such as water pressure but also the shape and quality of orifices. Hydroentangling is known to be a very cost-intensive process because of the necessity of high water pressures as well as water recycling (Moyo, 2012).

The specific energy is a commonly used measure to quantify the amount of energy carried by the water jets per unit mass (Batra & Pourdeyhimi, 2012, p. 126). Based on the kinetic energy in classical mechanics, energy carried by a single water jet \dot{E} can be estimated by the following equation.

$$\dot{E} = \frac{\pi}{8} \rho d_n^2 C_d v^3 \quad [\text{J s}^{-1}] \quad \text{Eq. 3- 1}$$

where ρ is the specific density of the fluid [Kg m^{-3}], d_n the nozzle diameter [m], C_d the discharge coefficient and v the jet velocity [m s^{-1}].

In order to calculate the kinetic energy carried by all water jets of the system \dot{E} has to be further multiplied by the number of manifolds and number of jets along the width of the

material. Thus, total energy \dot{E}_{Total} carried by all water jets of the system can be calculated as follows.

$$\dot{E}_{Total} = \left(\sum_{M=1}^n \dot{E}_M J_M \right) \times 1000^{-1} \text{ [KJ s}^{-1}\text{]} \quad \text{Eq. 3- 2}$$

where \dot{E} is the energy carried by a single water jet [J s⁻¹], n is the number of manifolds used during hydroentangling and J the number of jets per manifold. Based on that specific energy SE can be calculated by using the following equation.

$$SE = \frac{\dot{E}_{Total}}{\dot{M}} \text{ [KJ s}^{-1}\text{]} \quad \text{Eq. 3- 3}$$

where \dot{E}_{Total} is the summed energy of all jets [KJ s⁻¹] and \dot{M} is the mass flow rate of fabric [Kg s⁻¹]. Latter can be calculated as follows.

$$\dot{M} = s \times w \times v_B \text{ [Kg s}^{-1}\text{]} \quad \text{Eq. 3- 4}$$

where s is the fabric width [m], w is the basis weight of the material [g m⁻²] and v_B is the operating speed [m s⁻¹] (Pourdeyhimi, Minton et al., 2004).

Equations demonstrate jet spacing to be an important parameter in terms of energy consumption and clarify the necessity of this topic to be further investigated. Several patents and published papers mention the term jet spacing but just little is known about its influence on the structure and properties of nonwoven materials. US patent US4514455 A, titled “Nonwoven fabric for apparel insulating interliner”, claims on hydroentangled composite nonwoven interlining materials made from polyester staple fibers. Used jet spacing is mentioned to be in the range of 1.7 to 5 cm (Hwang, 1985). According to Batra et al. (Batra & Pourdeyhimi, 2012, p. 120), jet strips contain up to 1600 holes per meter, which is equivalent to a jet spacing of 600 μm. Jet spacing as low as 200 μm are mentioned in patent

US4442161 A (Kirayoglu & Zafiroglu, 1984). In another paper jet spacing was mentioned to be a critical factor in terms of potential interference between single jets. Latter could prevent the jets to maintain their constricted shape enormously affecting the energy transfer (Begenir, Tafreshi et al., 2004). Suragani studied the effect of jet spacing on fiber transfer as well as structure and properties of two-layered PA6/PET staple nonwovens. It has been conclusively shown that hydroentangling with narrow jet spacing (600 μm) and a water pressure of 100 bar results in less fiber penetration compared to structures bonded with larger jet spacing. Latter was explained by the interaction of neighboring fibers and restricted fiber mobility preventing deep fiber penetration. For higher hydroentangling pressures fiber penetration was found to be the same. Also, air permeability was reported to increase with larger jet spacing. Hydroentangling with jet spacing larger than 600 μm and pressures of 200 bar resulted in knot-like structures having higher air permeabilities and absorbency rates (Suragani Venu, 2012, p. 190).

However, there has been no literature published addressing the effect of jet spacing on bicomponent structures and filtration performance. The objective of this study is to determine the influence of jet spacing on the structure and properties of 37 island-in-the-sea nonwoven materials.

3.3 Methodology

3.3.1 Materials

Island-in-the-sea bicomponent nonwoven materials consisting of 37 islands and a fixed basis weight of 125 g m^{-2} with poly (propylene) (Braskem CP360H) as island and poly (lactic acid)

(Natureworks 6202D) as sea polymer (polymer ratio: 75 island to 25 sea) were manufactured at the Nonwovens Institute Partners facilities located at Centennial Campus, North Carolina State University. The cross-section of the island-in-the-sea fibers after meltspinning and fiber drawing can be seen in Figure 3- 3. Meltspinning was performed with a 0.5 meter Hills-Nordson spunbond line and subsequent hydroentangling with a 0.5 meter 5-manifold Fleissner Aquajet. Prior to hydroentangling webs were cold calendered and passed through a compaction roll. To study the effect of jet spacing different jet strips with same nozzle diameter, nozzle shape but different nozzle-to-nozzle spacing were used at fixed hydroentangling pressures and belt speed (see Table 3- 1). All webs were hydroentangled from face side with a total of five manifolds. After bonding materials were dried in a conveyor oven and rolled up. Figure 3- 2 shows a schematic of a jet strip along with a clarification of jet spacing (a) and nozzle diameter (b).

Table 3- 1: Structures and hydroentangling parameters

Fabric ID	Jet Spacing [μm]	Hydroentangling Pressure [bar]	Belt Speed [m min^{-1}]
3.-37-600-125	600	20 (Manifold 1)	10
3.-37-1200-125	1200	150 (Manifold 2)	
3.-37-1800-125	1800	200 (Manifold 3)	
3.-37-2400-125	2400	225 (Manifold 4)	
3.-37-4800-125	4800	225 (Manifold 5)	

Figure 3- 1 depicts the applied specific energy for all jet spacing during hydroentangling, which was calculated based on Eq. 3- 1 - Eq. 3- 4.

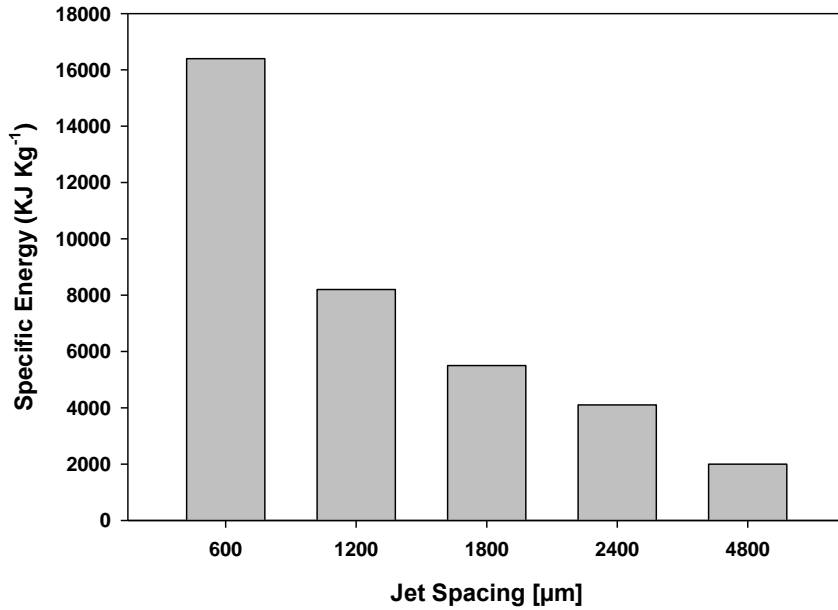


Figure 3- 1: Calculated specific energy

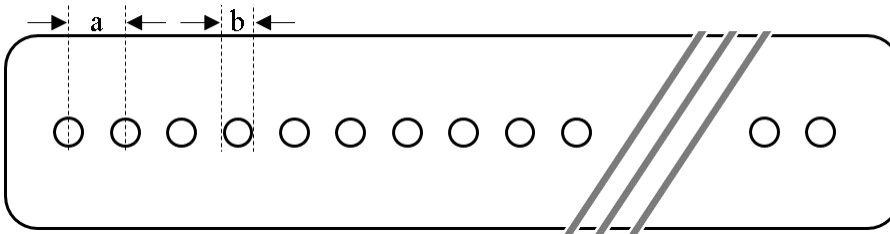


Figure 3- 2: Schematic of a hydroentangling jet strip (\rightarrow not true to scale)

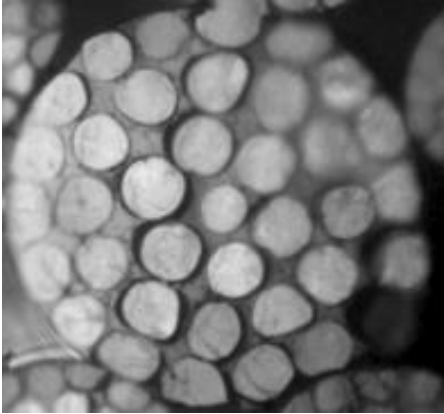


Figure 3- 3: Cross-sectional image of a drawn poly (propylene)/poly (lactic acid) 37 InS fiber

3.3.2 Sample Preparation

Bonded nonwoven materials were washed in a caustic soda solution to remove the poly (lactic acid) compound from the bicomponent fibers unveiling island fiber with smaller diameters. Sodium hydroxide-based solution was prepared in a steam kettle with a concentration of 8% w/w and temperature of 100 °C. Samples were washed for 10 min under continuous stirring before being drained, washed with cold water until pH neutralization and air-dried.

3.3.3 Characterization Methods

Basis Weight and Thickness

In order to measure basis weight and gravimetrically monitor the removal of poly (lactic acid), unit area mass of 10 replicates were measured by using a Denver Instrument XL-3100D top-loading balance prior and after the caustic treatment. Thickness was measured by using a hanatek FT3V-LAB high-precision thickness gauge.

Solid Volume Fraction (SVF)

Solidity (solid volume fraction) α was calculated by using the following equation.

$$\alpha = \frac{w}{\rho_f \times t} \quad \text{Eq. 3- 5}$$

where w is the basis weight [g m^{-2}], ρ_f the total fiber density [g m^{-3}] and t the thickness of the structure [m]. Total fiber density ρ_f is calculated as follows.

$$\rho_f = (\rho_{island} \times R_i) + (\rho_{sea} \times R_s) \text{ [g cm}^{-3}\text{]} \quad \text{Eq. 3- 6}$$

where ρ_{island} is the density of the island polymer [g cm^{-3}], R_i is the mass fraction of island polymer ρ_{sea} is the density of the sea polymer [g cm^{-3}] and R_s is the mass fraction of sea polymer.

Fiber Diameter Measurements

Fiber diameter of both unwashed and caustic-treated structure was determined by examining SEM images taken with a Phenom G2 Pro Desktop SEM unit. ImageJ was used to measure a total 100 fiber diameters of the unwashed material (10 images, 10 measurements each) and fiber distribution was determined. In addition, mean fiber diameter of islands was calculated based on random measurements of the intact bico-fiber and predicted by using the following equation.

$$d_{f,s,t} = d_f \sqrt{\frac{vol_i}{N}} \text{ [}\mu\text{m]} \quad \text{Eq. 3- 7}$$

where d_f is the diameter of the intact island-in-the-sea fiber [μm], vol_i is the volume fraction of the island polymer and N is the island count. Volume fraction of island polymer vol_i was

calculated from the mass fraction R_i , which was obtained from the metering pump during spunbond process. Volume fraction vol_i was determined by using the following equation.

$$vol_i = \frac{R_i \times \rho_i}{(R_i \times \rho_i) + (R_s \times \rho_s)} \quad \text{Eq. 3- 8}$$

where R_i is the mass fraction of island polymer, ρ_i is the specific density of the island polymer [g cm^{-3}], R_s is the mass fraction of sea polymer and ρ_s is the specific density of the sea polymer [g cm^{-3}].

Optical Analysis

SEM images of as-received and caustic soda treated samples were taken by using a Phenom G2 Pro Desktop SEM unit. To increase conductivity samples were Au/Pd sputter-coated prior image capturing. SEM images were taken at different magnifications to investigate the effect of washing and fiber spreading.

Jet Streak Analysis

Bonding with high-pressurized water jets causes the nonwoven web to deform and have depressions with pre-defined spacing in between. Depressions are designated as ridges or jet streaks and their intensity can be analyzed by a technique using image capturing and co-occurrence methods (Shim & Pourdeyhimi, 2005). The setup shown in Figure 3- 4 was used to capture macro images of specimens. Intensity of jet streaks was studied for unwashed and caustic-treated structures hydroentangled with 600 μm , 1800 μm and 4800 μm jet spacing.

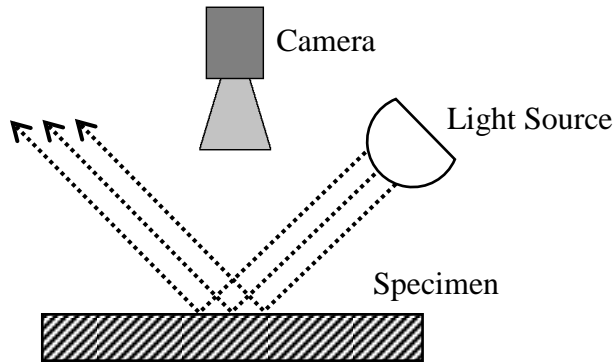


Figure 3- 4: Schematic of dark-field illumination image capturing

By illuminating specimens not perpendicular to the sample dark field illumination allows capturing jet streaks. By aligning the camera perpendicular to the surface of the sample lens is not exposed to direct light illumination. Image processing software was used to convert images to gray scale and histogram equalization to enhance the contrast. By means of spatial co-occurrence pixel pairs were examined in terms of gray intensity and pixel distance. This information was used to explain the intensity of jet streaks (Shim & Pourdeyhimi, 2005).

Air Permeability

Air permeability of caustic-treated samples was investigated according to ASTM D737 by using a TEXTTEST FX 3300. A total of 10 replicates per sample were tested.

Aerosol Filtration Properties

Aerosol filtration performance of IPA discharged samples (EN 779) was evaluated by using a TSI 3160 automated filter tester. Tests were performed with dioctyl phthalate (DOP) as challenging aerosol with a fixed particle diameter d_p of 0.3 μm , face velocity f_v of

5.33 cm s⁻¹ and testing area A of 100 cm². Particle penetration was measured by detecting particles before (upstream counter) and after (downstream counter) the filtration media using a CPC (condensation particle counter). Pressure drop (filter resistance) was measured by an electronic manometer (Yeom & Pourdeyhimi, 2011). Filtration efficiency E was calculated as follows.

$$E = 100 - P = 100 - \left(\frac{C_{down}}{C_{up}} \times 100 \right) [\%] \quad \text{Eq. 3- 9}$$

where P the penetration, C_{down} is the number of particles detected at the downstream and C_{up} the number of particles detected at the upstream side.

Quality factor QF was calculated to further evaluate the filtration performance of the materials.

$$QF = \frac{-\ln(P)}{\Delta p} [\text{Pa}^{-1}] \quad \text{Eq. 3- 10}$$

where P is the fractional particle penetration and Δp the pressure drop [Pa] of the material.

3.4 Results and Discussion

3.4.1 Removal of Sea Polymer from the Bicomponent Structure

Figure 3- 5 depicts the basis weight of as-received and caustic-soda washed materials. Basis weight of unwashed samples was measured to be higher after hydroentangling caused by shrinkage during bonding.

Basis weight reduction of caustic soda treated materials was expected to be about 25% due to the polymer ratio of 75 (island) to 25 (sea). However, weight loss was found to be in the range of 30% and therefore little higher. Latter could be explained by fluctuations

during polymer feed (most likely) and/or fiber loss during caustic soda treatment. Also, results indicated the weight loss during the treatment to be independent from jet spacing.

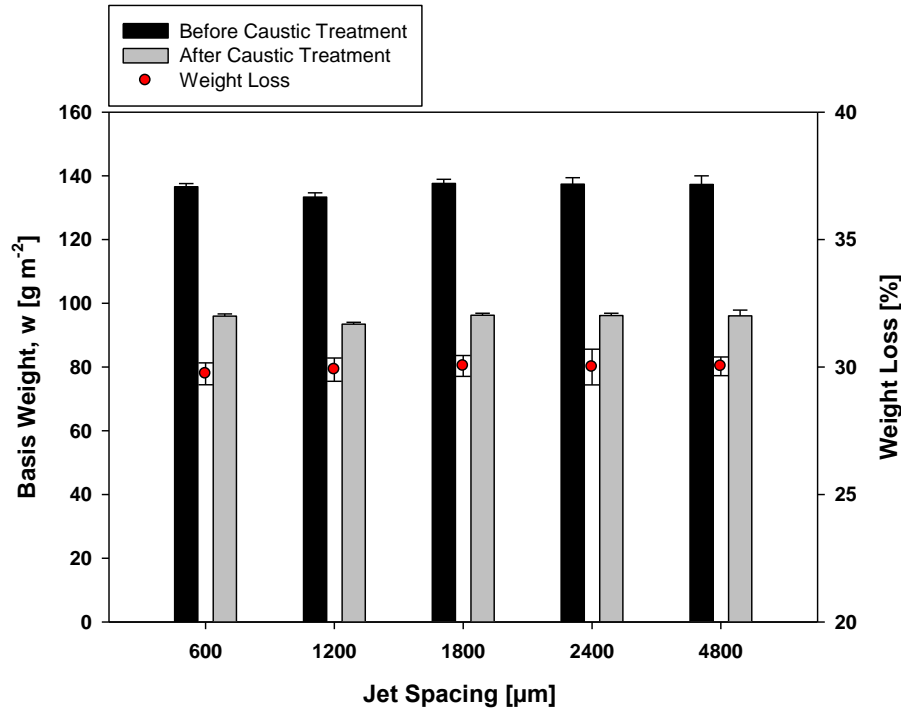


Figure 3- 5: Basis weight before/after caustic treatment

Successful removal of poly (lactic acid) was also confirmed by SEM images taken from the surface of the treated material (see Figure 3- 7). Poly (lactic acid) removal resulted in exposure of island compound as well as a sufficient degree of island separation.

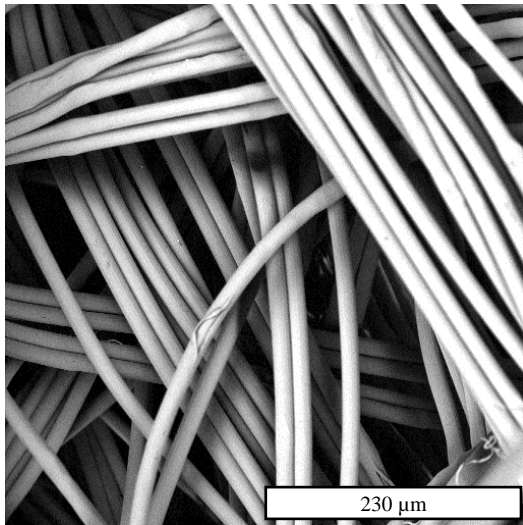


Figure 3- 6: 37 InS structure before caustic treatment

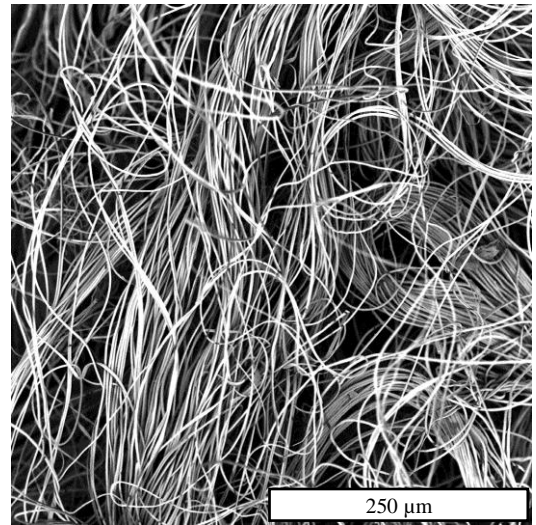


Figure 3- 7: 37 InS structure after caustic treatment

3.4.2 Jet Streak Analysis

Results of co-occurrence analysis along with corresponding dark-field illumination images are shown in the following. Results indicated the intensity of jet streaks (amplitude of wave) to decrease after the materials underwent the caustic washing. However, experiments proved the structures to still have the distinctive appearance after being treated with caustic.

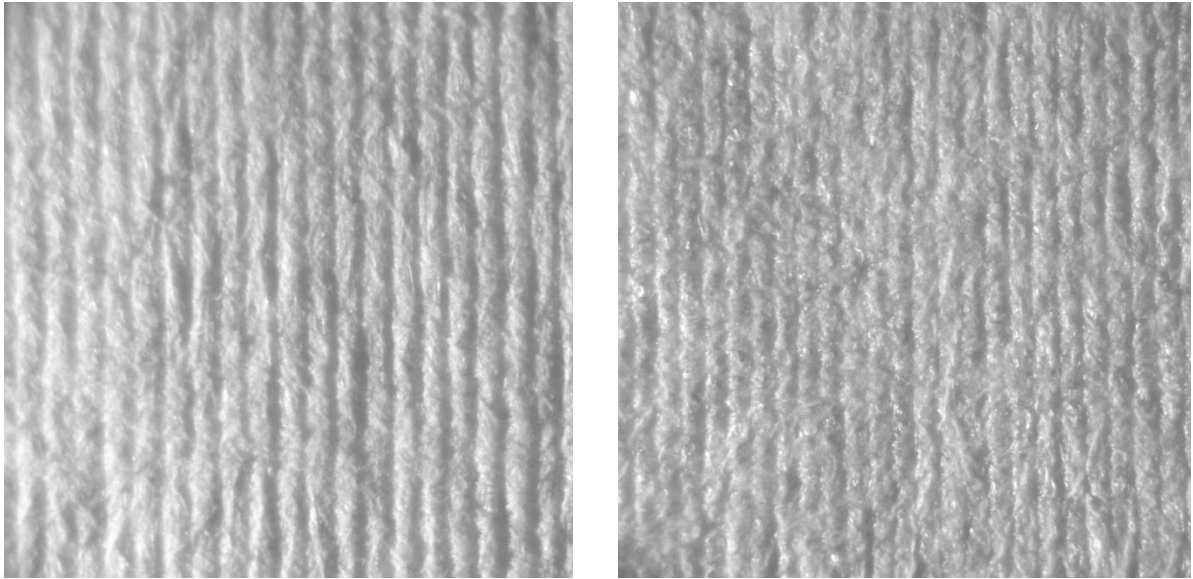


Figure 3- 8: Dark-field illumination images showing the surface of unwashed (left) and caustic-treated (right) 37 InS nonwoven structures hydroentangled with 600 μm jet spacing

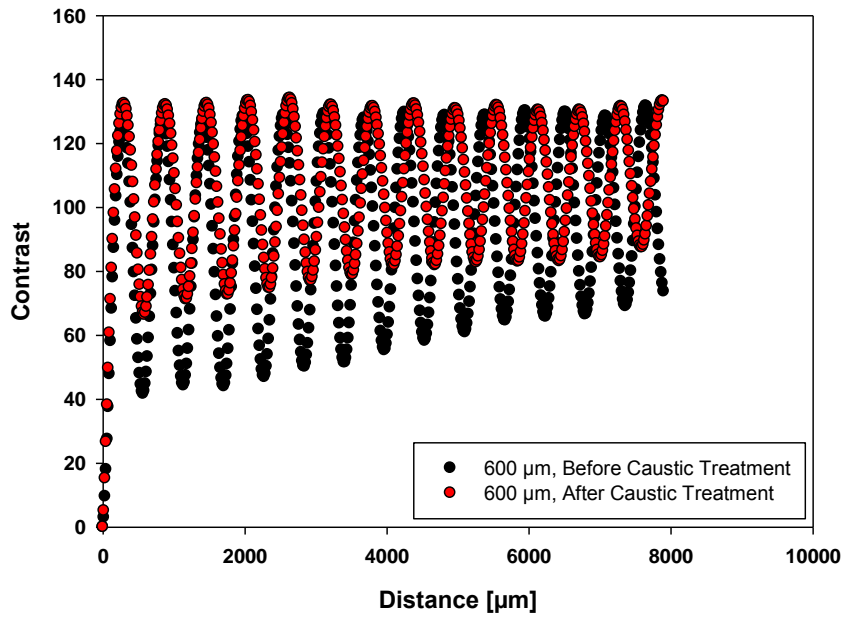


Figure 3- 9: Comparison co-occurrence results of unwashed/washed, 600 μm hydroentangled materials

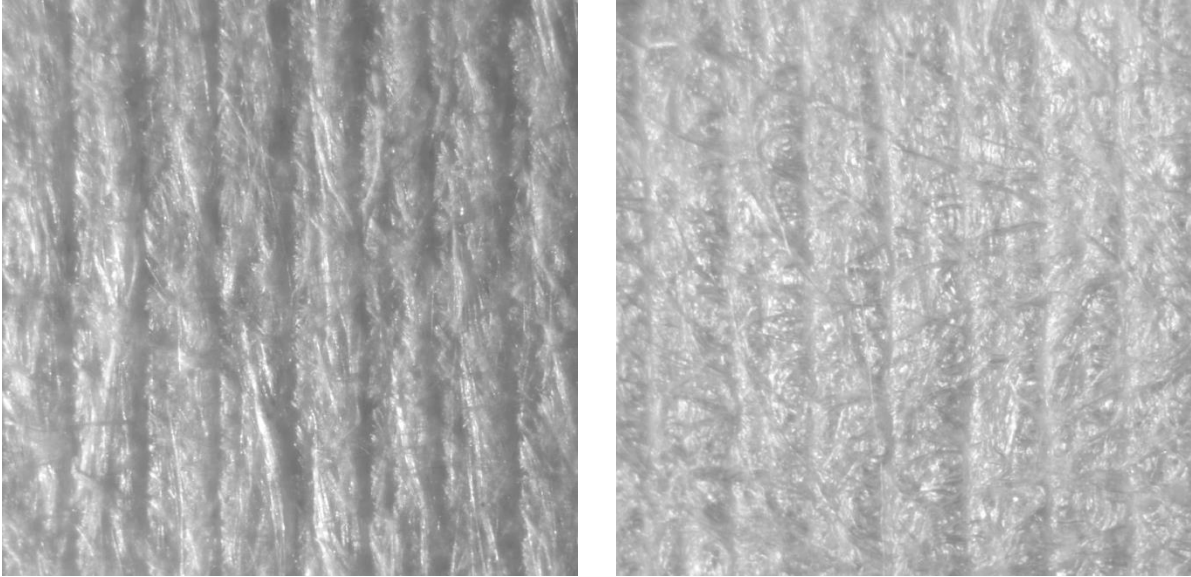


Figure 3- 10: Dark-field illumination images showing the surface of unwashed (left) and caustic-treated (right) 37 InS nonwoven structures hydroentangled with 1800 μm jet spacing

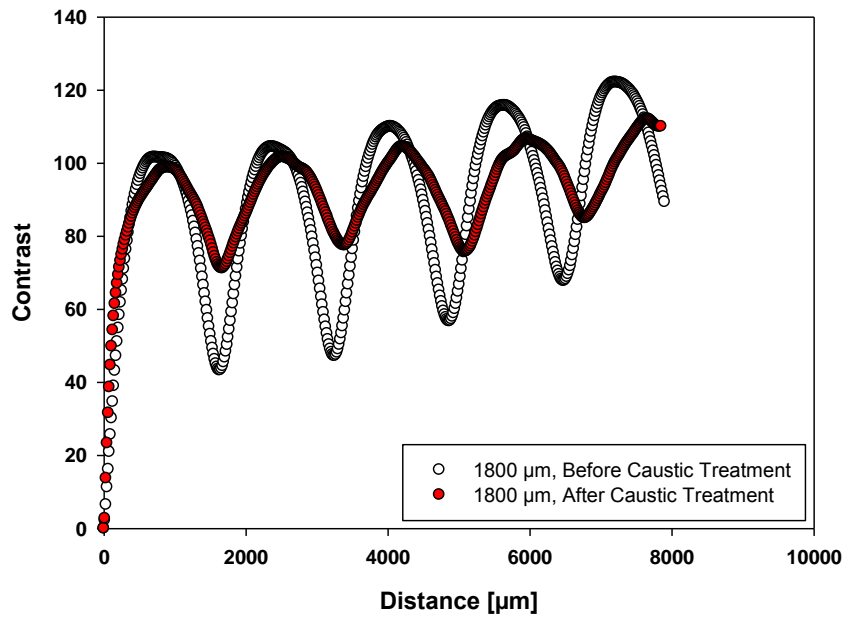


Figure 3- 11: Comparison co-occurrence results of unwashed/washed, 1800 μm hydroentangled materials

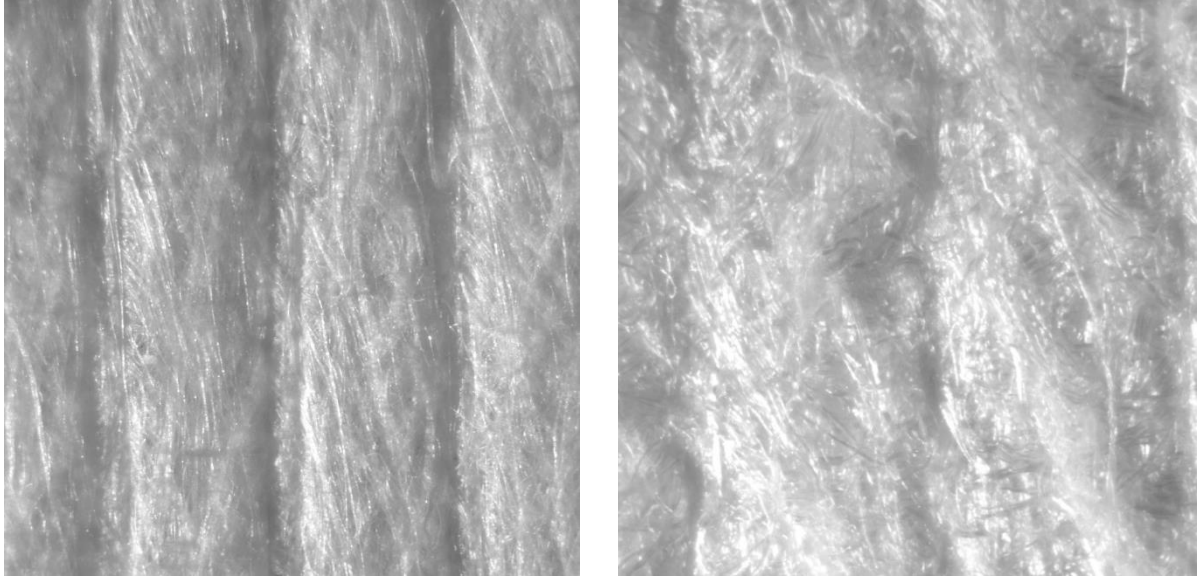


Figure 3- 12: Dark-field illumination images showing the surface of unwashed (left) and caustic-treated (right) 37 InS nonwoven structures hydroentangled with 4800 μm jet spacing

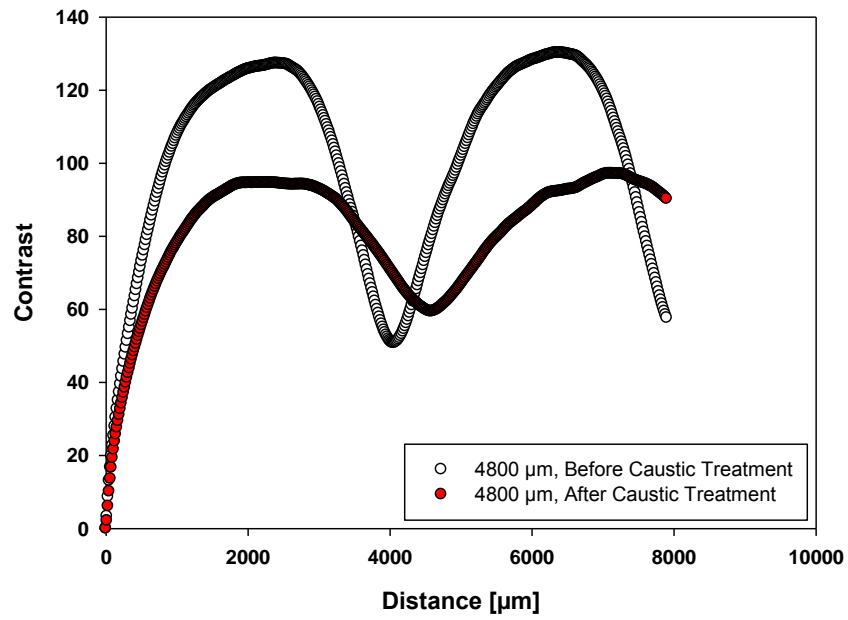


Figure 3- 13: Comparison co-occurrence results of unwashed/washed, 4800 μm hydroentangled materials

3.4.3 Fiber Diameter

Fiber diameter measurements before alkaline treatment are summarized in the following in Table 3- 2.

Table 3- 2: Results of fiber diameter measurements (before caustic treatment)

Mean, \bar{x} [μm]	SD, σ [μm]	CV, c_v [%]	Median [μm]
14.73	1.08	7.33	14.79

Average weight loss after washing the structure with caustic was measured to be ~29.94% (see Figure 3- 5). Thus, island-to-sea ratio of ~70/30 can be used to calculate theoretical island diameter. Both results of theoretical calculations along with SEM-based measurements can be found in the following and indicate the theoretical value to be in accordance with the measured diameters.

Table 3- 3: Theoretical and measured island diameter (after caustic treatment)

Method	$\bar{x} (d_{f, island})$ [μm]	$\sigma (d_{f, island})$ [μm]
Theoretical Calculation	2.12	
SEM Measurements	2.16	0.06

3.4.4 Influence of Jet Spacing on Thickness and Solidity

Figure 3- 14 depicts the influence of jet spacing on the thickness of caustic soda treated 37 island-in-the-sea fiber nonwoven materials.

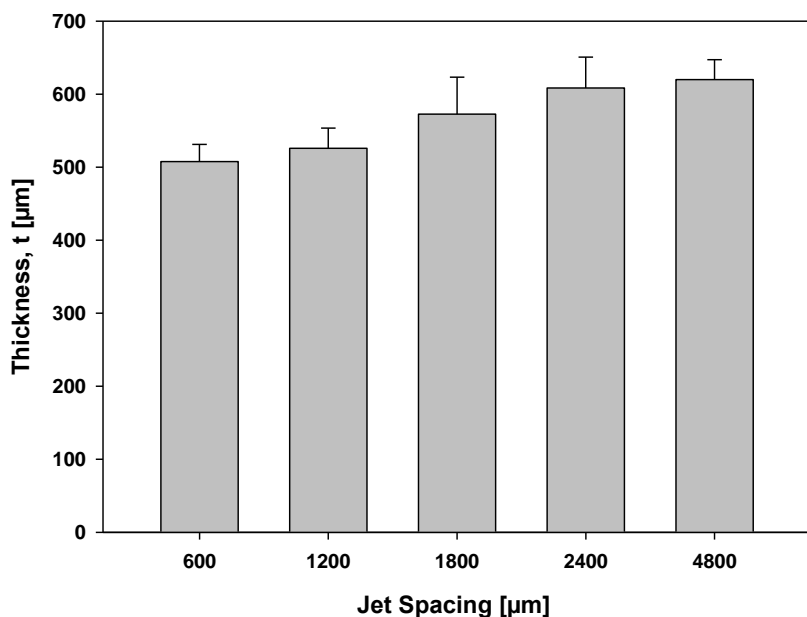


Figure 3- 14: Thickness of 37 InS structures after caustic treatment

As can be seen from the figure, thickness of samples increases with jet spacing. Same trend was reported for monocomponent structures by Suragani (Suragani Venu, 2012).

Solid volume fraction after removing the sea compound from the materials is depicted in Figure 3- 15. Data indicates the structures to be less dense when hydroentangled with larger jet spacing, which is related to the entanglement mechanism and formation of high and low density regions. Hydroentangling with high jet densities leads to more surface entanglement because of interaction of adjacent fibers. In contrast to that, hydroentangling with large jet spacing results in increased fiber penetration depths, less surface entanglement and pocket-like structures showing high- and low density regions (Suragani Venu, 2012).

Results prove the influence of jet spacing to be present even though samples underwent a series of steps to remove the sea compound from the bicomponent fibers.

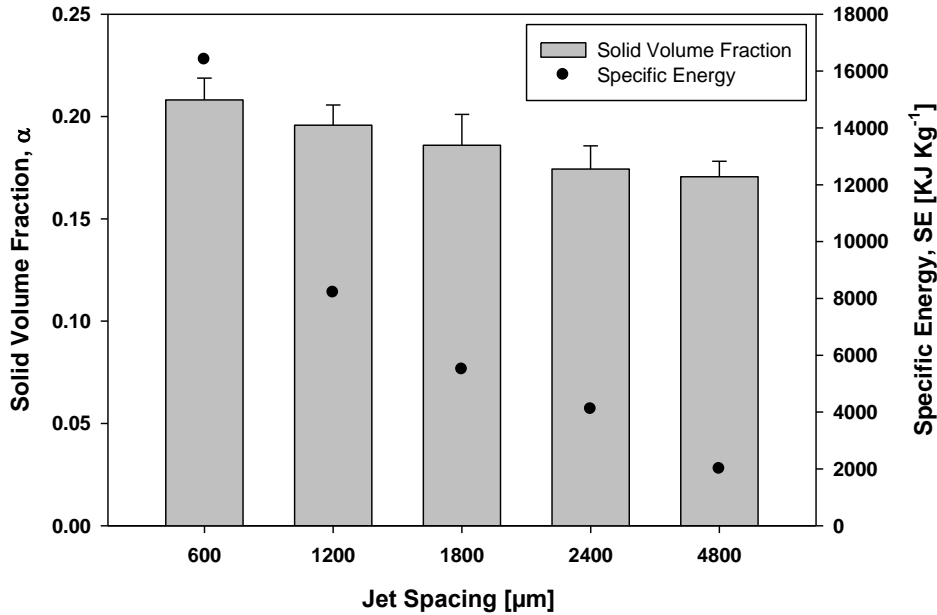


Figure 3- 15: Solidity of 37 InS structures after caustic treatment

3.4.5 Influence of Jet Spacing on Air Permeability and Filtration Properties

Figure 3- 16 depicts the effect of jet spacing on air permeability. It can be observed that air permeability first increases with increasing jet spacing but then levels off. Hydroentangling with jet spacing larger than 1800 μm resulted in comparable permeabilities. In contrast to that, Figure 3- 18 shows the pressure drop to continuously decrease as a function of jet spacing. It is assumed that the structure collapsed during air permeability tests resulting in denser, less permeable materials. Air permeability test was performed at 125 Pa, whereas

pressure drop of samples hydroentangled with jet spacing larger than 1800 μm is below 100 Pa.

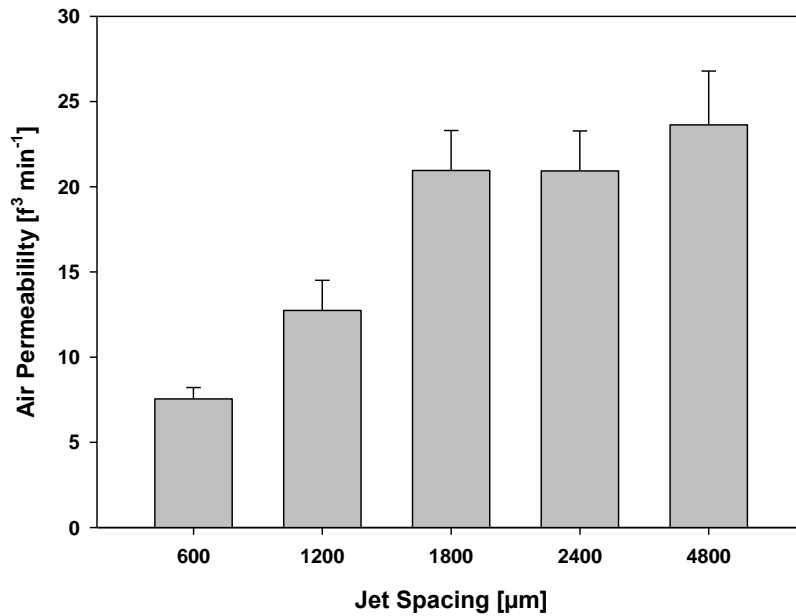


Figure 3- 16: Air permeability of 37 InS structures after caustic treatment

Figure 3- 17 and Figure 3- 18 depict the filtration performance of the materials. According to the results, filtration efficiency follows a non-linear relationship. Capture efficiency first decreases with larger jet spacing but then increases for jet spacing larger than 1800 μm . This may be explained by the increase in thickness and therefore longer trajectory particles are travelling within the material. Whereas materials hydroentangled with 600 μm jet spacing are characterized by a dense, closely-packed structure with high pressure drops, bonding with larger jet spacing resulted in more open, porous materials.

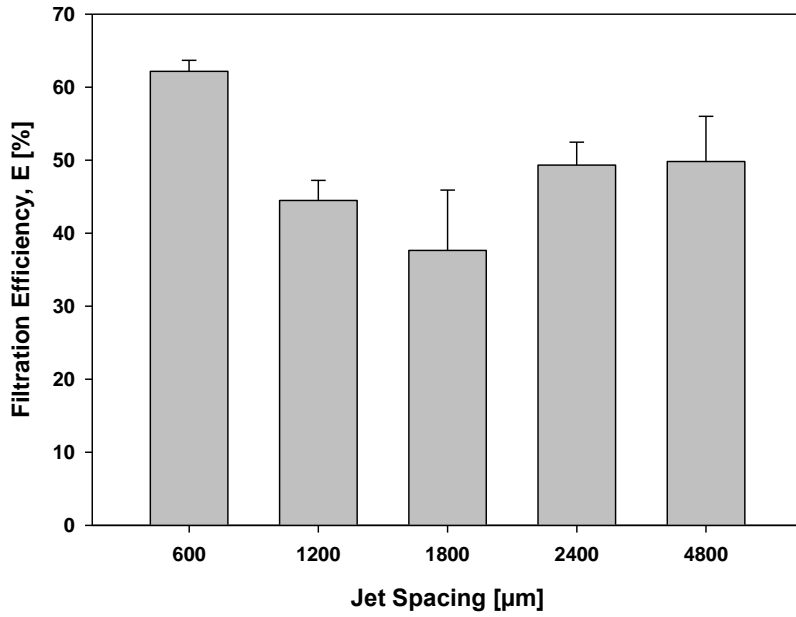


Figure 3- 17: Filtration efficiency as a function of jet spacing ($d_p: 0.3 \mu\text{m}$, $f_v: 5.33 \text{ cm s}^{-1}$, $A: 100 \text{ cm}^2$, DOP)

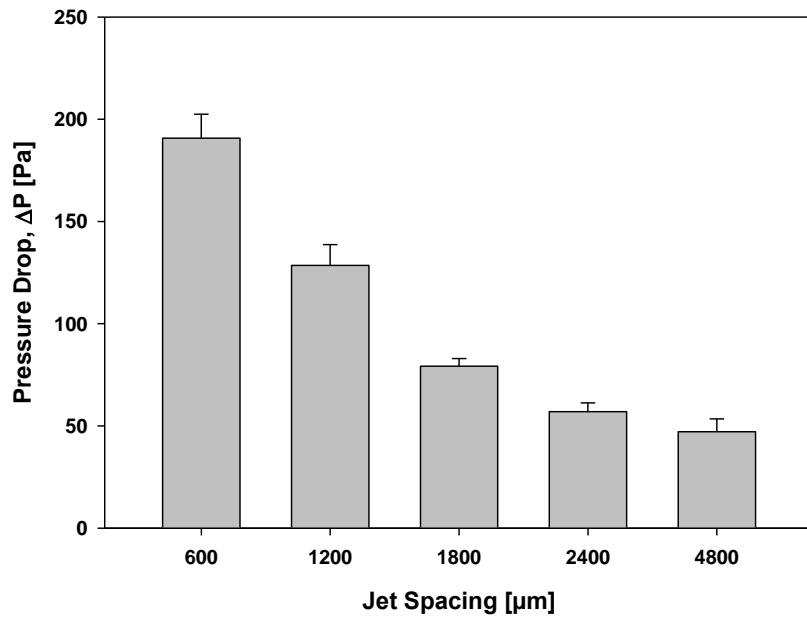


Figure 3- 18: Pressure drop as a function of jet spacing ($f_v: 5.33 \text{ cm s}^{-1}$)

Figure 3- 19 depicts the quality factor as a function of jet spacing. Depicted results provide confirmatory evidence that hydroentangling with larger jet spacing enhances the filtration performance of this type of material.

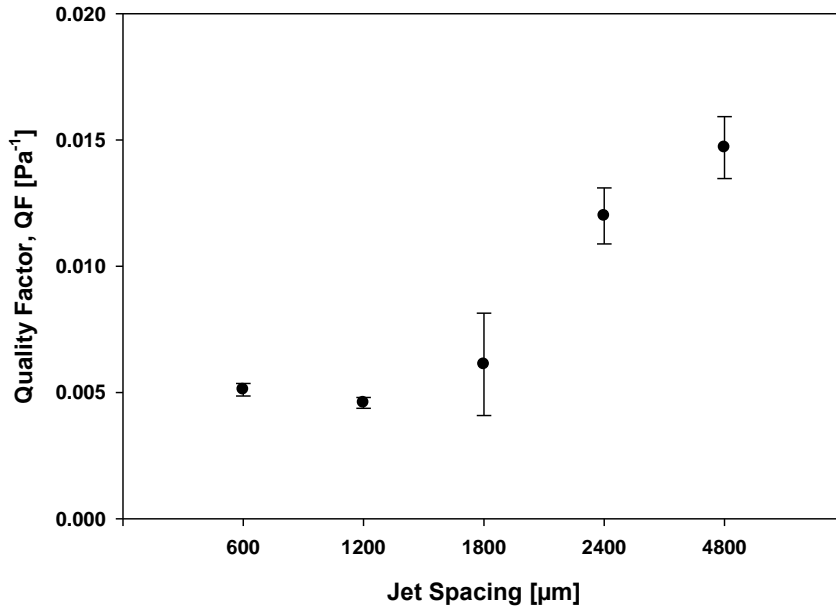


Figure 3- 19: Quality factor of caustic washed samples

3.5 Summary and Conclusion

The purpose of the present research was to investigate the influence of jet spacing in hydroentangling on the structure, properties and also filtration performance of 37 island-in-the-sea bicomponent nonwoven materials. Fiber diameter decreased from 15 μm (before removing sea polymer) to about 2 μm (after removing sea polymer). For both as-received and caustic soda treated materials thickness was found to increase with larger jet spacing.

Moreover, results proved the structures to be less dense and more permeable when hydroentangling with low jet densities. Air permeability was found to no further increase when bonding with jet spacing larger than 1800 μm . However, pressure drop was found to decrease even beyond 1800 μm indicating the structure to collapse during testing. Filtration efficiency was found to follow a non-linear relationship and to increase beyond 1800 μm jet spacing. Quality factor proved the filtration performance to increase the larger the distance between the jets is. In other words, materials hydroentangled with less energy showed considerably better filtration properties.

3.6 References

- Batra, S. K. & Pourdeyhimi, B. (2012). *Introduction to nonwovens technology*: DEStech Publications, Inc.
- Begenir, A., Tafreshi, H. V. & Pourdeyhimi, B. (2004). Effect of nozzle geometry on hydroentangling water jets: Experimental observations. *Textile Research Journal*, 74(2), 178-184.
- Hwang, S. H. (1985). US Patent No. US4514455 A.
- INDA (Association of the Nonwoven Fabric Industry). (n.d.). Spunlace Bonded Nonwovens (Hydroentangling). Retrieved Oct 10, 2014, from <http://www.inda.org/hydroentangling.html>
- Kirayoglu, B. & Zafiroglu, D. P. (1984). US Patent No. US4442161 A. U.S. Patent and Trademark Office.
- Majumdar, A., Das, A., Alagirusamy, R. & Kothari, V. (2012). *Process control in textile manufacturing*: Elsevier.
- Moyo, D. (2012). Energy transfer during the hydroentanglement of fibres Retrieved April 10, 2015, from http://researchspace.csir.co.za/dspace/bitstream/10204/6242/1/Moyo1_2012.pdf
- Pourdeyhimi, B., Minton, A. & Putnam, M. (2004). Structure-process-property relationships in hydroentangled nonwovens-part 1: preliminary experimental observations. *International Nonwovens Journal*, 13, 15-21.
- Russell, S. (2006). *Handbook of nonwovens*: Woodhead Publishing.
- Shim, E. & Pourdeyhimi, B. (2005). A note on jet streaks in hydroentangled nonwovens. *Textile Research Journal*, 75(7), 569-577.
- Suragani Venu, L. B. (2012). *A Study on Hydroentangling Mechanisms and Structures*. (Ph.D. - Fiber and Polymer Science), North Carolina State University.
- Yeom, B. Y. & Pourdeyhimi, B. (2011). Aerosol filtration properties of PA6/PE islands-in-the-sea bicomponent spunbond web fibrillated by high-pressure water jets. *Journal of materials science*, 46(17), 5761-5767.

CHAPTER 4

- Influence of Hydroentangling on Island-in-the-Sea Nonwoven Materials -

Part II: Effect of Hydroentangling Pressure

Sections of this chapter will be submitted for publication in a peer-reviewed journal

4.1 Abstract

Hydroentangling describes an effective and commonly used technique for bonding various types of nonwoven webs. By impinging fibrous materials with curtains of high-velocity water jets, fibers are redirected, interlocked and entangled. The speed of water jets and therefore extend with which the structure is bonded is usually controlled by manifold pressure. In this research discussion centers on the effect of hydroentangling pressure on the structure and properties of spunbond poly (propylene)/poly (lactic) acid 37 island-in-the-sea (InS) nonwoven materials. Webs were hydroentangled with two different water pressures P1 (high pressures) and P2 (reduced pressures) and three jet spacing (600 μm , 1800 μm and 4800 μm) before being washed with a caustic solution to remove the sea polymer from the structure. Aerosol filtration performance was determined with a TSI 3160 particle penetration tester after discharging the samples with isopropyl alcohol. Structure and properties were analyzed prior and after the caustic washing. Results indicated that for both P1 (high pressures) and P2 (reduced pressures) jet spacing significantly influences the properties of the material. Reducing the water pressure (P2) led to thicker, more permeable structures showing a lower packing density. Furthermore, materials hydroentangled with low water pressures (P2) showed greatly improved filtration properties at significantly reduced specific energies during operation.

4.2 Introduction

The idea of using constricted high-velocity water jets for fiber entanglement was not recently born and has been established in the early 1960s. According to Batra et al (Batra &

Pourdeyhimi, 2012, p. 113), Joseph Guerin was the first who had the idea of the concept and filed a patent. This technology, rather known as hydroentangling, spunlacing, water-jet entangling but also hydraulic needling uses a series of fine, high-speed water jets to induce fiber entanglement (Russell, 2006). Numerous researchers invested time in understanding the principle of hydroentangling and the factors influencing the final properties of the material. The water pressure (also called hydroentangling or jet pressure) used during operation influences different aspects of which some are discussed in the following section.

Apparently speed of water jets is mostly influenced by the hydroentangling pressure set during operation. Speed of an individual water jet v can be estimated by Bernoulli equation and calculated as follows.

$$v = \sqrt{\frac{2P}{\rho}} \text{ [m s}^{-1}\text{]} \quad \text{Eq. 4- 1}$$

where P is the water pressure [Pa] and ρ is the specific density of the fluid [Kg m^{-3}] (Anantharamaiah, 2006, p. 167).

Efficient bonding requires the water jets to be rather constricted than distorted. Cavitation and hydraulic flip are common terms in the language of hydroentangling and required to bond as efficient as possible. As soon as the water enters the sharp-edged inlet of the jet strip the horizontal momentum needs to be high enough to force the water to detach from the inner wall and cause subsequent cavitation (Tafreshi & Pourdeyhimi, 2004).

There is no doubt that the water pressure during hydroentangling directly affects the degree of bonding and therefore the properties of the final material. As the effect of water

pressure on the structure depends on many variables, e.g. solidity of material, fiber size and also bending rigidity et cetera, it is quite challenging to quantify the impact in any way.

Jet impact force and also specific energy are two measures commonly used to describe the intensity of hydroentangling. Equation for jet impact force F_{Impact} is given in the following.

$$F_{Impact} = \frac{\pi}{4} p v^2 d_j^2 \text{ [N]} \quad \text{Eq. 4- 2}$$

where p is the density of the fluid [Kg m^{-3}], v is the speed of the water jet [m s^{-1}] and d_j the diameter of the water jet [m] (Patanaik & Anandjiwala, 2010). As can be seen from the equation jet impact force is directly related to the actual jet velocity and therefore to the water pressure.

Suragani (Suragani Venu, 2012) reported data showing the effect of water pressure on the fiber penetration. By visualizing the bonded structure by DVI (digital volumetric imaging) technology, fiber penetration was found to increase with increasing water pressure.

Another work by Pourmohammadi et al. (Pourmohammadi, Russell et al., 2003) investigated the effect of pressure sequences on the mechanical properties of nonwoven materials. This research demonstrated that hydroentangling with one manifold from one side with 70 bar or bonding from both sides with two manifolds having pressures of 30 and 40 bar does make a difference. According to the study, hydroentangling both sides of the web with two manifolds led to enhanced mechanical properties.

Nevertheless, pressure during hydroentangling is rather limited by the material than the potential of the equipment. In other words, maximum pressure during hydroentangling is

determined by the web and above a critical pressure $P_{critical}$ mechanical properties get worse or the web even cut (Majumdar, Das et al., 2012, p. 286).

Most studies investigating the effect of pressure in hydroentangling are based on monocomponent structures and rarely consider the effect on filtration properties. There is no doubt that filtration is an extremely important sector for nonwoven materials with tremendous growth rates over the next years explaining the necessity of ongoing research (Smithers Apex, 2014).

This study represents an investigation to understand the influence of reduced hydroentangling pressures on the structure, physical and also filtration properties of caustic-washed 37 island-in-the-sea nonwoven materials.

4.3 Methodology

4.3.1 Materials

Island-in-the-sea nonwoven material with an island count of 37, made from poly (propylene) (Braskem CP360H) for the island and poly (lactic acid) (Natureworks 6202D) for the sea were produced and hydroentangled at the Nonwoven Institute Partners facilities located at Centennial Campus, North Carolina State University. A 0.5 meter Hills-Nordson spunbond line was used to manufacture the mentioned bicomponent webs. Materials were produced with a polymer ratio of 75/25 (island/sea) and a constant basis weight of 125 g m^{-2} . Right after passing through a compaction roll and being cold calendered bonding was performed with a 0.5 meter Fleissner Aquajet 5-manifold hydroentangling unit using different pressures and jet spacing (see Table 4- 1). Afterwards, materials were dried in a conveyor oven.

Table 4- 1: Structures and hydroentangling parameters

Fabric ID	Jet Spacing [μm]	Hydroentangling Pressure [bar]		Belt Speed [m min ⁻¹]
3.-37-600-125	600 1800 4800	P1	20 (Manifold 1)	10
3.-37-1800-125			150 (Manifold 2)	
3.-37-4800-125			200 (Manifold 3)	
4.-37-600-125		P2	225 (Manifold 4)	
4.-37-1800-125			225 (Manifold 5)	
4.-37-4800-125			20 (Manifold 1)	
			100 (Manifold 2)	
			100 (Manifold 3)	
			150 (Manifold 4)	
			150 (Manifold 5)	

For this study two different sets of hydroentangling pressures were used, P1 (hereinafter called “high hydroentangling pressures”) and P2 (hereinafter called “low hydroentangling pressures”). Also, materials were hydroentangled just from the face side of the structure.

Figure 4- 1 depicts a microscopy images taken from the cross-section of 37 island-in-the-sea spunbond fibers after drawing and before web formation.

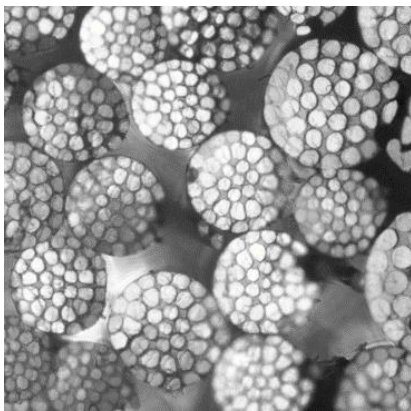


Figure 4- 1: Cross-sectional image of 37 island-in-the-sea fibers

Specific energy applied during hydroentangling was calculated based on Bernoulli equation and speed of water jet v calculated as follows.

$$v = (2P \rho^{-1})^{0.5} [\text{m s}^{-1}] \quad \text{Eq. 4- 3}$$

where P is the water pressure within the manifold [Pa] and ρ the specific gravity [Kg m^{-3}].

From the equation for Newtonian kinetic energy, single jet energy \dot{E} can be predicted as follows.

$$\dot{E} = \pi 8^{-1} \rho d_n^2 C_d v^3 [\text{J s}^{-1}] \quad \text{Eq. 4- 4}$$

where ρ the specific gravity of water [998.2 Kg m^{-3} at room temperature], d_n the nozzle diameter [m], C_d the discharge coefficient and V the jet velocity [m s^{-1}].

Based on that, total energy of all jets was calculated by multiplying the single jet energy \dot{E} with the number of jets having the same pressure. As hydroentangling pressure was not the same for all manifolds, energy emanated from each manifolds had to be calculated separately. Specific energy SE was predicted by using the equation shown below.

$$SE = \frac{\dot{E}_{Total}}{\dot{M}} [\text{KJ Kg}^{-1}] \quad \text{Eq. 4- 5}$$

where \dot{M} is the mass flow rate of fabric [Kg s^{-1}], which was determined by using the following term.

$$\dot{M} = s \times w \times v_B [\text{Kg s}^{-1}] \quad \text{Eq. 4- 6}$$

where s is the fabric width [m], w is the basis weight of the material [g m^{-2}] and v_B is the operating speed [m s^{-1}] (Pourdeyhimi, Minton et al., 2004). Specific energy based on the hydroentangling pressures shown in Table 4- 1 is given in the following.

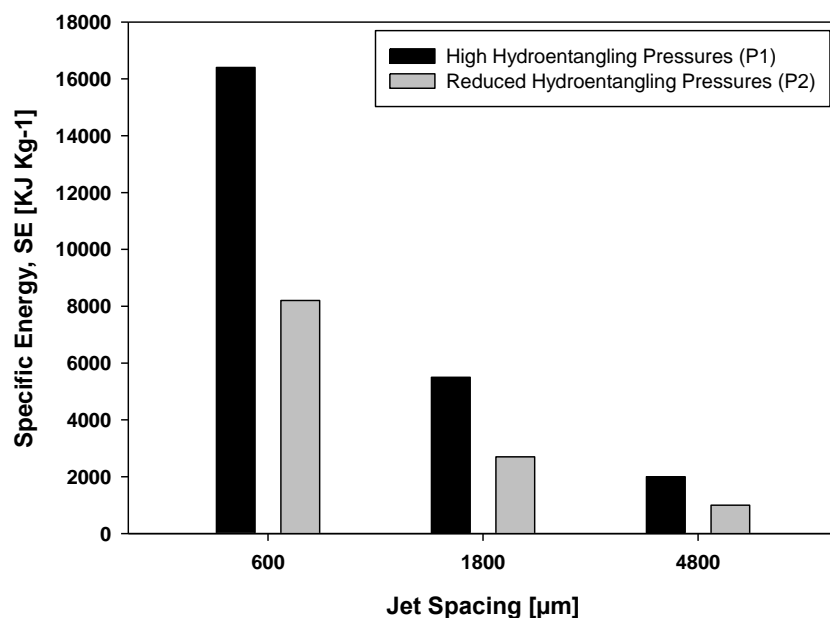


Figure 4- 2: Calculated specific energy of P1/P2 hydroentangled structures

4.3.2 Sample Preparation

After hydroentangling nonwoven materials were washed with caustic to remove the poly (lactic acid) compound from the bicomponent fibers resulting in fiber diameters considerably smaller. An 8 % w/w sodium hydroxide bath was prepared in a steam kettle and heated up to 100 °C. Nonwoven samples were treated for 10 minutes under continuous stirring before being drained and neutralized with cold water. Samples were air-dried on a rack.

4.3.3 Characterization Methods

Basis Weight and Thickness

A Denver Instrument XL-3100D top-loading balance was used to test weight loss and determine the effectiveness of the alkaline treatment. Thickness was measured by using a Hanatek FT3V-LAB high-precision thickness gauge. Analysis of both tests was performed prior and after the caustic washing with 10 replicates each.

Solid Volume Fraction

Solidity of materials was calculated by using the formula shown below.

$$\alpha = \frac{w}{\rho_f \times t} \quad \text{Eq. 4- 7}$$

where w is the basis weight (in g m^{-2}), ρ_f the total fiber density (in g m^{-3}) and t the thickness of the structure (in m). Total fiber density ρ_f is calculated as follows.

$$\rho_f = (\rho_{island} \times R_i) + (\rho_{sea} \times R_s) \text{ [g cm}^{-3}\text{]} \quad \text{Eq. 4- 8}$$

where ρ_{island} is the density of the island polymer [g cm^{-3}], R_i is the mass fraction of island polymer, ρ_{sea} is the density of the sea polymer [g cm^{-3}] and R_s is the mass fraction of sea polymer.

Air Permeability

Air permeability of materials was tested at 125 Pa with a TEXTEST FX 3300 air permeability tester according to ASTM D737. A total of 10 samples were tested after removing the sea compound from the bicomponent fibers.

Aerosol Filtration Properties

Filtration properties of caustic-washed structures were evaluated with a TSI 3160 particle penetration tester. Materials were challenged with dioctyl phthalate (DOP) particles having a diameter d_p of 0.3 μm . Face velocity f_v was fixed at 5.33 cm s^{-1} and tested area was 100 cm^2 . Prior testing samples were discharged with isopropanol alcohol according to EN 779.

Quality factor QF of materials was calculated based on the equation shown in the following.

$$QF = \frac{-\ln(P)}{\Delta p} [\text{Pa}^{-1}] \quad \text{Eq. 4-9}$$

where P is the fractional particle penetration and Δp the pressure drop [Pa] of the material.

4.4 Results and Discussion

4.4.1 Removal of Sea Polymer from the Bicomponent Structure

The data in Figure 4- 3 indicated the sea polymer to be completely removed from the island-in-the-sea bicomponent structure. As can be seen from the data average weight loss after treating the structures with alkaline was about 30%. The higher weight loss compared to initial polymer ratio of 75/25 can be explained by fluctuations of polymer throughput and also fiber loss during the caustic washing. Jet spacing did not influence the ability to remove the sea polymer from the structure. Also, removal of poly (lactic acid) seems to be independent from the intensity of hydroentangling pressure.

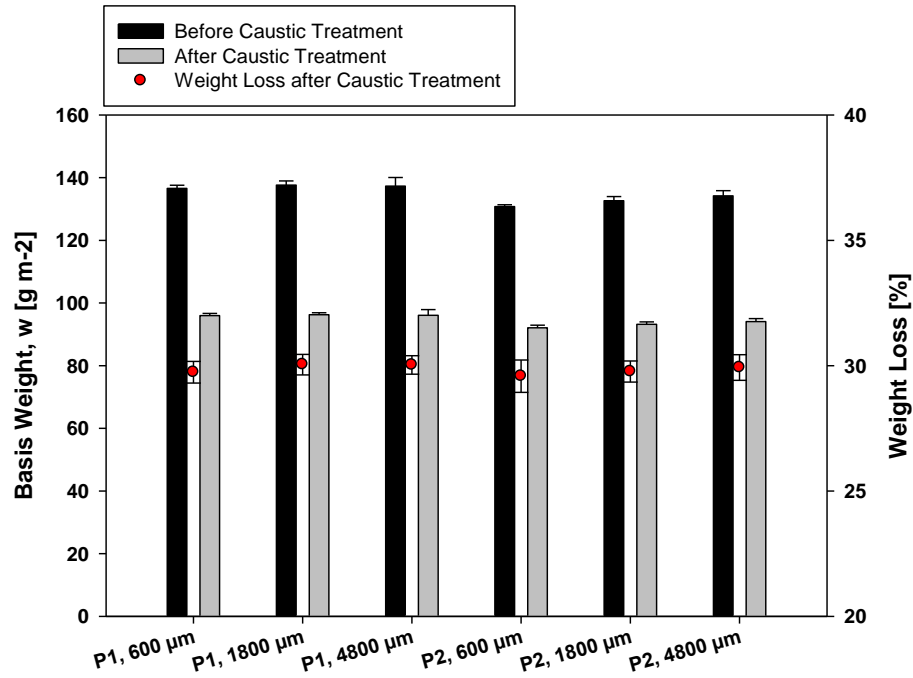


Figure 4- 3: Basis weight of P1/P2 hydroentangled structures before/after caustic treatment

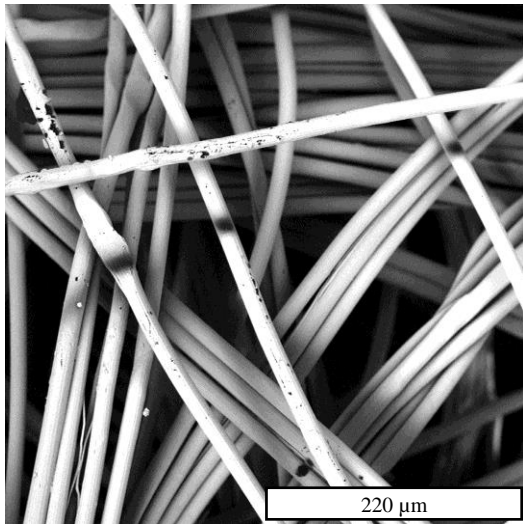


Figure 4- 4: 37 InS structure before caustic treatment

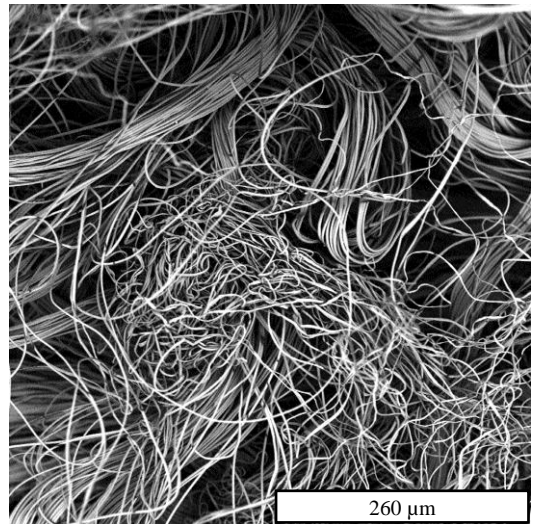


Figure 4- 5: 37 InS structure after caustic treatment

Information about fiber size of unwashed and caustic treated materials was taken from the previous experiments (3.4.3) as base material was the same. Results of fiber diameter measurements of unwashed and alkaline treated materials are shown in the following.

Table 4- 2: Results of fiber diameter measurements (before caustic treatment)

Mean, \bar{x} [μm]	SD, σ [μm]	CV, c_v [%]	Median [μm]
14.73	1.08	7.33	14.79

Table 4- 3: Results of fiber diameter measurements (after caustic treatment)

Method	$\bar{x} (d_{f, island})$ [μm]	SD, $\sigma (d_{f, island})$ [μm]
Theoretical Calculation	2.12	
SEM Measurements	2.16	0.06

4.4.2 Influence of Hydroentangling Pressure on Thickness and Solidity

In the previous chapter we discussed the jet spacing in hydroentangling to be a significant factor influencing the thickness of the materials. With increasing jet spacing the thickness of caustic-washed 37 island-in-the-sea nonwovens was found to increase. Figure 4- 6 indicates the thickness of low pressure-bonded (P2), caustic-treated samples to significantly increase for all jet densities. Comparison of P1 and P2 reveals the increase in thickness to be more dominant for P2-hydroentangled samples.

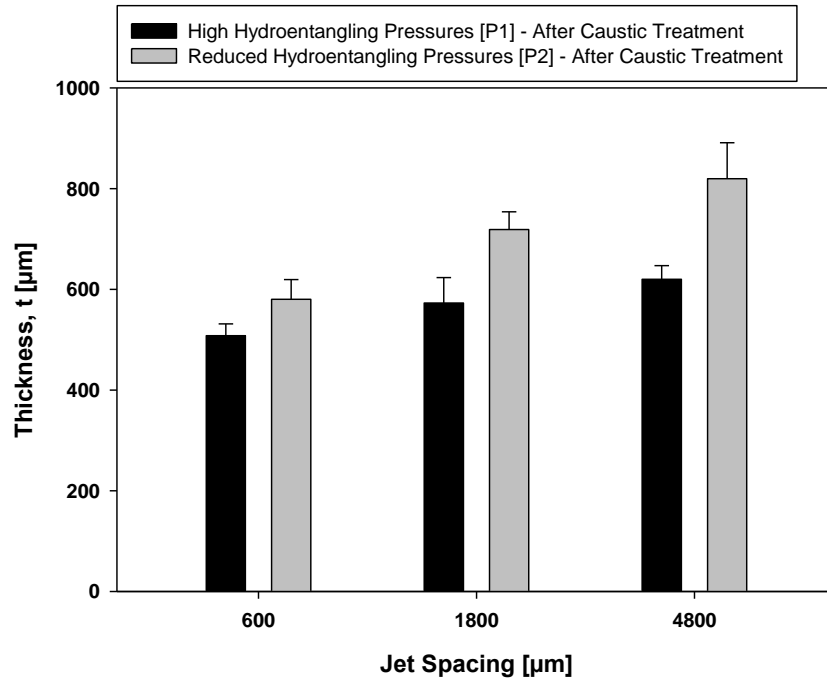


Figure 4- 6: Thickness of P1/P2 hydroentangled structures after caustic treatment

As can be seen from the following figure, structures hydroentangled with P1 seems to collapse and just slightly change in terms of thickness, whereas materials bonded with P2 show the opposite behavior. From this it can be assumed that the reduction in pressure and thus fiber interlocking allowed the fibers to reorient during the caustic-washing and the structure to further open. Data also suggests an island count of 37 and therefore island diameter of about 2 μm to be sufficient to prevent structure collapsing. In addition, hydroentangling pressure seems to be a crucial factor to control the thickness of island-in-the-sea nonwoven structures.

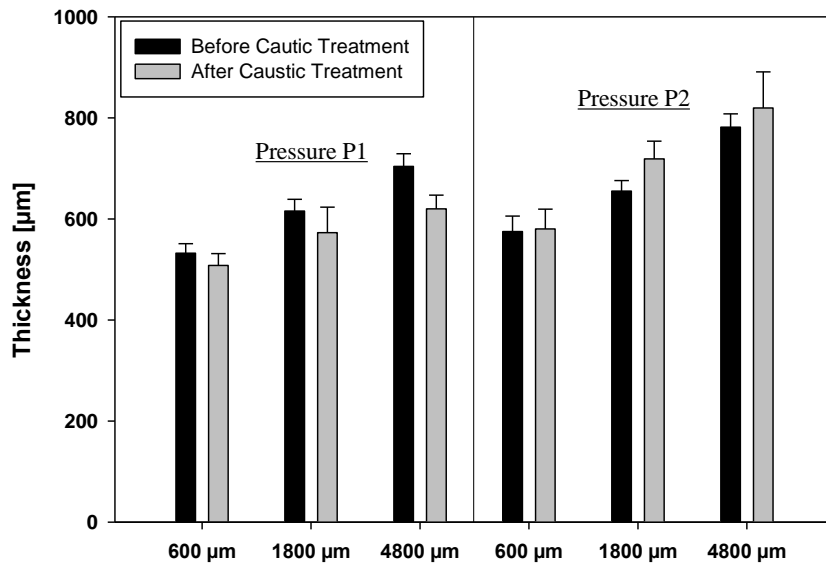


Figure 4- 7: Thickness of P1/P2 hydroentangled structures before/after caustic treatment

Following can be said from the discussed findings: 1) for both P1 and P2 thickness of structures increases as a function of jet spacing 2) lower hydroentangling pressures led to thicker materials, 3) in contrary to P1, structure of P2 materials opened during the caustic washing and 4) increase in thickness as a function of jet spacing is remarkably larger for materials hydroentangled with P2.

Figure 4- 8 depicts the influence of jet spacing and hydroentangling pressure on the solid volume fraction of caustic-washed 37 island-in-the-sea materials.

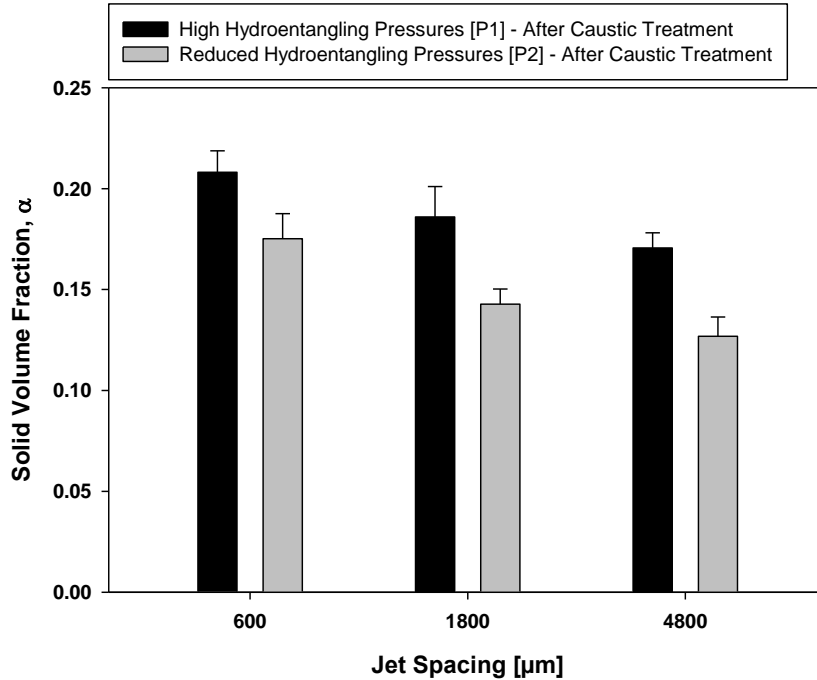


Figure 4- 8: Solidity of P1/P2 hydroentangled structures after caustic treatment

The data yielded by lowering the water pressure during operation provides evidence that even though the jet pressure was considerably reduced solidity is still influenced by jet spacing. Also, degree of consolidation is remarkably lowered by lowering the water pressure and thus the impact force. A closer look at the data indicates the bulk density of P2 to show a clear trend and no flattening. In other words, effect of jet spacing is still measurable despite the fact that structures were bonded with low manifold pressures and also jet densities and further underwent a subsequent treatment.

4.4.3 Air Permeability and Filtration Properties

Figure 4- 9 shows the change in air permeability as a function of jet spacing for caustic treated island-in-the-sea nonwoven materials hydroentangled with high (P1) and low (P2) water pressures.

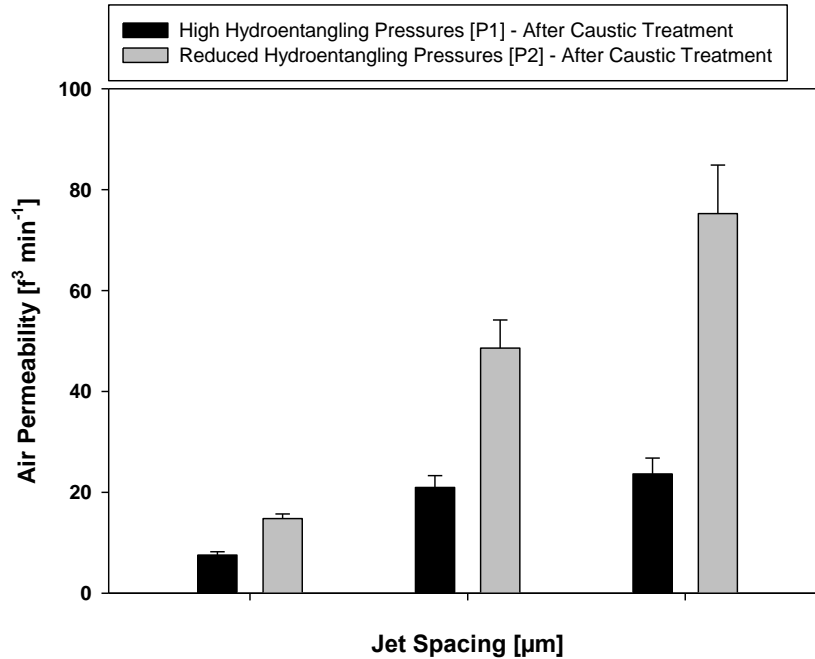


Figure 4- 9: Air permeability of P1/P2 hydroentangled structures after caustic treatment

Data implies the following: 1) air permeability increases with larger jet spacing for both P1 and P2, 2) increase in air permeability is significantly greater for P2-hydroentangled samples and 3) all structures hydroentangled with P2 show higher air permeability compared to P1-hydroentangled samples. This significant difference in permeability can be explained by the reduced structure consolidation affecting the porosity and permeability of the materials.

Filtration efficiency and pressure drop of IPA discharged, caustic-washed materials are given in Figure 4- 10 and Figure 4- 11. Results revealed the particle penetration of samples hydroentangled with reduced manifold pressures and 600 μm and 1800 μm jet spacing to be lower compared to structures hydroentangled with higher manifold pressures. In addition, pressure drop decreased for all materials hydroentangled with reduced manifolds pressures. As can be seen from the results, reducing the pressure during hydroentangling significantly improved the filtration properties compared to samples hydroentangled with significantly higher pressures.

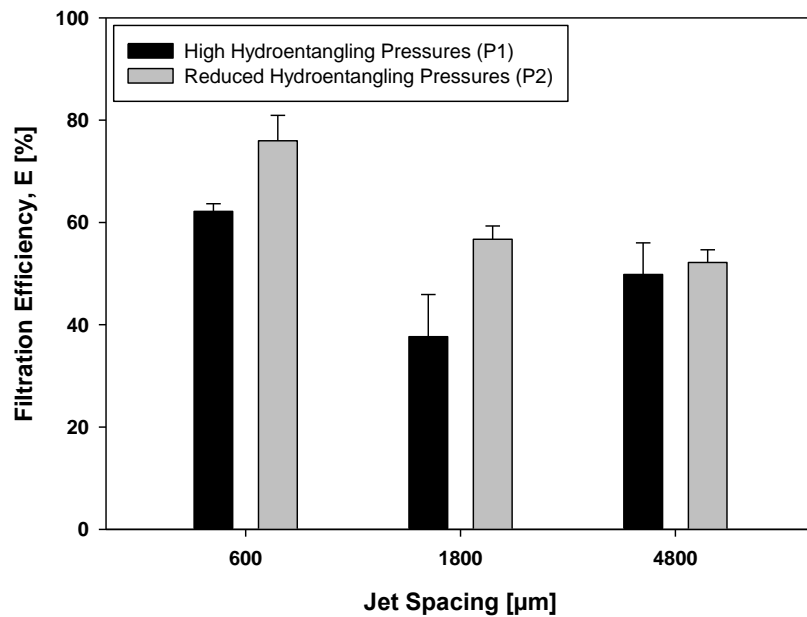


Figure 4- 10: Filtration efficiency of P1/P2 hydroentangled structures after caustic treatment ($d_p: 0.3 \mu\text{m}, f_v: 5.33 \text{ cm s}^{-1}, A: 100 \text{ cm}^2, DOP$)

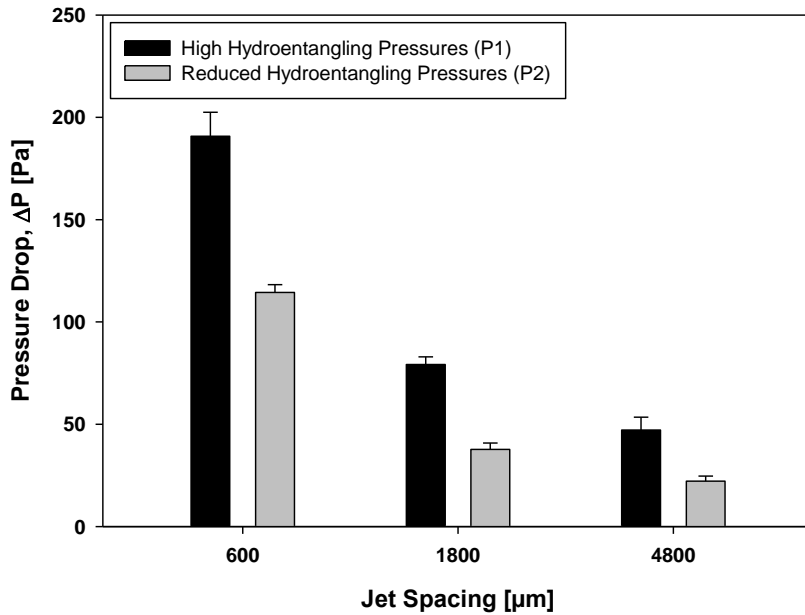


Figure 4- 11: Pressure drop of P1/P2 hydroentangled structures after caustic treatment ($f_p: 5.33 \text{ cm s}^{-1}$)

Quality factor of structures was calculated based on Eq. 4- 9 and indicated materials hydroentangled with large jet spacing to perform better. Also, hydroentangling with reduced manifold pressures resulted in nonwoven structures with greatly improved filtration properties.

However, reducing the hydroentangling pressure is limited as materials require a certain level of fiber interlocking to withstand the subsequent removal of sea polymer. Minimum degree of bonding depends on factors, such as fiber bending rigidity, polymer ratio but also required washing time and further finishing steps.

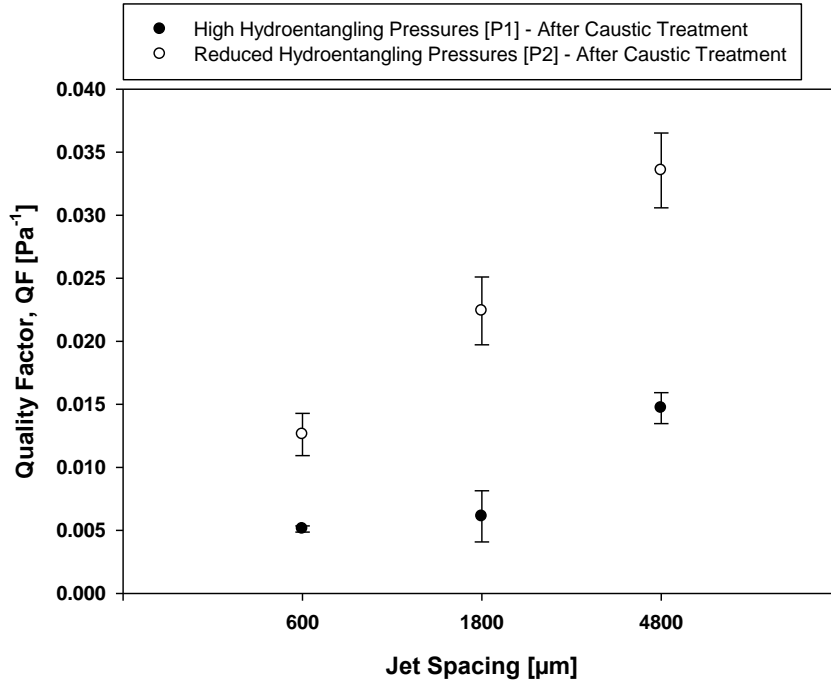


Figure 4- 12: Quality factor of P1/P2 hydroentangled structures after caustic treatment

Plotting these results in a different manner reveals the jet spacing to be not the all-important factor influencing the quality factor of the materials (see Figure 4- 13). As can be seen from the figure, hydroentangling with the largest amount of specific energy gave the worst quality factor, whereas hydroentangling with the least specific energy (less than one-eighth of the initial energy) resulted in the best quality factor.

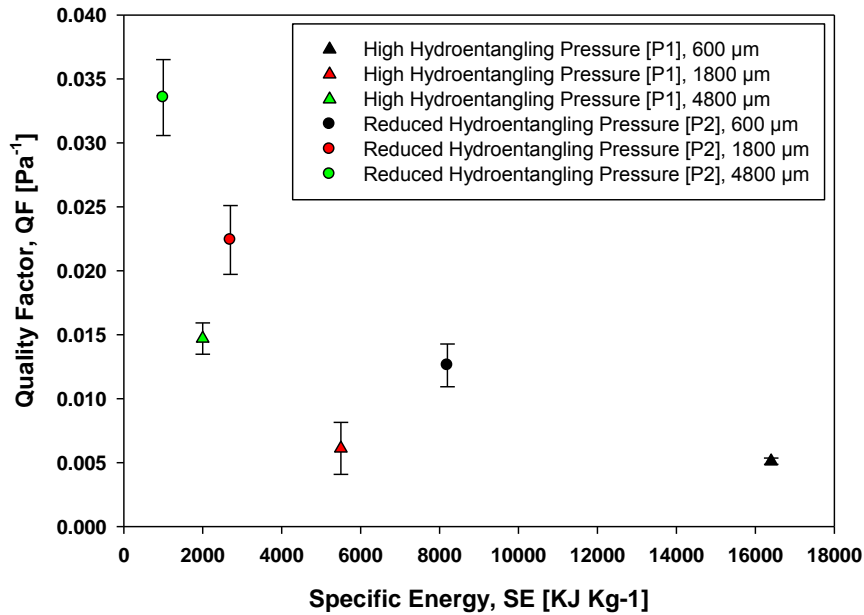


Figure 4- 13: Quality factor of P1/P2 hydroentangled structures as a function of specific energy

4.5 Conclusion

The purpose of the present study was to investigate the influence of reduced hydroentangling pressures on the structure and properties of caustic-soda treated 37 island-in-the-sea nonwoven materials. Furthermore, effect of three different jet spacing (600 μm, 1800 μm and 4800 μm) has been investigated. Bonding with reduced water pressures (P2) and variable jet spacing showed the same trend as reported for high water pressures (P1). Lowering the jet density led to an increase in thickness and air permeabilities and a decrease in solidity of the structures. In contrast to P1, structure of materials hydroentangled with reduced water pressures (P2) opened during the caustic washing resulting in higher thicknesses and air permeabilities and lower solidities. Data also showed the filtration properties to be dependent

on the specific energy and low specific energies to result in better filtration performance. In addition, reduced hydroentangling pressures have a larger effect on the performance of the filtration media than the jet spacing used during bonding.

4.6 References

- Anantharamaiah, N. (2006). *An investigation of the influence of nozzle geometry in the hydroentangling process*.
- Batra, S. K. & Pourdeyhimi, B. (2012). *Introduction to nonwovens technology*: DEStech Publications, Inc.
- Majumdar, A., Das, A., Alagirusamy, R. & Kothari, V. (2012). *Process control in textile manufacturing*: Elsevier.
- Patanaik, A. & Anandjiwala, R. D. (2010). Hydroentanglement nonwoven filters for air filtration and its performance evaluation. *Journal of Applied Polymer Science*, 117(3), 1325-1331.
- Pourdeyhimi, B., Minton, A. & Putnam, M. (2004). Structure-process-property relationships in hydroentangled nonwovens-part 1: preliminary experimental observations. *International Nonwovens Journal*, 13, 15-21.
- Pourmohammadi, A., Russell, S. J. & Höffele, S. (2003). Effect of water jet pressure profile and initial web geometry on the physical properties of composite hydroentangled fabrics. *Textile Research Journal*, 73(6), 503-508.
- Russell, S. (2006). *Handbook of nonwovens*: Woodhead Publishing.
- Smithers Apex. (2014). Nonwovens Market Still Spreads Thick Across the Globe. Retrieved May 5th, 2015, from <http://news.thomasnet.com/imt/2014/10/28/nonwovens-market-still-spreads-thick-across-the-globe>
- Suragani Venu, L. B. (2012). *A Study on Hydroentangling Mechanisms and Structures*. (Ph.D. - Fiber and Polymer Science), North Carolina State University.
- Tafreshi, H. V. & Pourdeyhimi, B. (2004). Simulating cavitation and hydraulic flip inside hydroentangling nozzles. *Textile Research Journal*, 74(4), 359-364.

CHAPTER 5

- Effect of Island Count of Island-in-the-sea Nonwoven Materials -

Sections of this chapter will be submitted for publication in a peer-reviewed journal

5.1 Abstract

The island-in-the-sea technology describes a technique used to create nonwoven materials with small fiber diameters at high output rates. Because of increased specific surface areas, such structures are known to be superior in terms of filtration and because of enhanced absorption properties great for other kind of application (e.g. wipes etc.). This study investigated spunbond island-in-the-sea materials with three different island counts (37, 108 and 360) and hydroentangled with three different jet spacing (600 μm , 1800 μm and 4800 μm) in terms of their structure and properties. Structures were made from spunbond poly (propylene)/poly (lactic acid) bicomponent fibers with a fixed basis weight of 125 g m^{-2} and a polymer ratio of 75 (island) to 25 (sea). After bonding, samples were washed with an alkaline solution to remove the sea compound from the structures and unveil island fibers. Analysis indicated the treatment time to be adequate for materials with 37 and 108 islands but insufficient for higher island counts. Results demonstrated the jet spacing to be the dominant parameter influencing most properties. Also, combination of small fibers and large jet spacing was found to be critical as structures tend to collapse. Contrary to initial exception, best aerosol filtration performance was tested for 37 island-in-the-sea samples.

5.2 Introduction

Since the early 1930s bicomponent fibers are subject of research activities and acknowledged as materials being advantageous in many aspects (Koslowski, 2009). By definition, bicomponent fibers are nowadays known as fibers spun by co-extrusion of two immiscible polymers having different chemical and physical properties (Pohl, 2010, p. 17).

Island-in-the-sea fibers describe one type of bicomponent fibers and the beginnings can be traced back to the 1970s (Batra & Pourdeyhimi, 2012, p. 14). Island-in-the-sea fibers consist of two different polymers having similar or different properties, whereas one polymer is declared as the sea (sheath) and the other as island (core) polymer. An illustration showing the general structure of this type of fiber is depicted in the following.

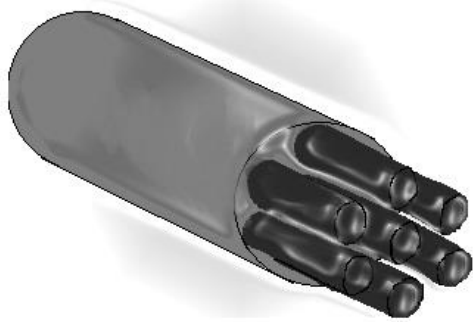


Figure 5- 1: Illustration of the structure of an island-in-the-sea fiber

Multiple techniques of how to release the island fibers are described in literature. These techniques can broadly grouped into two categories: 1) fibrillation of island-in-the-sea fibers by mechanical means (e.g. hydroentangling) and 2) removing of the sea polymer (Anantharamaiah, Verenich et al., 2008; Pourdeyhimi, 2008). Since fibrillation of island-in-the-sea fibers requires the island polymer to separate from the sea both polymers have to be incompatible in terms of their chemical nature.

One advantage of using micro- or even nanofiber structures is the enormous specific surface, such materials can provide. The relation between high specific surface area and enhanced filtration properties is mentioned by many authors in today's literature (Chapman,

2010, p. 15). Anantharamaiah et al. investigated the properties of water jet fibrillated island-in-the-sea nonwoven materials with island counts ranging between 1 and 108. According to the results, smaller fiber sizes led to decreasing mean pore sizes and increasing moisture vapor transport rates. Latter was found to reach a plateau for island counts higher than 19 (Anantharamaiah, Durany et al., 2009). Yeom et al. studied the effect of fibrillated island-in-the-sea nonwoven materials on the filtration performance. According to the results, filtration efficiency is the highest for structures containing 108 islands and the lowest for materials containing only one island (Yeom & Pourdeyhimi, 2011).

Hills, a pioneer in bicomponent fiber spinning, successfully spun island-in-the-sea fibers consisting of up to 1200 individual islands (Prokop, 2014, p. 12). Assuming an initial fiber diameter of about 15 μm and an island-to-sea ratio of 75/25 this would result in islands of about 380 nm in diameter. In case that all islands are completely separated from each other and made from poly (propylene) this kind of structure would provide a specific surface area of more than 11 $\text{m}^2 \text{g}^{-1}$. Another source mentions the highest island count ever spun to be 10,000 (Dugan, 2010).

However, there has been no research about the interaction of island count and jet spacing of caustic-treated island-in-the-sea nonwovens. This study examines a total of three different island counts (37, 108 and 360) and, contrary to previous studies, also reports on effect of jet spacing (600-4800 μm). Aerosol filtration performance of caustic-washed samples is also addressed and sea compound was removed by treating the structures with caustic instead of fibrillating via mechanical forces.

5.3 Methodology

5.3.1 Materials

We report on spunbond island-in-the-sea nonwoven webs made from poly (propylene) (Braskem CP360H) for the island and poly (lactic acid) (Natureworks 6202D) for the sea with a polymer ratio of 75 (island) to 25 (sea) and a fixed basis weight of 125 g m⁻². Island-in-the-sea webs with three different island counts (37, 108 and 360) were manufactured with a 0.5 meter Hills-Nordson spunbond line. SEM images of the fibers' cross-section are depicted in Figure 5- 2 - Figure 5- 4. Prior hydroentangling webs passed through a compaction and calender roll (cold calendered). Hydroentangling was performed with a total of five different jet spacing and fixed water manifold pressures. A 0.5 meter Fleissner Aquajet 5-manifold unit was used for hydroentangling and both web formation and bonding performed at the Nonwoven Institute pilot facilities located at Centennial Campus, North Carolina State University. Additional information about the samples and bonding conditions can be found in the following.

Table 5- 1: Structures and hydroentangling parameters

Fabric ID	Island Count	Jet Spacing [μm]	Hydroentangling Pressure [bar]	Belt Speed [m min⁻¹]
3.- 37-JetSpacing-125	37	600	20 (Manifold 1)	10
5.- 108-JetSpacing-125	108	1200	150 (Manifold 2)	
5.- 360-JetSpacing-125	360	1800	200 (Manifold 3)	
		2400	225 (Manifold 4)	
		4800	225 (Manifold 5)	

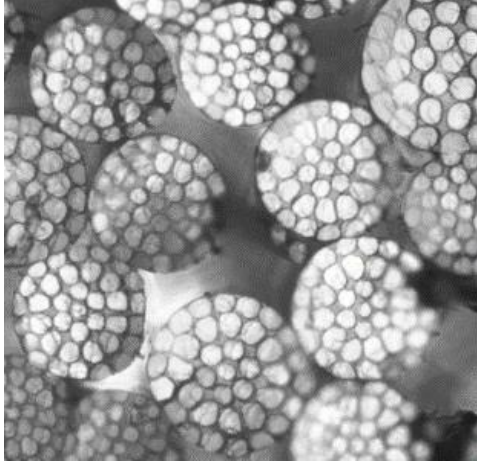


Figure 5- 2: Cross-sectional microscopy image of 37 InS fibers

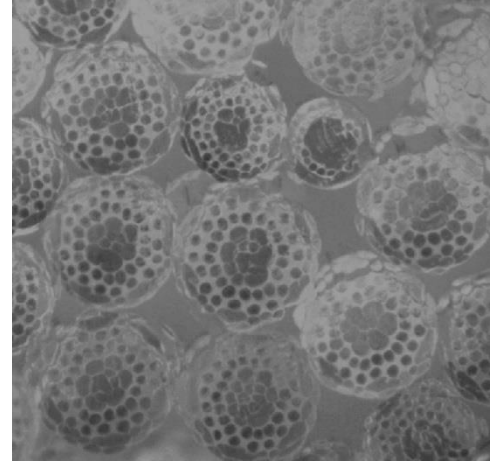


Figure 5- 3: Cross-sectional microscopy image of 108 InS fibers

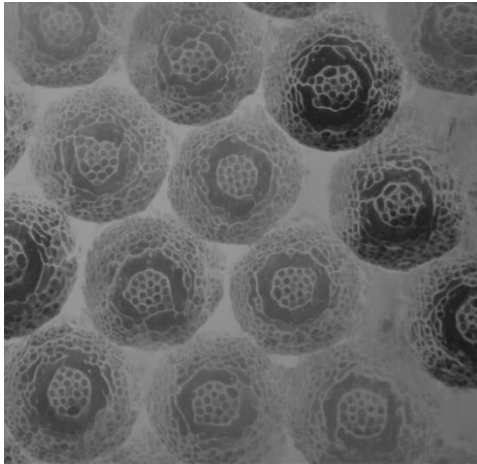


Figure 5- 4: Cross-sectional microscopy image of 360 InS fibers

Specific energy is given in Figure 5- 5 and was estimated based on the energy \dot{E} carried by a single water jet. That energy can be calculated by the following equation.

$$\dot{E} = \frac{\pi}{8} \rho d_n^2 C_d v^3 \text{ [J s}^{-1}\text{]} \quad \text{Eq. 5- 1}$$

where ρ is the specific density of the fluid [998.2 Kg m⁻³ for H₂O at 20 °C], d_n the nozzle diameter [m], C_d the discharge coefficient and v the jet velocity [m s⁻¹].

By multiplying the single jet energy \dot{E} with the number of jets of a manifold and adding the energy of all respective manifolds together, total energy \dot{E}_{Total} can be calculated as shown in the following.

$$\dot{E}_{Total} = \left(\sum_{M=1}^n \dot{E}_{MJM} \right) \times 1000^{-1} \text{ [KJ s}^{-1}\text{]} \quad \text{Eq. 5- 2}$$

where n is the number of manifolds used during hydroentangling and J the number of jets per manifold.

Specific energy SE is the energy applied by the water jets per kilogram of fabric and can be estimated by using the following equation.

$$SE = \frac{\dot{E}_{Total}}{\dot{M}} \text{ [KJ Kg}^{-1}\text{]} \quad \text{Eq. 5- 3}$$

where \dot{M} is the mass flow rate of fabric [Kg s⁻¹]. Latter can be calculated with the following equation.

$$\dot{M} = s \times w \times v_B \text{ [Kg s}^{-1}\text{]} \quad \text{Eq. 5- 4}$$

where s is the fabric width [m], w is the basis weight of the material [g m⁻²] and v_B is the operating speed [m s⁻¹] (Pourdeyhimi, Minton et al., 2004).

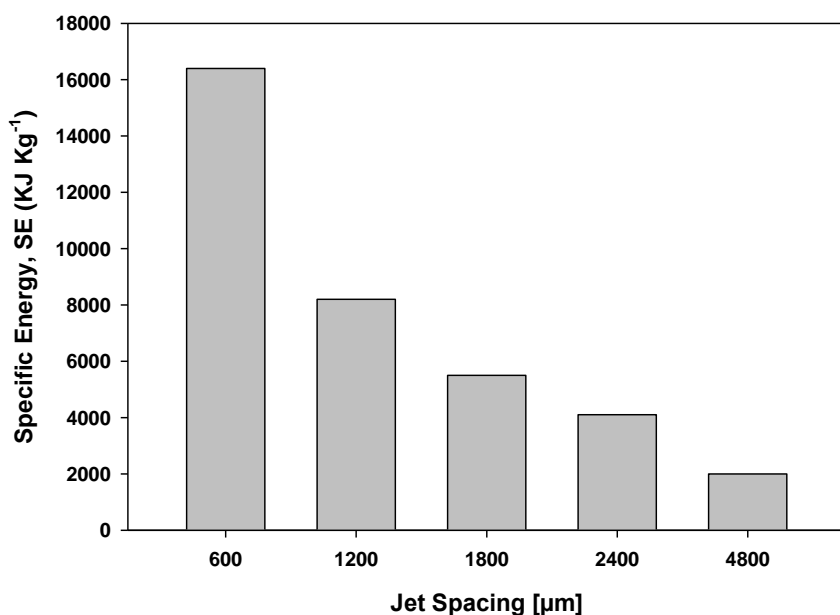


Figure 5- 5: Calculated specific energy during hydroentangling

5.3.2 Sample Preparation

Hydroentangled materials were washed with a caustic-soda solution to remove sea polymer from the bicomponent structure. Samples were washed in an 8% w/w sodium hydroxide solution at 100 °C for 10 minutes under continuous stirring. Afterwards, samples were washed-out with cold water until pH neutralization and dried in the open air on a rack.

5.3.3 Characterization Methods

Basis Weight and Thickness

Basis weight was measured with a Denver Instrument XL-3100D top-loading balance and thickness with a Hanatek FT3V-LAB high-precision thickness gauge. All experiments were performed prior and after removing the sacrificial polymer and 10 replicates were tested per

structure. Basis weight was used as an indicator whether the sacrificial polymer was successfully removed.

Solid Volume Fraction

Solid volume fraction α of samples was determined based on the following equation.

$$\alpha = \frac{w}{\rho_f \times t} \quad \text{Eq. 5- 5}$$

where w the basis weight [in g m^{-2}], ρ_f the total fiber density [g cm^{-3}] and t the thickness of the structure [m]. Total fiber density ρ_f is calculated as follows.

$$\rho_f = (\rho_{island} \times R_i) + (\rho_{sea} \times R_s) \quad [\text{g cm}^{-3}] \quad \text{Eq. 5- 6}$$

where ρ_{island} is the density of the island polymer [g cm^{-3}], R_i is the mass fraction of island polymer, ρ_{sea} is the density of the sea polymer [g cm^{-3}] and R_s is the mass fraction of the sea polymer.

Fiber Diameter

Fiber diameter of unwashed and caustic-washed materials was measured by analyzing SEM images with image processing software (ImageJ). Images were taken from Au/Pd (gold/palladium) sputter-coated samples with a Phenom G2 Pro Desktop SEM unit.

Theoretical fiber diameter of structures was calculated based on the volume fraction vol_i of the island polymer, which was obtained from the mass fraction of island polymer (determined by the percentage of island-to-sea polymer fed by the metering pump).

$$vol_i = \frac{R_i \times \rho_i}{(R_i \times \rho_i) + (R_s \times \rho_s)} \quad \text{Eq. 5-7}$$

where R_i is the mass fraction of island polymer, ρ_i is the specific density of the island polymer [g cm^{-3}], R_s is the mass fraction of sea polymer and ρ_s is the specific density of the sea polymer [g cm^{-3}].

Equation to calculate the average island diameter $d_{f,s,t}$ is given in the following.

$$d_{f,s,t} = d_f \sqrt{\frac{vol_i}{N}} \quad [\mu\text{m}] \quad \text{Eq. 5-8}$$

where d_f is the diameter of the intact island-in-the-sea fiber [μm], vol_i is the volume fraction of the island polymer and N is the island count.

Specific Surface Area

Theoretical accessible specific surface area A_S of materials was determined as follows.

$$A_S = \alpha \sqrt{\frac{4\pi \times 10^6}{\rho D}} \quad [\text{m}^2 \text{g}^{-1}] \quad \text{Eq. 5-9}$$

where α is the solid volume fraction, ρ is the specific density of the material [g cm^{-3}] and D the fiber denier [g 9000m^{-1}] (Anantharamaiah, Durany et al., 2009).

BET surface area was tested experimentally by using a Quantachrome Autosorb iQ2. Samples were outgassed for about 16-18 hours at 40°C before being analyzed. Krypton ($\rho; 2.413 \text{ g cm}^{-3}$) was used for physisorption.

Air Permeability

For each structure 10 replicates of unwashed and caustic-washed materials were tested for air permeability with a TEXTEST FX 3300 air permeability tester. Samples were examined according to ASTM D737 with a pressure of 125 Pa.

Aerosol Filtration Properties

Filtration properties of caustic-treated, IPA discharged (EN 779) structures were evaluated with a TSI 3160 particle penetration tester. All samples were challenged with dioctyl phthalate (DOP) with a particle diameter d_p of 0.3 μm . Face velocity f_v was set at 5.33 cm s^{-1} and the tested area was 100 cm^2 .

Quality factor QF of materials was calculated based on the following equation.

$$QF = \frac{-\ln(P)}{\Delta p} [\text{Pa}^{-1}] \quad \text{Eq. 5- 10}$$

where P is the fractional particle penetration and Δp the pressure drop [Pa] of the material.

5.4 Results and Discussion

5.4.1 Removal of Sea Compound from the Bicomponent Structure

As mentioned polymer ratio of all island-in-the-sea structures was chosen to be 75 (island) to 25 (sea). Figure 5- 6 depicts the basis weight before and after washing the structure with the caustic solution. For the purpose of illustration results of narrowest and largest jet spacing are shown for all island counts. Results indicate the sea polymer to be completely removed for structures consisting of fibers with 37 islands. Structures with an island count of 108 and 360

showed less weight removal after the treatment. Structures with 360 islands lost about 5% less weight compared to materials made from fibers with 37 islands.

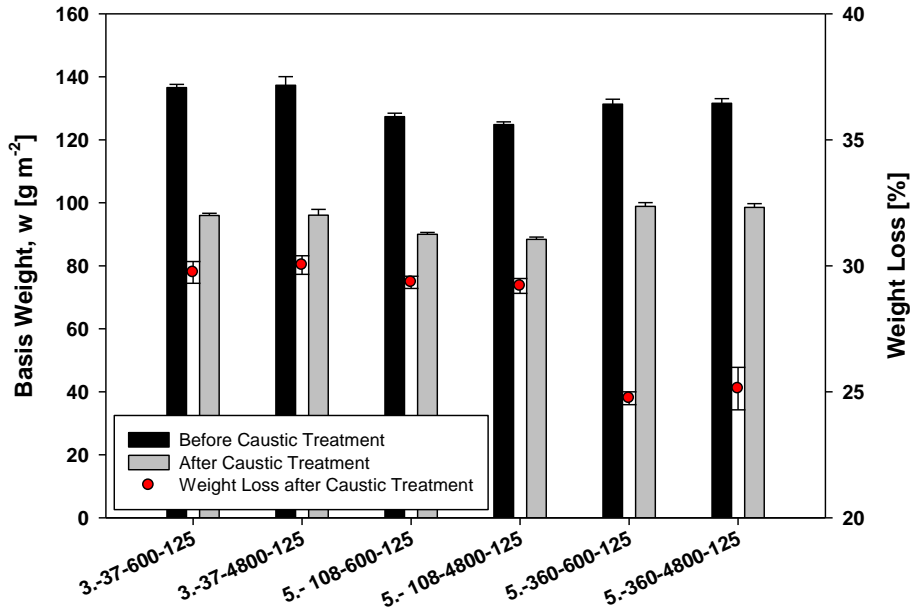


Figure 5- 6: Basis weight before/after caustic treatment

Figure 5- 7 and Figure 5- 8 depict SEM images taken from the surface of the materials before and after poly (lactic acid) removal. Images indicate successful removal of poly (lactic acid) from 37 island-in-the-sea structures. Images also show the fibers to be fibrillated and no intact bicomponent fibers to be present.

As can be seen from Figure 5- 10 caustic-treated 108 island-in-the-sea structures still show few intact bicomponent fibers. Even though poly (lactic acid) was removed from the majority of bicomponent fibers some remained in bundles. It is assumed that insufficient

agitation during the washing process and/or poly (lactic) residues between islands, which prevent fibrillation, are responsible for that.

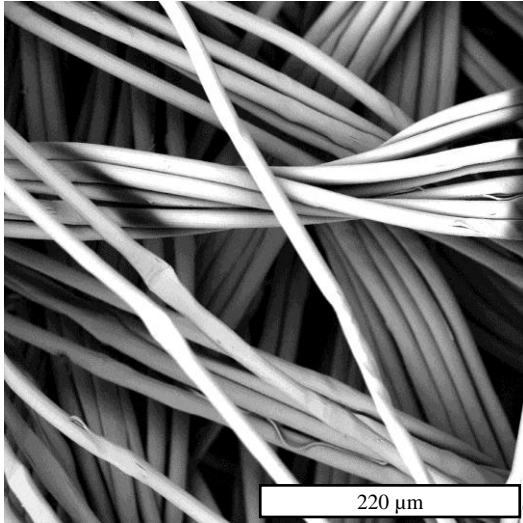


Figure 5- 7: 37 InS structure before caustic treatment

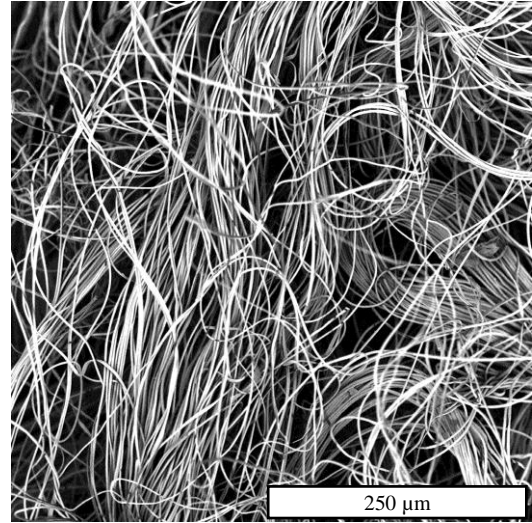


Figure 5- 8: 37 InS structure after caustic treatment

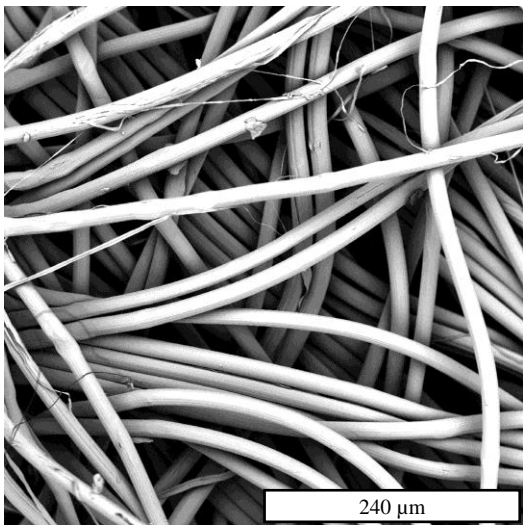


Figure 5- 9: 108 InS structure before caustic treatment

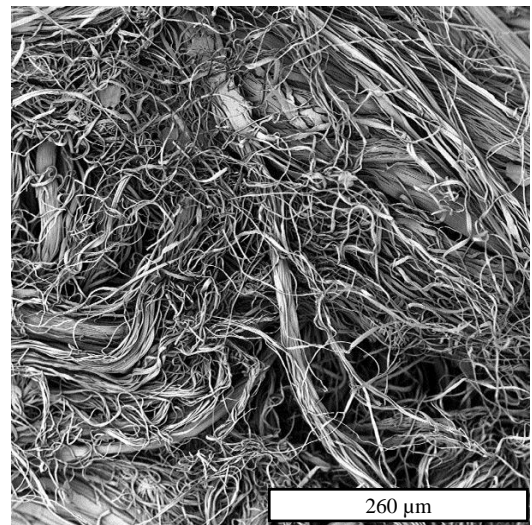


Figure 5- 10: 108 InS structure after caustic treatment

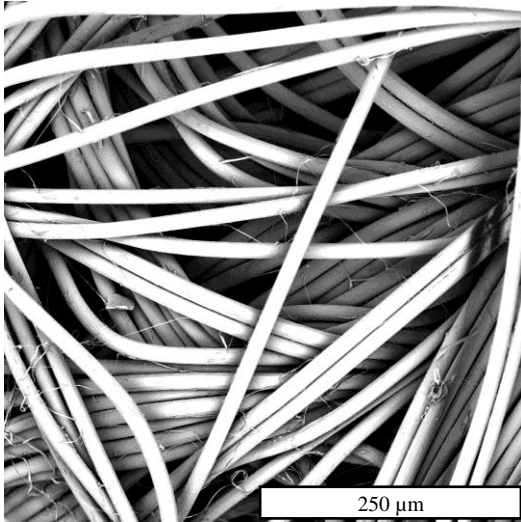


Figure 5- 11: 360 InS structure before caustic treatment

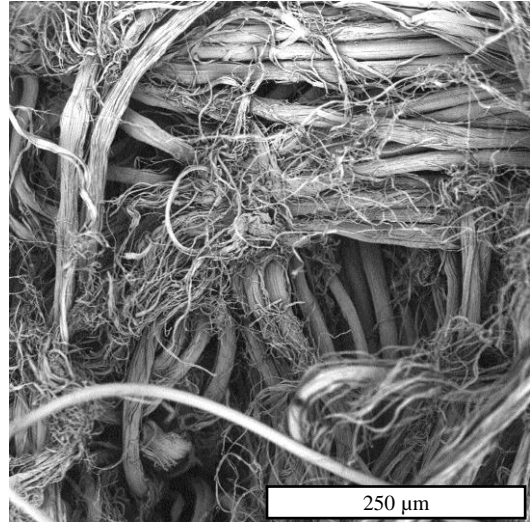


Figure 5- 12: 360 InS structure after caustic treatment

Figure 5- 12 shows the surface of a 360 island-in-the-sea structure after being treated with the alkaline solution for 10 minutes. In contrast to the other structures, many bicomponent fibers are either intact with minimal or no sea removal or insufficiently fiber spread.

5.4.2 Influence of Island Count on Fiber Diameter

Results of fiber size distribution are shown in Figure 5- 13. Data shows intact bicomponent fibers of all island counts to have similar fiber sizes after being spun and drawn. Diameter distribution indicates the majority of fibers to have fiber sizes between 14-16 μm.

Table 5- 2: Results of fiber diameter measurements (before caustic treatment)

Island Count	$\bar{x}(d_{f,bico})$ [μm]	SD, σ [μm]	CV, c_v [%]	Median [μm]
37	14.7	1.1	7.3	14.8
108	15.2	1.1	7.5	15.2
360	15.1	1.2	8.1	15.1

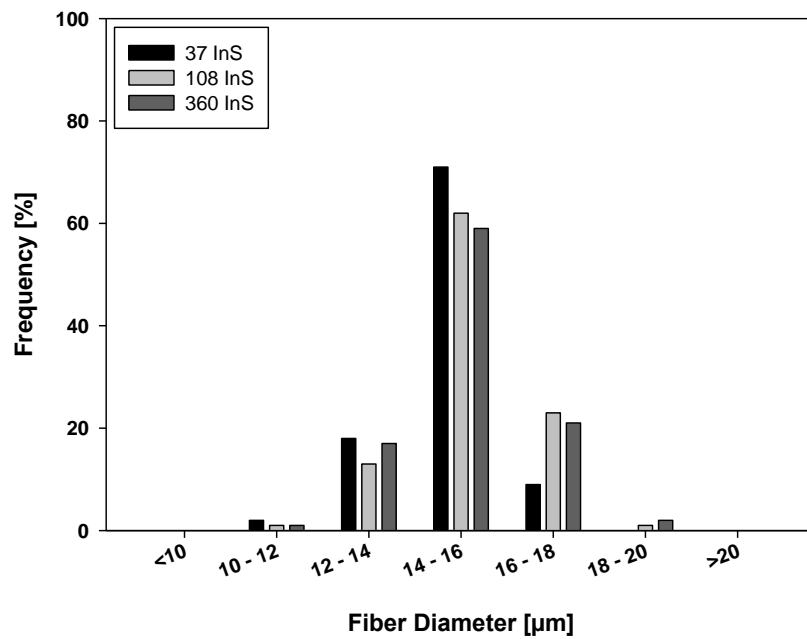


Figure 5- 13: Fiber size distribution of intact island-in-the-sea fibers of structures with intact 37, 108 and 360 InS fibers

Average weight loss for island size estimation was taken from basis weight measurements and calculated to be ~29.94% (SD: 0.13) for 37 island-in-the-sea structures, ~29.29% for 108 island-in-the-sea structures and 24.97% for 360 island-in-the-sea structures. Since SEM images and also FTIR analysis proved poly (lactic acid) to be completely removed from 37 island-in-the-sea structures the measured polymer ratio was used to calculate theoretical island diameters. Calculated and measured island sizes from 37, 108 and 360 island-in-the-sea structures can be seen in Table 5- 3.

Table 5- 3: Results of island diameter measurements (after caustic treatment)

Island Count	$\bar{x}(d_{f,island})$ [μm] (Theoretical)	$\bar{x}(d_{f,island})$ [μm] (Measured)	SD, σ ($d_{f,island}$) [μm]
37	2.1	2.2	0.1
108	1.3	1.4	0.2
360	0.7	0.5	0.03

Results demonstrate the calculated island diameter to be in accordance with measured values. However, measurements revealed islands of 360 island-in-the-sea structures to be smaller than predicted.

5.4.3 Influence of Island Count on Specific Surface Area

Results of theoretical accessible specific surface area are depicted in Figure 5- 14.

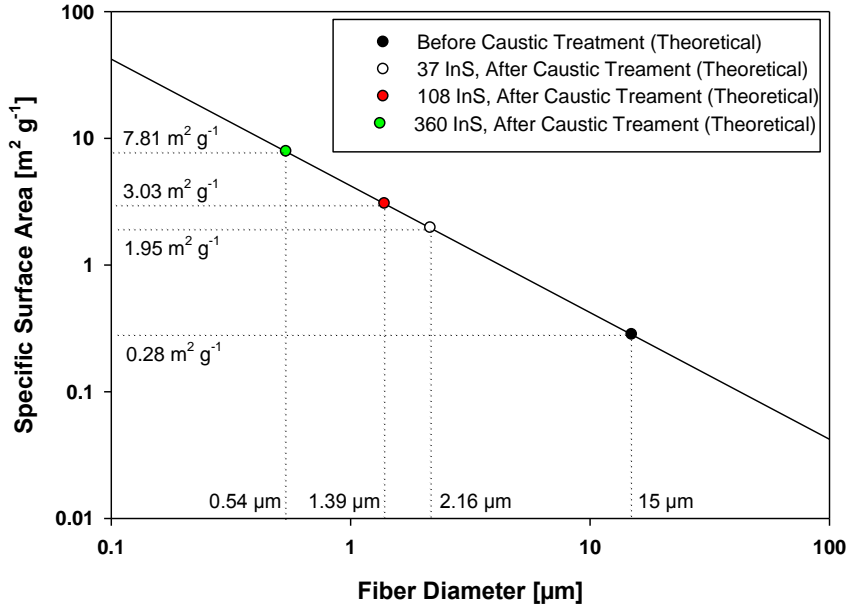


Figure 5- 14: Calculated theoretical accessible specific surface area based on fiber size measurements

Theoretical specific surface area represents the ideal case with all islands to be separated and accessible. BET specific surface areas are shown in the following table and indicate just little variation from theoretical calculations. However, BET measurements of 360 island-in-the-sea structures revealed the samples to have just half of the calculated specific surface area. This is in accordance with weight loss results and optical analysis of SEM images indicating incomplete removal of poly (lactic acid) from the bicomponent structure. Intact island-in-the-sea fibers showed little higher BET specific surface areas, which might be correlated to water jet fibrillation during hydroentangling.

Table 5- 4: Results of BET specific surface area measurements

	Intact InS	37 InS	108 InS	360 InS
Theoretical SSA [m² g⁻¹]	0.28	1.95	3.03	7.81
BET SSA [m² g⁻¹]	0.4	2.22	2.83	3.55

5.4.4 Effect of Island Count and Jet Spacing on Structure Properties

Figure 5- 15 depicts the results of normalized thickness (nominal basis weight: 95 g m⁻²) after removing the sea polymer from the island-in-the-sea structures. Data indicates the jet spacing to influence the thickness of the materials. 2-Way ANOVA has been applied to understand the relationship between island count, jet spacing and resulting thickness.

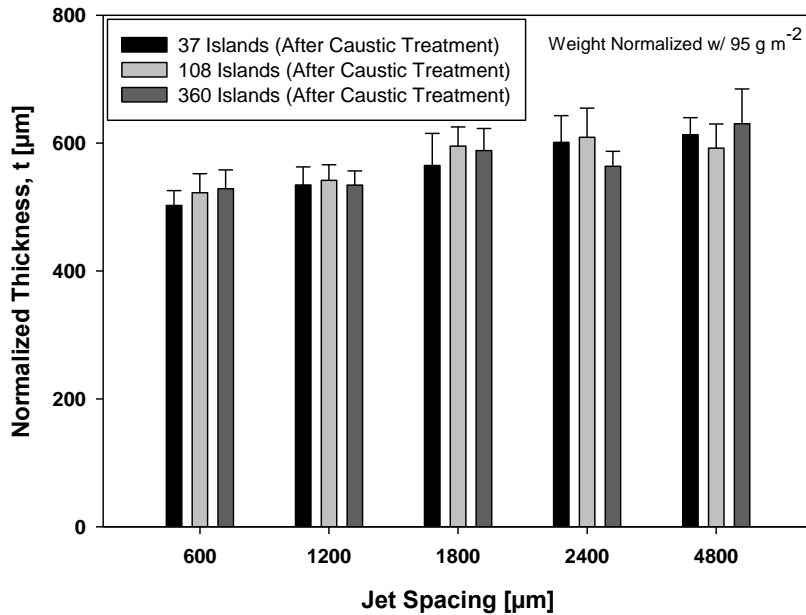


Figure 5- 15: Influence of island count and jet spacing on normalized thickness after caustic treatment

ANOVA results indicate jet spacing to influence the thickness of the caustic-washed island-in-the-sea structures. However, no evidence was found for the island count to affect the thickness of the samples. Also, there was no interaction found between island count and jet spacing after the structures underwent the caustic washing.

Table 5- 5: 2-Way ANOVA ($\alpha: 0.05$), Influence of island count and jet spacing on normalized thickness, after caustic treatment (performed with JMP Pro)

Island Count [Prob > F]	Jet Spacing [Prob > F]	Island Count * Jet Spacing [Prob > F]
.1990	<.0001 (<i>REJECT H₀</i>)	.1975

Results of solid volume fraction after treating the materials with caustic are given in Figure 5- 16. Comparison of the results reveals the solidity of materials to generally decrease with increasing jet spacing. We reported this trend for 37 island-in-the-sea structures but it seems also to be valid for higher island counts. However, both 108 and 360 island-in-the-sea structures show no further decrease in bulk density beyond 1800 μm jet spacing. This may be explained by the interaction of low density regions and reduced fiber sizes.

ANOVA results indicate the jet spacing but not island count to influence the solid volume fraction of caustic-washed island-in-the-sea samples.

Table 5- 6: 2-Way ANOVA ($\alpha: 0.05$), Influence of island count and jet spacing on SVF, before/after caustic treatment (performed with JMP Pro)

Island Count [Prob > F]	Jet Spacing [Prob > F]	Island Count * Jet Spacing [Prob > F]
.137	<.0001 (<i>REJECT H₀</i>)	.1623

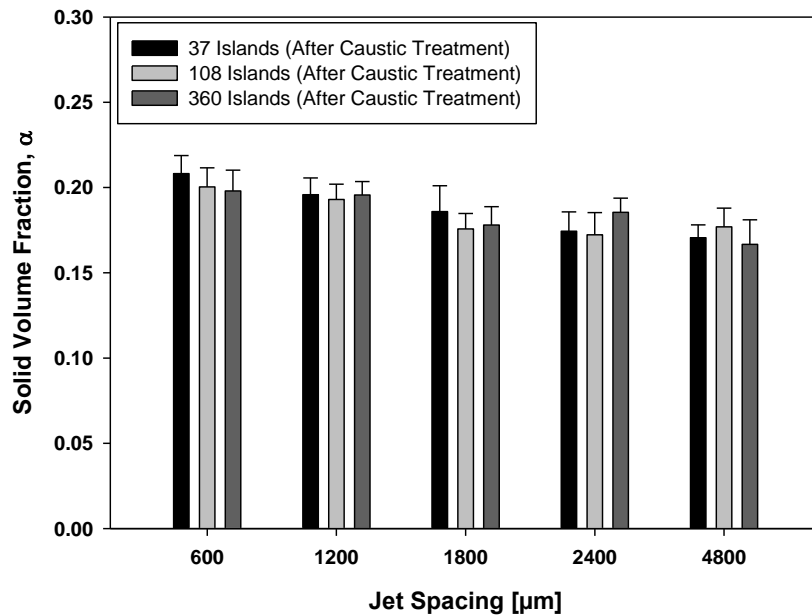


Figure 5- 16: Influence of island count and jet spacing on solid volume fraction after caustic treatment

5.4.5 Influence of Island Count on Air Permeability and Filtration Properties

To enhance comparability air permeability results were normalized by a nominal basis weight of 95 g m^{-2} . Air permeability results of caustic-washed island-in-the-sea structures hydroentangling with different jet spacing are shown in Figure 5- 17 and indicate the air permeability to increase with jet spacing. Also, 108 and 360 island-in-the-sea structures showed higher permeabilities compared to bicomponent structures with 37 islands. This can be explained by the difficulties to completely remove sea compound and evenly spread islands of both 108 and 360 island-in-the-sea structures. Intact island-in-the-sea fibers have larger diameters and lead to increased pore sizes within the material. This correlation is confirmed by analysis of variances, which is shown in Table 5- 7.

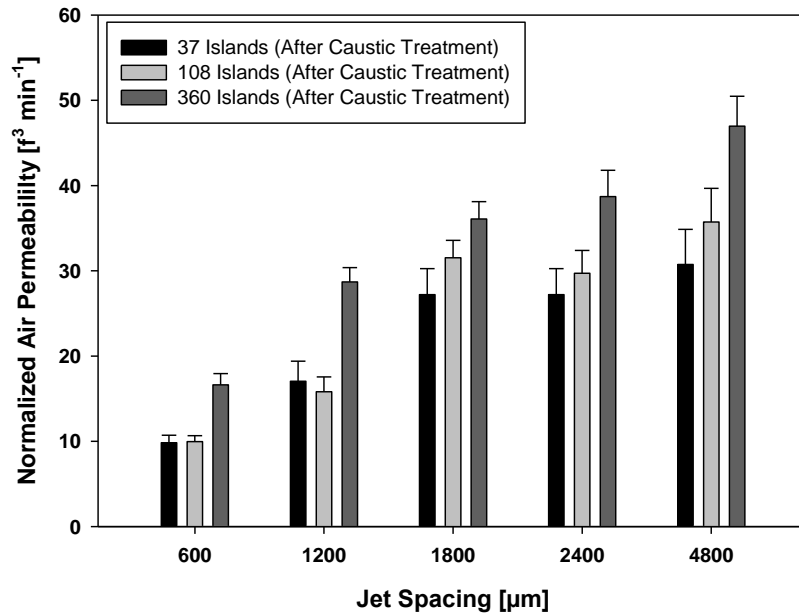


Figure 5- 17: Influence of island count and jet spacing air permeability after caustic treatment

Table 5- 7: 2-Way ANOVA ($\alpha: 0.05$), Influence of island count and jet spacing on air permeability, before/after caustic treatment (performed with JMP Pro)

Island Count [Prob > F]	Jet Spacing [Prob > F]	Island Count * Jet Spacing [Prob > F]
.0002 (<i>REJECT H₀</i>)	<.0001 (<i>REJECT H₀</i>)	.0019 (<i>REJECT H₀</i>)

Figure 5- 18 depicts the influence of fiber size on the filtration properties. Figure shows the capture efficiency of unwashed and caustic-soda treated 37 island-in-the-sea nonwoven materials. Both materials were IPA discharged prior testing and indicate the filtration efficiency to be comparable for 600 µm jet spacing but to be higher for larger jet spacing. Thus, smaller fibers are not enhancing the filtration efficiency for narrow jet spacing. However, results from Figure 5- 19 indicate the caustic treatment to loosen the structure

resulting in lower pressure drops. Capture efficiency of nonwovens bonded with a jet spacing larger than 600 μm was found to be higher compared to materials with intact bicomponent fibers. Filtration efficiency of unwashed island-in-the-sea structures hydroentangled with jet spacing larger than 600 μm performed almost the same, whereas the opposite was found for caustic-treated nonwovens.

Pressure drop of both materials decreased with increasing jet spacing but caustic-treated materials hydroentangled with jet spacing larger than 600 μm showed a higher resistance to flow. This is because of the reduction of fiber size after removing the sea compound from the structure.

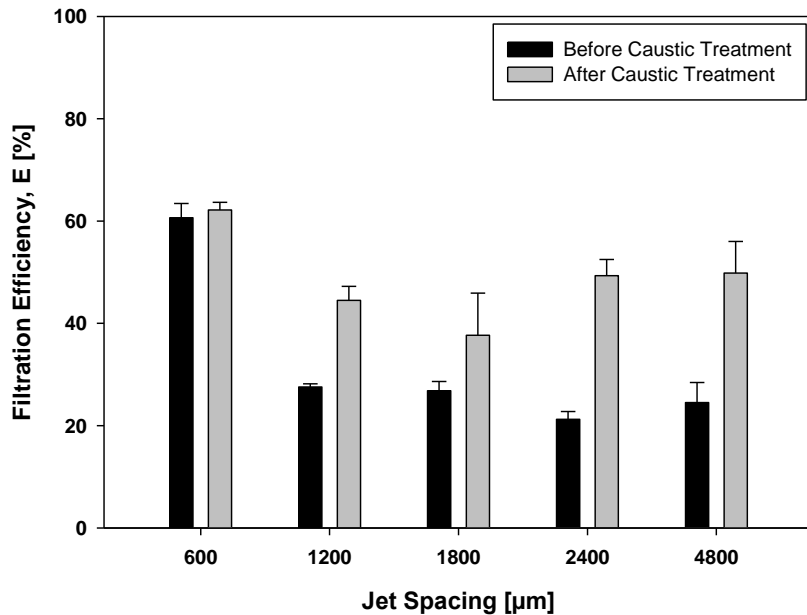


Figure 5- 18: Filtration efficiency as a function of jet spacing ($d_p: 0.3 \mu\text{m}, f_v: 5.33 \text{ cm s}^{-1}, A: 100 \text{ cm}^2, DOP$)

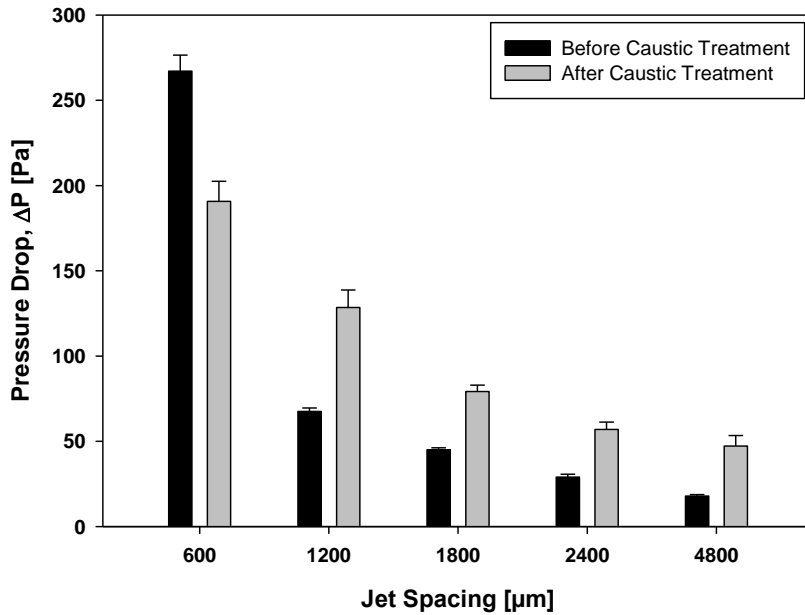


Figure 5- 19: Pressure drop as a function of jet spacing (5.33 cm s^{-1})

Capture efficiency of caustic-treated 37, 108 and 360 island-in-the-sea structures is given in Figure 5- 20. Data indicates the filtration efficiency to decrease with larger jet spacing except for 37 island-in-the-sea structures. 360 island-in-the-sea nonwoven showed lowest capture efficiency and 37 and 108 island-in-the-sea materials comparable particle penetrations for 600 μm, 1200 μm and 1800 μm jet spacing.

Pressure drop of samples is shown in Figure 5- 21 and shows the pressure drop of 37 island-in-the-sea structures to decrease with larger jet spacing. In contrast to that, pressure drop of 108 island-in-the-sea materials levels off until 1800 μm before increasing again. This may be explained by the difference in fiber diameter as islands of 37 island-in-the-sea structure have about twice the diameter. Thus, affinity to bend and cause structure collapsing

is significantly lower. 360 island-in-the-sea structures showed lowest pressure drop indicating incomplete removal of the sea compound.

Results indicate not the reduction of island diameter and therefore increase in specific surface area to enhance the filtration properties but rather the interaction of fiber size and structure. Even though BET specific surface area was measured to be the highest for 360 island-in-the-se structures materials showed lowest filtration performance.

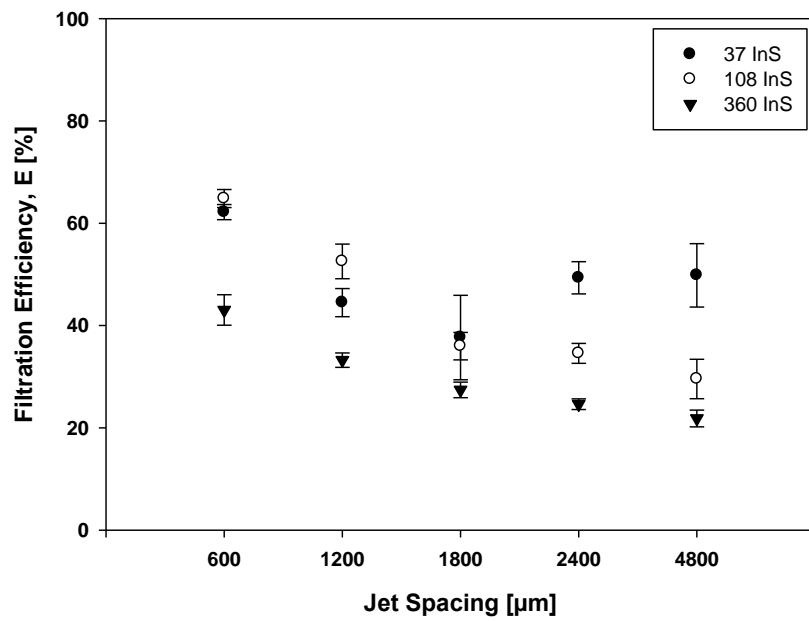


Figure 5- 20: Filtration as a function of jet spacing ($d_p: 0.3 \mu\text{m}$, $f_v: 5.33 \text{ cm s}^{-1}$, $A: 100 \text{ cm}^2$, DOP)

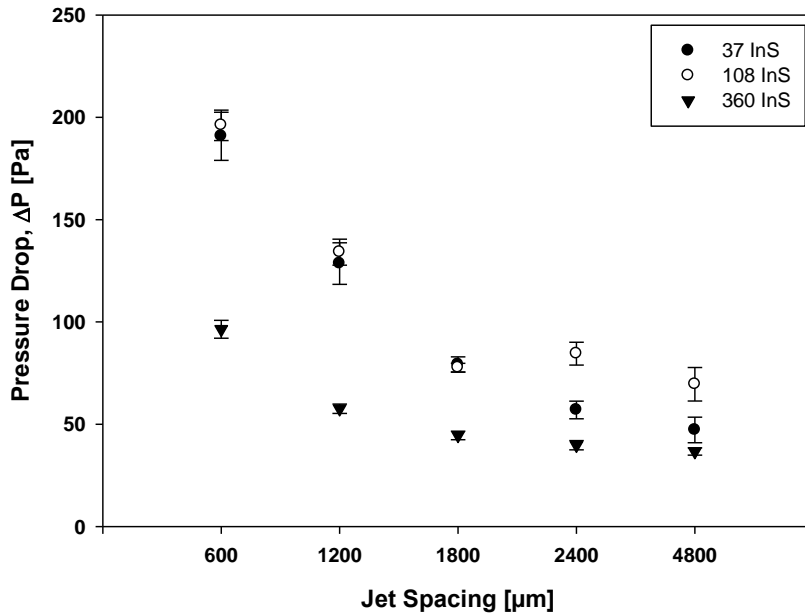


Figure 5- 21: Pressure drop as a function of jet spacing ($f_p: 5.33 \text{ cm s}^{-1}$)

Quality factors of all structures are depicted in Figure 5- 22. From the results it can be seen that 37 island-in-the-sea structures hydroentangled with large jet spacing have better filtration properties compared to the other materials. Quality factor results can be divided into two different regions. First region indicates 108 and 360 but also 37 island-in-the-sea structures hydroentangled with narrow jet spacing to show similar quality factors. Second region includes 37 island-in-the-sea materials hydroentangled with jet spacing larger than 1800 μm. Islands of these samples are strong enough to prevent the pocket-like structure from collapsing.

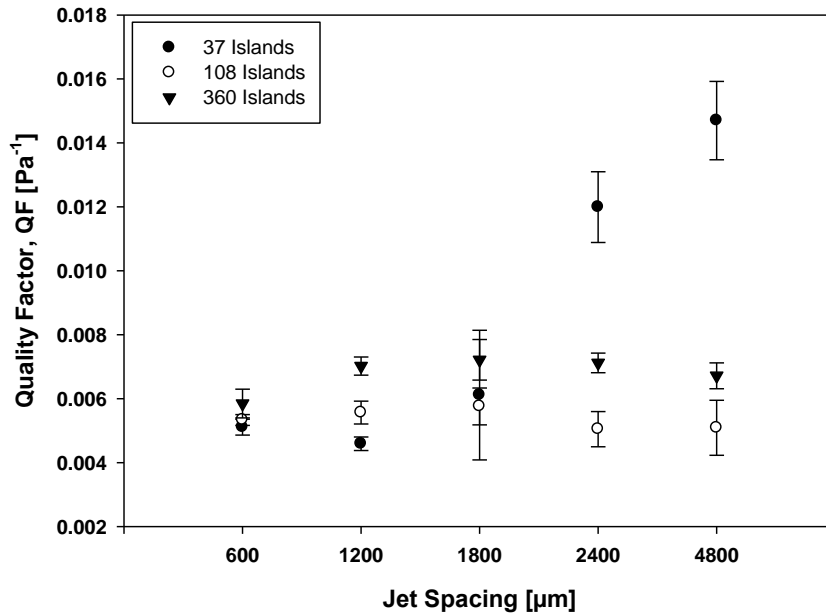


Figure 5- 22: Quality factor as a function of jet spacing

5.5 Summary and Conclusion

Spunbond island-in-the-sea materials with three different island counts (37, 108 and 360) were hydroentangled with same pressures but varying jet spacing. Structures underwent a caustic-soda washing to remove the sea compound from the bicomponent structure. Smallest average island diameter was measured to be about $0.5 \mu\text{m}$ resulting in a BET specific surface area of about $3.5 \text{ m}^2 \text{ g}^{-1}$, which was not in accordance with theoretical calculations. Results indicated the sea removal to work for 37, partially for 108 but not 360 island-in-the-sea structures. Experiments indicated the solid volume fraction of sodium hydroxide washed island-in-the-sea nonwoven materials to be a function of the jet spacing during hydroentangling. However, air permeability of materials was found to be dependent on island

count and also jet spacing. Filtration performance was reported to be a function of structure and fiber size and 37 island-in-the-sea nonwovens hydroentangled with jet spacing larger than 1800 μm to be superior.

5.6 References

- Anantharamaiah, N., Durany, A. & Pourdeyhimi, B. (2009). High surface area nonwovens via fibrillating spunbonded nonwovens comprising Islands-in-the-Sea bicomponent filaments: structure–process–property relationships. *Journal of materials science*, 44(21), 5926-5934.
- Anantharamaiah, N., Verenich, S. & Pourdeyhimi, B. (2008). Durable nonwoven fabrics via fracturing bicomponent islands-in-the-sea filaments. *Journal of Engineered Fibers and Fabrics*, 3(3), 1-9.
- Batra, S. K. & Pourdeyhimi, B. (2012). *Introduction to nonwovens technology*: DEStech Publications, Inc.
- Chapman, R. (2010). *Applications of nonwovens in technical textiles*: Elsevier.
- Dugan, J. S. (2010). Specialty Markets - Bicomponent Fibers. Retrieved May 26, 2015, from [http://www.textileworld.com/Issues/2010/July-August/Nonwovens-Technical Textiles/Specialty Markets --Bicomponent Fibers](http://www.textileworld.com/Issues/2010/July-August/Nonwovens-Technical%20Textiles/Specialty%20Markets%20--Bicomponent%20Fibers)
- Koslowski, H. (2009). Man-Made Fibres Congress: Dornbirn Austria:16-18th Sept 2009. Retrieved September 9th, 2014
- Pohl, G. (2010). *Textiles, polymers and composites for buildings*: Elsevier.
- Pourdeyhimi, B. (2008). Comments on the paper entitled “Splitting of islands-in-the-sea fibers (PA6/COPET) during hydroentangling of nonwovens”. *Journal of Engineered Fibers and Fabrics*, 3, 32-35.
- Pourdeyhimi, B., Minton, A. & Putnam, M. (2004). Structure-process-property relationships in hydroentangled nonwovens-part 1: preliminary experimental observations. *International Nonwovens Journal*, 13, 15-21.
- Prokop, A. (2014). *Intracellular Delivery Ii: Fundamentals and Applications*: Springer London, Limited.
- Yeom, B. Y. & Pourdeyhimi, B. (2011). Aerosol filtration properties of PA6/PE islands-in-the-sea bicomponent spunbond web fibrillated by high-pressure water jets. *Journal of materials science*, 46(17), 5761-5767.

CHAPTER 6

- High Surface Area Mixed Media Nonwovens Materials -

Sections of this chapter will be submitted for publication in a peer-reviewed journal

6.1 Abstract

Mixed media are hybrid structures consisting of homo- and bicomponent fibers in a pre-defined pattern. Depending on the spinpack design both fiber types can be spun in an alternating or layered configuration providing and combining the advantages of different fiber sizes and/or cross-sections. The purpose of this study is to advance understanding of the influence of hydroentangling and different jet spacing (600 μm , 1800 μm and 4800 μm) on mixed media island-in-the-sea structures. Research also examines how mixed media structures differ in terms of structure, properties and aerosol filtration performance from conventional island-in-the-sea materials. Spunbond technique was used to manufacture poly (propylene)/poly (lactic acid) mixed media island-in-the-sea webs in an alternating configuration with two different island counts (37 and 108 islands) and a basis weight of 125 g m^{-2} . The study's findings revealed the hydroentangling pressures used for island-in-the-sea webs to be too low for mixed media structures. Materials hydroentangled with large jet spacing fell apart during the caustic washing due to insufficient fiber entanglement. Increasing the pressure but not the specific energy led to mixed media structures with adequate strength. It was proven that implementing larger fibers led to decreased pressure drops but also lower filtration efficiencies. Insufficient fiber spreading and lower specific surface area might be reasonable explanations for that. Nevertheless, calculated quality factors indicated mixed media structures to be superior in terms of filtration performance compared to 37 island-in-the-sea structures.

6.2 Introduction

The idea of using more than one polymer within a single fiber to benefit from its properties is certainly nothing new. It is believed that this concept first appeared in 1930s when the former German company IG Farben AG used side-by-side viscose fibers to increase crimp (Koslowski, 2009). Since then, numerous bi- and multicomponent fibers have been introduced to either change the cross-section or reduce the fiber diameter. Common examples are splittable bicomponent fibers, such as segmented pie, tipped-trilobal or side-by-side fibers (Fedorova, 2006, p. 22; Pourdeyhimi, 2011a). Researchers used hydroentangling to split such fibers and obtain structures with much smaller mean fiber sizes (Anantharamaiah, Verenich et al., 2008; Yeom & Pourdeyhimi, 2011). Splittable fibers require the polymers to be immiscible and thus share no similarities. Island-in-the sea fibers describe another fiber type containing much smaller fibers (islands) embedded in a matrix (sea). Island-in-the-sea fibers are not classified as splittable bicomponent fibers as just the sea polymer is exposed to the surface. Island fibers can be either fibrillated by mechanical force (e.g. hydroentangling) or unveiled by chemical treatments (dissolving sea polymer) (Fedorova, 2006, p. 26; Pourdeyhimi, 2008). Using island-in-the-sea nonwoven materials along with suitable post-treatments can result in micro- or even nanofibers offering a variety of interesting properties. Reducing fiber size and thus increasing the specific surface areas of nonwoven materials has the potential to improve properties, such as filtration performance, textile hand but also fluid absorption (Shim, Pourdeyhimi et al., 2010).

If product demands require the material to have multiple properties, which cannot be achieved by a single fiber type, hybrid structures can be used to overcome limitations. These

structures can either be made by layers of different materials or by implementing different fiber types into a structure. SMS (spunbond-meltblown-spunbond) nonwoven materials, which were first patented by Kimberly-Clark in 1977, are the prime example of composite nonwovens (Hutten, 2007, p. 97). Whereas the spunbond layer has the purpose to provide additional strength the meltblown layers acts as a barrier. Other variations of SMS nonwovens are SMMS or SSMMMSS (Das & Pourdeyhimi, 2014, p. 8). SMS nonwoven materials are traditionally produced by using a series of beams followed by point bonding (Batra & Pourdeyhimi, 2012, pp. 304-305).

Over the past years more and more patents have been filed and papers published about mixed fiber structures, i.e. materials consisting fibers, which are different in size, shape or other characteristics (Iyama, Kuroda et al., 2014; Marmon & Creagan, 1999). Such structures can either be produced by using finite (staple) or continuous (filaments) fibers. A process to directly spin mono- and multicomponent fibers in a predetermined configuration is mentioned in patent US7981336 B2. Fibers within the material can be organized differently, such as in an alternating, layered or random configuration (Pourdeyhimi, 2011b). Mentioned mixed media island-in-the-sea configurations are depicted in Figure 6- 1 - Figure 6- 3. Hollowell studied layered and alternating configurations of mixed media segmented pie and island-in-the-sea structures. According to the study, implementation of larger fibers led to less compact, more permeable structures with higher specific surface areas (Hollowell, 2012). However, there is no literature covering mixed media structures hydroentangled with different jet spacing and their impact on aerosol filtration performance. This study reports on

mixed media alternating 37 and 108 island-in-the-sea materials hydroentangled with different jet spacing and manifold pressures.

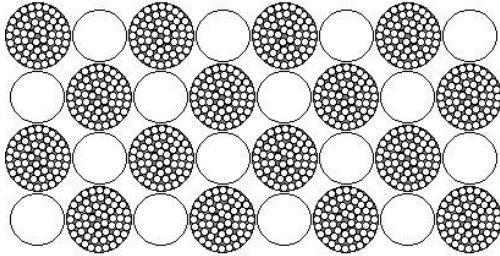


Figure 6- 1: Illustration of an alternating mixed media island-in-the-sea configuration

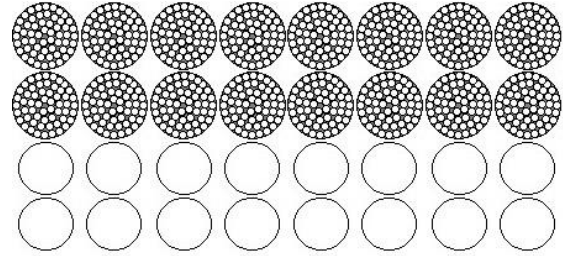


Figure 6- 2: Illustration of a layered mixed media island-in-the-sea configuration

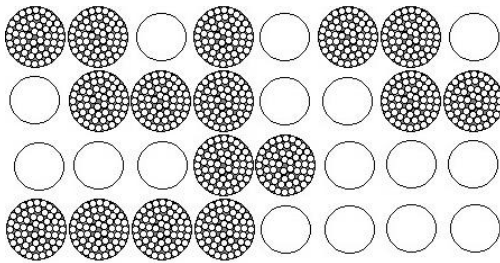


Figure 6- 3: Illustration of a random mixed media island-in-the-sea configuration

6.3 Methodology

6.3.1 Materials

Mixed media alternating 37 and 108 island-in-the-sea structures made from poly (propylene) (Braskem CP360H) for the homocomponent part and the islands and poly (lactic acid) (Natureworks 6202D) for the sea compound were produced at the Nonwovens Institute pilot facilities located at Centennial Campus, North Carolina State University. A 0.5 meter Hills-Nordson spunbond line was used for web formation with a fixed polymer ratio of 75 (PP) to

25 (PLA). Structures were spun with a homo- to bicomponent ratio of 50 to 50 in an alternating fiber configuration. Basis weight of materials was fixed at 125 g m^{-2} . After web formation materials went through a compaction roll with 75 psi pressure to enhance the self-adherence of fibers before being cold calendered. A 0.5 meter Fleissner Aquajet 5-manifold hydroentangling unit was used for subsequent hydroentangling. Webs were hydroentangled with different jet spacing but fixed manifold pressures before being dried in a conveyor oven. All structures along with information about hydroentangling parameters can be seen in the following table.

Table 6- 1: Structures and hydroentangling parameters

Fabric		Jet Spacing [μm]	Island Count	Hydroentangling Pressure [bar]		Belt Speed [m min^{-1}]
4.-37-Jet Spacing-125 (37 InS)	Mono	600 1800 4800	37	P1	20 (Manifold 1)	10
6.-37MM-Jet Spacing-125-1 (37 Alt. Mixed Media InS)	Mixed Media				100 (Manifold 2)	
6.-37MM-600-125-2 (37 Alt. Mixed Media InS)			100 (Manifold 3)			
6.-108MM-600-125 (108 Alt. Mixed Media InS)			150 (Manifold 4)			
			108	P2	150 (Manifold 2)	
					200 (Manifold 3)	

Cross-sectional microscopy images of drawn fibers of mixed media 37 and 108 island-in-the-sea structures are shown in the following.

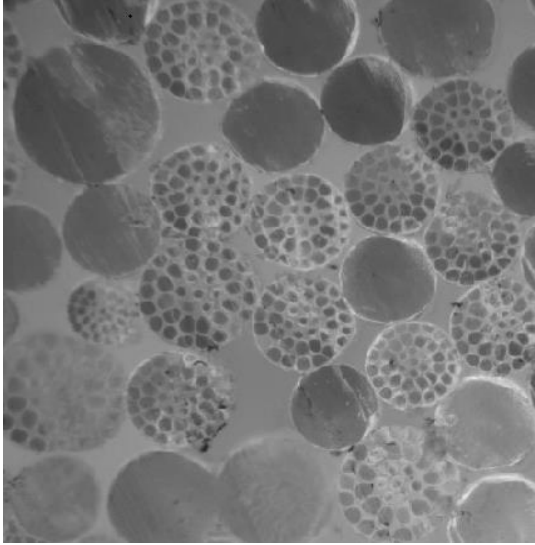


Figure 6- 4: Microscopy image of cross-section of drawn fibers of MM 37 InS structure

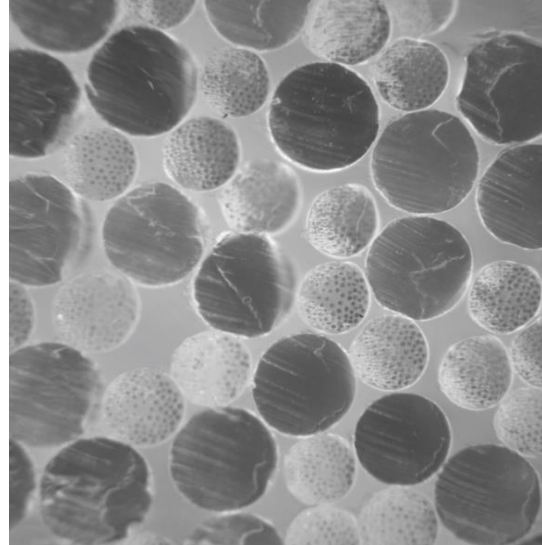


Figure 6- 5: Microscopy image of cross-section of drawn fibers of MM 108 InS structure

Influence of manifold pressure and jet spacing on specific energy is shown in Figure 6- 6.

Specific energy was calculated for all structures and calculated based on the following equations. Energy carried by a single water jet \dot{E} was estimated as follows:

$$\dot{E} = \frac{\pi}{8} \rho d_n^2 C_d v^3 \text{ [J s}^{-1}\text{]} \quad \text{Eq. 6- 1}$$

where ρ is the specific density of the fluid [998.2 Kg m⁻³ for H₂O at 20 °C], d_n the nozzle diameter [m], C_d the discharge coefficient and v the jet velocity [m s⁻¹].

Total energy \dot{E}_{Total} was calculated by multiplying jet energy \dot{E} with the number of jets emanating from the same manifold and adding all together.

$$\dot{E}_{Total} = \left(\sum_{M=1}^n \dot{E}_{JM} \right) \times 1000^{-1} \text{ [KJ s}^{-1}\text{]} \quad \text{Eq. 6- 2}$$

where n is the number of manifolds used during hydroentangling and J the number of jets per manifold.

Afterwards, specific energy SE , which is the energy applied by the water jets per kilogram of fabric, was estimated as follows.

$$SE = \frac{\dot{E}_{Total}}{\dot{M}} [\text{KJ Kg}^{-1}] \quad \text{Eq. 6- 3}$$

where \dot{M} is the mass flow rate of fabric [Kg s^{-1}] and can be determined by using the following equation.

$$\dot{M} = s \times w \times v_B [\text{Kg s}^{-1}]. \quad \text{Eq. 6- 4}$$

where s is the fabric width [m], w is the basis weight of the material [g m^{-2}] and v_B is the operating speed [m s^{-1}] (Pourdeyhimi, Minton et al., 2004).

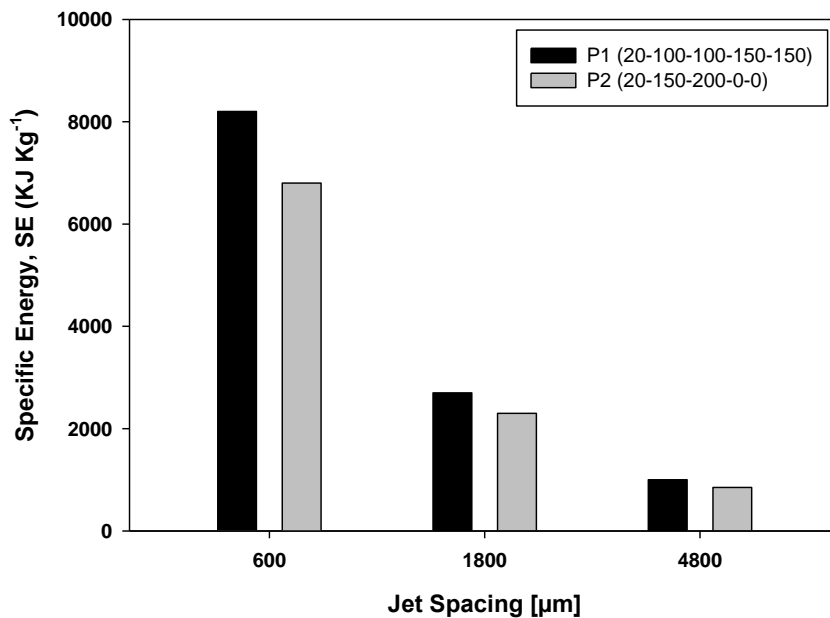


Figure 6- 6: Calculated specific energy during hydroentangling

6.3.2 Sample Preparation

After hydroentangling structures were treated with alkaline to remove the sea compound from the structure. Caustic solution with a concentration of 8% w/w was prepared in a steam-kettle and heated up to 100 °C. Samples were treated for 10 minutes under manual stirring before being washed-out with cold water until pH-neutralization and dried in the open air.

6.3.3 Characterization Methods

Basis Weight and Thickness

Basis weight of all samples was measured with a Denver Instrument XL-3100D top-loading balance and thickness with a Hanatek FT3V-LAB high-precision thickness gauge. A total of 10 samples were tested and weight loss after treatment was used as an indicator whether or not the sea polymer was completely removed.

Solid Volume Fraction

Results of basis weight and thickness were used to calculate the bulk density of all samples by using the following equation.

$$\alpha = \frac{w}{\rho_f \times t} \quad \text{Eq. 6- 5}$$

where w is the basis weight [in g m^{-2}], ρ_f the total fiber density [g cm^{-3}] and t the thickness of the structure [m].

As fiber density is different for intact and caustic treated mixed media structures, total fiber density ρ_f was calculated as follows.

$$\rho_f = (\rho_{P1} \times R_{P1}) + (\rho_{P2} \times R_{P2}) \text{ [g cm}^{-3}\text{]} \quad \text{Eq. 6- 6}$$

where ρ_{P1} is the density of the first polymer [g cm⁻³], R_{P1} is the mass fraction of the first polymer, ρ_{P2} is the density of the second polymer [g cm⁻³] and R_{P2} is the mass fraction of the second polymer.

Specific Surface Area

Island-in-the-sea and mixed media island-in-the-sea structures require different approaches to estimate the accessible specific surface area within the material. Calculation of both is discussed in the following.

a) Estimating Specific Surface Area of Island-in-the-Sea Nonwoven Materials

Fiber diameter of intact island-in-the-sea fiber and individual islands was measured from SEM images with image processing software. Also, island diameter was estimated using the following equation.

$$d_{f,s,t} = d_f \sqrt{\frac{vol_i}{N}} \text{ [}\mu\text{m]} \quad \text{Eq. 6- 7}$$

where d_f is the diameter of the intact island-in-the-sea fiber [μm], vol_i is the volume fraction of the island polymer and N is the island count. After that, accessible specific surface area A_S was calculated using the following equation.

$$A_S = \alpha \sqrt{\frac{4\pi \times 10^6}{\rho D}} [\text{m}^2 \text{g}^{-1}] \quad \text{Eq. 6- 8}$$

where α is the solid volume fraction, ρ is the specific density of the material [g cm^{-3}] and D the fiber denier [g 9000 m^{-1}] (Anantharamaiah, Durany et al., 2009).

b) Estimating Specific Surface Area of Island-in-the-Sea Nonwoven Materials

In contrast to the previous calculation, estimating the specific surface area of mixed media island-in-the-sea nonwoven materials requires further information about the structure. To determine the relation between mono- and bicomponent fibers and calculate the specific surface area of the mixed media structure following information had to be determined.

- Fiber diameter of monocomponent fibers $d_{f,mono}$
- Fiber diameter of bicomponent fibers d_f
- Fiber diameter of islands $d_{f,istand}$

From the settings of the metering pumps during web formation ratio of poly (propylene) to poly (lactic acid) is known to be 75%/25%. Nevertheless, actual amount of poly (propylene) within the monocomponent fibers $R_{PP Mono}$ and bicomponent fibers $R_{PP Bico}$ is not known as this depends, among other factors, on the design of the spinpack. However, knowing these two values is crucial to calculate the specific surface area of the structure. Figure 6- 7 depicts a mixed media island-in-the-sea structure with all abbreviations used for the following calculations.

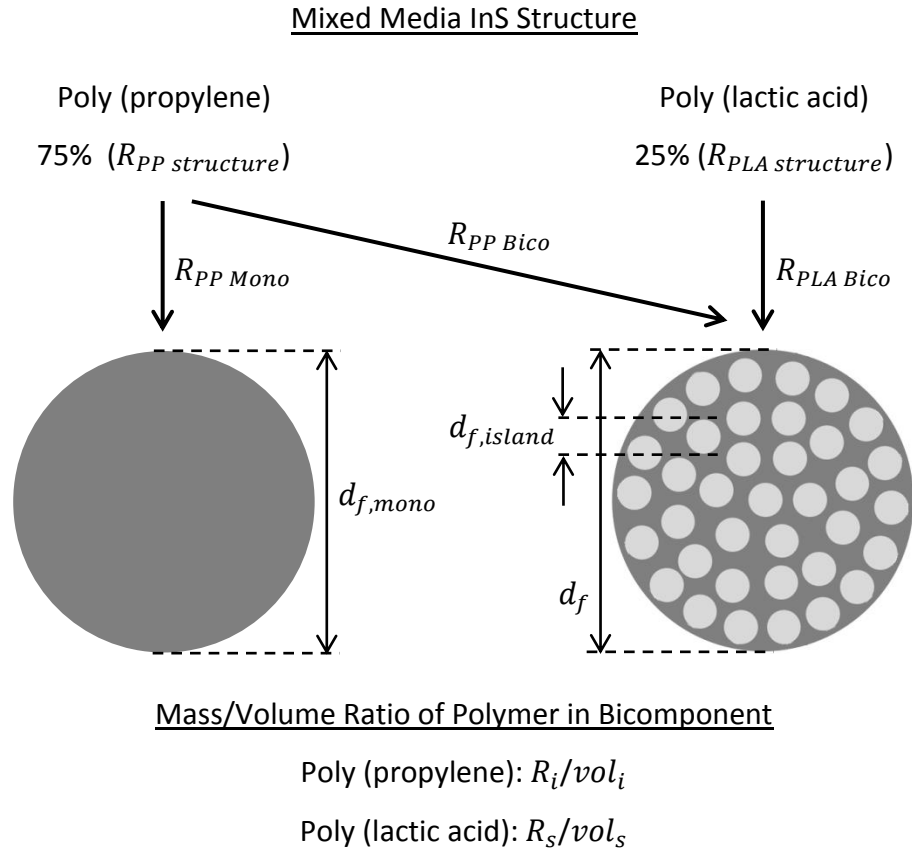


Figure 6- 7: Abbreviations used for specific surface area calculation of MM InS structures

Following calculations are valid for: 1) mixed media alternating island-in-the-sea structures with a 50/50 distribution and 2) mixed media structures where monocomponent fibers are made from the same polymer as island fibers.

After measuring the fiber diameter, volume fraction of island polymer vol_i and volume fraction of sea polymer vol_s were calculated as follows.

$$vol_i = \frac{d_{f,island}^2 N}{d_f^2} \tag{Eq. 6- 9}$$

and volume fraction of sea polymer vol_s can be determined by

$$vol_s = 1 - vol_i \quad \text{Eq. 6- 10}$$

where $d_{f, island}$ [μm] is the measured island diameter, N is the island count and d_f [μm] is the diameter of the intact bicomponent fiber.

Converting the volume fraction to the mass fraction of island polymer R_i was done as shown in the following.

$$R_i = \frac{vol_i \times \rho_i}{(vol_i \times \rho_i) + (vol_s \times \rho_s)} \quad \text{Eq. 6- 11}$$

where vol_i is the volume fraction of island polymer, ρ_i is the specific density of the island polymer [g cm^{-3}], vol_s is the volume fraction of sea polymer and ρ_s is the specific density of the sea polymer [g cm^{-3}].

As poly (propylene) was distributed to the mono- and bicomponent fiber but the ratio is not known mass fraction of poly (propylene) within the structure $R_{PP structure}$ can assumed to be the following.

$$R_{PP structure} = R_{PP Mono} + R_{PP Bico} \quad \text{Eq. 6- 12}$$

where $R_{PP Mono}$ is the mass fraction of poly (propylene) of the monocomponent fiber and $R_{PP Bico}$ is the mass fraction of poly (propylene) of the bicomponent fiber.

Because $R_{PLA structure} = R_{PLA Bico}$ it can be assumed that the mass fraction of poly (propylene) of the bicomponent fiber $R_{PP Bico}$ is defined as follows.

$$R_{PP Bico} = \frac{R_i \times R_{PLA structure}}{1 - R_i} \quad \text{Eq. 6- 13}$$

and

$$R_{PP Mono} = R_{PP structure} - R_{PP Bico} \quad \text{Eq. 6- 14}$$

where R_i is the mass fraction of island polymer, $R_{PLA\ structure}$ the mass fraction of poly (lactic acid) within the structure, $R_{PP\ Mono}$ the mass fraction of poly (propylene) of the monocomponent fiber, $R_{PP\ Mono}$ the mass fraction of poly (propylene) of the monocomponent fiber and $R_{PP\ structure}$ the mass fraction of poly (propylene) within the structure.

Fraction of poly (propylene) within the monocomponent fiber PP_{Mono} and the bicomponent fiber PP_{Bico} can be obtained as follows.

$$PP_{Mono} = \frac{R_{PP\ Mono}}{R_{PP\ Mono} + R_{PP\ Bico}} \quad \text{Eq. 6- 15}$$

$$PP_{Bico} = 100 - PP_{Mono} \quad \text{Eq. 6- 16}$$

where $R_{PP\ Mono}$ is the mass fraction of poly (propylene) of the monocomponent fiber and $R_{PP\ Bico}$ the mass fraction of poly (propylene) of the bicomponent fiber.

Calculated proportions allow calculating the specific surface area of a mixed media alternating island-in-the-sea structure $A_{MM\ Alt\ IS}$ and the corresponding equation is given in the following:

$$A_{MM\ Alt\ IS} = \left(\left(\frac{\sqrt{4\pi \times 10^6}}{\sqrt{\rho D_{Mono}}} \right) \times PP_{Mono} \right) + \left(\left(\frac{\sqrt{4\pi \times 10^6}}{\sqrt{\rho D_{island}}} \right) \times PP_{Bico} \right) [\text{m}^2 \text{g}^{-1}] \quad \text{Eq. 6- 17}$$

where ρ is the specific gravity of the mono-/island polymer [g cm^{-3}], D_{Mono} is the fiber denier for the monocomponent fibers [g 9000 m^{-1}], PP_{Mono} is the fraction of poly (propylene) within the monocomponent fiber, D_{island} is the fiber denier for the island fibers [g 9000 m^{-1}] and PP_{Bico} is the is the fraction of poly (propylene) within the bicomponent fiber.

Air Permeability

All alkaline-washed and unwashed structures were tested for air permeability with a TEXTEST FX 3300 air permeability tester according to ASTM D737. A total of 10 replicates were examined per structure and statistically evaluated.

Aerosol Filtration Properties

Aerosol filtration properties of caustic treated mixed media structures were examined with a TSI 3160 particle penetration tester. Prior testing samples were discharged with isopropyl alcohol according to EN 779. Dioctyl phthalate (DOP) was used as challenging aerosol with a particle size d_p of 0.3 μm . Face velocity f_v was set at 5.33 cm s^{-1} and the tested area was 100 cm^2 .

Quality factor QF was calculated as follows.

$$QF = \frac{-\ln(P)}{\Delta p} [\text{Pa}^{-1}] \quad \text{Eq. 6- 18}$$

where P is the fractional particle penetration and Δp the pressure drop [Pa] of the material.

6.4 Results and Discussion

Discussion of this study is split into the following three parts.

Part I: Comparison of 37 InS structures and mixed media alt. 37 InS structures

Part II: Mixed media alt. 37 InS structures hydroentangled with different manifold pressures

Part III: Comparison of mixed media alt. 37 and 108 InS structures

6.4.1 Part I: Comparison of 37 InS and 37 Mixed Media Alt. InS Structures

6.4.1.1 Removal of Sea Compound

Results of basis weight measurements of unwashed and also caustic-treated structures are depicted in Figure 6- 8. In contrast to 37 island-in-the-sea structures, not all mixed media structures showed sufficient strength to sustain the caustic washing. Materials hydroentangled with 4800 μm jet spacing fell apart during the treatment indicating the requirements in terms of bonding to be different for this type of structure. In contrast to that, structures hydroentangled with 600 μm and 1800 μm jet spacing showed sufficient strength.

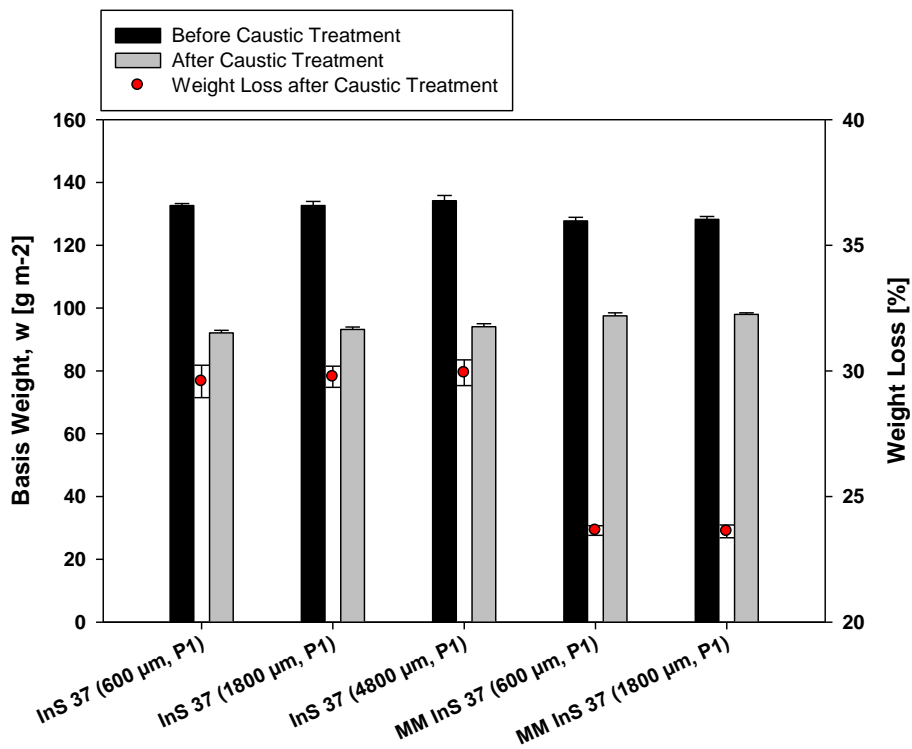


Figure 6- 8: Basis weight before/after caustic treatment

Basis weight measured before and after the caustic washing indicated the weight loss of mixed media materials to be about 25% (measurements: 23.71% PLA, 76.29% PP). Analysis of SEM images provided evidence all poly (lactic acid) to be removed from the structure.

Figure 6- 9 and Figure 6- 10 indicate the island fibers of the 37 island-in-the-sea structure to be evenly distributed after removing the sea polymer from the structure. In contrast to that, SEM images of mixed media structures, which are shown in Figure 6- 11 and Figure 6- 12, show the sea polymer to be removed but less fiber spreading. One explanation for this phenomenon could be the larger fibers hindering the islands to freely move, separate and distribute during the washing process.

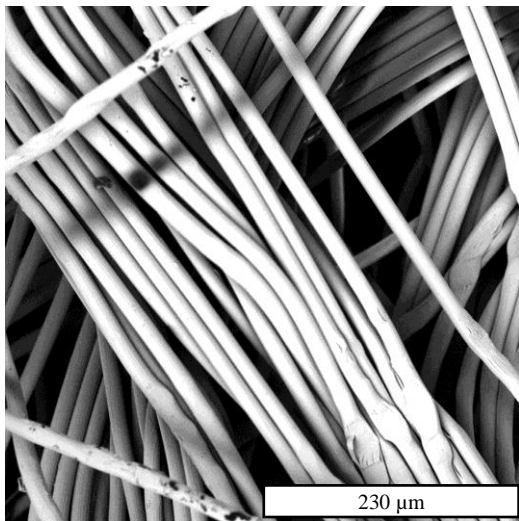


Figure 6- 9: SEM image of 37 InS structure before caustic treatment

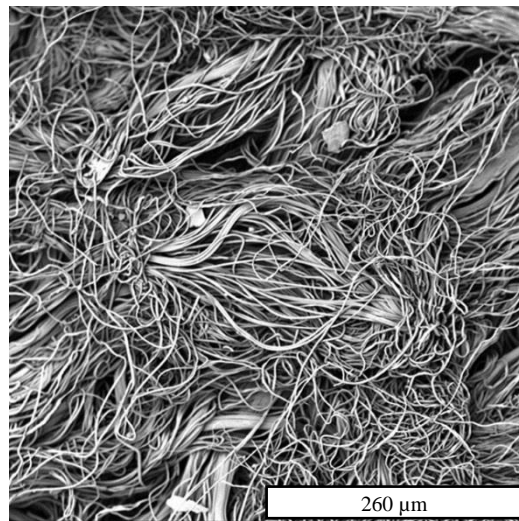


Figure 6- 10: SEM image of 37 InS structure after caustic treatment

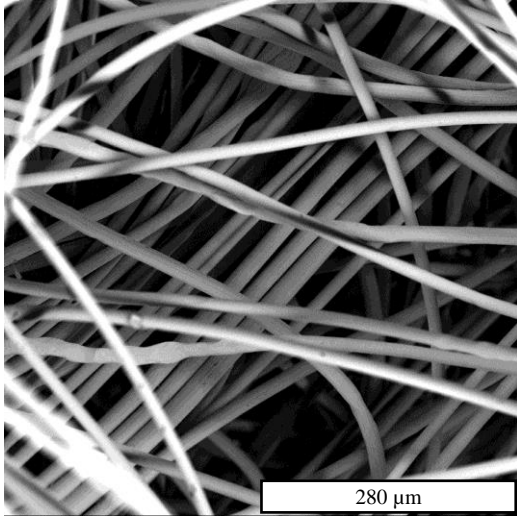


Figure 6- 11: SEM image of mixed media alt 37. InS structure before caustic treatment

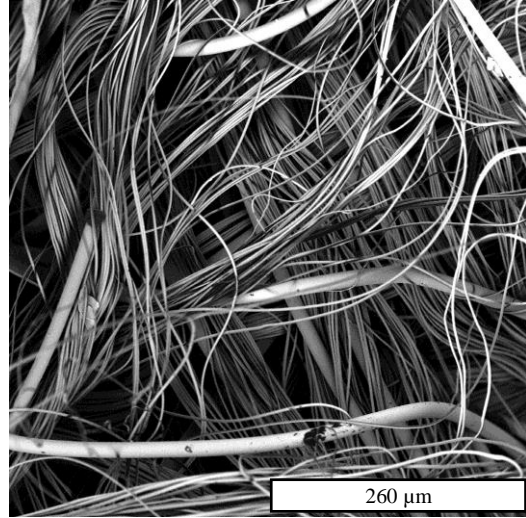


Figure 6- 12: SEM image of mixed media alt. 37 InS structure after caustic treatment

6.4.1.2 Fiber Size and Specific Surface Area

Fiber diameter distribution results of both structures before the caustic treatment can be seen in Figure 6- 13. Measurements indicated the diameter of 37 island-in-the-sea fibers to be different from the intact bicomponent fibers within the mixed media structure. Mean diameters of both structures (before and after the caustic washing) are given in Table 6- 2.

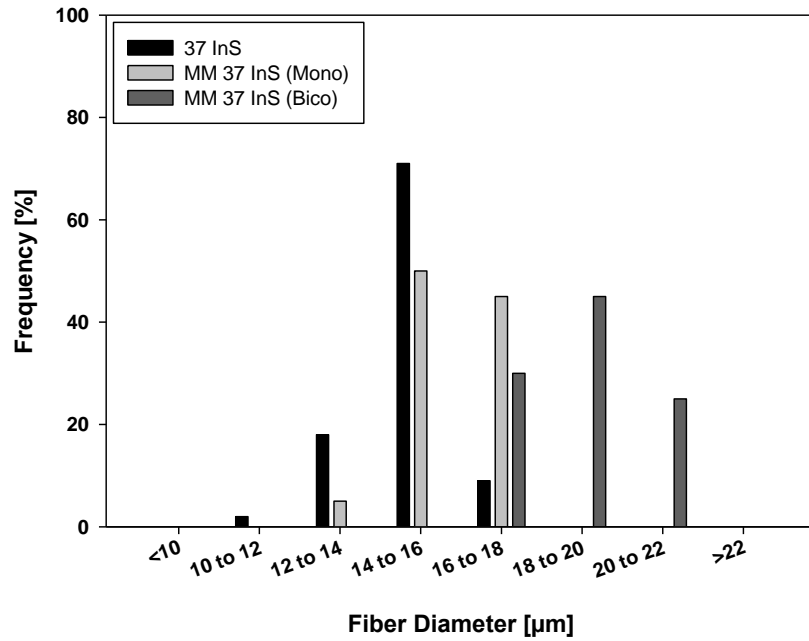


Figure 6- 13: Fiber size distribution of 37 InS and MM alt. 37 InS structure

Table 6- 2: Results of fiber diameter measurements (before/after caustic treatment)

Fiber	$\bar{x}, \sigma (d_{f,bico}) [\mu\text{m}]$ (Measured)	$\bar{x} (d_{f,istand}) [\mu\text{m}]$ (Measured)	$\bar{x}, \sigma (d_{f,homo}) [\mu\text{m}]$ (Measured)
37 InS	14.7 / 1.1	2.2	
MM Alt. 37 InS	19.1 / 1.7	2.6	15.6 / 0.8

Based on the empirical data given in Table 6- 2, calculations of mass ratio of poly (propylene) within the monocomponent fibers $R_{PP Mono}$ and bicomponent fibers $R_{PP Bico}$ revealed poly (propylene) to be evenly distributed between both fiber types. In other words, mass of poly (propylene), which is about 75% of the mass of the whole structure, is

evenly shared by homo- and bicomponent fibers. Following table summarizes mass- and volume fractions of both homo- and bicomponent fibers of the mixed media structure.

Table 6- 3: Calculated mass/volume fractions of the used mixed media structure

Fiber		$R_{structure}$	R/vol	R_{PP}	R_{PLA}
Homo	PP	0.75		0.375	
Bico	PP		0.6/0.67	0.375	
	PLA	0.25	0.4/0.33		0.25

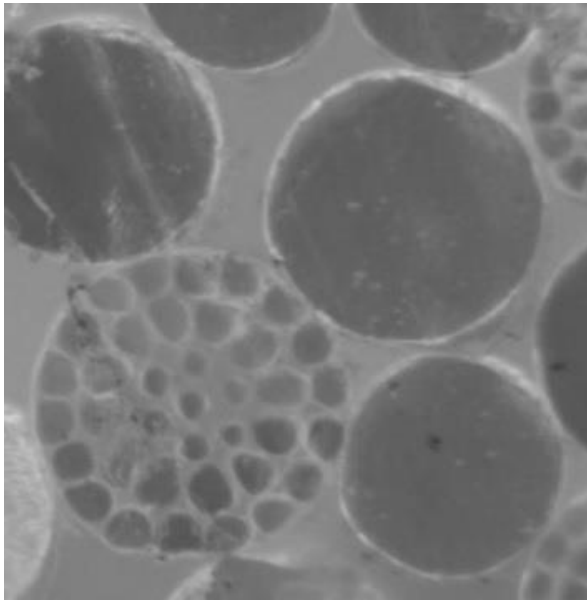


Figure 6- 14: Cross-sectional image of MM 37 InS structure, polymer distribution: 50/50 poly(propylene) homo/mono, 60/40 poly(propylene)/poly (lactic acid) island/sea

Theoretical accessible specific surface area was calculated based on Eq. 6- 7 and Eq. 6- 17 and is depicted in the following. Calculations are based on the data shown in Table 6- 2 and Table 6- 3.

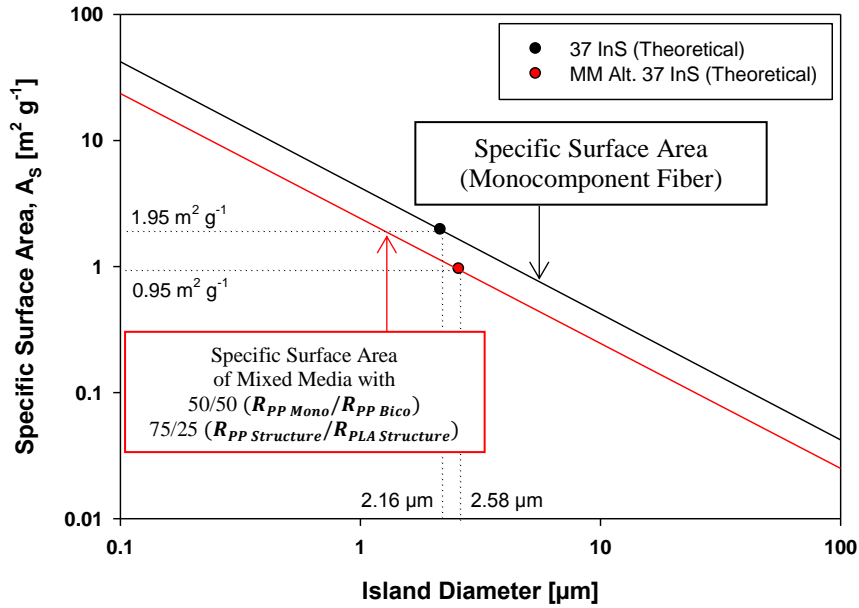


Figure 6- 15: Comparison of specific surface area of 37 InS & MM Alt. 37 InS Structures

As can be seen from the graph, specific surface area of mixed media structures is about half of the specific surface area of the island-in-the-sea structure. This is because of the combination of small (islands) and large (homocomponent part) fibers within the material. Red line designates the relationship of specific surface of and mixed media island-in-the-sea structures with an equal distribution of homo- and bicomponent fibers.

6.4.1.3 Thickness and Solidity

Figure 6- 16 depicts the normalized thickness (nominal weight: 95 g m^{-2}) of both structures as a function of jet spacing. It can be seen that even though webs were hydroentangled with the same pressure mixed media structures show higher thicknesses compared to island-in-the-sea structures. Increased bending rigidities could be responsible for that. Thus, hydroentangling mixed media materials require more intense bonding to achieve comparable consolidation as island-in-the-sea structures. Furthermore, both structures show increasing thicknesses with decreasing jet densities.

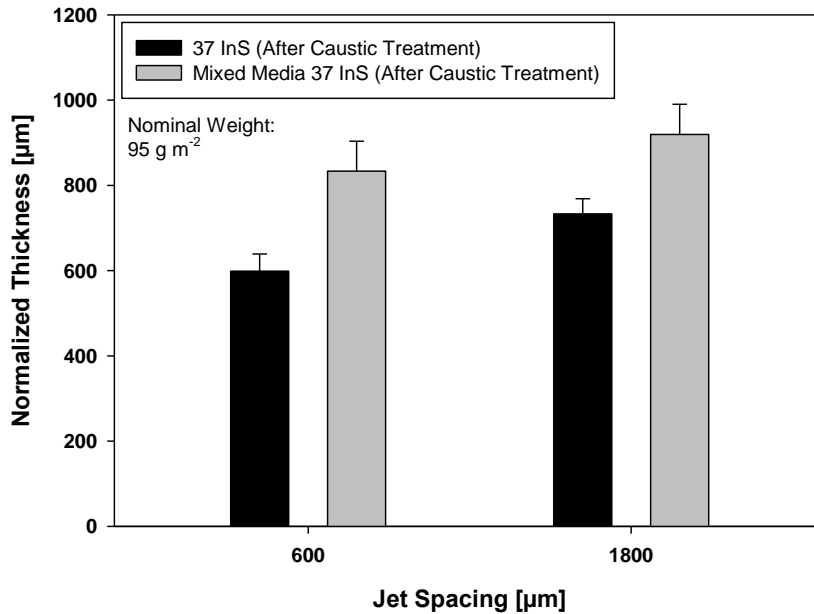


Figure 6- 16: Normalized thickness as a function of jet spacing of caustic-treated 37 InS and MM 37 InS structures

Results of solid volume fraction are depicted in Figure 6- 17 and indicate the density of mixed media structures to decrease with increasing jet spacing. In addition, caustic-treated mixed media structures showed lower solidities than island-in-the-sea materials.

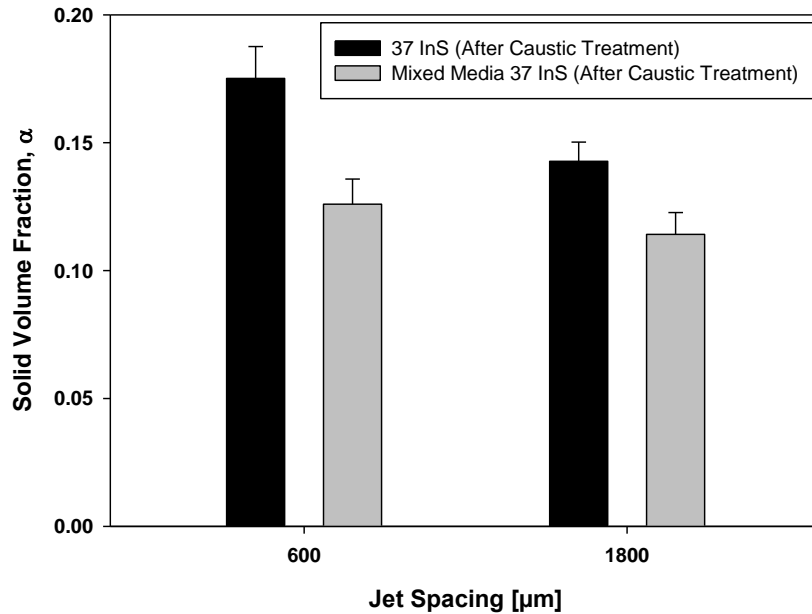


Figure 6- 17: Solidity as a function of jet spacing of caustic-treated 37 InS and MM 37 InS structures

6.4.1.4 Air Permeability and Filtration Performance

Figure 6- 18 depicts the air permeability of caustic-treated structures and indicates the mixed media nonwovens to show significantly higher permeabilities. This is related to the hybrid structure containing a mixture of macro- and microfibers. Results also reveal the air permeability of mixed media island-in-the-sea nonwovens to increase with jet spacing. We previously reported this trend for various island-in-the-sea materials.

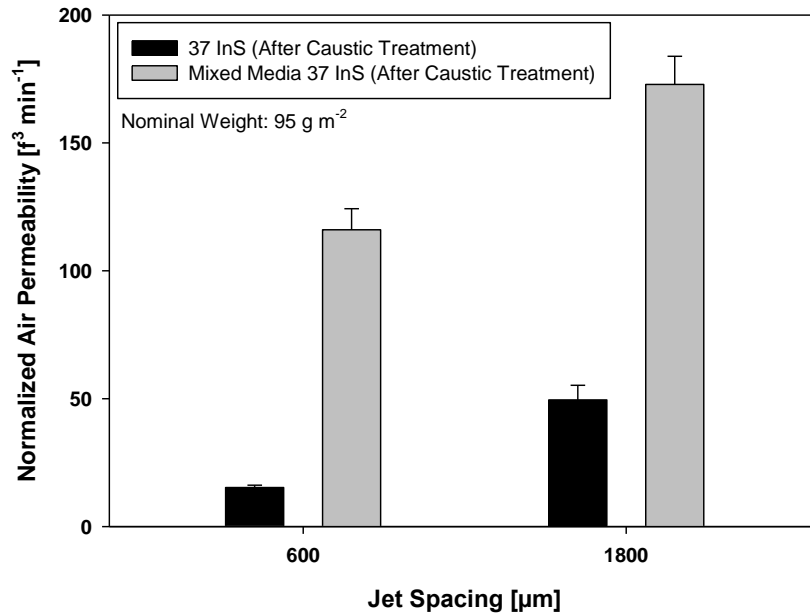


Figure 6- 18: Normalized air permeability as a function of jet spacing of caustic-treated 37 InS and MM 37 InS

As can be seen from Figure 6- 19 mixed media and island-in-the-sea structures show decreasing capture efficiency with increasing jet spacing. Comparing both structures side-by-side reveals mixed media materials to show lower filtration efficiencies. We assume this to be related to larger pore sizes because of fewer microfibers and insufficient island separation and spreading. Pressure drop is shown in Figure 6- 20 and indicates pressure drop of mixed media structures to be significantly lower compared to island-in-the-sea structures. However, plotting the quality factor of the materials (Figure 6- 21) indicates mixed media structures to perform better in terms of filtration performance.

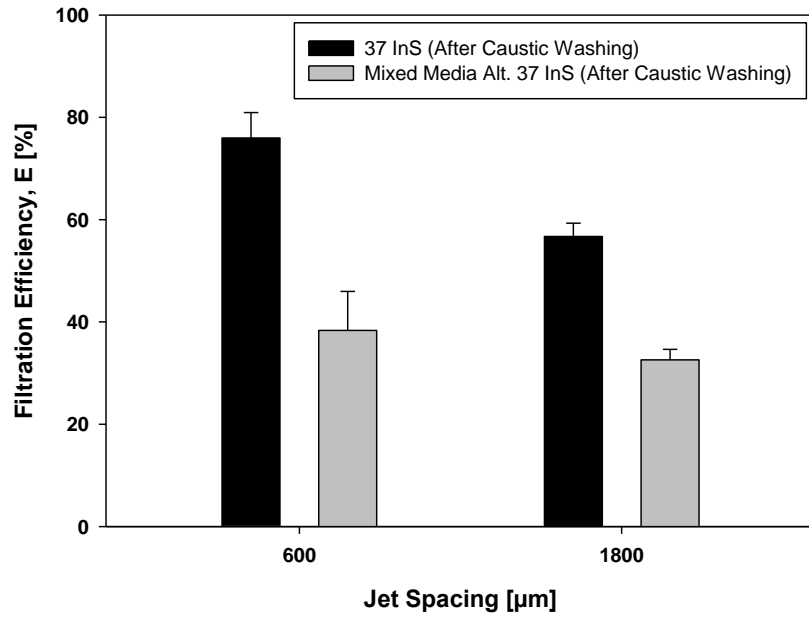


Figure 6- 19: Filtration efficiency as a function of jet spacing ($d_p: 0.3 \mu\text{m}$, $f_v: 5.33 \text{ cm s}^{-1}$, $A: 100 \text{ cm}^2$, DOP)

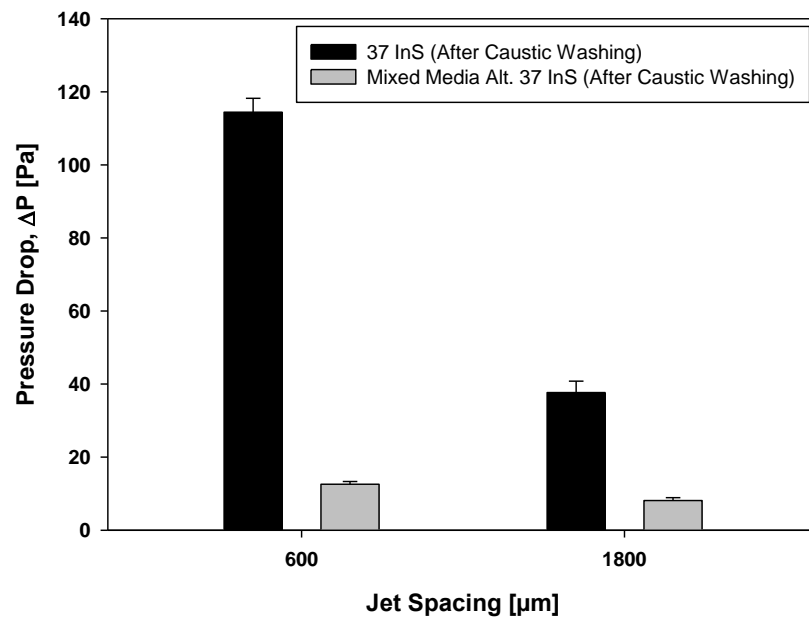


Figure 6- 20: Pressure drop as a function of jet spacing ($f_v: 5.33 \text{ cm s}^{-1}$)

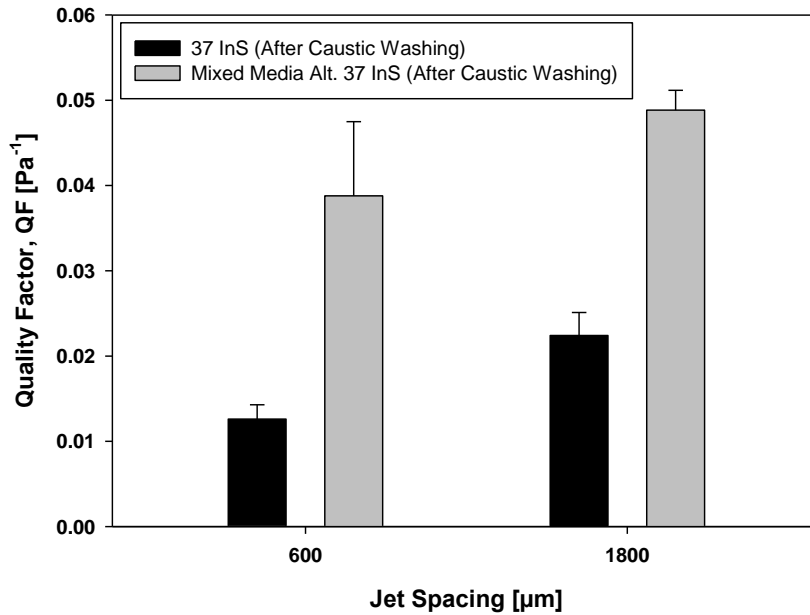


Figure 6- 21: Quality factor as a function of jet spacing

6.4.1.5 Summary (Part I)

The study of 37 island-in-the-sea and mixed media alternating 37 island-in-the-sea structures has shown the homocomponent fibers to influence and change the web's response to hydroentangling. Both materials were hydroentangled under identical conditions but mixed media structures hydroentangled with 4800 μm jet spacing did not show sufficient strength during the caustic treatment. This may be explained by increased bending rigidities because of large homocomponent fibers. Compared to island-in-the-sea nonwovens, mixed media samples showed higher thicknesses, lower solid volume fractions and higher air permeabilities. We assume this to be related to the different response to hydroentangling and larger pore sizes because of homocomponent fibers. SEM images indicated the island

separation during the caustic washing to be different from island-in-the-sea materials. In contrast to island-in-the-sea structures, islands of mixed media samples are not well distributed with many parallel lying microfibers. Latter might be attributed to homocomponent fibers hindering small island fibers to move, rotate and completely separate from each other. Quality factor proved mixed media nonwovens to have superior filtration properties compared to island-in-the-sea structures.

6.4.2 Part II: Mixed Media Alt. 37 InS Hydroentangled with Higher Pressures

6.4.2.1 Removal of Sea Compound

We previously reported hydroentangling of mixed media island-in-the-sea webs to be different from webs consisting of just bicomponent fibers. Figure 6- 22 show the basis weight of unwashed and caustic-treated mixed media nonwovens hydroentangling with different peak pressures and varying jet spacing. Hydroentangling mixed media webs with higher peak pressures but less specific energy resulted in nonwovens with sufficient fiber interlocking withstanding the caustic-treatment. Even materials hydroentangled with 4800 μm jet spacing did not fall apart during the caustic bath.

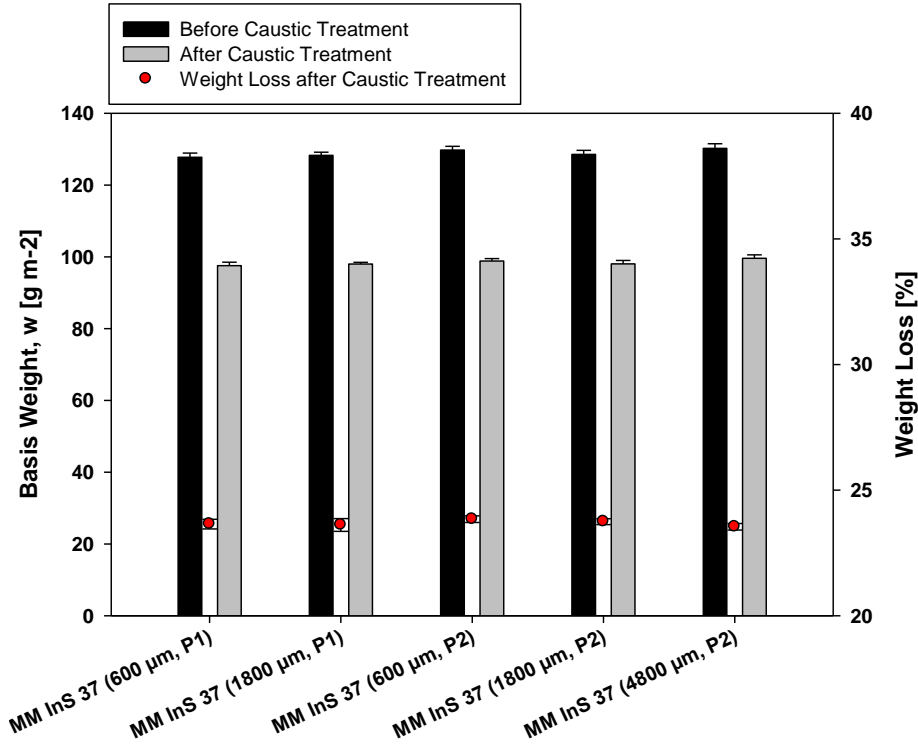


Figure 6- 22: Basis weight as a function of jet spacing of caustic-treated P1/P2 MM 37 InS structures

6.4.2.2 Influence on Structure and Properties

Figure 6- 23 depicts the solidity of caustic-treated mixed media nonwovens hydroentangled with manifold pressures P1 and P2. According to the results, increasing the peak manifold pressure (P2) led to higher solid volume fractions. Effect of jet spacing is measurable for both materials. Figure 6- 24 shows same trend and air permeability is remarkably reduced when bonding with pressure range P2. This is remarkably as just the peak manifold pressure was enhanced but not the specific energy per se.

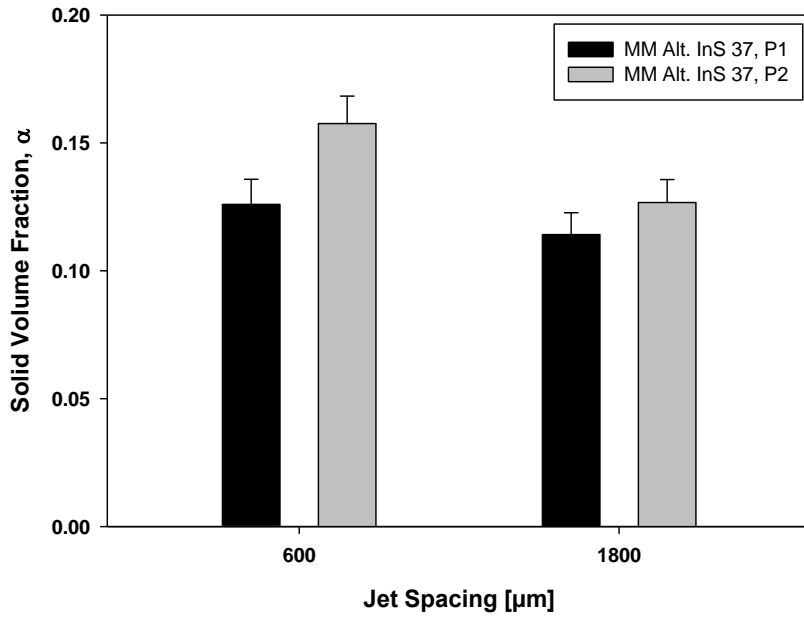


Figure 6- 23: Solidity as a function of jet spacing of caustic-treated P1/P2 MM 37 InS structures

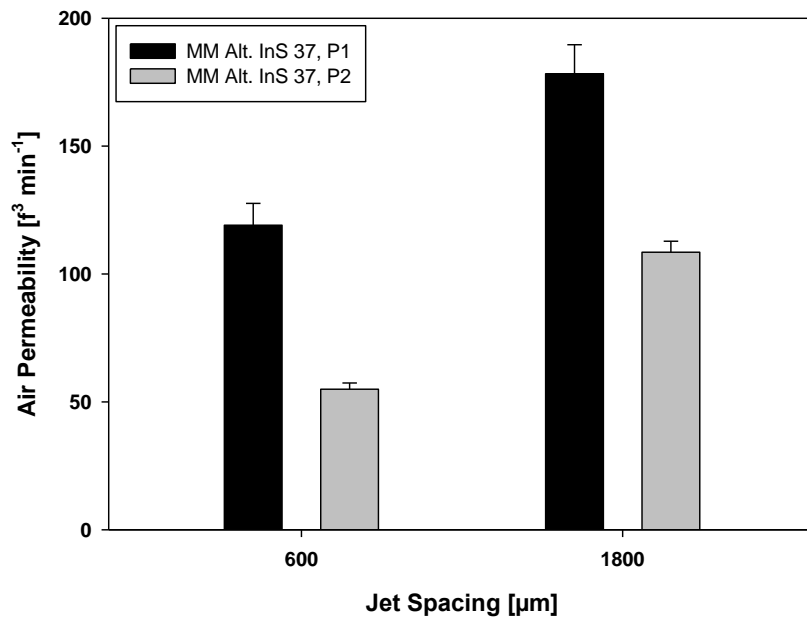


Figure 6- 24: Air permeability as a function of jet spacing of caustic-treated P1/P2 MM 37 InS structures

Filtration efficiency of mixed media structures is shown in the following. Data indicated both structures and jet spacing to show comparable capture efficiencies. However, hydroentangling with higher peak manifold pressures led to significantly higher pressure drops. In addition, hydroentangling with higher jet spacing led to materials with lower pressure drops. Increase in pressure for P2-bonded materials can be explained by the increase in structure density and is in accordance with the measured permeabilities.

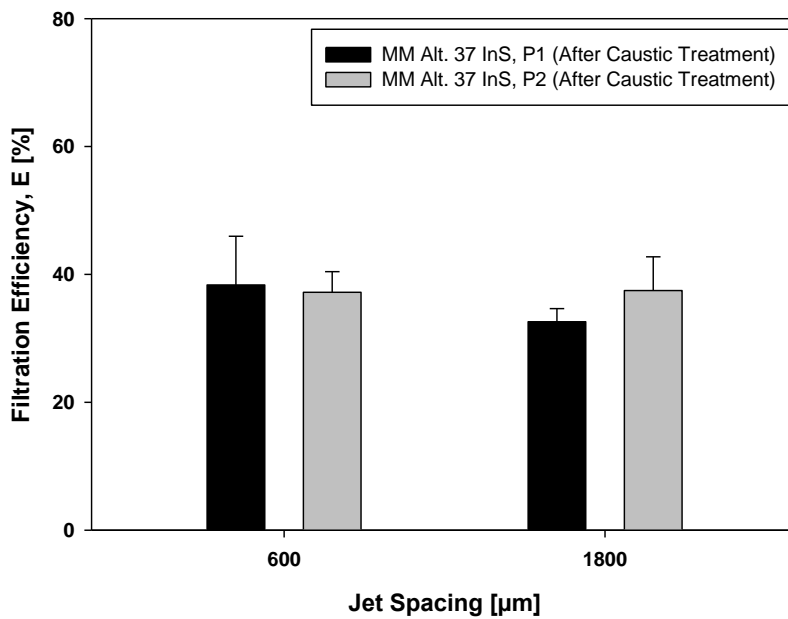


Figure 6- 25: Filtration efficiency as a function of jet spacing ($d_p: 0.3 \mu\text{m}$, $f_v: 5.33 \text{ cm s}^{-1}$, $A: 100 \text{ cm}^2$, DOP)

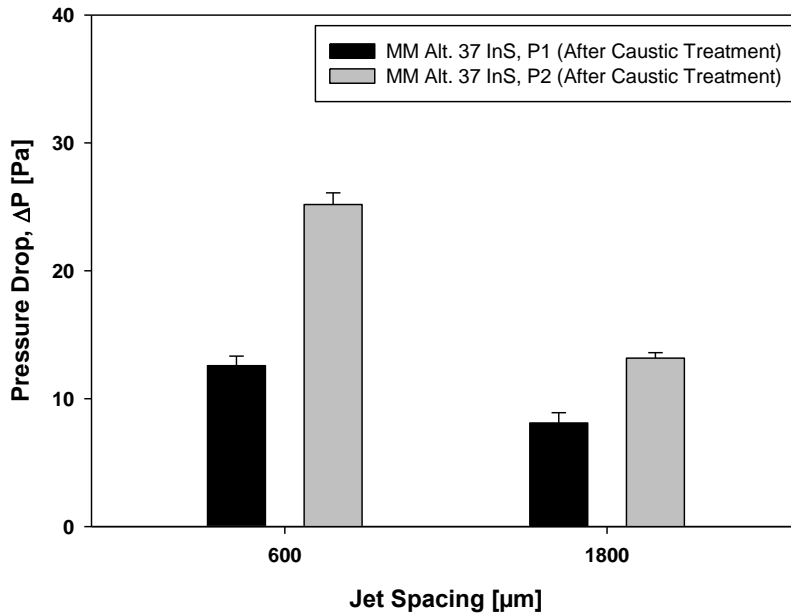


Figure 6- 26: Pressure drop as a function of jet spacing (5.33 cm s^{-1})

6.4.2.3 Summary (Part II)

Results provide confirmatory evidence that response to hydroentangling of mixed media structures is different compared to island-in-the-sea materials. Increasing the peak pressure but not the specific energy led to nonwoven materials strong enough to withstand the caustic washing. Even structures hydroentangled with jet densities as low as $4800 \mu\text{m}$ did not fall apart during the treatment. We attribute this to an increase in fiber penetration because of higher impact forces. However, increasing the manifolds pressures led to higher bulk densities and lower air permeabilities and also higher pressure drops. Filtration efficiency did not change compared to structures hydroentangled with lower peak pressures.

6.4.3 Part III: Mixed Media Alt. 37 and 108 Island-in-the-Sea Structures

6.4.3.1 Removal of Sea Polymer from Structures

Figure 6- 27 depicts the basis weight as well as change of weight of mixed media structures with 37 and 108 islands after treating with caustic. It follows that materials lost about 25% of their initial weight and samples with 108 islands about 2.5% more compared to mixed media structures with 37 islands (average weight loss of MM alt. 37 InS: 23.71%, average weight loss of MM alt. 108 InS: 26.21%).

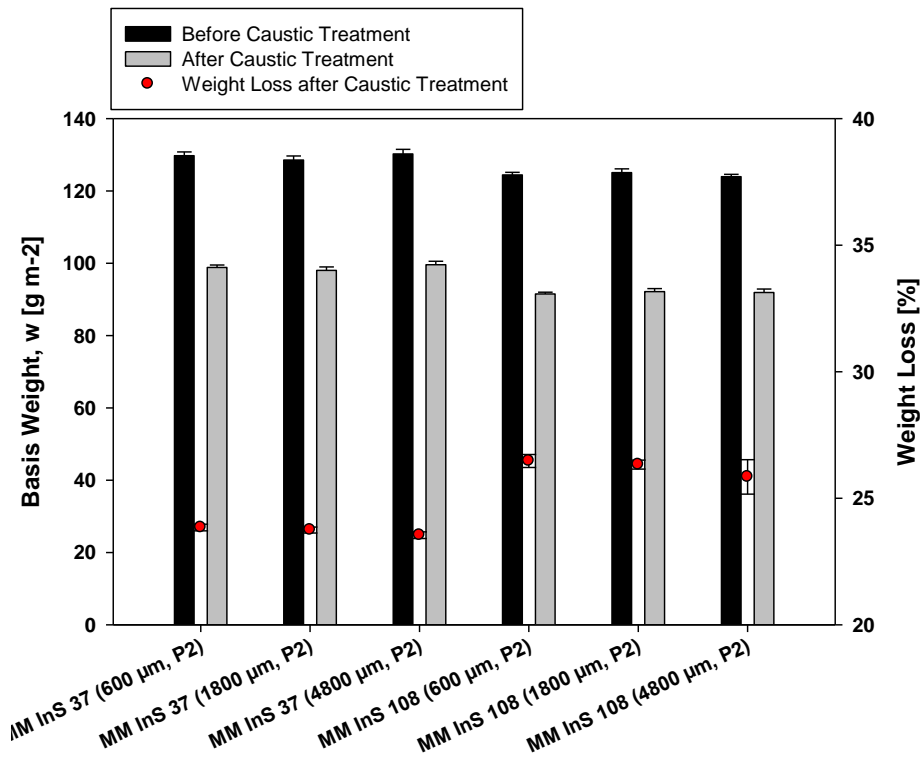


Figure 6- 27: Basis weight caustic-treated MM 37/108 InS structures hydroentangled with P2

SEM images of mixed media nonwovens with 108 islands taken before and after the alkaline treatment can be seen in Figure 6- 28 and Figure 6- 29. SEM images show the individual islands to be fibrillated but insufficiently distributed. Same phenomenon has been reported for caustic-treated mixed media nonwovens with 37 islands.

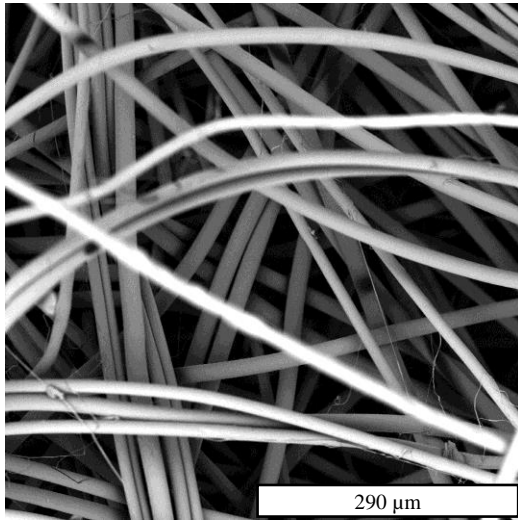


Figure 6- 28: SEM image of MM alt. 108 InS structure before caustic treatment

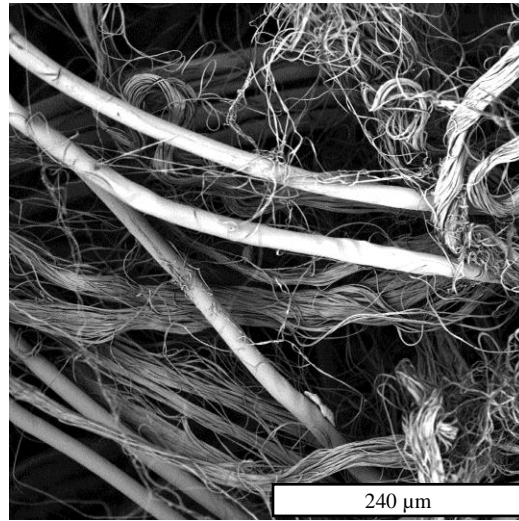


Figure 6- 29: SEM image of MM alt. 108 InS structure after caustic treatment

6.4.3.2 Fiber Size and Specific Surface Area

Fiber size distribution of mixed media 108 island-in-the-sea structures is shown in Figure 6- 30. Results indicate the homocomponent fibers to be larger than the bicomponent fibers. Mean diameters of both mixed media 37 and 108 island-in-the-sea structures (before and after caustic treatment) can be seen in Table 6- 4. Data reveals the homocomponent fibers of the mixed media 108 island-in-the-sea structure to be about 23% bigger in size

compared to its counterpart. From this it can be expected that percentage of poly (propylene) within the homocomponent fiber is higher compared to the bicomponent fibers.

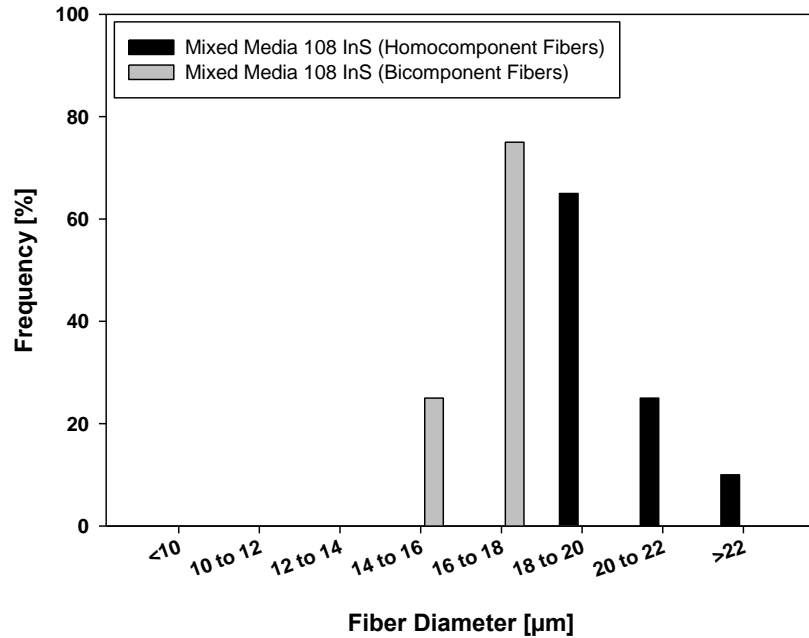


Figure 6- 30: Fiber size distribution of MM alt. 108 InS structure

Table 6- 4: Results of fiber diameter measurements of MM 37/108 InS (before/after caustic treatment)

Fiber	$\bar{x}, \sigma (d_{f,bico}) [\mu\text{m}]$ (Measured)	$\bar{x} (d_{f,island}) [\mu\text{m}]$ (Measured)	$\bar{x}, \sigma (d_{f,homo}) [\mu\text{m}]$ (Measured)
MM Alt. 37 InS	19.1 / 1.7	2.6	15.6 / 0.8
MM Alt. 108 InS	16.3 / 0.36	1.1	20 / 1

Information shown in Table 6- 4 provided the basis to calculate poly (propylene) distribution within the structure. Calculations indicated the distribution of poly (propylene) within the mixed media materials with 108 islands to be different from the mixed media structures with 37 islands. Poly (propylene) portion, which is about 75% of the structure’s weight, is shared unequally. Calculations revealed that mass of island fibers is about 19% and mass of homocomponent about 57% giving a distribution of 75% for $R_{PP\ Mono}$ and 25% for $R_{PP\ Bico}$. This is different from mixed media 37 island-in-the-sea, which shared the poly (propylene) portion. Calculated polymer ratios are given in Table 6- 5.

Table 6- 5: Calculated mass/volume fractions of the used mixed media structure

Fiber		$R_{structure}$	R/vol	R_{PP}	R_{PLA}
Homo	PP	0.75		0.56	
Bico	PP		0.43/0.51	0.19	
	PLA	0.25	0.57/0.49		0.25

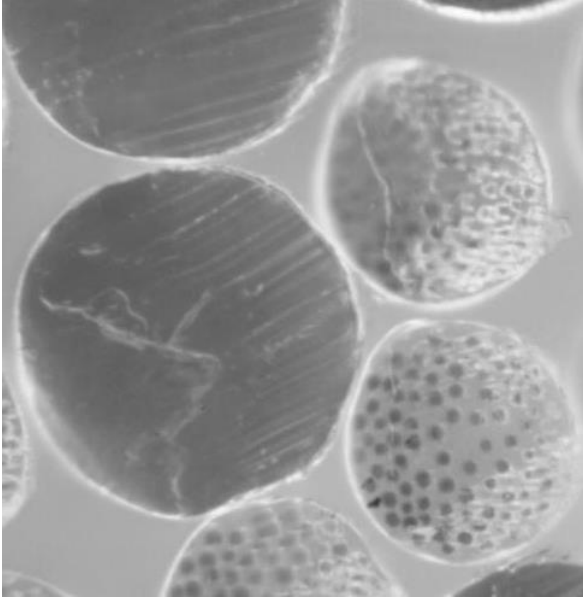


Figure 6- 31: Cross-sectional image of MM 108 InS structure, polymer distribution: 75/25 poly(propylene) homo/mono, 40/60 poly(propylene) / poly (lactic acid) island/sea

Theoretical accessible specific surface area of 37 island-in-the-sea as well as mixed media alternating 37 and 108 island-in-the-sea structures can be seen in Figure 6- 15. Since $R_{PP\ Mono} \neq R_{PP\ Bico}$ relation between island diameter and specific surface area is different for mixed media nonwovens with 108 islands compared to relation shown for mixed media nonwovens with 37 islands. This relation is shown as a green line in the following graph.

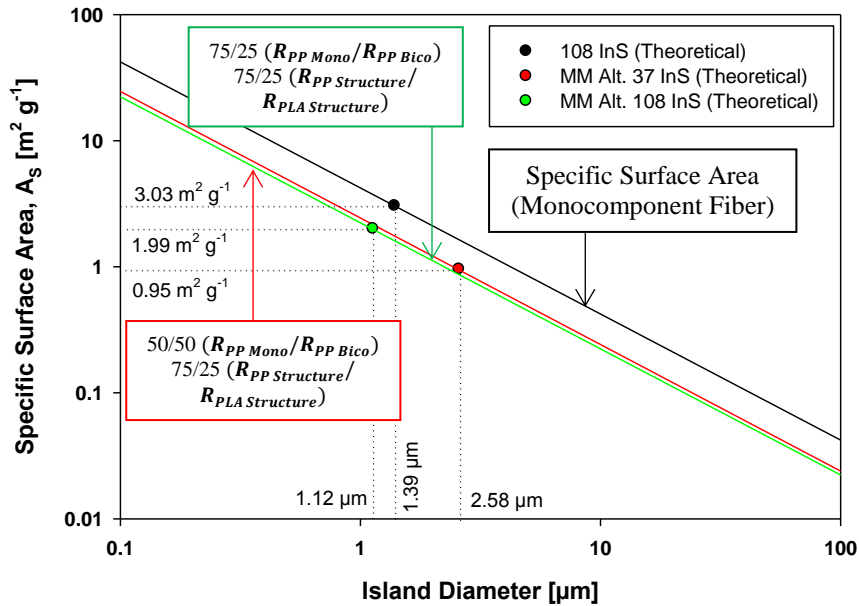


Figure 6- 32: Comparison of specific surface area of 37 InS, MM 37 InS, MM 108 InS structures

Solving the equations revealed the theoretical accessible specific surface area of mixed media nonwovens with 108 island-in-the-sea bicomponent fibers to be about $\sim 2 \text{ m}^2 \text{ g}^{-1}$. Results also indicated the poly (propylene) distribution to have only little effect on the actual specific surface of the hybrid structure.

6.4.3.3 Structure and Properties

Solid volume fractions of mixed media 37 and 108 island-in-the-sea materials are depicted in Figure 6- 33. Experimental results indicated the solid volume fraction to be lower compared to mixed media structures with 37 islands. Furthermore, jet spacing larger than 1800 μm seems to have only little influence on the solidity of both structure types.

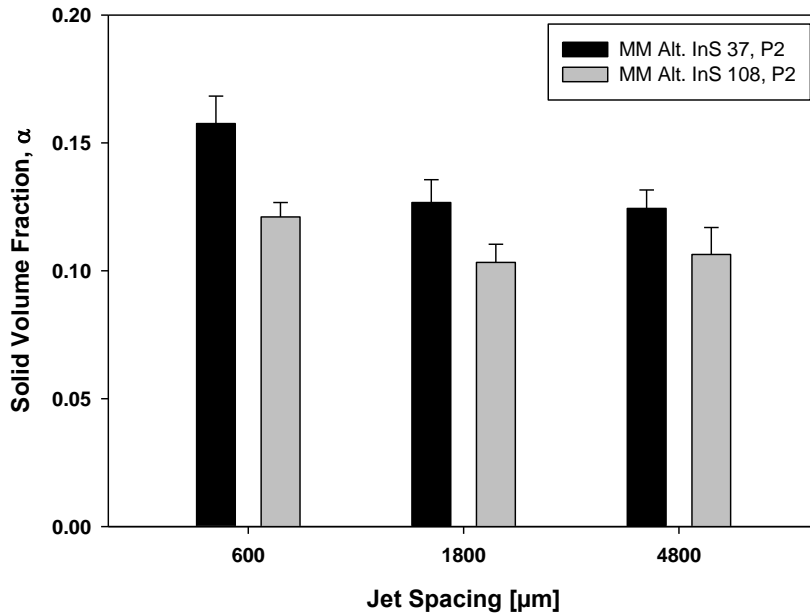


Figure 6- 33: Solidity as a function of jet spacing of caustic-treated, P2 hydroentangled MM 37 InS, MM 108 InS structures

As can be seen from the following figure air permeability is following a similar trend and mixed media 108 island-in-the-sea nonwovens have significantly lower permeabilities. As seen for solidity jet spacing seems to play no role beyond 1800 μm jet spacing. Results are not in accordance with the results initially expected. Since mixed media structures with 108 islands have smaller fibers air permeability was expected to be lower. We attribute this to the insufficient fiber spreading, which was previously shown and mentioned. Homocomponent fibers are assumed to hinder island fibers to move and separate. As nonwovens hydroentangled with jet spacing larger than 1800 μm did not show any difference it can be assumed that degree of consolidation cannot be further reduced.

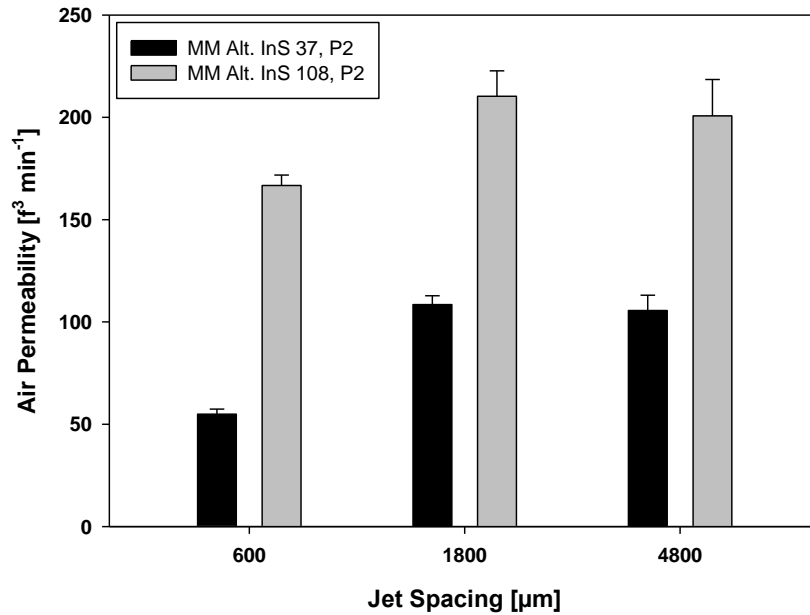


Figure 6- 34: Air permeability as a function of jet spacing of caustic-treated, P2 hydroentangled MM 37 InS, MM 108 InS structures

Filtration properties are shown in the following and indicate mixed media nonwovens with 37 islands to have higher capture efficiencies but also higher pressure drops. Jet spacing seems to have no major influence on the capture efficiency of both mixed media 37 and 108 island-in-the-sea structures. Mixed media nonwovens with 108 islands showed no difference in pressure drop when hydroentangling with different jet spacing. As mentioned before, this is not in accordance with the results initially expected. Removing the sea compound and separating island fibers was found to be difficult for both structures but easier for mixed media structures with lower island counts.

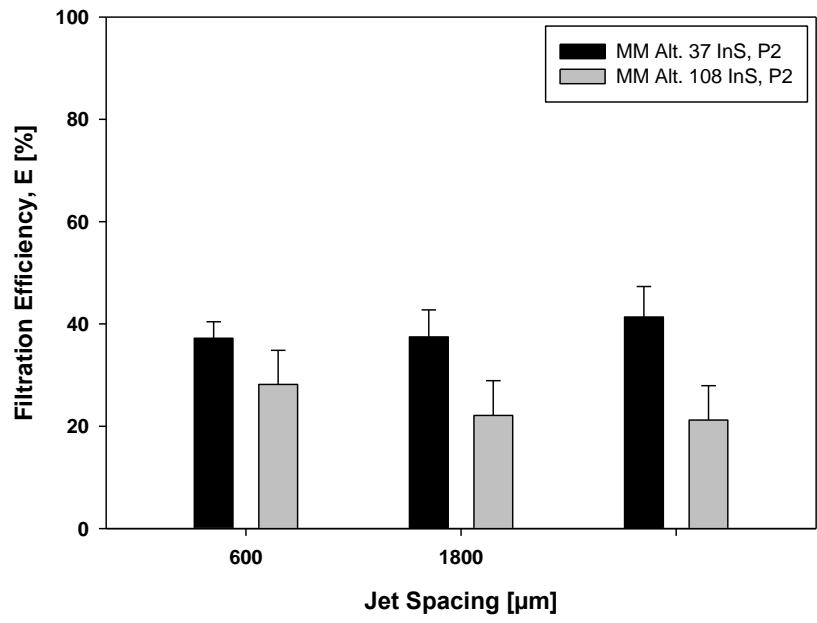


Figure 6- 35: Filtration efficiency as a function of jet spacing ($d_p: 0.3 \mu\text{m}$, $f_v: 5.33 \text{ cm s}^{-1}$, $A: 100 \text{ cm}^2$, DOP)

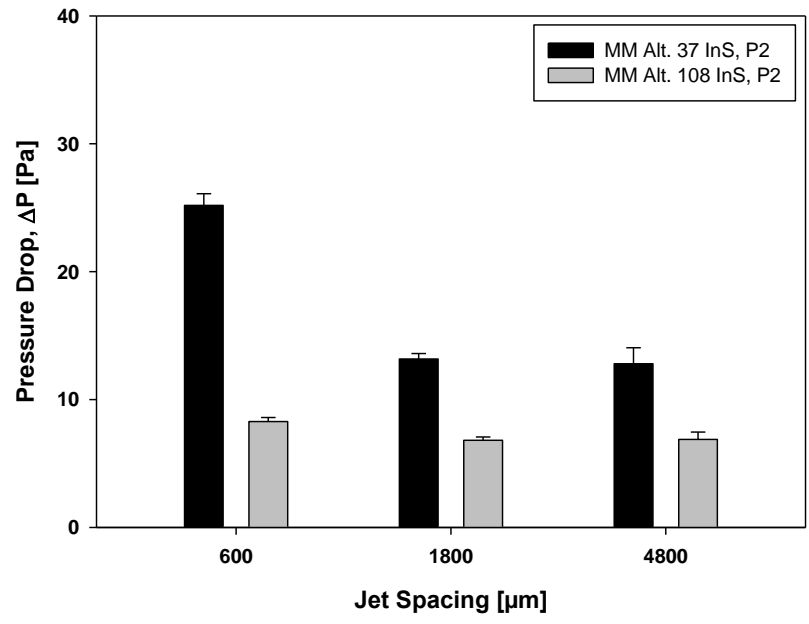


Figure 6- 36: Pressure drop as a function of jet spacing ($f_v: 5.33 \text{ cm s}^{-1}$)

Quality factor results are summarized in the following table. Data proves mixed media structures to show better quality factors than island-in-the-sea structures.

Structure	QF @ 600 μm [Pa^{-1}]	QF @ 1800 μm [Pa^{-1}]	QF @ 4800 μm [Pa^{-1}]
37 InS, P1	0.0126	0.0224	0.0336
MM Alt. 37 InS, P1	0.0388	0.0488 (<u>best</u>)	Fell Apart
MM Alt. 37 InS, P2	0.0186	0.0359	0.0423
MM Alt. 108 InS, P2	0.0406	0.0370	0.0348

6.5 Summary and Conclusion

Mixed media alternating island-in-the-sea structures were spun with different island counts and hydroentangled with different water pressures and three different jet spacing. Sea compound was dissolved by washing the nonwoven materials with an alkaline solution for 10 minutes. Analysis of SEM images revealed the fiber spreading to be less compared to conventional island-in-the-sea fabrics. It is assumed that homocomponent fibers prevented small islands to move and distribute. Investigation revealed the requirements in terms of hydroentangling pressure to be different for mixed media compared to island-in-the-sea structures. Hybrid structures hydroentangled with large jet spacing fell apart during the caustic treatment, whereas island-in-the-sea nonwovens hydroentangled with the exact same conditions showed sufficient strength. Increased bending rigidities, caused by the implementation of larger fibers, might be one reason for that. Mixed media structure showed

lower solid volume fractions and higher air permeabilities compared to island-in-the-sea materials. Both capture efficiency and pressure drop of mixed media nonwovens were tested to be lower, whereas quality factor improved.

Increasing the peak manifold pressure but not the specific energy led to mixed media structures strong enough to withstand the removal process. Also, structures showed higher densities and lower permeabilities, comparable capture efficiencies but higher pressure drops.

Caustic treatment of mixed media nonwovens with higher island counts turned out to be even more challenging. Even though poly (lactic acid) was successfully removed insufficient island separation resulted in materials with lower air permeability, lower capture efficiency and lower flow resistance.

6.6 References

- Anantharamaiah, N., Durany, A. & Pourdeyhimi, B. (2009). High surface area nonwovens via fibrillating spunbonded nonwovens comprising Islands-in-the-Sea bicomponent filaments: structure–process–property relationships. *Journal of materials science*, 44(21), 5926-5934.
- Anantharamaiah, N., Verenich, S. & Pourdeyhimi, B. (2008). Durable nonwoven fabrics via fracturing bicomponent islands-in-the-sea filaments. *Journal of Engineered Fibers and Fabrics*, 3(3), 1-9.
- Batra, S. K. & Pourdeyhimi, B. (2012). *Introduction to nonwovens technology*: DEStech Publications, Inc.
- Das, D. & Pourdeyhimi, B. (2014). *Composite Nonwoven Materials: Structure, Properties and Applications*: Elsevier Science.
- Fedorova, N. (2006). *Investigation of the utility of islands-in-the-sea bicomponent fiber technology in the spunbond process, 2006*. (Ph.D. - Fiber and Polymer Science), North Carolina State University.
- Hollowell, K. B. (2012). *Hybrid Mixed Media Nonwovens: An Investigation of Structure-Property Relationships*. (Ph.D. - Fiber and Polymer Science), North Carolina State University.
- Hutten, I. M. (2007). *Handbook of nonwoven filter media*: Elsevier.
- Iyama, Y., Kuroda, A. & Yakake, Y. (2014). EP2787108 A1.
- Koslowski, H. (2009). Man-Made Fibres Congress: Dornbirn Austria:16-18th Sept 2009. Retrieved September 9th, 2014
- Marmon, S. E. & Creagan, C. C. (1999). US Patent No. US5965468 A.
- Pourdeyhimi, B. (2008). Comments on the paper entitled “Splitting of islands-in-the-sea fibers (PA6/COPET) during hydroentangling of nonwovens”. *Journal of Engineered Fibers and Fabrics*, 3, 32-35.
- Pourdeyhimi, B. (2011a). Durable Nonwovens. Retrieved November 18, 2014, from http://www.textileworld.com/Issues/2011/May-June/Nonwovens-Technical_Textiles/Durable_Nonwovens
- Pourdeyhimi, B. (2011b). US Patent No. US7981336 B2.

- Pourdeyhimi, B., Minton, A. & Putnam, M. (2004). Structure-process-property relationships in hydroentangled nonwovens-part 1: preliminary experimental observations. *International Nonwovens Journal*, 13, 15-21.
- Shim, E., Pourdeyhimi, B. & Latifi, M. (2010). Three-dimensional analysis of segmented pie bicomponent nonwovens. *The Journal of The Textile Institute*, 101(9), 773-787.
- Yeom, B. Y. & Pourdeyhimi, B. (2011). Aerosol filtration properties of PA6/PE islands-in-the-sea bicomponent spunbond web fibrillated by high-pressure water jets. *Journal of materials science*, 46(17), 5761-5767.

CHAPTER 7

- Influence of Jet Intensity and Manifolds in Hydroentangling -

Part I: Specific Energy and Force

Sections of this chapter will be submitted for publication in a peer-reviewed journal

7.1 Abstract

Specific energy is a term used in hydroentangling and can be defined as energy applied per unit mass of material (Batra & Pourdeyhimi, 2012, p. 126). In the industry the term is rather used than the actual hydroentangling pressure as it can be used as a measure for the energy consumption during the process. Specific energy and its influence on the material parameters was subject of various discussions published in the past. In this study we investigate the influence of specific energy and force on the structure and properties of mono- and bicomponent nonwoven materials. Poly (propylene) and poly (lactic acid) monocomponent and 37 and 108 island-in-the-sea bicomponent webs were produced with a fixed basis weight of 125 g m^{-2} and hydroentangled with different water pressures and also jet spacing (600 μm , 1800 μm and 4800 μm). Bicomponent nonwovens were washed with caustic to remove the sea compound from the structure. This study demonstrated that varying the manifold pressure and the number of manifolds but keeping the specific energy constant does affect the structure and properties of nonwoven materials. Hydroentangling with higher manifold pressures but less manifolds most often resulted in more oriented materials with higher mechanical properties. It was also found that this configuration led to island-in-the-sea materials with superior properties. Lowering the specific energy showed the same trend with a greater impact of higher than lower manifold pressures.

7.2 Introduction

Hydroentangling describes a mechanical bonding technique using ultra-fine, high-speed water jets to entangle and interlock fibers (Hutten, 2007, p. 73; Schäfer, Fane et al., 2005, p. 204). Bonding nonwoven webs with jet velocities faster than 200 m s^{-1} is not uncommon and different researchers attempted to understand the constitution of jets, the impact on the structure as well as the structure's response to that (Groz-Beckert KG, 2012).

The specific energy is a measure often used in hydroentangling to describe the amount of energy applied per unit mass of material (Batra & Pourdeyhimi, 2012, p. 126). To estimate the specific energy during hydroentangling, single water jet energy \dot{E} has to be calculated first.

$$\dot{E} = \frac{\pi}{8} \rho d_n^2 C_d v^3 \text{ [J s}^{-1}\text{]} \quad \text{Eq. 7- 1}$$

where ρ is the specific density of the fluid [998.2 Kg m^{-3} for H_2O at $20 \text{ }^\circ\text{C}$], d_n the nozzle diameter [m], C_d the discharge coefficient and v the jet velocity [m s^{-1}].

Single water jet energy \dot{E} has to be calculated for each pressure and multiplied by the number of jets having the same velocity. Thus, energy of all jets \dot{E}_{Total} can be calculated as follows.

$$\dot{E}_{Total} = \left(\sum_{M=1}^n \dot{E}_{MJM} \right) \times 1000^{-1} \text{ [KJ s}^{-1}\text{]} \quad \text{Eq. 7- 2}$$

where n is the number of manifolds used during hydroentangling and J the number of jets per manifold. Dividing the total jet energy \dot{E}_{Total} by the mass flow rate of fabric gives the specific energy applied per unit mass of fabric.

$$SE = \frac{\dot{E}_{Total}}{\dot{M}} [\text{KJ Kg}^{-1}] \quad \text{Eq. 7- 3}$$

where \dot{M} is the mass flow rate of fabric [Kg s^{-1}]. Fabric mass flow rate can be estimated by using the following equation.

$$\dot{M} = s \times w \times v_B [\text{Kg s}^{-1}] \quad \text{Eq. 7- 4}$$

where s is the fabric width [m], w is the basis weight of the material [g m^{-2}] and v_B is the operating speed [m s^{-1}] (Pourdeyhimi, Minton et al., 2004).

As can be seen from the equations specific energy is not only a function of water pressure but also machine speed, basis weight, jet diameter and many others. Literature provides several studies investigating different hydroentangling parameters on the structure. Moyo et al. (Moyo, Patnaik et al., 2014) reported the specific energy to be a function of various parameters and that varying them but keeping the energy constant would not certainly result in equivalent structure properties. Study showed other factors than the water pressure to be influencing the actual fiber entanglement. In another work researchers confirmed the jet pressure and not the specific energy to be the all-important parameter in hydroentangling (Seyam, Shiffler et al., 2005). The specific energy ratio is a term often discussed in literature and describes the quotient of energy applied to the face side to the back side of the material (Connolly & Parent, 1993). In other words, a specific energy ratio of 50 means the total specific energy to be applied equally on both sides of the web. Connolly and his co-workers (Connolly & Parent, 1993) assumed a specific energy ratio of 50 to be not ideal and low specific energy ratios to decrease fiber loss. Authors also stated the specific energy to be correlated to the strength of the material. Pourmohammadi et al.

(Pourmohammadi, Russell et al., 2003) reported that bonding with multiple manifolds with the same absolute pressure as a single manifold can result in enhanced fabric strengths even though the total specific energy is lowered. Tausif et al. (Tausif & Russell, 2012) studied the effect of specific energy on the dimensional and mechanical properties of layered poly (ethylene terephthalate) and glass/poly (ethylene terephthalate) (80/20) nonwoven webs. Results indicated the tensile strength to be affected by the interaction between conveyor speed and nozzle diameter as well as water pressure and number of manifolds. It was further stated that hydroentangling with same specific energies can result in nonwoven materials with different properties. Pourdeyhimi et al. (Pourdeyhimi, Minton et al., 2004) reported increasing fabric bending rigidity and tensile strength with increasing specific energy. However, after reaching a critical specific energy properties declined. Ghassemieh et al. (Ghassemieh, Acar et al., 2001) worked on the influence of hydroentangling on viscose/poly (ethylene terephthalate), poly (ethylene terephthalate) and Twaron webs. According to their results, tensile strength increased with increasing water pressures and decreased beyond a critical value.

Current literature provides no information about the relation and effect of manifold pressure and specific energy on island-in-the-sea nonwovens. The purpose of this study is to explore the influence of hydroentangling with different manifold pressures but constant specific energy on monocomponent and also caustic-washed island-in-the-sea nonwoven materials.

7.3 Methodology

7.3.1 Materials

Following nonwoven webs were spun with a 0.5 meter Hills-Nordson spunbond line and hydroentangled with a 0.5 meter Fleissner Aquajet at the Nonwoven Institute Partners facilities located at Centennial Campus, North Carolina State University.

Monocomponent Materials

Spunbond poly (propylene) (Braskem CP360H) and poly (lactic acid) (Natureworks 6202D) monocomponent nonwoven materials were spun with a fixed basis weight of 125 g m^{-2} before passing a compaction and calender roll (cold calendered). Subsequent hydroentangling was performed with different jet spacing, pressures and number of manifolds. Varying these parameters allowed bonding with same specific energy but different peak pressures (see Table 7- 1). Hydroentangling was performed on a 100 mesh poly (ethylene terephthalate) forming belt with a constant speed of 10 m min^{-1} . After bonding all structures were dried in a conveyor oven.

Island-in-the-Sea Materials

Research also reports on spunbond island-in-the-sea nonwoven materials with two different island counts (37 and 108) and a fixed basis weight of 125 g m^{-2} . Braskem CP360H poly (propylene) was used as island and Natureworks 6202D poly (lactic acid) as sea polymer. Materials were spun with a polymer ratio of 75 (island) to 25 (sea) and passed

through a compaction and calender roll (cold calendered). Bonding was performed under the same conditions as mentioned for the monocomponent structures.

Table 7- 1: Structures and hydroentangling parameters

Structure	Hydroentangling Pressure [bar]		600 μm	1800 μm	4800 μm
			Specific Energy [KJ Kg^{-1}]		
37 InS 108 InS PP Mono PLA Mono	P1	20-175-225-0-0 (M1-M5)	8200	2700	1000
	P2	20-100-100-150-150 (M1-M5)	8200	2700	1000
37 InS	P3	20-150-150-0-0 (M1-M5)	5400	1800	700
	P4	20-80-100-100-100 (M1-M5)	5400	1800	700
Belt Speed: 10 m min⁻¹					
→ Structure IDs: 7.-Structure.JetSpacing-125-Pressure ←					

7.3.2 Sample Preparation

Bonded bicomponent structures were treated in a boiling caustic solution to remove the sea polymer from the fibers. Sodium hydroxide solution was prepared in a steam kettle with a concentration of 8% w/w and a temperature of 100 °C, which was controlled with a digital lab thermometer. Samples were treated for 10 minutes under manual stirring before being washed out with cold water until pH neutralization. All samples were dried on a sample rack.

7.3.3 Structure Analysis

Basis Weight and Thickness

Basis weight was tested with a Denver Instrument XL-3100D top-loading balance and thickness measured with a hanatek FT3V-LAB high-precision thickness gauge. A total of 10 replicates per structures were tested.

Solid Volume Fraction (SVF)

The packing density of all structures was calculated for unwashed and caustic-treated samples by using the following equation

$$\alpha = \frac{w}{\rho_f \times t} \quad \text{Eq. 7- 5}$$

where w the basis weight [g m^{-2}], ρ_f the total fiber density [g m^{-3}] and t the thickness of the structure [m]. Total fiber density ρ_f has to be calculated for bicomponent structures and is obtained as follows.

$$\rho_f = (\rho_{island} \times R_i) + (\rho_{sea} \times R_s) \quad \text{Eq. 7- 6}$$

where ρ_{island} is the density of the island polymer [g cm^{-3}], R_i is the mass fraction of island polymer ρ_{sea} is the density of the sea polymer [g cm^{-3}] and R_s is the mass fraction of sea polymer.

Fiber Diameter Measurements

Fiber size was examined from SEM images taken from sputter-coated (Au/Pd) mono- and bicomponent samples. A Phenom G2 Pro Desktop unit was used to take surface images and

ImageJ was used to measure the fiber sizes (total of 100 measurements from 10 SEM images). Island diameter was estimated based on the mass fraction of the island polymer R_i , which was obtained from the metering pumps during melt spinning. This requires conversion of mass fraction to volume fraction of island polymer vol_i , which can be calculated as follows.

$$vol_i = \frac{R_i \times \rho_i}{(R_i \times \rho_i) + (R_s \times \rho_s)} \quad \text{Eq. 7-7}$$

where R_i is the mass fraction of island polymer, ρ_i is the specific density of the island polymer [g cm^{-3}], R_s is the mass fraction of sea polymer and ρ_s is the specific density of the sea polymer [g cm^{-3}].

From this theoretical island diameter d_f can be predicted as follows.

$$d_{f,s,t} = d_f \sqrt{\frac{vol_i}{N}} \quad [\mu\text{m}] \quad \text{Eq. 7-8}$$

where d_f is the diameter of the intact island-in-the-sea fiber [μm], vol_i is the volume fraction of the island polymer and N is the island count.

Air Permeability

Air permeability of mono- and bicomponent structures (prior/after caustic treatment) was tested with a TEXTTEST FX 3300 air permeability tester. Experiments were performed according to ASTM D737 and a total of 10 replicates were examined per structure.

Mechanical Properties (Ball Burst)

Burst strength of monocomponent as well as bicomponent materials was tested with an Instron 4400r universal testing system. Bicomponent nonwovens were tested prior and after the caustic washing and all experiments were performed according to ASTM D6797 (5 replicates per structure).

Mechanical Properties (Strip Tensile)

Strip tensile test was performed according to ASTM D5035 with 5 replicates per structure. Mono- and bicomponent structures (prior/after caustic treatment) were tested in both machine- (MD) and cross direction (CD) with an Instron 4400r universal testing system.

Mechanical Properties (Tongue Tear)

Tongue tear tests was done according do ASTM D5735 with a total of 5 replicates per structure. Both mono- and bicomponent materials (prior/after caustic) were tested in machine- (MD) and cross direction (CD). Analysis of mechanical properties was performed with an Instron 4400r universal testing system.

7.4 Results and Discussion

Discussion about the influence of specific energy and force is organized as follows.

Part I: Mono- and bicomponent nonwovens

Part II: Caustic-treated 37 island-in-the-sea nonwovens

Part III: Effect of changing the specific energy

7.4.1 Part I: Mono- and Bicomponent Nonwovens

7.4.1.1 Fiber Diameter Distribution

Fiber diameter distribution results are shown in Figure 7- 1 and Table 7- 2.

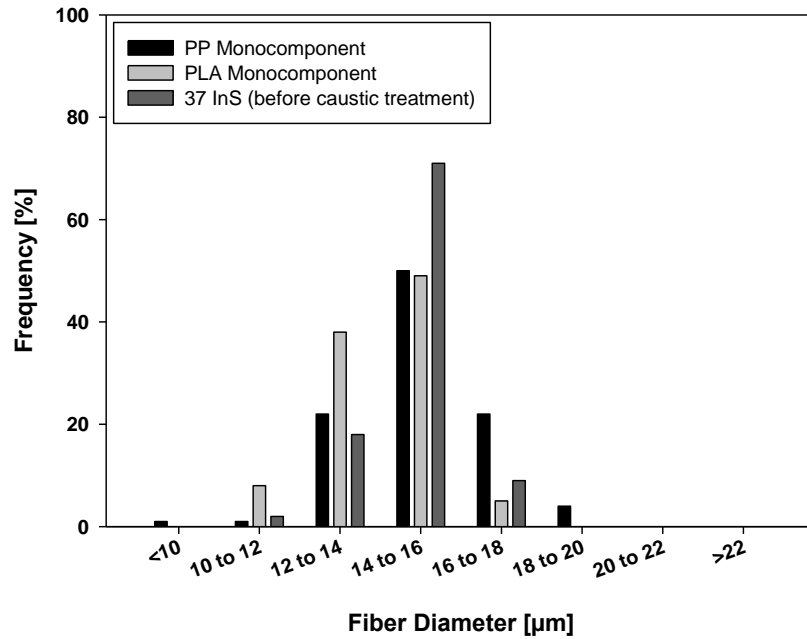


Figure 7- 1: Fiber size distribution of intact PP and PLA monocomponent and 37 InS fibers (PP, PLA, 37 InS)

Measurements indicated mono- and bicomponent fibers to have comparable fiber sizes.

Table 7- 2: Results of fiber diameter measurements

Structure	$\bar{x} (d_{f, Mono/Bico})$ [μm]	SD, σ [μm]	CV, c_v [%]	Median [μm]
PP Mono	14.9	2	13.3	14.9
PLA Mono	14	1.2	8.5	14.1
37 InS	14.7	1.1	7.3	14.8

7.4.1.2 Solid Volume Fraction and Air Permeability

Solid Volume fraction of mono- and 37 island-in-the-sea structures (before caustic treatment) hydroentangled with 600 μm jet spacing is shown in the following.

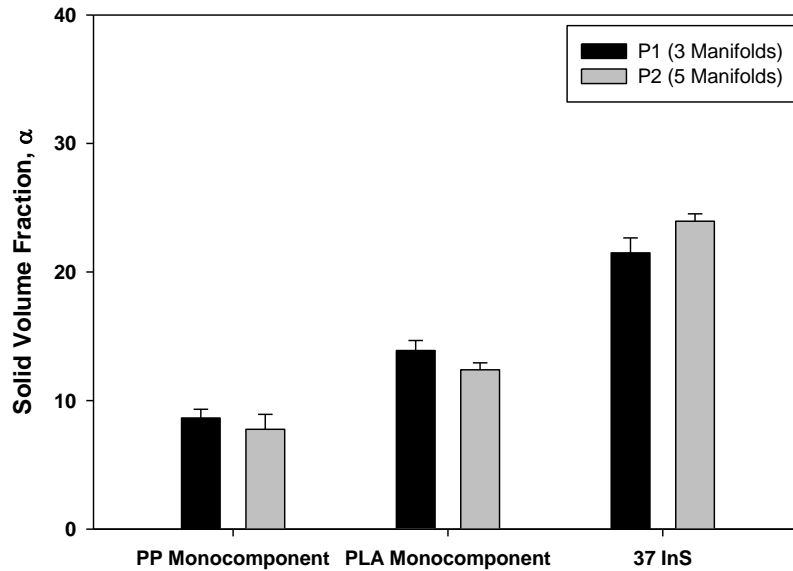


Figure 7- 2: Solidity of 600 μm , P1/P2 hydroentangled mono- and bicomponent structures (before caustic treatment)

Experiments indicated that hydroentangling monocomponent structures results in lower solidities compared to the island-in-the-sea material. Since structures are bonded with the same manifold pressure and bicomponent fibers are larger in diameter compared to poly (lactic acid) fibers flexural rigidity of fibers might be responsible for that.

Comparing the influence of manifold pressures P1 and P2 shows that hydroentangling with three manifolds but higher manifold pressures led to slightly higher bulk densities for monocomponent materials but less dense 37 island-in-the-sea structures. Latter might be associated with fiber fibrillation when bonding with five manifolds. Hydroentangling with

more manifolds may enhance fiber fibrillation, which unveils islands resulting in structures with higher solid volume fractions.

Plotting air permeability of structures (Figure 7- 3, normalized with a nominal weight of 130 g m⁻²) reveals P1-hydroentangled nonwovens to show lower air permeabilities. Comparable air permeabilities were found for P1/P2-bonded 37 island-in-the-sea materials.

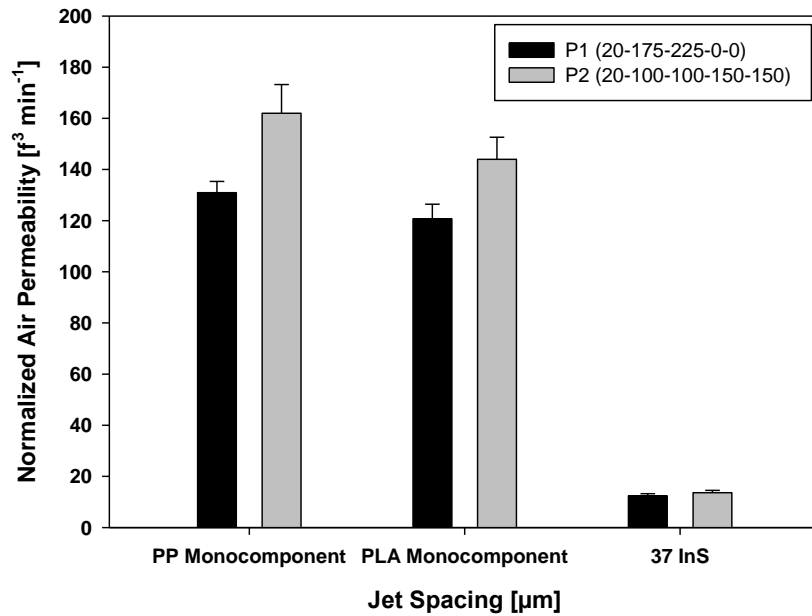


Figure 7- 3: Air permeability of 600 µm, P1/P2 hydroentangled mono- and bicomponent structures (before caustic treatment)

7.4.1.3 Influence on Mechanical Properties

Figure 7- 4 and Figure 7- 5 depict the tensile properties of P1/P2 hydroentangled structures. Hydroentangling with higher jet pressures but fewer passes led to higher tensile strengths in machine direction. Poly (lactic acid) monocomponent and island-in-the-sea structures showed significantly higher tensile strengths compared to poly (propylene structure).

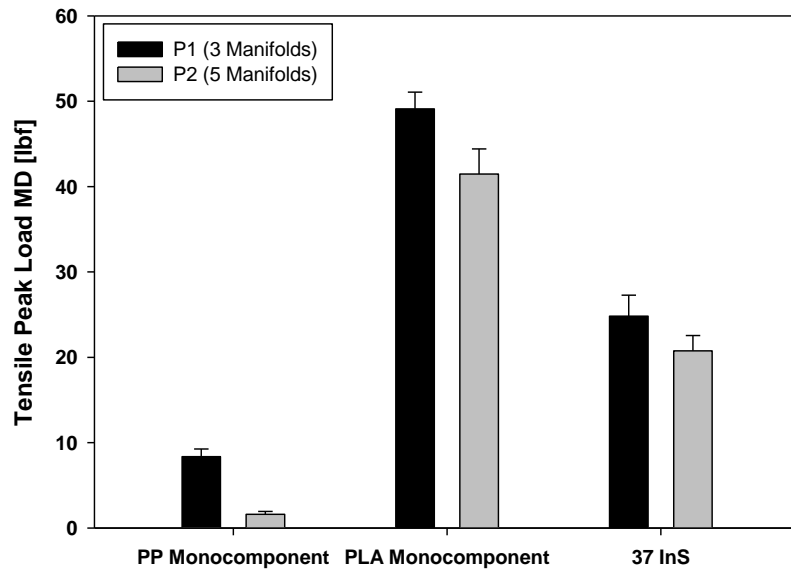


Figure 7- 4: Strip tensile strength (MD) of 600 μm , P1/P2 hydroentangled mono- and bicomponent structures (before caustic treatment)

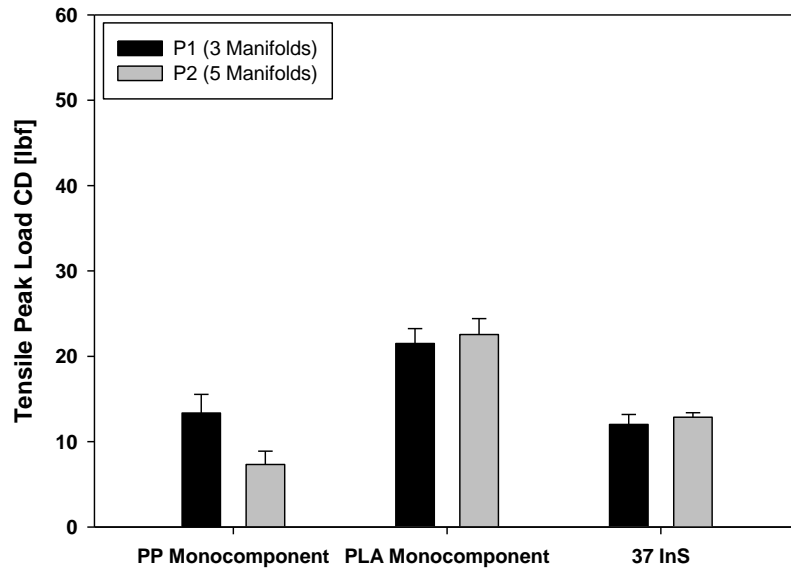


Figure 7- 5: Strip tensile strength (CD) of 600 μm , P1/P2 hydroentangled mono- and bicomponent structures (before caustic treatment)

Fiber orientation of nonwoven structures can be interpreted from the ratio of tensile strength in machine direction (MD) to cross-direction (CD). Results are given in Figure 7- 6 and indicate hydroentangling with three manifolds and higher jet pressures led to more MD-oriented structures. Poly (lactic acid) monocomponent and 37 island-in-the-sea structures revealed to be oriented in machine direction. Difference in orientation between poly (propylene) and the other two structures can be explained by the hydrophilicity of the respective materials.

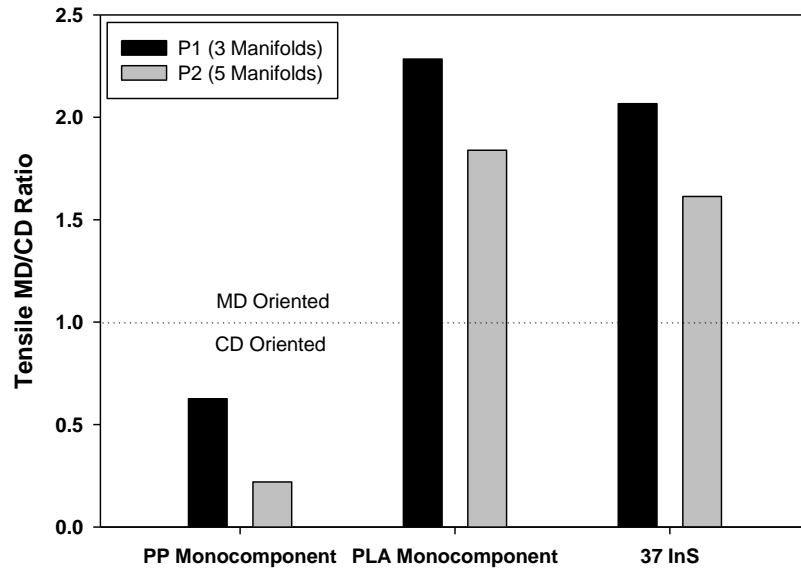


Figure 7- 6: Tensile MD/CD ratio of 600 μm , P1/P2 hydroentangled mono- and bicomponent structures (before caustic treatment)

Figure 7- 7 and Figure 7- 8 depict the tear strength of the hydroentangled materials. It can be seen that hydroentangling poly (propylene) nonwovens with higher jet pressures but fewer passes led to materials with high tear strengths. Tear strength is related to the mobility of fibers and formation of bundles preventing structure failure. From this it can be said that P1-hydroentangled poly (propylene) nonwovens provide more fiber mobility, whereas increasing the number of passes and decreasing the peak jet pressures led to less fiber mobility. Burst strength, which is shown in Figure 7- 9, indicated P1-hydroentangled poly (propylene) structures to have higher burst strength. Contrary to that, tear and burst strength of poly (lactic acid) and island-in-the-sea materials hydroentangled with P2 showed lower strengths, which is a result of less fiber mobility.

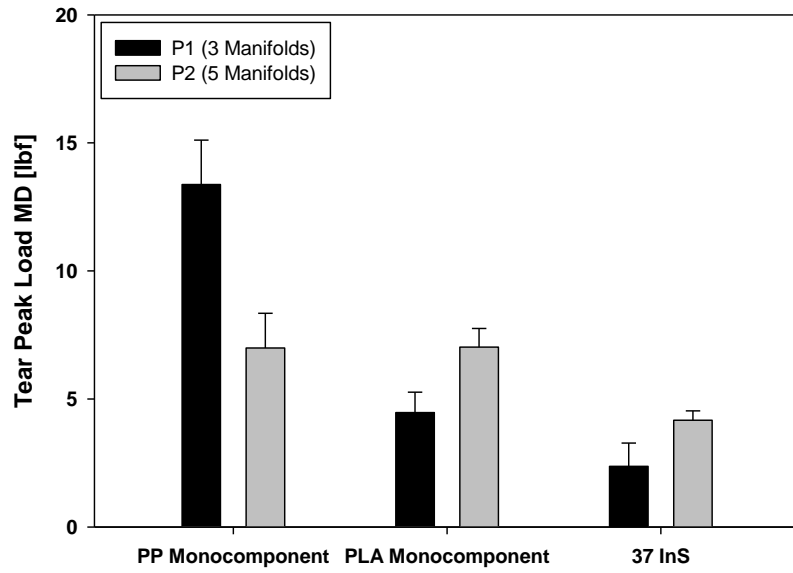


Figure 7- 7: Tongue tear strength (MD) of 600 μ m, P1/P2 hydroentangled mono- and bicomponent structures (before caustic treatment)

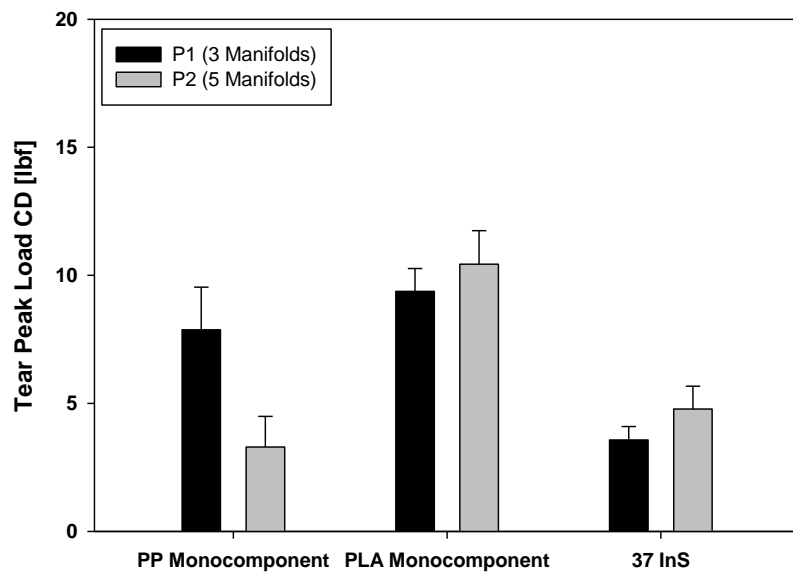


Figure 7- 8: Tongue tear strength (CD) of 600 μ m, P1/P2 hydroentangled mono- and bicomponent structures (before caustic treatment)

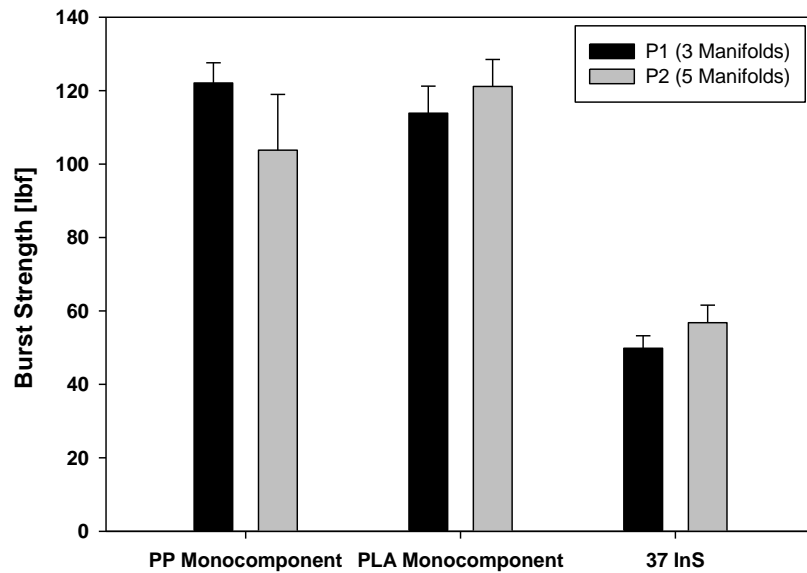


Figure 7- 9: Burst strength of 600 μm , P1/P2 hydroentangled mono- and bicomponent structures (before caustic treatment)

7.4.1.4 Summary (Part I)

This section demonstrated that hydroentangling nonwoven webs with different manifold pressures but same specific energy results in materials different in terms of their bulk density, permeability, fiber orientation and also mechanical properties. Experiments showed that hydroentangling monocomponent webs with high pressures but less manifolds results in higher bulk densities. Opposite was found for bicomponent materials and was attributed to a higher degree of island fibrillation when bonding with more manifolds but lower pressures. This was in agreement with the tested air permeability. Also, hydroentangling with higher manifold pressures but less passes resulted in more oriented materials. Moreover, tensile strengths were found to be higher for P1-hydroentangled materials.

7.4.2 Part II: Effect on Caustic-Treated 37 InS Nonwovens

7.4.2.1 Fiber Diameter Distribution

Fiber diameter distribution measurements of unwashed island-in-the-sea fibers were taken from previous measurements and are given in the following.

Table 7- 3: Results of fiber diameter measurements (before caustic treatment)

Mean, \bar{x} [μm]	SD, σ [μm]	CV, c_v [%]	Median [μm]
14.73	1.08	7.33	14.79

Experimental and theoretical island diameter of 37 island-in-the-sea materials is shown in the following table.

Table 7- 4: Results of fiber diameter measurements (after caustic treatment)

Method	$\bar{x} (d_{f, island})$ [μm]	SD, $\sigma (d_{f, island})$ [μm]
Theoretical Calculation	2.12	
SEM Measurements	2.16	0.06

7.4.2.2 Influence on Structural Properties

It was previously discussed that bonding bicomponent structures led to higher solid volume fractions, which could be the result of lower bending rigidities and also fibrillating fibers. Solidity after the caustic treatment empirical data (Figure 7- 10) indicates the solidity of P1-bonded nonwovens to be lower. Same trend was found to be valid for unwashed

structures. Furthermore, results imply the difference in solidity for P1- and P2-hydroentangled materials to increase with increasing jet spacing. This could be explained by knot-like structures obtained when hydroentangled with larger jet spacing. Such structures consist of high- and low density regions (see Figure 7- 11). These regions are assumed to be different for P2-bonded materials and less developed resulting in denser structures. Previous research has shown the fiber penetration and also pocket-structure to be a function of the water pressure used during bonding (Suragani Venu, 2012, pp. 187-188).

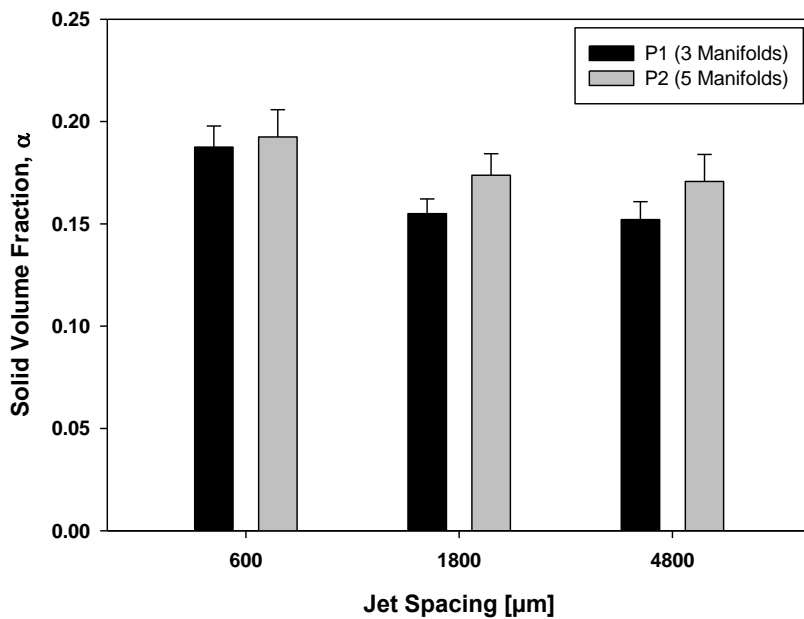


Figure 7- 10: Solidity of P1/P2 hydroentangled 37 island-in-the-sea structures (after caustic treatment)

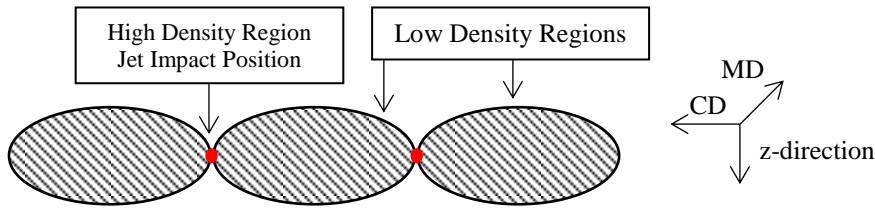


Figure 7- 11: Illustration of high and low density regions

Two-way analysis of variances was applied to further understand the influence of pressure on the solid volume fraction. Even though there is only little difference in solidity, 2-way ANOVA showed both pressure intensity (P1/P2) and jet spacing to influence the solid volume fraction of caustic washed 37 island-in-the-sea nonwoven materials.

Table 7- 5: 2-Way ANOVA ($\alpha: 0.05$), Influence of pressure (P1/P2) and jet spacing on solidity, after caustic treatment (JMP Pro)

Pressure P1/P2 [Prob > F]	Jet Spacing [Prob > F]	Pressure P1/P2 * Jet Spacing [Prob > F]
<.0001 (<i>REJECT H₀</i>)	<.0001 (<i>REJECT H₀</i>)	0.07

Air permeability of samples was normalized with nominal weight of 90 g m^{-2} and is shown in the following. Results are in accordance with solidity results shown in Figure 7- 10.

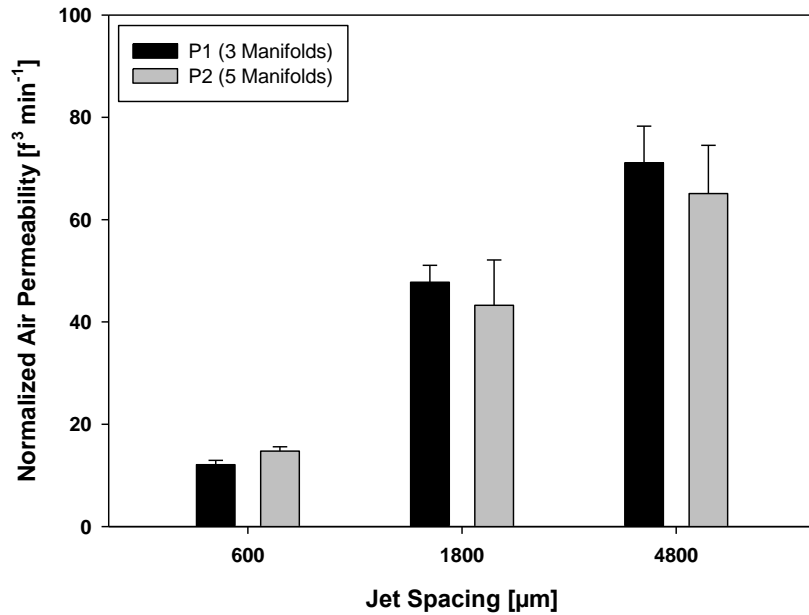


Figure 7- 12: Normalized air permeability of P1/P2 hydroentangled 37 InS structures (after caustic treatment)

Figure 7- 13 compares the solid volume fraction of 37 and 108 island-in-the-sea structures hydroentangled with P1/P2 and treated with alkaline. As can be seen from the results solidity of P1/P2 hydroentangled 108 island-in-the-sea structures turned out to be comparable. However, air permeability of both structures (Figure 7- 14) demonstrates that bonding with higher manifold pressures but less passes led to higher air permeabilities. Air permeability of samples was normalized with nominal weight of 90 g m^{-2} .

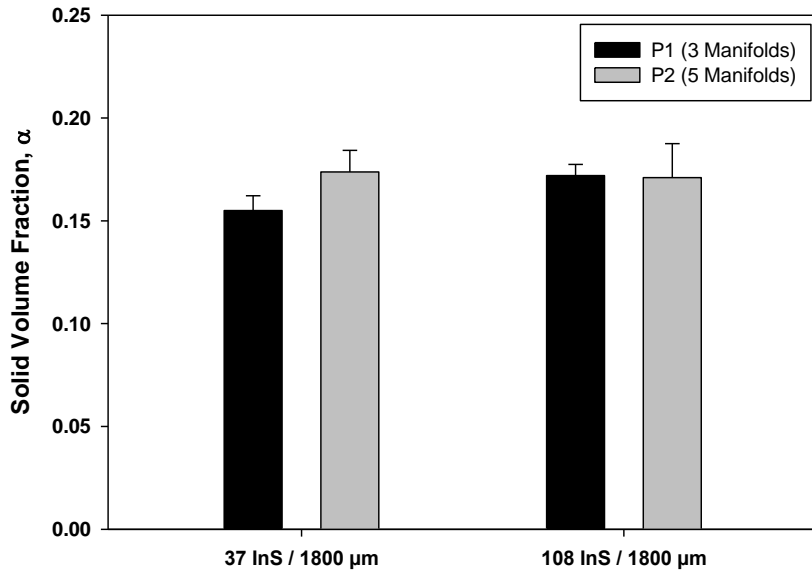


Figure 7- 13: Solid volume fraction of P1/P2 hydroentangled 37 and 108 InS structures (after caustic treatment)

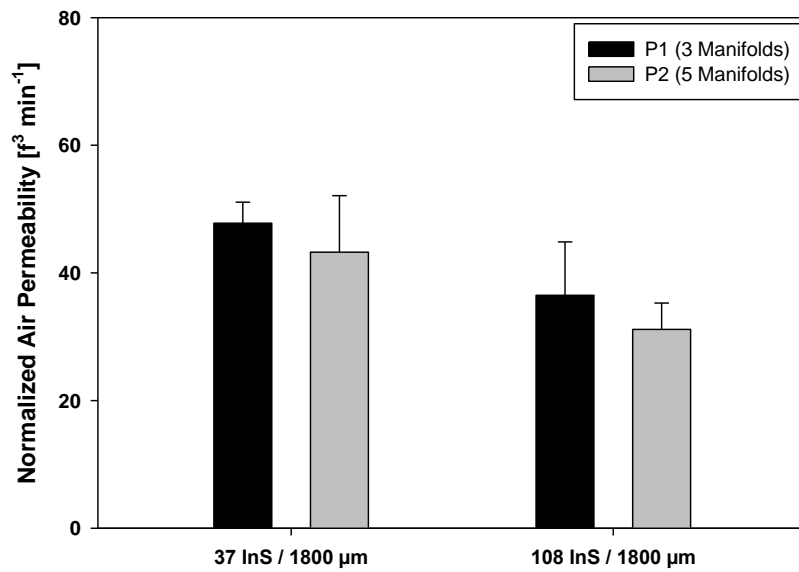


Figure 7- 14: Normalized air permeability of P1/P2 hydroentangled 37 and 108 InS structures (after caustic treatment)

MD/CD ratio of unwashed and caustic-treated 37 island-in-the-sea structures is shown below. Fiber orientation was tested to be in machine direction (MD) for both P1- and P2-hydroentangled materials. Despite the fact that the caustic treatment caused the ODF to change towards a random orientation, P1-hydroentangled structures still showed a bias in machine direction (MD), whereas P2-hydroentangled materials were randomly oriented.

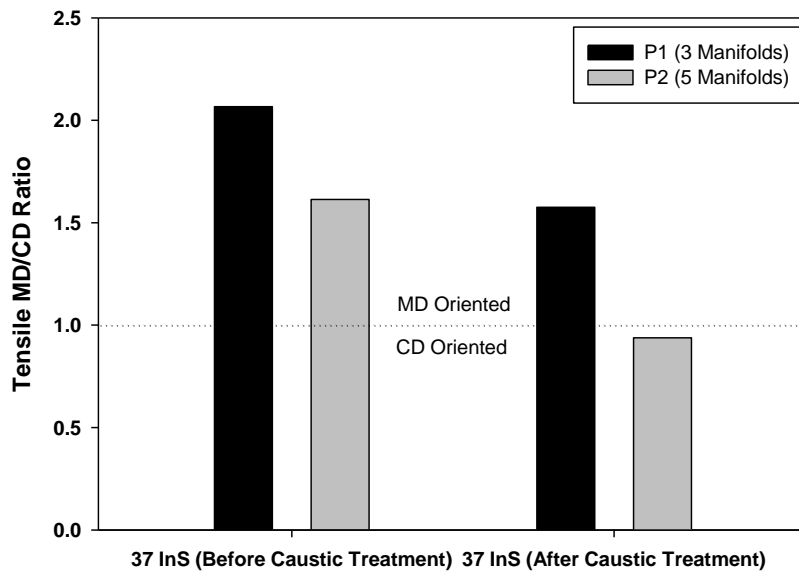


Figure 7- 15: Tensile MD/CD ratio of 600 μm , P1/P2 hydroentangled 37 InS structures (before/after caustic treatment)

7.4.2.3 Mechanical Properties

As can be seen from Figure 7- 16 - Figure 7- 18 hydroentangling with high jet pressures but fewer passes resulted in higher tensile strengths in machine direction and, except 600 μm jet spacing, in cross-direction. Moreover, materials revealed to be more oriented in machine direction than samples hydroentangled with more manifolds but lower injector pressures.

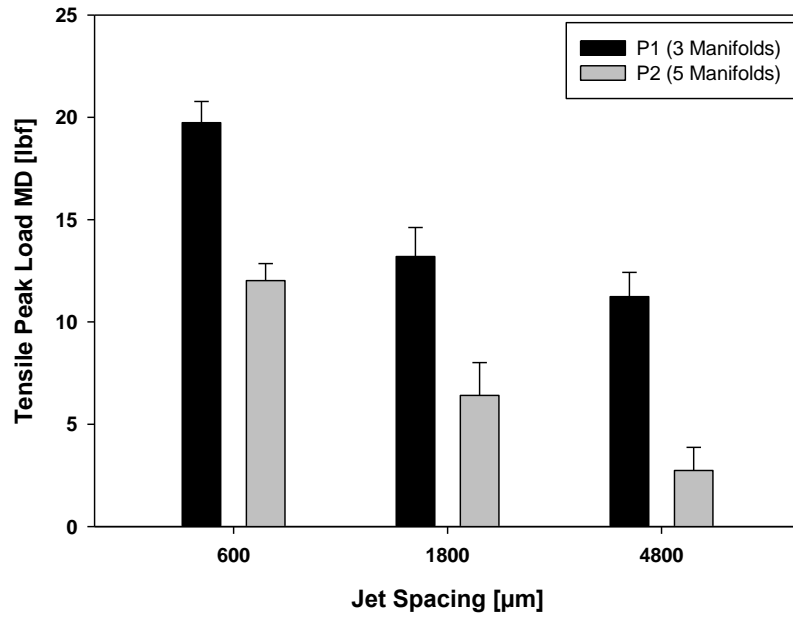


Figure 7- 16: Strip tensile strength (MD) of P1/P2 hydroentangled 37 island-in-the-sea structures (after caustic treatment)

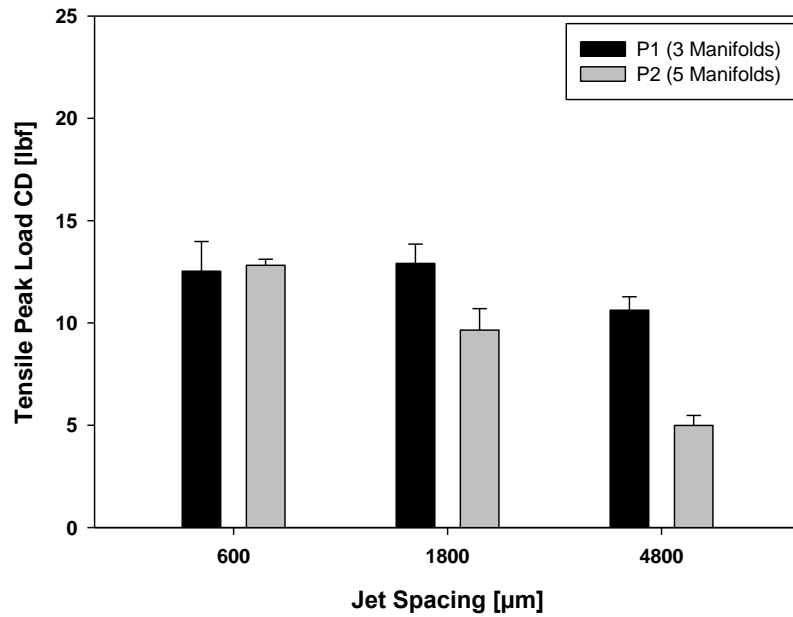


Figure 7- 17: Strip tensile strength (CD) of P1/P2 hydroentangled 37 island-in-the-sea structures (after caustic treatment)

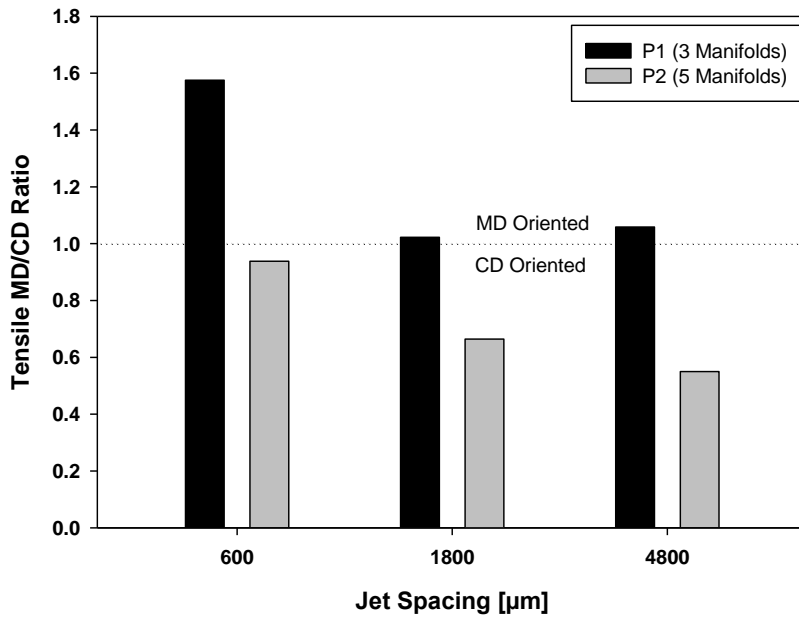


Figure 7- 18: Tensile MD/CD ratio of P1/P2 hydroentangled 37 island-in-the-sea structures (after caustic treatment)

According to Figure 7- 19 and Figure 7- 20, tear strength follows a different trend for P1- and P2-hydroentangled structure. Whereas tear strength of materials hydroentangled with higher jet pressures but fewer manifolds increases with jet spacing, opposite was found for structures hydroentangled with five injectors but lower pressures. Decrease in tear strength corresponds to a decrease in fiber mobility and we assume the difference in entanglement mechanism for large jet spacing to be responsible. However, further investigation of this phenomenon is necessary.

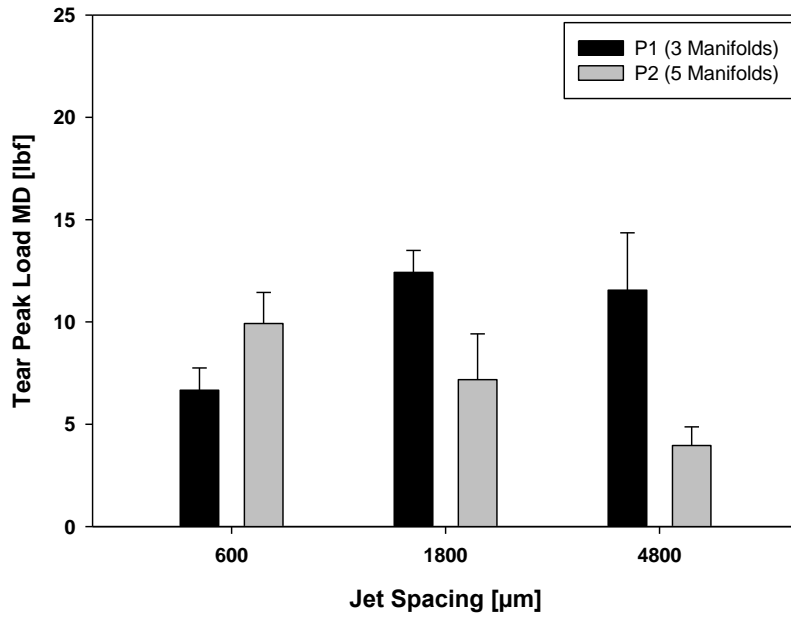


Figure 7- 19: Tongue tear strength (MD) of P1/P2 hydroentangled 37 island-in-the-sea structures (after caustic treatment)

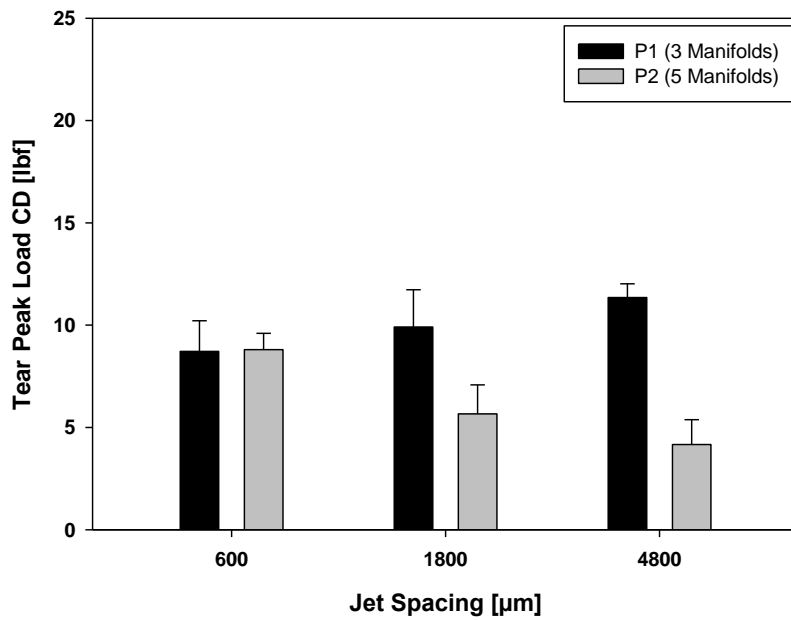


Figure 7- 20: Tongue tear strength (CD) of P1/P2 hydroentangled 37 island-in-the-sea structures (after caustic treatment)

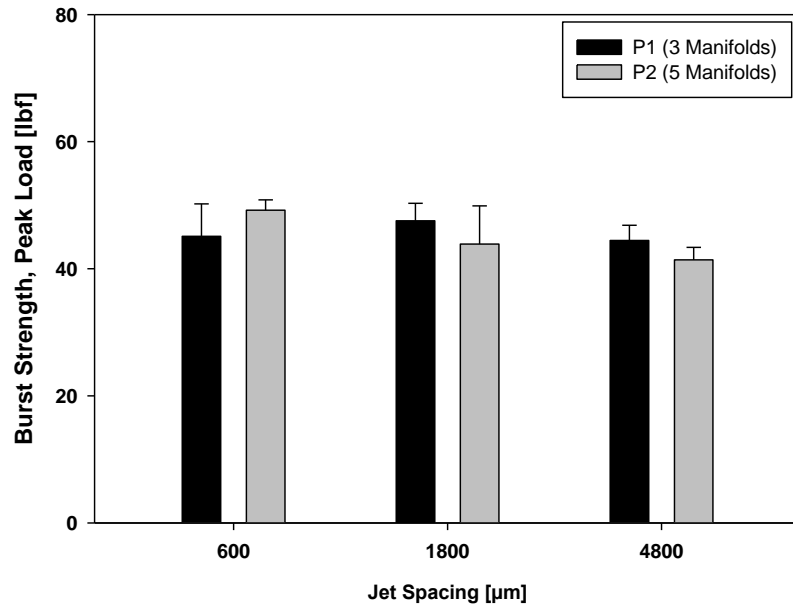


Figure 7- 21: Burst strength of P1/P2 hydroentangled 37 island-in-the-sea structures (after caustic treatment)

7.4.2.4 Summary (Part II)

We demonstrated that specific energy is not an adequate measure to describe the structure and properties of hydroentangled, caustic-treated island-in-the-sea structures. Bicomponent webs bonded with different pressures and manifolds but same specific energy and washed with an alkaline solution revealed to be different in terms of solid volume fraction, air permeability, fiber orientation as well as mechanical properties. Mechanical properties were found to be higher for nonwovens hydroentangled with higher manifold pressures but less passes.

7.4.3 Part III: Changing Specific Energy

7.4.3.1 Solid Volume Fraction and Air Permeability

Following results show that lowering the specific energy (P3/P4, 600 μm ~44% lower than P1/P2 and P3/P4, 4800 μm ~30% lower than P1/P2) did not result in solidities significantly different from higher specific energies. In contrast to that, air permeability (shown in Figure 7- 23) was found to be higher when hydroentangling with lower specific energies. Hydroentangling with fewer manifolds led to higher permeabilities.

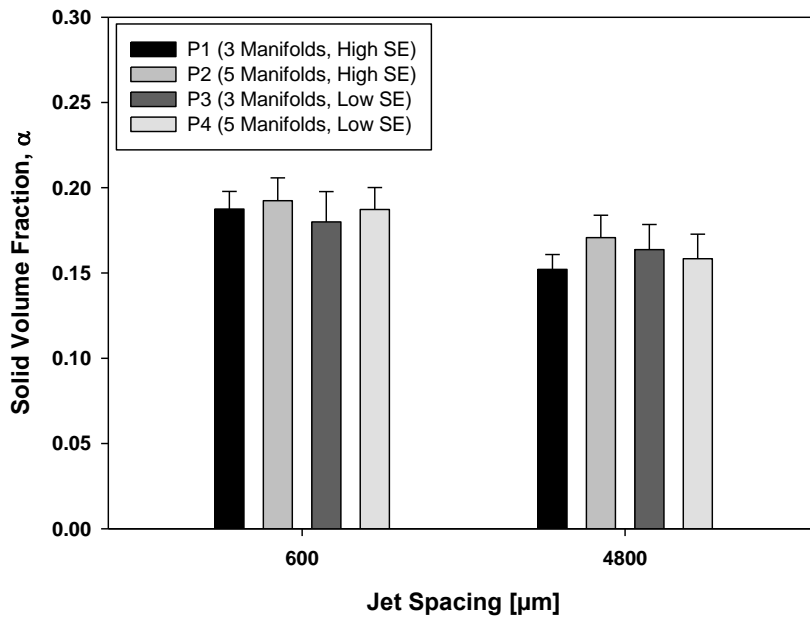


Figure 7- 22: Influence of specific energy and jet spacing on the solidity of caustic-treated 37 island-in-the-sea nonwoven materials

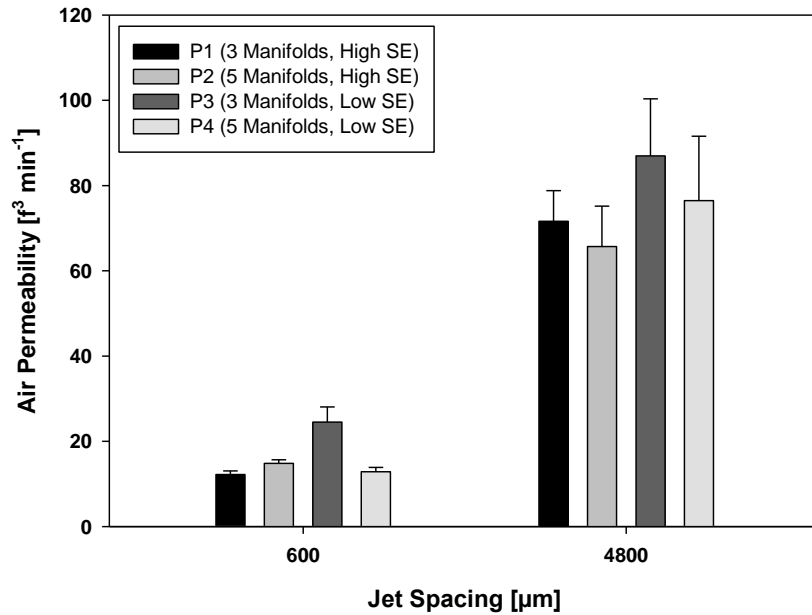


Figure 7- 23: Influence of specific energy and jet spacing on the solidity of caustic-treated 37 island-in-the-sea nonwoven materials

7.4.3.2 Tensile and Tear Strength

Comparison of strip tensile peak load and tongue tear strength is shown in Figure 7- 24 to Figure 7- 27. Both machine- (MD) and cross-direction (CD) are shown separately and indicate the mechanical properties to decrease when hydroentangling with lower specific energies. Reducing the specific energy and hydroentangling with three manifolds and 4800 µm jet spacing did not result in significantly stronger materials compared to five manifolds. The opposite can be seen for higher specific energies. This indicates the specific energy to play a crucial role and higher manifold pressures at same energy levels to be not a guarantor for stronger materials. Data also showed that results are less meaningful for materials hydroentangled with narrow jet spacing.

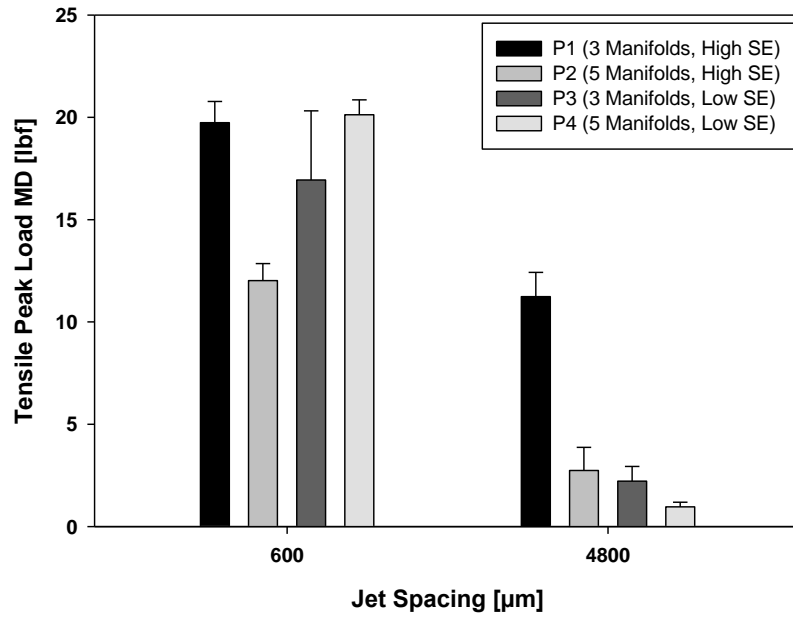


Figure 7- 24: Tensile strength (MD) of caustic-treated 37 island-in-the-sea nonwoven materials hydroentangled with P1/P2 and P3/P4 with 600 μm and 4800 μm jet spacing

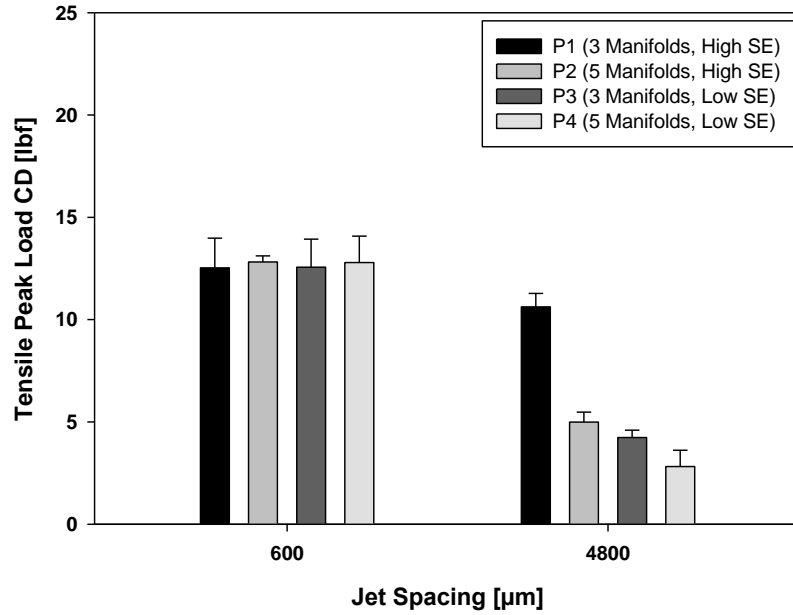


Figure 7- 25: Tensile strength (CD) of caustic-treated 37 island-in-the-sea nonwoven materials hydroentangled with P1/P2 and P3/P4 with 600 μm and 4800 μm jet spacing

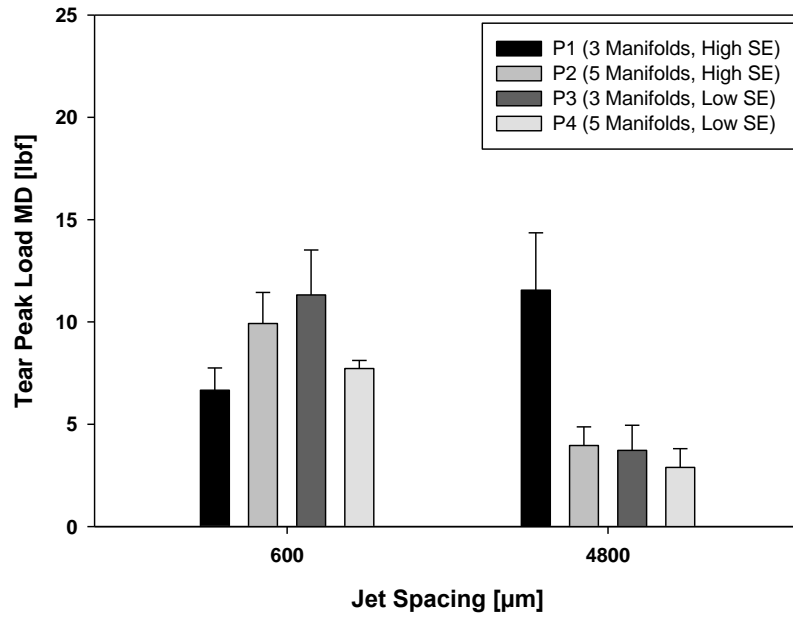


Figure 7- 26: Tear strength (MD) of caustic-treated 37 island-in-the-sea nonwoven materials hydroentangled with P1/P2 and P3/P4 with 600 μm and 4800 μm jet spacing

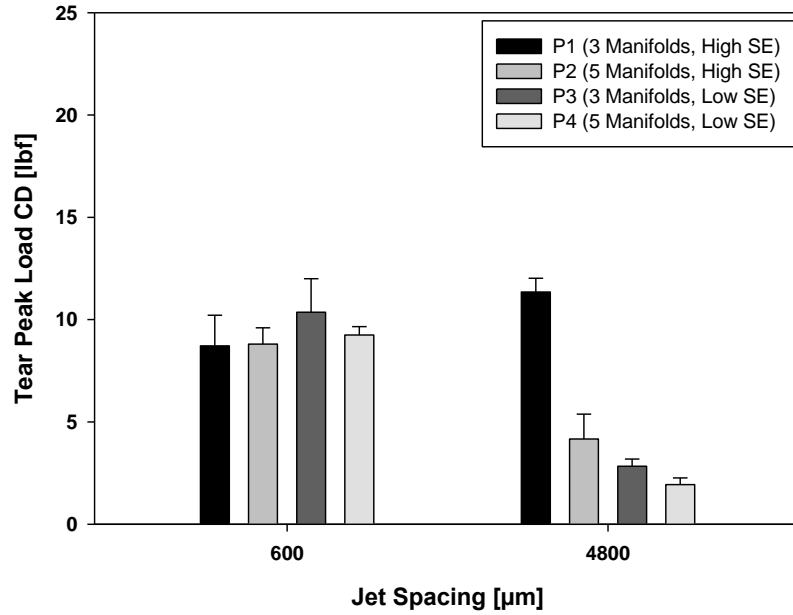


Figure 7- 27: Tear strength (CD) of caustic-treated 37 island-in-the-sea nonwoven materials hydroentangled with P1/P2 and P3/P4 with 600 μm and 4800 μm jet spacing

7.5 Overall Summary

This study examined the interaction of manifold pressure and number of manifolds at same specific energy during hydroentangling. Results indicated that specific energy is not an adequate measure to describe the influence of hydroentangling on mono- and bicomponent nonwoven materials. Mono- and bicomponent structures behaved differently and dissimilar fiber properties are assumed to be the reason. Study proved higher manifold pressures but less passes to result in more MD-oriented structures showing higher tensile strengths.

Caustic-treated island-in-the-sea nonwovens also showed a different response to manifold peak pressure and the number of passes. Hydroentangling with higher peak pressures but less manifolds led to more MD-oriented structures showing higher tensile strengths. However, hydroentangling with five manifolds but lower peak pressures resulted in denser structures with reduced air permeabilities. This phenomenon was observed to increase with jet spacing. Prior studies reported the development of knot-like structures to be better with higher manifold pressures and our findings could be related to that.

Third section of this study showed the influence of manifold peak pressure and number of passes at same energy levels to be different when lowering specific energy.

7.6 References

- Batra, S. K. & Pourdeyhimi, B. (2012). *Introduction to nonwovens technology*: DEStech Publications, Inc.
- Connolly, T. & Parent, L. (1993). Influence of specific energy on the properties of hydroentangled nonwoven fabrics. *Tappi journal*, 76(8), 135-141.
- Ghassemieh, E., Acar, M. & Versteeg, H. (2001). Improvement of the efficiency of energy transfer in the hydro-entanglement process. *Composites Science and Technology*, 61(12), 1681-1694.
- Groz-Beckert KG. (2012). HyTec® The jet strip from Groz-Beckert for hydroentanglement systems Retrieved Oct 20, 2014, from <http://www.groz-beckert.de/home/getFileCh.php?chbid=36&lang=en&file=content&download=true>
- Hutten, I. M. (2007). *Handbook of nonwoven filter media*: Elsevier.
- Moyo, D., Patnaik, A. & Anandjiwala, R. D. (2014). Optimization of energy usage in the hydroentanglement process. *Textile Research Journal*, 84(9), 913-923.
- Pourdeyhimi, B., Minton, A. & Putnam, M. (2004). Structure-process-property relationships in hydroentangled nonwovens-part 1: preliminary experimental observations. *International Nonwovens Journal*, 13, 15-21.
- Pourmohammadi, A., Russell, S. J. & Höffele, S. (2003). Effect of water jet pressure profile and initial web geometry on the physical properties of composite hydroentangled fabrics. *Textile Research Journal*, 73(6), 503-508.
- Schäfer, A. I., Fane, A. G. & Waite, T. D. (2005). *Nanofiltration: Principles and Applications*: Elsevier Advanced Technology.
- Seyam, A., Shiffler, D. & Zheng, H. (2005). An examination of the hydroentangling process variables. *International Nonwoven Journal*, 14(1), 25-33.
- Suragani Venu, L. B. (2012). *A Study on Hydroentangling Mechanisms and Structures*. (Ph.D. - Fiber and Polymer Science), North Carolina State University.
- Tausif, M. & Russell, S. J. (2012). Influence of hydroentangling variables on the properties of bi-layer polyethylene terephthalate–glass fabrics. *Textile Research Journal*, 82(16), 1677-1688.

CHAPTER 8

- Influence of Jet Intensity and Manifolds in Hydroentangling -

Part II: Number of Manifolds

Sections of this chapter will be submitted for publication in a peer-reviewed journal

8.1 Abstract

Hydroentangling is known to be a very cost-intensive process and many authors studied the correlation between energy transfer, fiber reorientation and effect on the structure. This relationship defines the ability to produce more efficient with an optimal cost-performance ratio. In a previous study we demonstrated reduced manifold pressures to be superior for low density island-in-the-sea structures in terms of filtration performance. This research has the purpose to investigate the effect of multiple manifolds with same water pressures on mono- and bicomponent nonwoven structures and also the effect on the filtration performance of the materials. Poly (propylene)/poly (lactic acid) 37 island-in-the-sea bicomponent and poly (propylene) and poly (lactic acid) monocomponent structures were produced with a basis weight of 125 g m^{-2} before being hydroentangled. After pre-wetting webs were exposed to multiple manifolds with same low jet pressures ($\leq 100 \text{ bar}$). Following webs were hydroentangled with same pressures but less manifolds before being analyzed in terms of structure and properties. Results indicated that hydroentangling with multiple manifolds with same low pressure does affect the structure and also properties. It was found that air permeability and also strength are highly affected and that even though pressures are not increased structure is changing. In addition, influence of multiple manifolds with same jet pressures also depends on the actual jet spacing during bonding.

8.2 Introduction

Techniques for bonding nonwoven webs are generally divided into mechanical, thermal and chemical processes (Chapman, 2010, p. 11). Hydroentangling describes a mechanical bonding technique using impinging, ultra-fast columns of water jets to reorient, interlock and entangle fibers (Goddard III, Brenner et al., 2007; Hutten, 2007, p. 73). However, application of this technique is not just limited to bond nonwoven webs as the jets' force can also be used to obtain microfibers by either splitting or fibrillating multicomponent fibers. Splittable bicomponent fibers are fibers containing two immiscible polymers (different in their chemical and physical properties) both facing the surface of the fiber. Examples for splittable fibers are segmented pie, segmented ribbon or tipped trilobal fibers (Goddard III, Brenner et al., 2007; Pourdeyhimi, 2008). Evolon[®] by Freudenberg is a commercially available 16-segmented pie poly (ethylene terephthalate)/poly (amide-6) spunlaid, hydroentangled nonwoven materials (Das & Pourdeyhimi, 2014, p. 95). Another bico-fiber technique is described by island-in-the-sea, which is characterized by small fibers (islands) embedded within the matrix of another polymer (sea). Compared to splittable fibers islands are not exposed to the outside of the fiber and sea has either to be cracked or dissolved to unveil islands. Depending on the final application sea fragments can have adventitious or undesirable effects, such as increased pressure drops due to blocked pores. Spinnability and properties of island-in-the-sea fibers made from a variety of polymers were studied and reported by Fedorova (Fedorova, 2006). If sea polymer is intended to be dissolved in a subsequent process structure requires sufficient fiber entanglement to withstand the subsequent treatment, which not only induces weight loss but also structural changes.

Poly (lactic acid), a biodegradable polymer with great spinnability, describes a suitable candidate to be used in an island/sea matrix (Belgacem & Gandini, 2011, p. 433; Fedorova, 2006, pp. 54, 66, 195). We previously reported reduced hydroentangling pressures and large jet spacing ($> 1800 \mu\text{m}$) to result in island-in-the-sea nonwoven materials with superior filtration properties. We also reported island-in-the-sea structures hydroentangled with manifold pressures of 20-80-100-100-100 (manifold 1 to 5) and jet spacing varying from $600 \mu\text{m}$ to $4800 \mu\text{m}$ to be strong enough to withstand the caustic washing. However, it is unknown whether a series of manifolds with same hydroentangling pressures affect the structure in terms of washability, structure and properties. Suragani (Suragani Venu, 2012, pp. 152-173) studied the effect of the number of manifolds on carded, cross-lapped poly (amide-6)/poly (ethylene terephthalate) monocomponent nonwovens. Webs were hydroentangled with 1 to 8 manifolds having a pressure of 100 bar each. According to the results, hydroentangling with multiple manifolds resulted in areas with deep and also restrained fiber penetration depths.

The principal objective of this study is to understand whether hydroentangling with multiple manifolds and same pressures affects the structural and physical properties of caustic-washed island-in-the-sea nonwoven materials. Study strives to understand whether the caustic treatment removes the effect of multiple manifolds with equal water pressures and whether or not optimized structures can be achieved. For this study an optimized material is declared to be more permeable (lower pressure drop) and cost-effective (lower specific energy during bonding). Based on our previous findings, which showed low hydroentangling pressures to be favorable to produce optimized filtration media, we chose manifold pressures

$\leq 100 \text{ bar}$ for this study. Multiple manifolds with equal pressures are often used in hydroentangling but the actual impact rather unknown. In addition, this study addresses the influence of jet spacing and investigates the effect of multiple manifolds with same hydroentangling pressure on monocomponent structures.

8.3 Methodology

8.3.1 Materials

Mono- and bicomponent nonwoven materials were produced with a 0.5 meter Hills-Nordson spunbond line and subsequently hydroentangled with a 0.5 meter Fleissner Aquajet at the Nonwoven Institute Partners facilities located at Centennial Campus, North Carolina State University.

Monocomponent Materials

Poly (propylene) (Braskem CP360H) and poly (lactic acid) (Natureworks 6202D) spunbond monocomponent nonwoven webs were produced with a basis weight of 125 g m^{-2} . Webs passed through a compaction and calender roll before being hydroentangled with different manifold pressures and jet spacing. Hydroentangling conditions are given in Table 8- 1.

Island-in-the-Sea Materials

Island-in-the-sea nonwoven webs were produced with a fixed basis weight of 125 g m^{-2} with poly (propylene) (Braskem CP360H) as island polymer and poly (lactic acid) (Natureworks 6202D) as sea polymer. Polymer mass ratio was kept constant at 75% for the island and 25%

for the sea polymer. After melt spinning webs passed through a compaction and calender roll before being hydroentangled with a different jet spacing and number of manifolds. Webs were hydroentangled on a 100 mesh poly (ethylene terephthalate) forming belt running with constant speed. All webs were dried in a conveyor oven. Table 8- 1 provides additional information about the bonding of the webs.

Table 8- 1: Structures and hydroentangling parameters

Structure	Hydroentangling Pressure [bar]		600 μm	1800 μm	4800 μm
			Specific Energy [kJ Kg^{-1}]		
37 InS PP Mono PLA Mono	P1	20-80-100-100-100 (M1-M5)	5400	1800	700
	P2	20-80-100-100-0 (M1-M5)	4000	1300	500
	P3	20-80-100-0-0 (M1-M5)	2600	900	300
Belt Speed: 10 m min⁻¹					
→ Structure IDs: 8.-Structure.JetSpacing-125-Pressure ←					

8.3.2 Sample Preparation

Island-in-the-sea samples were treated with caustic to remove the poly (lactic acid) compound from the bicomponent structure. Bath was prepared in a steam kettle with a sodium hydroxide concentration of 8% w/w and a temperature of 100 °C. Samples were washed under continuous stirring for 10 minutes before being washed-out and neutralized with cold water. Caustic-treated structures were dried in the open air on a sample rack.

8.3.3 Structure Analysis

Basis Weight and Thickness

A Denver Instrument XL-3100D top-loading balance and a hanatek FT3V-LAB high-precision thickness gauge were used to analyze weight and thickness respectively. 10 replicates were tested for each structure.

Solid Volume Fraction (SVF)

The solid volume fraction of all samples was determined by using the following equation.

$$\alpha = \frac{w}{\rho_f \times t} \quad \text{Eq. 8- 1}$$

where w is the basis weight [g m^{-2}], ρ_f the total fiber density [g m^{-3}] and t the thickness of the structure [m]. Total fiber density ρ_f has to be calculated for bicomponent structures and is obtained as follows.

$$\rho_f = (\rho_{island} \times R_i) + (\rho_{sea} \times R_s) \text{ [g cm}^{-3}\text{]} \quad \text{Eq. 8- 2}$$

where ρ_{island} is the density of the island polymer [g cm^{-3}], R_i is the mass fraction of island polymer ρ_{sea} is the density of the sea polymer [g cm^{-3}] and R_s is the mass fraction of sea polymer.

Mechanical Properties (Ball Burst)

Burst strength of mono- and bicomponent materials (prior/after caustic treatment) was tested with an Instron 4400r universal testing system according to ASTM D6797 (5 replicates per structure).

Mechanical Properties (Strip Tensile)

Strip tensile test was tested according to ASTM D5035 with 5 replicates per structure. An Instron 4400r universal testing system was used and mono- and bicomponent structures (prior/after caustic treatment) were tested in both machine- (MD) and cross direction (CD).

Mechanical Properties (Tongue Tear)

Tongue tear tests was done according do ASTM D5735 with a total of 5 replicates per structure. Both mono- and bicomponent materials (prior/after caustic) were tested in machine- (MD) and cross direction (CD). Analysis of mechanical properties was performed with an Instron 4400r universal testing system.

Aerosol Filtration Properties

Pressure drop and filtration efficiency of as-received samples were measured with a TSI 3160 particle penetration tester. Dioctyl phthalate (DOP) was used as challenging aerosol with a particle size d_p of 0.3 μm . Face velocity f_v was set at 5.33 cm s^{-1} and the tested area was 100 cm^2 . Quality factor QF was calculated as follows.

$$QF = \frac{-\ln(P)}{\Delta p} [\text{Pa}^{-1}] \quad \text{Eq. 8- 3}$$

where P is the fractional particle penetration and Δp the pressure drop [Pa] of the material.

8.4 Results and Discussion

The following discussion is divided into three individual sections discussing the effect the number of manifolds on the structure and properties of hydroentangled mono- and bicomponent nonwoven structures.

Part I: Caustic-treated 37 island-in-the-sea nonwovens

Part II: Caustic-treated 37 island-in-the-sea nonwovens with varying jet spacing

Part III: Mono- and bicomponent structures

8.4.1 Part I: Effect of Number of Manifolds on 37 InS Nonwoven Materials

8.4.1.1 Solid Volume Fraction and Air Permeability

Figure 8- 1 depicts the effect of hydroentangling with five, four and three manifolds and 600 μm jet spacing on the solid volume fraction of caustic-washed 37 island-in-the-sea nonwovens. Results indicated the solid volume fraction of P2- and P3-hydroentangled samples to be slightly lower compared to P1.

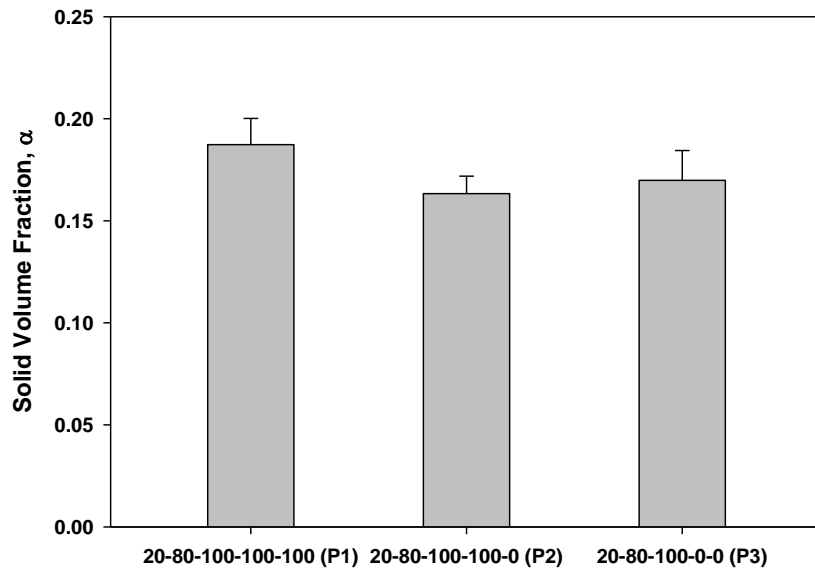


Figure 8- 1: Solid volume fraction of caustic-treated 37 InS structures hydroentangled with P1-P3 and 600 μm jet spacing

Air permeability measurements, which are shown in Figure 8- 2, indicated hydroentangling with multiple equal manifold pressures to significantly affect the permeability of the samples. According to the results, air permeability increased the more manifolds were deactivated. This result is interesting as air permeability was expected to follow the same trend as solid volume fraction. From this it can be assumed that hydroentangling with multiple manifolds with low pressures rather affect the entanglement on the surface than the actual consolidation of the material.

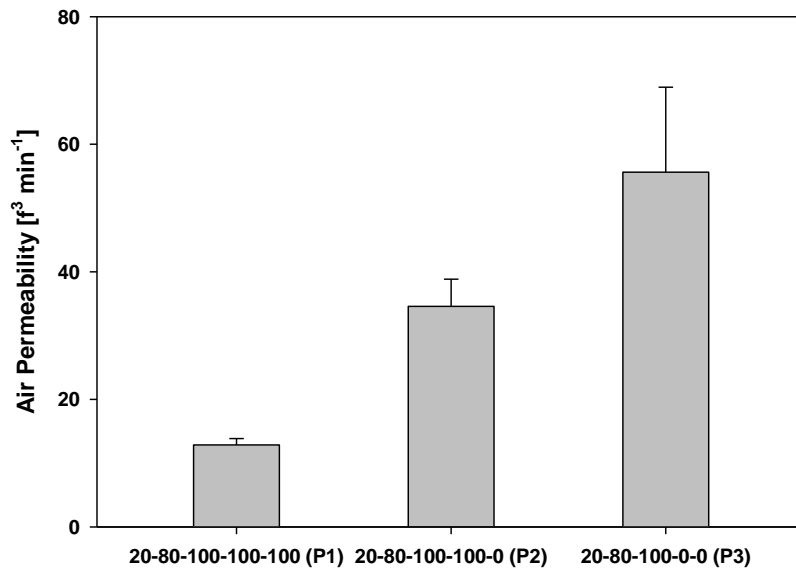


Figure 8- 2: Air permeability of caustic-treated 37 InS structures hydroentangled with P1-P3 and 600 μm jet spacing

8.4.1.2 Mechanical Properties

Burst strength of caustic-washed materials is shown in Figure 8- 3. Results revealed hydroentangling with consistent water pressure to have no effect on the burst strength of the samples.

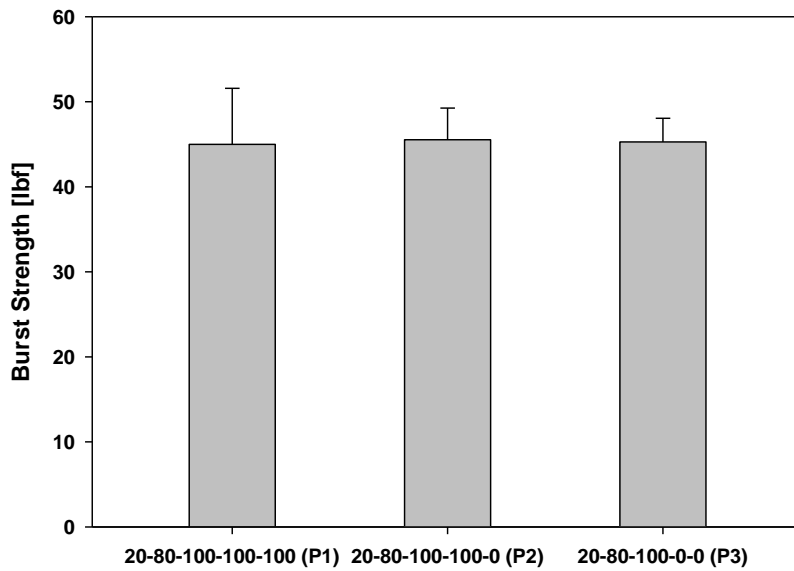


Figure 8- 3: Burst strength of caustic-treated 37 InS structures hydroentangled with P1-P3 and 600 μm jet spacing

According to the results, hydroentangling with three manifolds with equal water pressures showed significantly higher tensile strengths in machine-direction compared to samples hydroentangled with less repeating pressures. Tensile strength in cross-direction decreased the less manifolds were active and the same trend can be seen from tongue tear results. These results prove that hydroentangling island-in-the-sea materials with multiple, equal manifold pressures does affect the strength of the materials even after the caustic treatment.

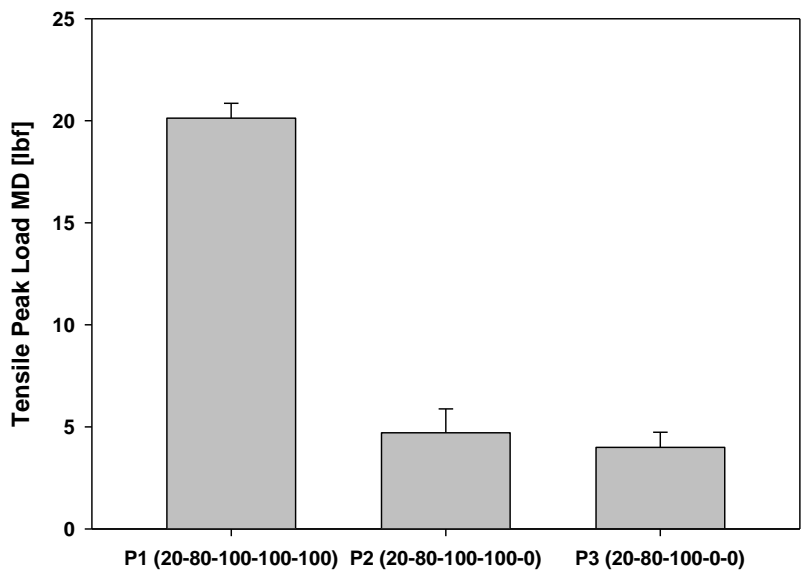


Figure 8- 4: Tensile strength (MD) of caustic-treated 37 InS structures hydroentangled with P1-P3 and 600 μm jet spacing

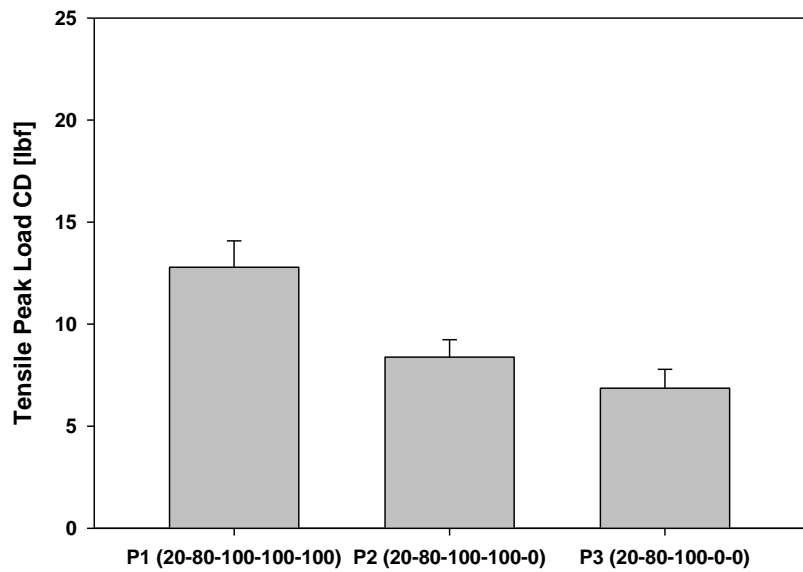


Figure 8- 5: Tensile strength (CD) of caustic-treated 37 InS structures hydroentangled with P1-P3 and 600 μm jet spacing

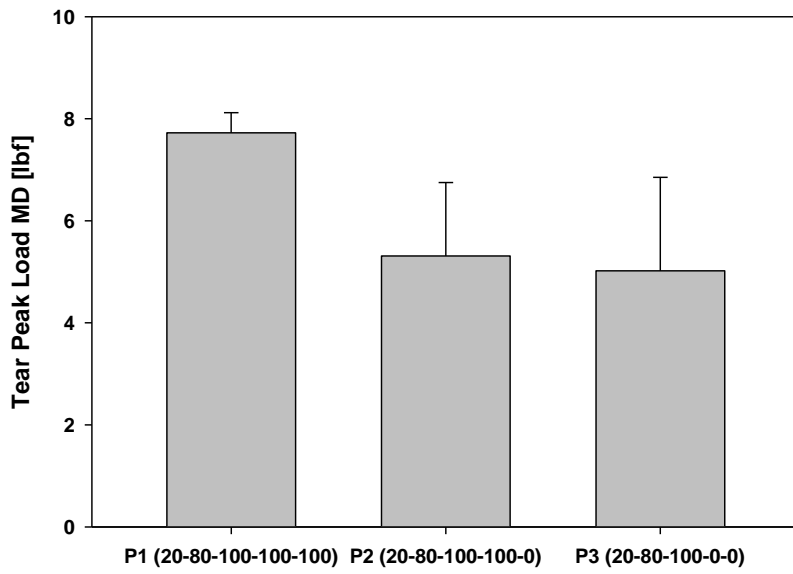


Figure 8- 6: Tongue tear strength (MD) of caustic-treated 37 InS structures hydroentangled with P1-P3 and 600 μm jet spacing

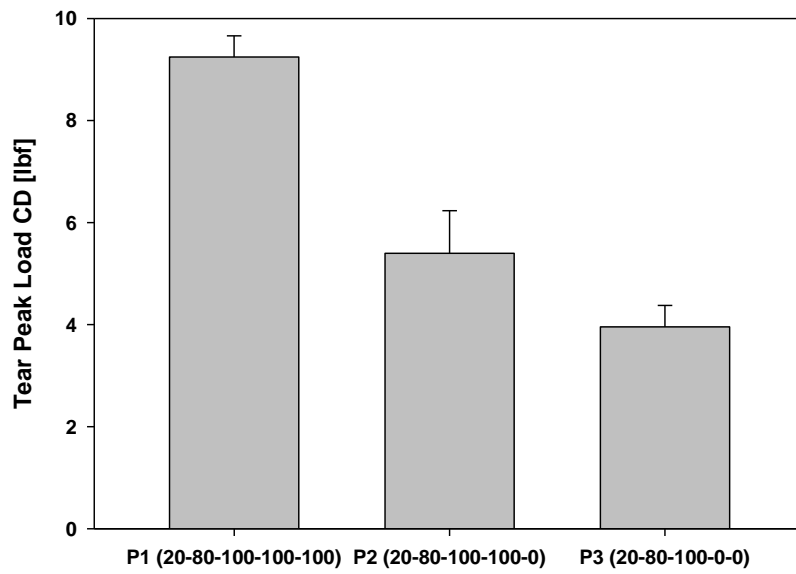


Figure 8- 7: Tongue tear strength (CD) of caustic-treated 37 InS structures hydroentangled with P1-P3 and 600 μm jet spacing

It was previously shown that air permeability increased the less manifolds with same pressures were used. Pressure drop of samples, which is given in Figure 8- 9, follows the same trend and decreases with less active manifolds. According to the quality factor, which is shown in Table 8- 2, samples hydroentangling with two manifolds with equal jet pressure performed best.

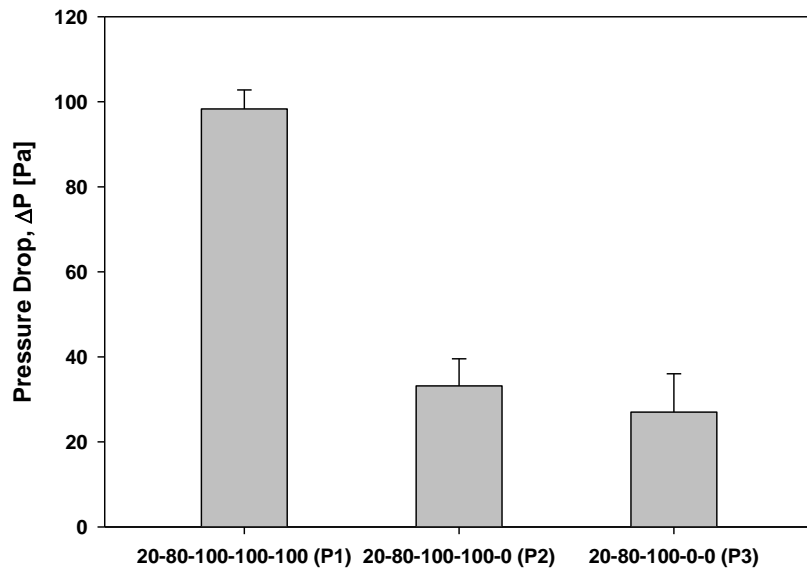


Figure 8- 8: Pressure drop of caustic-treated 37 InS structures hydroentangling with manifold pressures P1-P3 and 600 μm jet spacing ($f_j: 5.33 \text{ cm s}^{-1}$)

Table 8- 2: Quality factor of caustic-treated 37 InS structures hydroentangling with manifold pressures P1-P3 and 600 μm jet spacing

Structure	QF @ P1 [Pa^{-1}]	QF @ P2 [Pa^{-1}]	QF @ P3 [Pa^{-1}]
37 InS (P1-P3)	0.0065	0.0125	0.0105

8.4.1.3 Summary (Part I)

We demonstrated that even with low manifold pressures hydroentangling with multiple injectors with same pressure does affect the structure and properties of caustic-washed island-in-the-sea nonwoven materials. Samples hydroentangled with three equal manifold pressures showed highest solidity, lowest air permeability and highest strip tensile and tongue tear strengths.

8.4.2 Part II: Effect of Jet Spacing

8.4.2.1 Solid Volume Fraction and Air Permeability

The solid volume fraction of caustic-washed island-in-the-sea fabrics hydroentangled with different jet spacing and manifolds with same water pressures can be seen in Figure 8- 9.

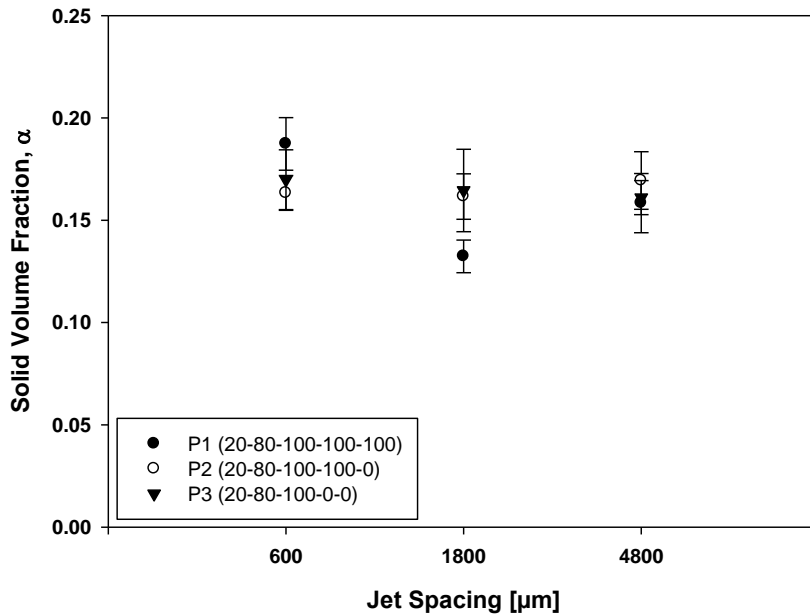


Figure 8- 9: Solid volume fraction of caustic-treated 37 InS structures hydroentangled with P1-P3 and 600, 1800 and 4800 μm jet spacing

Results indicated jet spacing to have only little influence on the solidity when hydroentangling with multiple similar manifold pressures.

Materials hydroentangled with 600 and 4800 μm jet spacing showed higher solidities compared to 1800 μm jet spacing. Hydroentangling with five manifolds (three identical manifold pressures) showed highest solidity for 600 μm but lowest for 1800 μm jet spacing. One reason could be knot-like structures obtained when hydroentangling with larger jet spacing. Following figures displays the air permeability results.

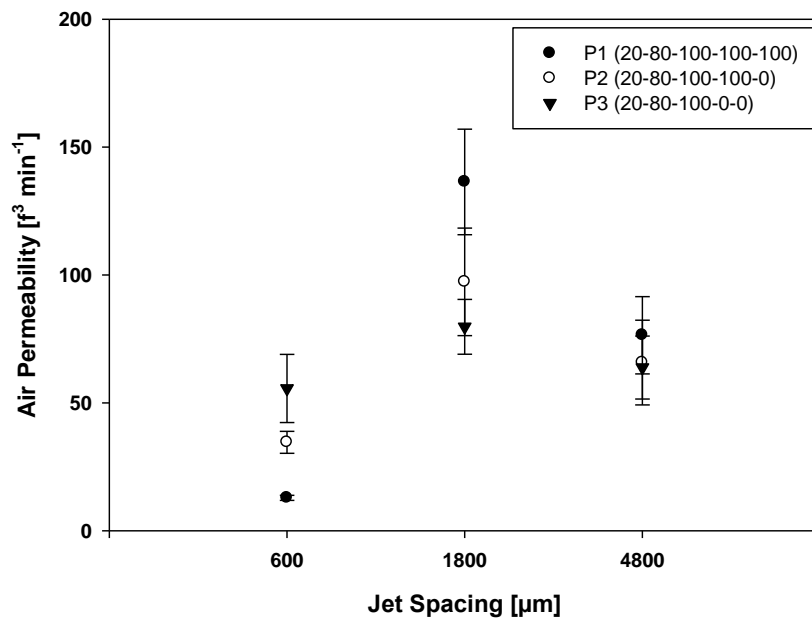


Figure 8- 10: Air permeability of caustic-treated 37 InS structures hydroentangled with P1-P3 and 600, 1800 and 4800 μm jet spacing

As can be seen from the data air permeability follows the trend shown for the solid volume fraction. Nonwovens hydroentangled with 600 μm jet spacing showed less permeability compared to structures hydroentangled with 1800 μm jet spacing. It is assumed that the

combined effect of low manifold pressures and 4800 μm did not result in sufficient fiber entanglement and structure collapsed after the caustic-treatment. This would explain the increase in solidity and decrease in air permeability.

8.4.2.2 Mechanical Properties

Figure 8- 11 and Figure 8- 12 show the tensile strength of caustic-washed island-in-the-sea samples as a function of jet spacing. According to the results, hydroentangling with 600 μm jet and three equal manifold pressures resulted in significantly stronger fabrics compared to webs hydroentangled with P2 or P3. Tensile strength was found to be comparable for larger jet spacing and tear results indicated a similar trend.

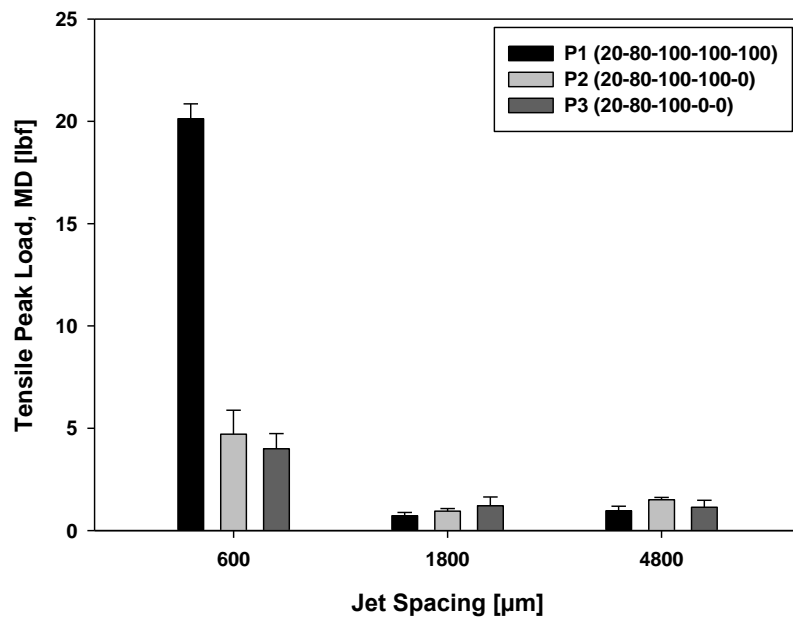


Figure 8- 11: Tensile strength (MD) of caustic-treated 37 InS structures hydroentangled with P1-P3 and 600, 1800 and 4800 μm jet spacing

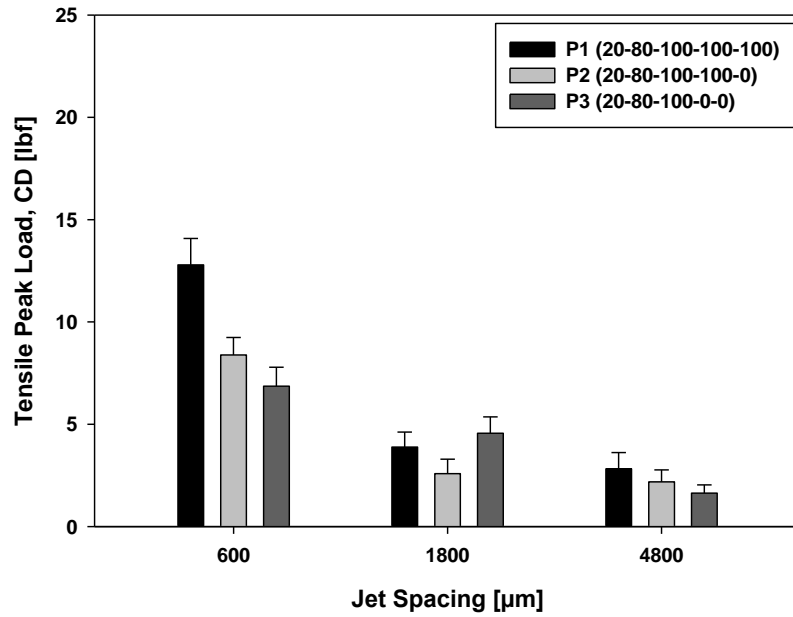


Figure 8- 12: Tensile strength (CD) of caustic-treated 37 InS structures hydroentangled with P1-P3 and 600, 1800 and 4800 μm jet spacing

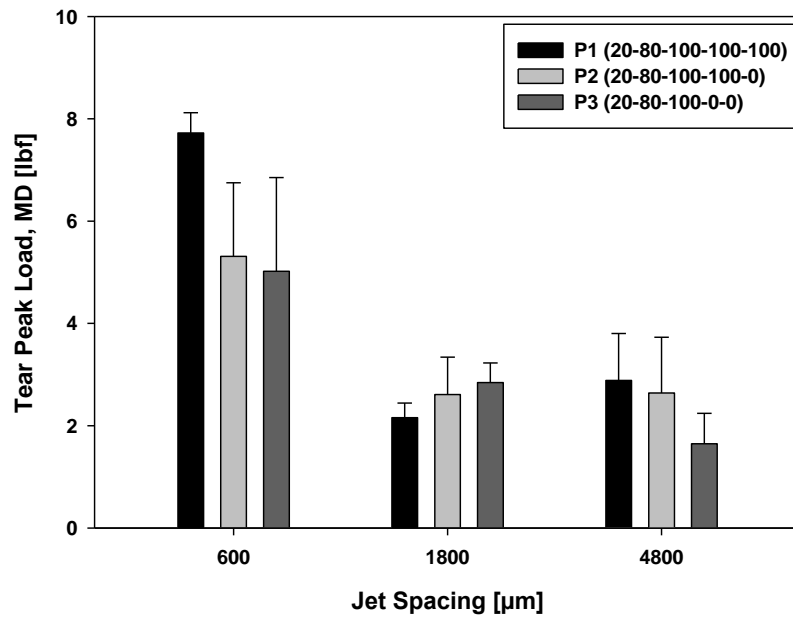


Figure 8- 13: Tear strength (MD) of caustic-treated 37 InS structures hydroentangled with P1-P3 and 600, 1800 and 4800 μm jet spacing

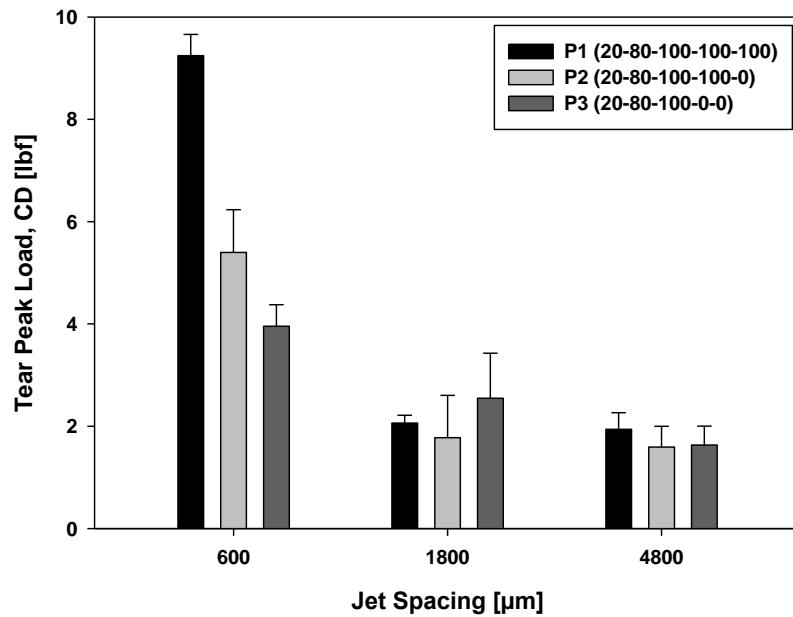


Figure 8- 14: Tear strength (CD) of caustic-treated 37 InS structures hydroentangled with P1-P3 and 600, 1800 and 4800 µm jet spacing

8.4.2.3 Summary (Part II)

Results demonstrated jet spacing to play a prominent role when hydroentangling with multiple manifolds with same pressures. Whereas hydroentangling with 600 µm jet spacing and multiple manifolds with one, two or three equal pressures clearly showed differences in terms of permeability and strength, results were vaguer for larger jet spacing. 1800 µm hydroentangled samples showed less dense and more permeable structures but both 1800 µm and 4800 µm showed significantly lower strengths.

8.4.3 Part III: Mono- and Bicomponent Nonwoven Structures

8.4.3.1 Solid Volume Fraction and Air Permeability

Effect of hydroentangling with equal manifold pressures on the solid volume fraction of mono- and bicomponent (before caustic-treatment) nonwovens is shown in Figure 8- 15.

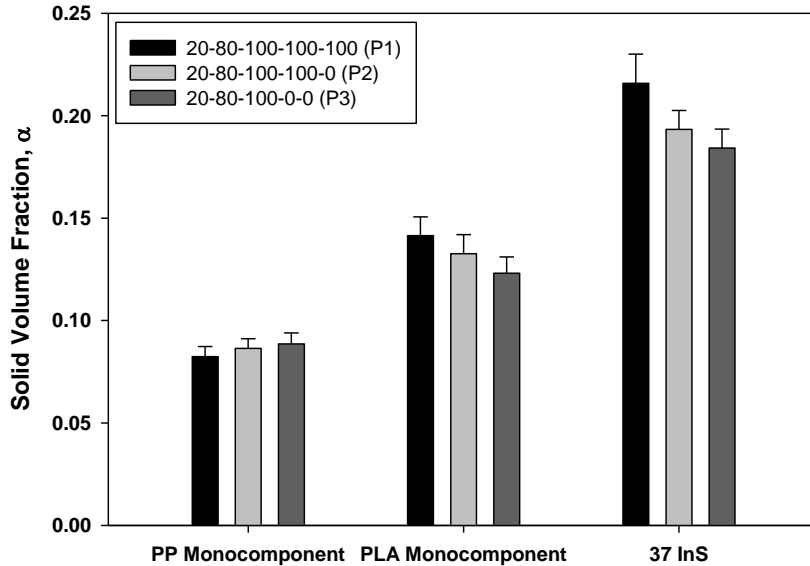


Figure 8- 15: Solidity of mono- and bicomponent nonwovens hydroentangled with P1-P3 and 600 μm jet spacing

It was observed that both poly (lactic acid) and island-in-the-sea structures followed the same trend with increasing solidities the more manifolds with same jet pressures were used. Air permeability of samples, which is shown in Figure 8- 16, confirmed that. However, poly (propylene) materials did show the opposite trend and it is assumed that combined effect of low hydrophilicity and low manifold pressures did not induce sufficient fiber transfer. Instead repeating water jets caused the structure to open. In contrast to that, hydroentangling

poly (lactic acid) monocomponent and island-in-the-sea structures with repeating manifold pressures caused the structure to consolidate.

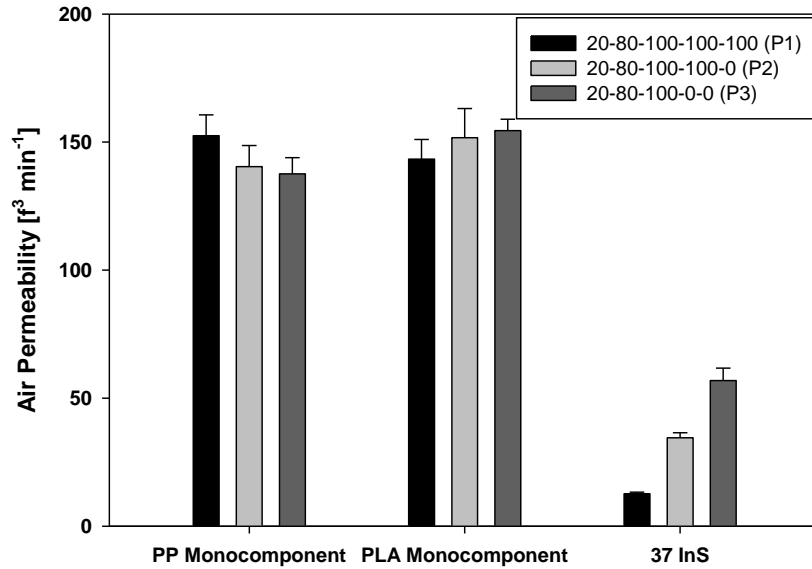


Figure 8- 16: Air permeability of mono- and bicomponent nonwovens hydroentangled with manifold pressures P1-P3 and 600 µm jet spacing

8.4.3.2 Mechanical Properties

Tensile and tear properties of samples are shown in the following. From the results it can be observed that poly (lactic acid) monocomponent nonwovens showed highest tensile and also tear strengths. However, there seems little or no influence of the number of manifolds on the mechanical properties of mono- and unwashed island-in-the-sea structures.

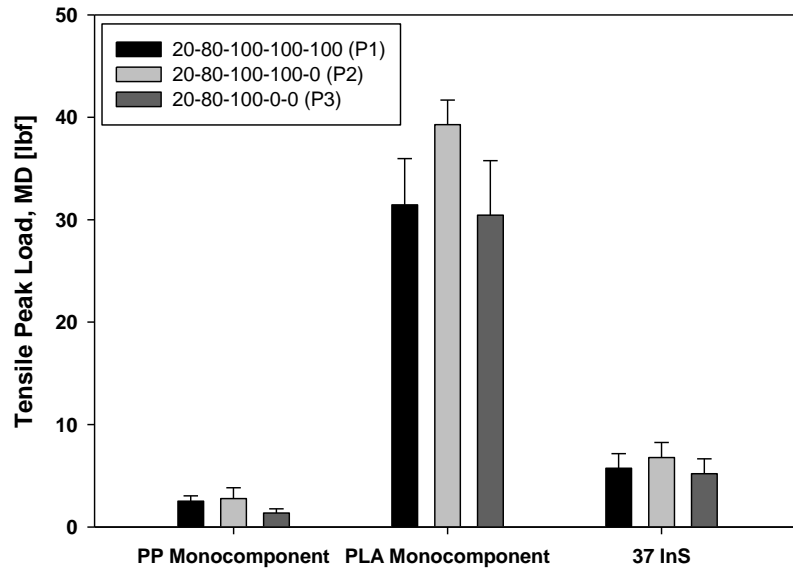


Figure 8- 17: Tensile strength (MD) of mono- and bicomponent structures hydroentangled with P1-P3

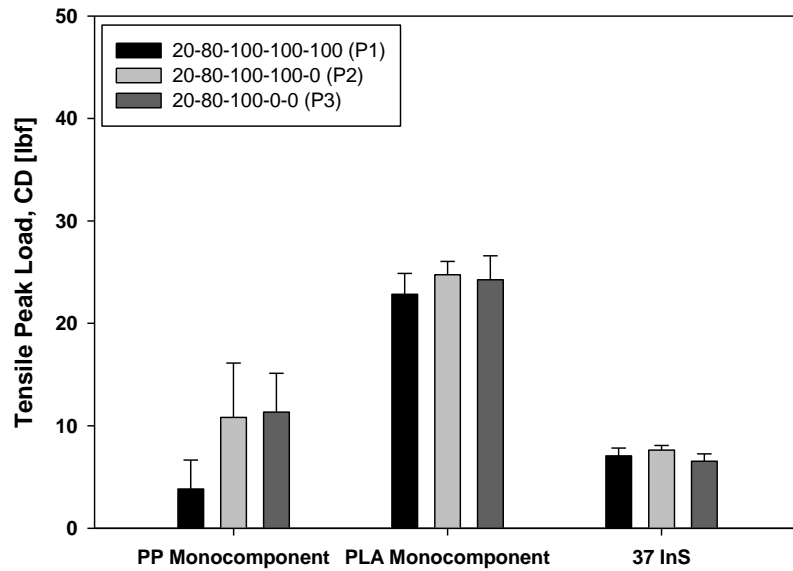


Figure 8- 18: Tensile strength (CD) of mono- and bicomponent structures hydroentangled with P1-P3

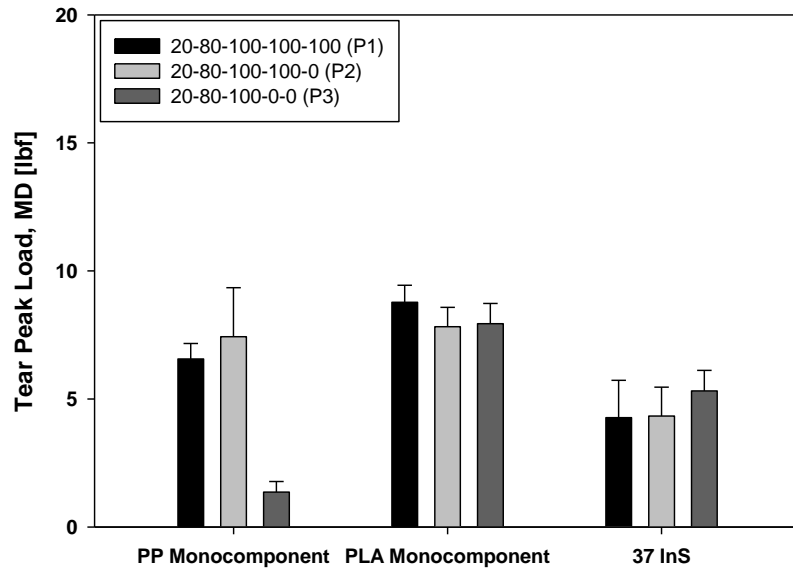


Figure 8- 19: Tear strength (MD) of mono- and bicomponent structures hydroentangled with P1-P3

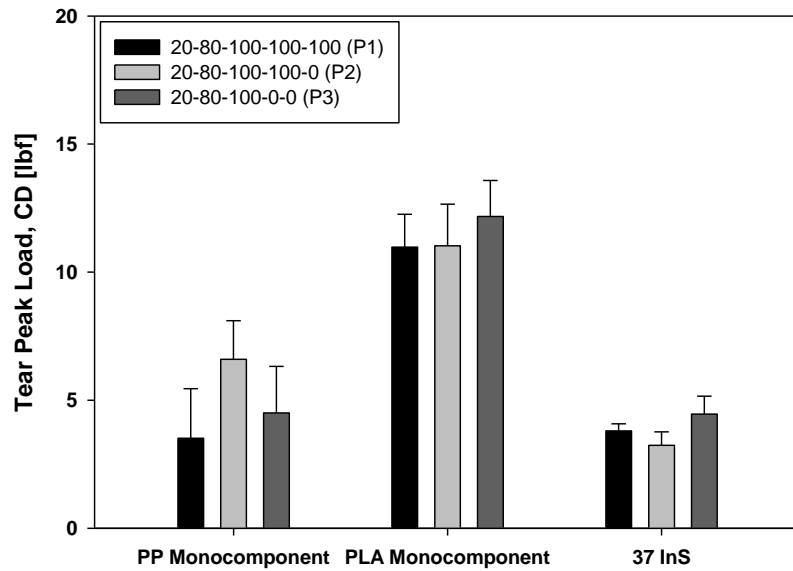


Figure 8- 20: Tear strength (CD) of mono- and bicomponent structures hydroentangled with P1-P3

8.4.3.3 Overall Conclusion

This study demonstrated that hydroentangling with different number of manifolds but same jet pressure influences the structure and properties of nonwoven materials. The first part of this work proved that hydroentangling with up to three manifolds with the same pressure does influence the properties of caustic-treated 37 island-in-the-sea nonwovens. Using multiple manifolds with same pressures led to decreased air permeabilities but also higher mechanical properties. However, quality factor of the samples was found to decrease. In the second part we demonstrated that hydroentangling with multiple manifolds with same pressures is rather important for 600 μm than larger jet spacing. Third part of this study showed that hydroentangling with multiple manifolds with same jet pressure influences the solidity and air permeability of poly (propylene) and poly (lactic acid) monocomponent and also unwashed island-in-the-sea nonwoven materials, whereas the mechanical properties were less affected.

8.5 References

- Belgacem, M. N. & Gandini, A. (2011). *Monomers, Polymers and Composites from Renewable Resources*: Elsevier Science.
- Chapman, R. (2010). *Applications of nonwovens in technical textiles*: Elsevier.
- Das, D. & Pourdeyhimi, B. (2014). *Composite Nonwoven Materials: Structure, Properties and Applications*: Elsevier Science.
- Fedorova, N. (2006). *Investigation of the utility of islands-in-the-sea bicomponent fiber technology in the spunbond process, 2006*. (Ph.D. - Fiber and Polymer Science), North Carolina State University.
- Goddard III, W. A., Brenner, D., Lyshevski, S. E. & Iafrate, G. J. (2007). *Handbook of nanoscience, engineering, and technology*: CRC press.
- Hutten, I. M. (2007). *Handbook of nonwoven filter media*: Elsevier.
- Pourdeyhimi, B. (2008). Comments on the paper entitled “Splitting of islands-in-the-sea fibers (PA6/COPET) during hydroentangling of nonwovens”. *Journal of Engineered Fibers and Fabrics*, 3, 32-35.
- Suragani Venu, L. B. (2012). *A Study on Hydroentangling Mechanisms and Structures*. (Ph.D. - Fiber and Polymer Science), North Carolina State University.

CHAPTER 9

- A Study on Winged Fiber Nonwoven Materials -

Sections of this chapter will be submitted for publication in a peer-reviewed journal

9.1 Abstract

Winged fibers describe a relatively young technology offering exceptional surface areas at high throughput rates. These oval-shaped, channel fibers provide specific surface areas of $14 \text{ m}^2 \text{ g}^{-1}$ or higher and have linear densities of about 1 to 2 denier (Pourdeyhimi & Chappas, 2012a). In this study spunbond winged fiber structures with 32 projections (wings, lobes) and an initial basis weight of 115 g m^{-2} were hydroentangled with different parameters. Afterwards, materials underwent a caustic treatment to remove the sheath polymer from the fibers, unveil the wings and obtain structures with much higher specific surface area. Structure, physical properties, aerosol filtration performance and also the influence of specific surface area and fiber diameter were analyzed. Results indicated the necessary water pressure during hydroentangling to be much higher for winged than round fiber webs. This can be explained by the different fiber flexural rigidities and the fibers' response to impinging water jets. BET specific surface area of winged materials was experimentally analyzed by Krypton gas adsorption and found to be in the range of circular fibers with diameters of about $1 \text{ }\mu\text{m}$. Winged structures revealed to be highly permeable and low in density, which can be related to their relatively large effective fiber diameter. Even though winged fibers might be superior as dust holding layers (DHC), efficiency at MPPS was slightly lower compared to structures with smaller fiber diameters. Unwashed and washed winged fiber structures showed comparable capture efficiencies demonstrating the specific surface area to be not the only important characteristic in terms of filtration efficiency.

9.2 Introduction

Over the past years much research has been performed to increase the amount of area provided by fibrous materials. Simply researching for patents and using the terms specific surface area and nonwovens results in a variety of approaches to create structures from modified, often non-round fiber types. The term specific surface area describes the theoretical accessible area within a structure per unit weight (Erdem & Trinkaus, 2008). Patent search revealed methods, such as the creation of micro- and or nanofibers by means of bicomponent techniques (Haggard, Wilkie et al., 2008) or fibers with extraordinary cross-sectional shapes ((Pourdeyhimi & Chappas, 2012b). Thus, increasing the specific surface area can either be made by reducing the fiber size or changing the cross-section of the fibers. Nonwoven manufacturing technologies being capable to produce fibers in the micro- or even nanometer region are often limited by low productivity (e.g. electrospinning) (Yeom & Pourdeyhimi, 2011). In contrast to that, bicomponent technologies allow production of structures with high specific surface areas at reasonable output rates. However, in contrast to electrospun or meltblown webs, subsequent processes are required to either remove one polymer or separate both from each other. Winged fibers describe a relatively young technology characterized by fibers with multiple projections (also called wings or lobes). These projections are attached to the center region of the fiber and the fiber is surrounded by a matrix polymer, which has to be removed in a subsequent process. Due to its shape this oval shaped fiber type can provide tremendous amounts of specific surface area. Winged fibers look similar to 4DG fiber but are, in contrast to 4DG fibers, not directly spun.

Figure 9- 1 depicts an illustration of a 32 lobes winged fiber before and after the removal of the sheath compound.

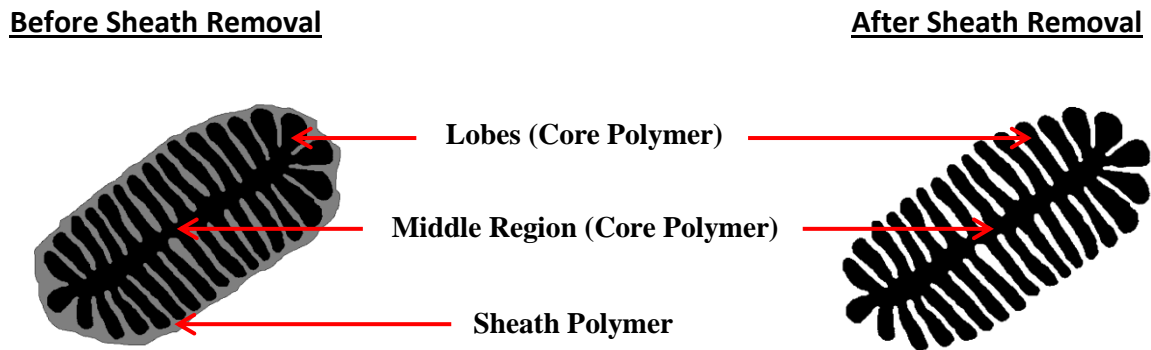


Figure 9- 1: Winged fiber before/after removing sheath polymer (Pourdeyhimi & Chappas, 2012b)

Contrary to bicomponent fibers, such as segmented pie or island-in-the-sea fibers, winged fibers are neither be split or fibrillated as hydroentangling with manifold pressures beyond a critical pressure $P_{critical}$ could cause the projections to tear off.

Peer-reviewed articles dealing with winged fiber nonwovens are very limited. Yeom et al. (Yeom & Pourdeyhimi, 2011) worked with winged fiber structures made from different polymer compositions. Spunbond winged fiber webs with poly (ethylene terephthalate), poly (propylene), poly (butylene terephthalate) and poly (lactic acid) as core and EastONE™ (a water-soluble co-polyester from Eastman Chemical Company) and poly (lactic acid) as sheath polymer. According to the results, aspects ratios of winged fibers were <0.7 depending on the polymer used during meltspinning. Also, specific surface area of winged fibers was reported to be much higher compared to 4DG or conventional circular fibers. For instance, fibrous materials with circular fiber and a linear density of 1 denier would provide a

specific surface area of about $0.35 \text{ m}^2 \text{ g}^{-1}$. In contrast to that, structures with winged fibers of the same linear density and polymer would have a theoretical specific surface area of more than $10 \text{ m}^2 \text{ g}^{-1}$. Winged fibers can have up to 64 projections and higher numbers are mentioned to be possible but difficult to spin. Width between channels is in the range between 200 and 500 nm (Pourdeyhimi & Chappas, 2012b). A study on winged fibers and their sound absorption behavior compared to round fiber showed improvements for middle but not high or low frequencies (Mohan, 2011). Different applications for winged fiber nonwovens are mentioned to be wipes, substrate materials (e.g. for artificial leather), protective clothing (better cooling and moisture transport), acoustic or thermal insulation materials, battery separator membranes, scaffolds for cell growth, filtration materials and also materials for particle separation or retention (Pourdeyhimi, Chappas et al., 2013).

To date just little is published about hydroentangled winged fiber nonwovens, their properties as well filtration properties. This study uses different manifold pressures and jet spacing to hydroentangle winged fiber webs. This study also reports on the structure, properties and filtration performance of winged fiber nonwovens after removing the sea compound by means of a caustic bath. Winged fiber nonwovens were compared to nonwoven materials with similar specific surface area and also tested in terms of their salt loading capacity.

9.3 Methodology

9.3.1 Materials

Spunbond winged fiber webs (32 lobes) were received from Baiksan Lintex. Materials had an initial basis weight of 115 g m^{-2} , a polymer ratio of about 50 (poly (propylene)) to 50 (poly (lactic acid)) and were hydroentangled with a 0.5 meter Fleissner Aquajet 5-manifold hydroentangling unit at the Nonwoven Institute pilot facilities located at Centennial Campus, North Carolina State University. Hydroentangling was performed with a total of five different pressures and three different jet spacing. After spunlacing nonwoven materials went through a conveyor oven. Hydroentangling conditions can be found in Table 9- 1.

Table 9- 1: Structures and hydroentangling parameters

Structure	Manifold Pressure [bar]		600 μm	4800 μm
			Specific Energy [KJ Kg^{-1}]	
Winged Fiber Media (32 Lobes)	P1	20-100-150-150-150 (M1-M5) Face Side	10200	1300
	P2	20-130-150-180-200 (M1-M5) Face Side	13400	1700
	P3	20-150-200-200-225 (M1-M5) Face Side	17000	2100
	P4	20-150-200-200-225 (M1-M5) Face (M1-M3), Back (M4-M5)	17000	2100
	P5	20-150-225-225-225 Face (M1-M3), Back (M4-M5)	19000	2300
➔ Structure IDs: 9.-Structure-JetSpacing-115-Pressure ←				

9.3.2 Sample Preparation

After bonding the samples via hydroentangling nonwoven materials underwent a caustic-soda treatment to remove the sheath compound from the winged fibers. Sodium hydroxide solution with a concentration of 8 % w/w was heated-up to 100 °C in a steam kettle. Samples were washed for 10 minutes under stirring before being pH-neutralized with cold tap water and dried in the open air on a sample rack.

9.3.3 Structure Analysis

Basis Weight and Thickness

Basis weight was measured with a Denver Instrument XL-3100D top-loading balance. Thickness of winged fiber materials was examined with a hanatek FT3V-LAB high-precision thickness gauge. Both analyses were performed with a total of 10 replicates.

Solid Volume Fraction (SVF)

Packing density of winged fiber materials was calculated by using the following equation:

$$\alpha = \frac{w}{\rho_f \times t} \quad \text{Eq. 9- 1}$$

where w is the basis weight [g m^{-2}], ρ_f the total fiber density [g m^{-3}] and t the thickness of the structure [m]. Total fiber density ρ_f is calculated as follows.

$$\rho_f = (\rho_{island} \times R_i) + (\rho_{sea} \times R_s) \text{ [g cm}^{-3}\text{]} \quad \text{Eq. 9- 2}$$

where ρ_{island} is the density of the island polymer [g cm^{-3}], R_i is the mass fraction of island polymer ρ_{sea} is the density of the sea polymer [g cm^{-3}] and R_s is the mass fraction of sea polymer.

Air Permeability

Air permeability of caustic soda treated samples was investigated according to ASTM D737 by using a TEXTEST FX 3300. A total of 10 samples were tested per structure.

Aerosol Filtration Properties

Aerosol filtration performance of IPA discharged and corona discharged samples was evaluated by using a TSI 3160 automated filter tester. Samples were tested with dioctyl phthalate (DOP) as challenging aerosol with particle sizes d_p ranging from 0.02 μm to 0.4 μm . Face velocity f_v was set at 5.33 cm s^{-1} and the tested area was 100 cm^2 . TSI 3160 uses a CPC (condense particle counter) to examine the particle penetration and filtration efficiency is determined as follows.

$$E = 100 - P = 100 - \left(\frac{C_{down}}{C_{up}} \times 100 \right) [\%] \quad \text{Eq. 9- 3}$$

where E is the filtration efficiency, P the penetration, C_{down} is the number of particles detected at the downstream and C_{up} the number of particles detected at the upstream side.

Filtration media was negatively charged by using a Haug Tristat TR 25 high voltage charging generator with a voltage of 22 kV and short-circuit current of 3000 μ A. Distance between the charging electrode and the material was 3.5 cm. Filtration media was charged for 10 seconds on each side before being tested. Laboratory climate was recorded to be ~ 20 $^{\circ}$ C and $\sim 35\%$ RH.

Quality factor QF was calculated to further evaluate the filtration performance of the materials.

$$QF = \frac{-\ln(P)}{\Delta p} [\text{Pa}^{-1}] \quad \text{Eq. 9- 4}$$

where P is the fractional particle penetration and Δp the pressure drop [Pa] of the material.

Salt Loading Capacity

Unwashed and caustic-soda treated winged fiber nonwoven materials were IPA discharged and corona discharged and tested for their salt loading capacity. A PALAS MFP 3000 filter test system and potassium chloride with a concentration of 2.5% were used to generate polydisperse particles.

Multiple salt loading cycles were performed until the filtration media achieved an overall filtration efficiency of 99.97%. Each loading step consisted of five upstream ($t_{upstream,single} = 40s$) and five downstream measurements ($t_{downstream,single} = 40s$). Filtration efficiency and pressure drop were recorded after each loading step and the weight of the gravimetric filter reported. Filtration media was not moved during the salt loading study and fixed in the filter holder. Aerosol loading was calculated based on the initial and

final weight of the filtration media $w_{filter,initial}$ $w_{filter,final}$ and gravimetric filter $w_{gravi,initial}$ $w_{gravi,final}$ as well as the increase in weight of the gravimetric filter after each loading step $w_{gravi,cycle}$. Based on this amount of salt generated per loading cycle $w_{salt,cycle}$ was calculated as follows.

$$w_{salt,cycle} = \frac{\Delta w_{filter} + \Delta w_{gravi}}{\# \text{ of Loading Cycles}} [\text{g}] \quad \text{Eq. 9- 5}$$

where Δw_{filter} is the weight difference of the filter before and after the salt loading and Δw_{gravi} the weight difference of the gravimetric filter before and after the salt loading.

From this salt loading on the filtration media after each loading cycle $w_{load,cycle}$ can be estimated as follows.

$$w_{load,cycle} = (w_{salt,cycle} - \Delta w_{gravi,cycle}) \times 100 [\text{g m}^{-2}] \quad \text{Eq. 9- 6}$$

where $w_{salt,cycle}$ is the amount of salt generated per loading cycle and $\Delta w_{gravi,cycle}$ is the difference in weight of the gravimetric filter before and after each loading step.

SEM Images

High magnification images were taken with a Hitachi S-3200 scanning electron microscope. Specimens were not sputter coated before imaging (better visibility and no loss of particles).

Specific Surface Area

BET surface area was determined by using a Quantachrome Autosorb iQ2. Samples were outgassed for about 16-18 hours at 40 °C before being analyzed. Krypton (ρ ; 2.413 g cm⁻³) was used for physisorption.

9.4 Results and Discussion

9.4.1 Removal of Sea Compound

Winged fiber nonwovens hydroentangled with manifold pressures P1, P2 and P3 fell apart during the caustic treatment. In contrast to that, structures hydroentangled with manifold pressures P4 and P5 and 600 μm jet spacing showed enough integrity. Removing the sea compound winged fiber nonwovens hydroentangled manifold pressures P4 and P5 and 4800 μm jet spacing fell apart. We previously reported the successful caustic treatment of various hydroentangled island-in-the-sea nonwovens webs. Materials showed sufficient structure integrity even though hydroentangled with considerably lower pressures compared to the winged fiber webs. We attribute this to the fiber bending rigidity, which is different for circular and non-circular fibers. Fiber bending or flexural rigidity F_{fiber} is defined as follows.

$$F_{fiber} = 1\eta ET^2(4\pi\rho)^{-1} \quad \text{Eq. 9- 7}$$

where η is the shape factor (1 for a round fiber), E is the specific bending modulus (in Nm Kg^{-1}), T is the fiber linear density (in Kg m^{-1}) and ρ is the fiber density (in Kg m^{-3}) (Fan & Hunter, 2009, p. 108)

The shape factor η , defined by the ratio of fiber perimeter to the corresponding area of a circular fiber, is much greater for winged than circular fibers. Thus, bending rigidity and required force during hydroentangling is expected to be higher for winged than island-in-the-sea webs. Basis weight measured prior and after the caustic washing along with the corresponding weight loss can be seen in the following.

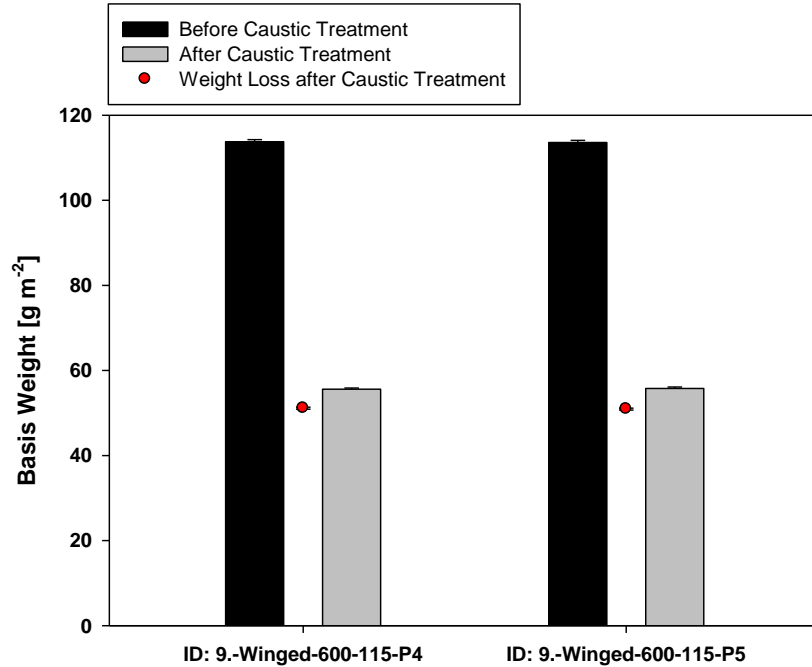


Figure 9- 2: Basis weight before/after caustic treatment (structure 9.-Winged.600-115-P4 to 9.-Winged.600-115-P5)

Results indicate the polymer ratio of winged fiber nonwovens to be about 50% (poly (propylene)) to 50% (poly (lactic acid)). SEM images showing the cross-section prior and after the alkaline treatment are shown in Figure 9- 3 and Figure 9- 4. After treating the structures with caustic-soda poly (lactic acid) residues are barely visible and channels between individual projections clearly visible.

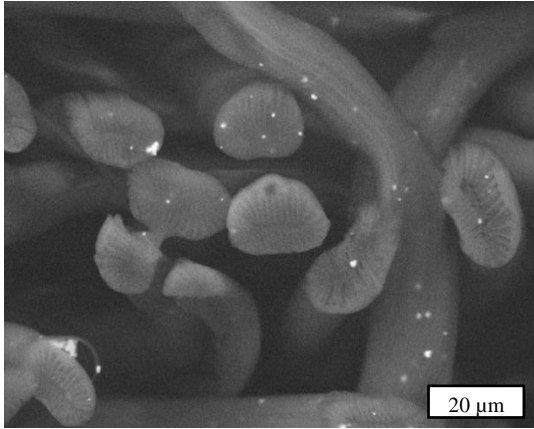


Figure 9- 3: Winged fiber nonwoven before caustic treatment

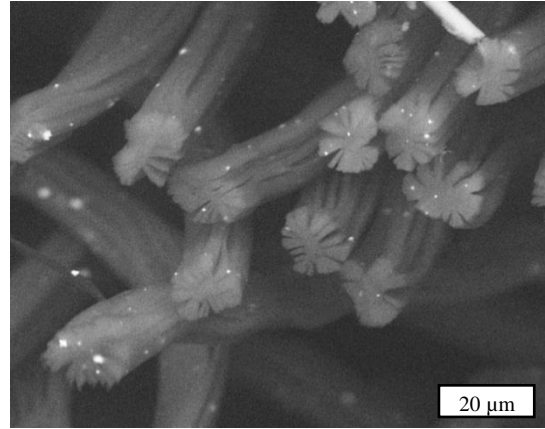


Figure 9- 4: Winged fiber nonwoven after caustic treatment

9.4.2 Solid Volume Fraction and Air Permeability

Solid volume fraction of both winged fiber structures is shown in the following figure.

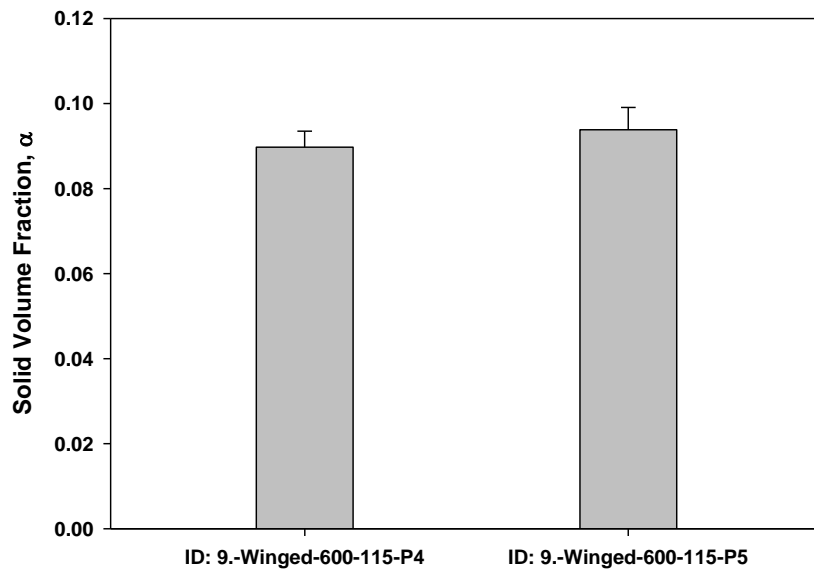


Figure 9- 5: Solid volume fraction of P4/P5 hydroentangled winged fiber nonwovens (after caustic treatment)

As can be seen from the results hydroentangling with higher manifold pressure led to winged fiber structures with increased solidities. We previously reported packing densities of a variety of island-in-the-sea structures, which were significantly higher.

Figure 9- 6 shows the air permeability of caustic-treated 32 lobes winged fiber materials. According to the results, hydroentangling with higher manifold pressures led to winged fiber structures with reduced air permeability. This is related to the increase in solidity and enhanced degree of consolidation.

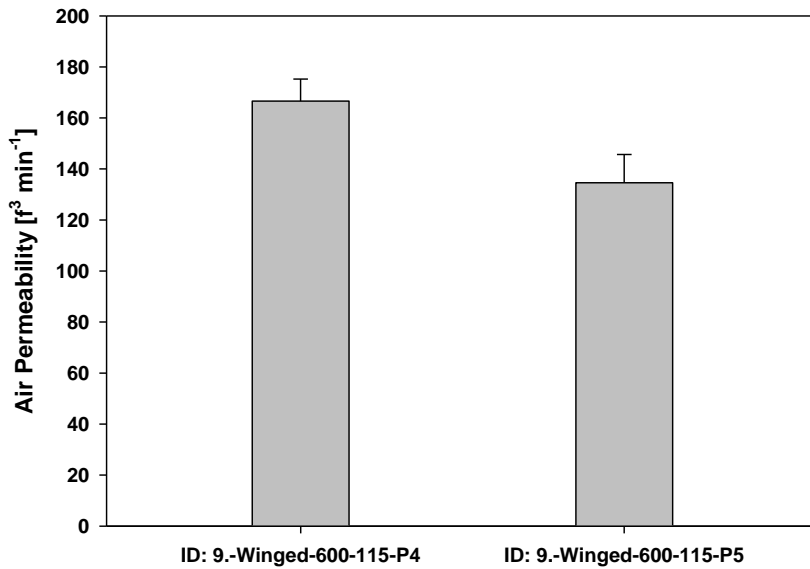


Figure 9- 6: Air permeability of P4/P5 hydroentangled winged fiber nonwovens (after caustic treatment)

9.4.3 Effect of Specific Surface Area on Filtration Properties

We previously reported the BET specific surface area of intact and caustic treated island-in-the-sea materials. Following figure compares these results with the BET specific surface area of unwashed and caustic treated winged fiber materials. Data indicates the BET

specific surface area of winged fiber materials to be about $2.6 \text{ m}^2 \text{ g}^{-1}$. Nonwovens with intact bicomponent fibers show lower BET specific surface area compared to island-in-the-sea structures. This is related to a certain degree of fiber fibrillation during hydroentangling, which occurs for island-in-the-sea but not winged fiber structures.

Table 9- 2: Comparison of BET specific surface area of intact/caustic-treated InS and winged fiber nonwovens

	Intact	37 InS	108 InS	32 Lobes
InS	0.4	2.22	2.83	
Winged	0.16			2.62

The following compares the filtration efficiency of winged and island-in-the-sea materials with comparable weight and specific surface area. Surface area based on BET tests was calculated to be 1.4 m^2 for both materials and a testing area of 100 cm^2 .

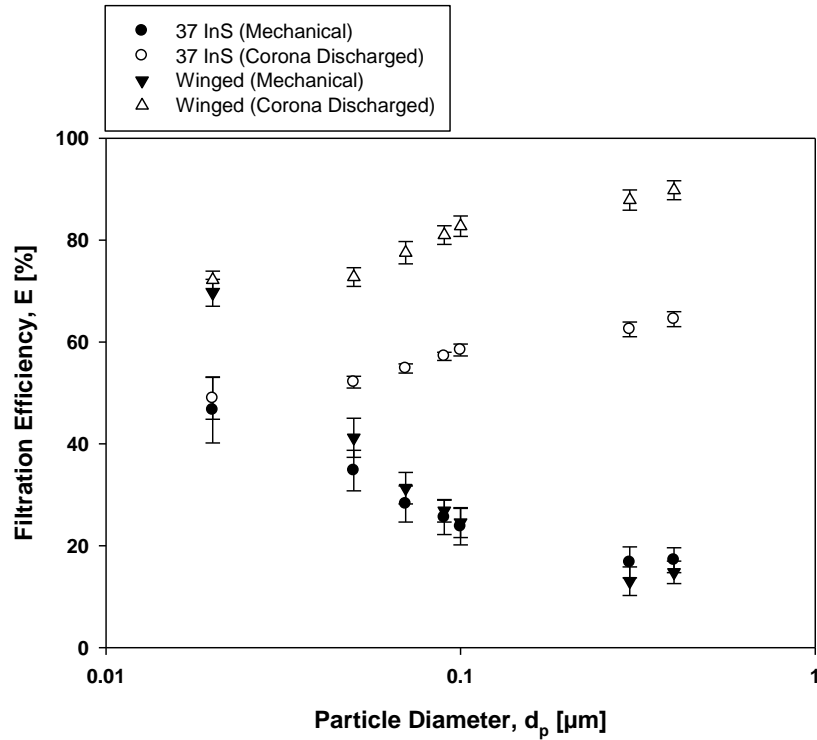


Figure 9- 7: Filtration properties of IPA discharged/corona discharged 32 winged and 37 InS nonwovens

Mechanical capture efficiency of winged fiber nonwovens was tested to be lower for particle sizes $>0.1 \mu\text{m}$ but higher for particle diameters smaller than that. Corona discharged winged fiber nonwovens showed higher filtration efficiencies for all particle sizes and a better charging potential. MPPS (most penetrating particle size) was tested to be $0.3 \mu\text{m}$ for both IPA discharged materials and $0.02 \mu\text{m}$ for both corona discharged structures.

Figure 9- 8 depicts the pressure drop of both structures after IPA and corona discharging. Island-in-the-sea structures showed higher resistance to flow compared to winged fiber materials. Measurements after corona discharge indicated pressure drop of island-in-the-sea to be higher and pressure drop of winged fiber nonwovens to be the same.

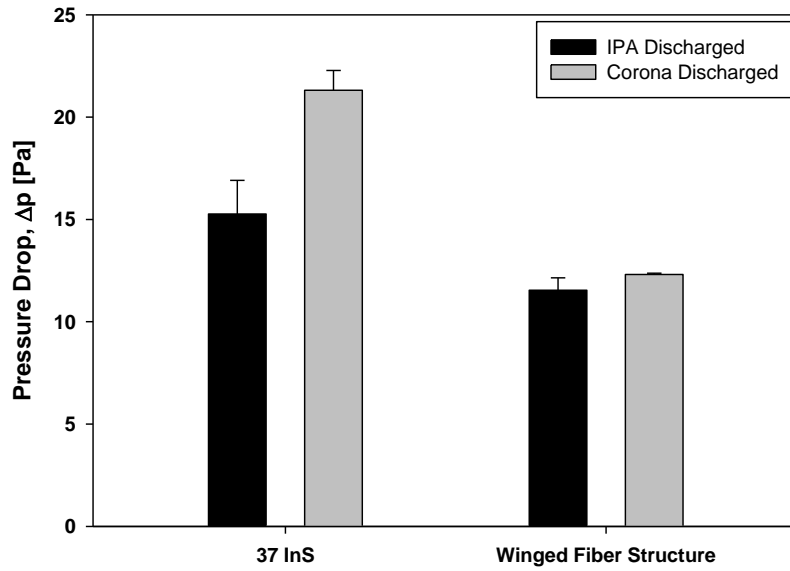


Figure 9- 8: Pressure drop of IPA and corona discharged InS and winged fiber nonwovens

Mean pore size measurements are depicted in Figure 9- 9 and indicate the pore size of island-in-the-sea structures to decrease after corona discharge. In contrast to that, winged fiber nonwovens show the same mean pore size after corona discharge. Fibers of winged materials are bigger in diameter and do not show the same behavior. Reason for this needs further investigation but was confirmed by multiple tests.

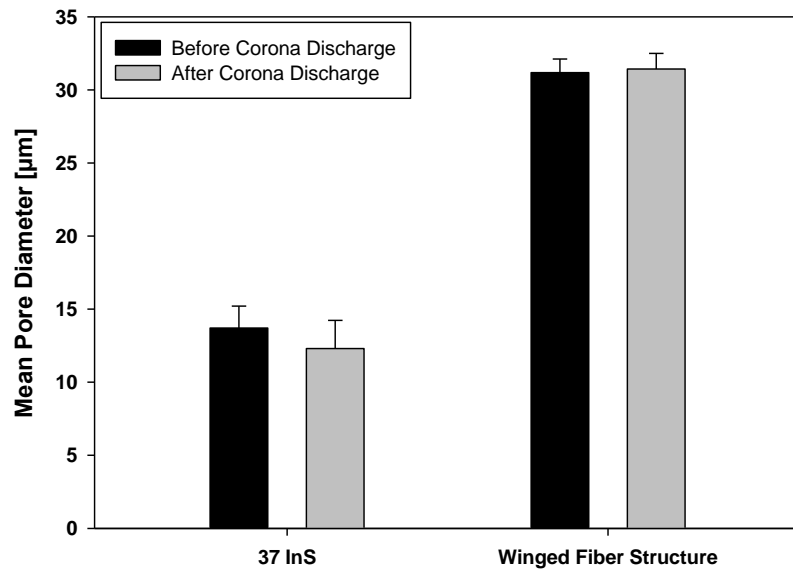


Figure 9- 9: Mean pore size of IPA/corona discharged 37 InS and 32 winged fiber nonwovens

9.4.4 Salt Loading Capacity

Results of salt loading study of IPA discharged unwashed and IPA discharged caustic-treated winged fiber materials are shown in the following. Data indicates the increase in efficiency and pressure drop to be significantly faster for unwashed winged fiber materials. Figure 9- 12 and Figure 9- 13 show this to be related to the change of fiber cross-section after the caustic treatment. Particles are trapped more within the lamella structure instead of slipping off the fibers and clogging the pores. Also, caustic-washed winged fiber nonwovens are able to hold about twice of the amount of potassium chloride compared to the unwashed samples. However, pressure drop at 99.97% efficiency is comparable for both structures. Figure 9- 14 depicts the salt loading as a function of time and reveals the caustic-washed structure to load slightly slower. Transition from depth to surface filtration started after 130 min.

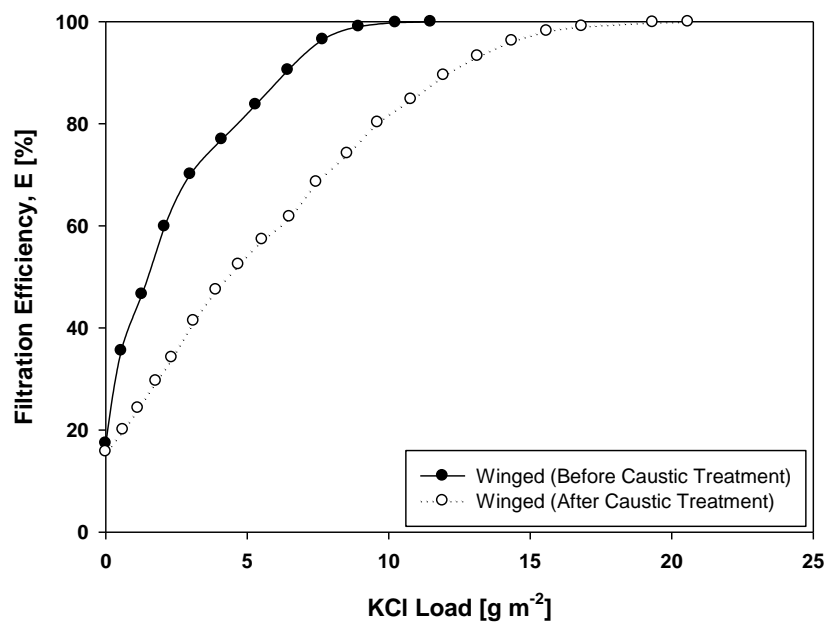


Figure 9- 10: Filtration efficiency as a function of salt load of unwashed/caustic-treated winged fiber nonwovens

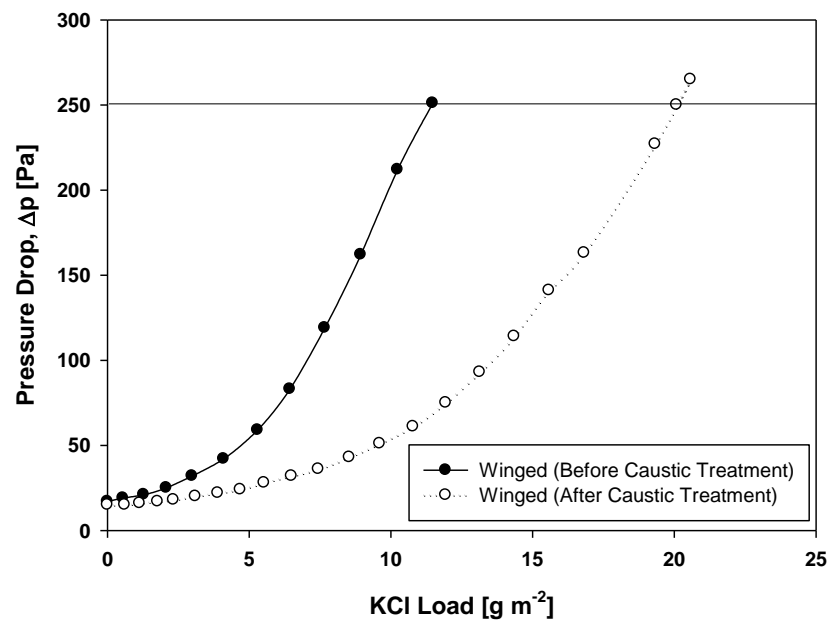


Figure 9- 11: Pressure drop as a function of salt load of unwashed/caustic-treated winged fiber nonwovens

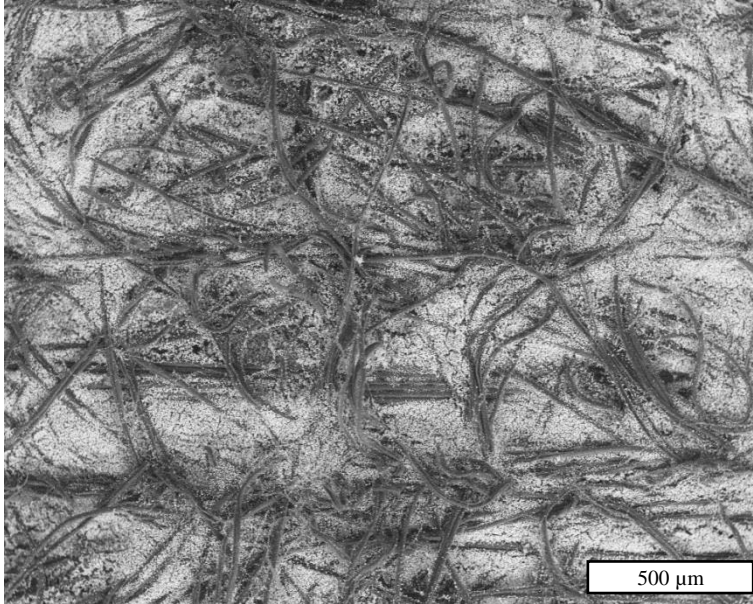


Figure 9- 12: SEM image taken from the surface of an unwashed winged fiber structure (IPA discharged)

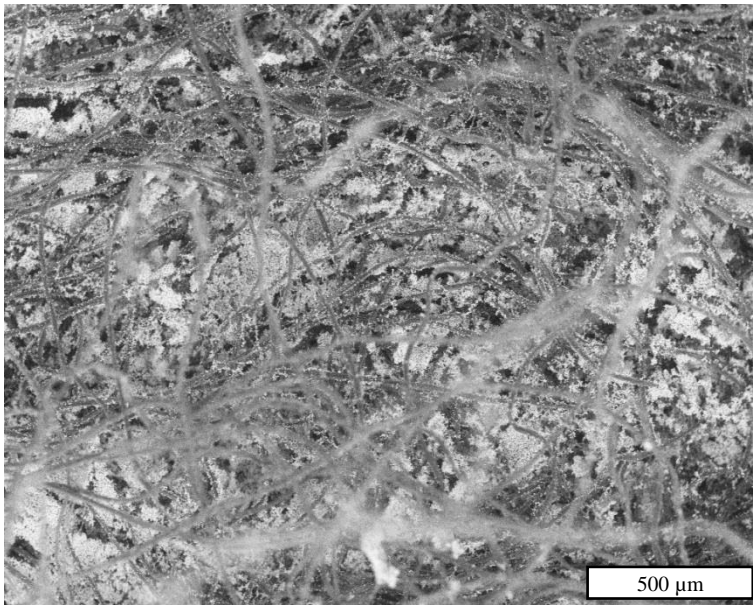


Figure 9- 13: SEM image taken from the surface of a caustic-treated winged fiber structure (IPA discharged)

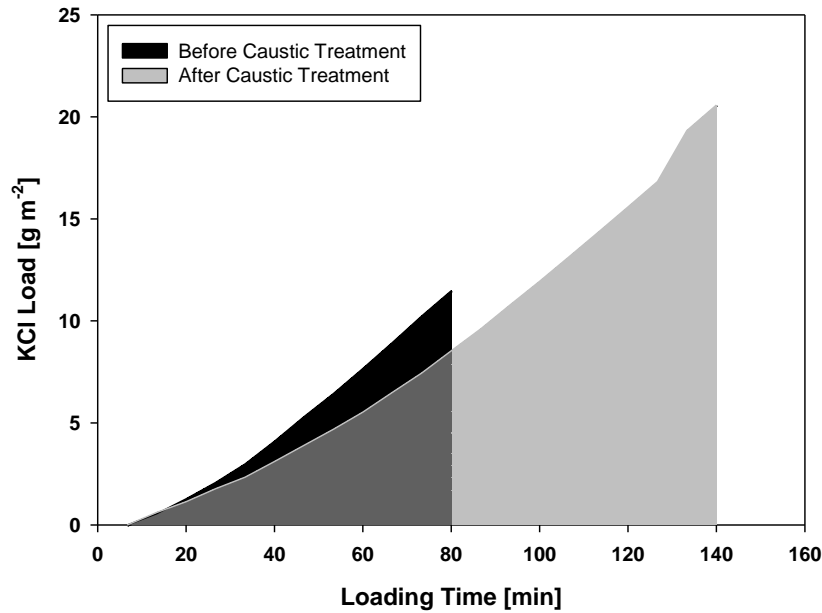


Figure 9- 14: Salt loading over time of unwashed/caustic-treated IPA discharged winged fiber materials

Results of salt loading study of corona discharged and IPA discharged caustic-treated winged fiber materials are shown in Figure 9- 15 and Figure 9- 16. According to the data, corona discharged samples collected significantly less KCl before reaching 99.97% efficiency. Difference in pressure drop is significant and corona discharged samples show much lower resistance to flow at 99.97% efficiency. However, from extrapolating that curve pressure drop of corona discharged material can be expected to be higher at same load ($\sim 20 \text{ g/m}^2$). In contrast to that, particles are evenly distributed within the structures of IPA discharged winged fiber nonwovens.

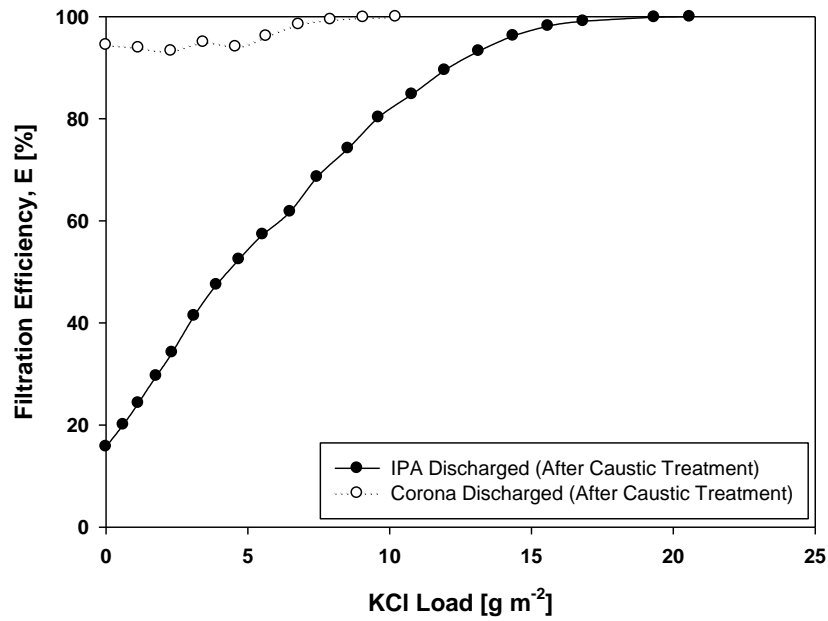


Figure 9- 15: Filtration efficiency as a function of salt load of IPA/Corona discharged caustic-treated winged fiber nonwovens

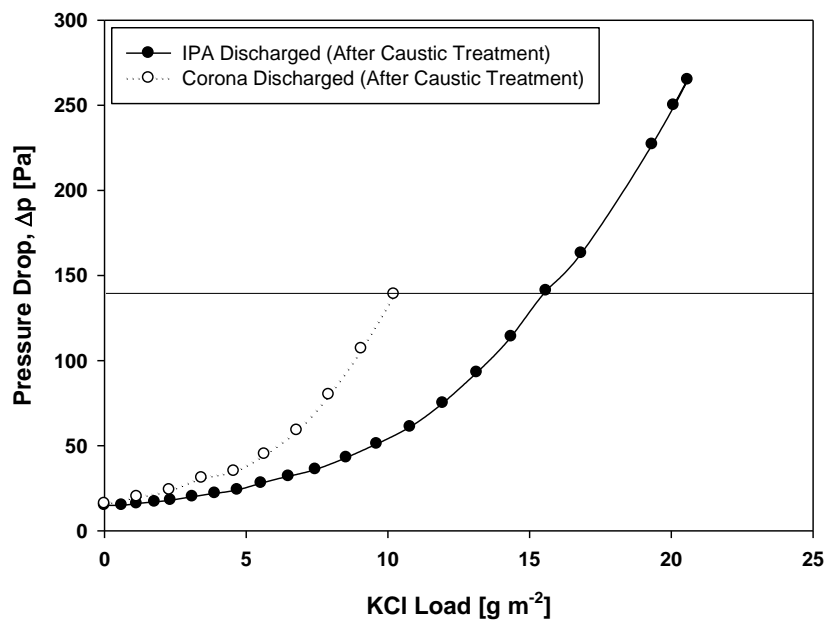


Figure 9- 16: Pressure drop as a function of salt load of IPA/Corona discharged caustic-treated winged fiber nonwovens

Figure 9- 17 indicates corona discharged materials to load faster than IPA discharged samples. Cross-sectional images of both structures are shown in Figure 9- 18 and Figure 9- 19 and indicate particle accumulation to take place on the surface (cake formation) of corona discharged materials. Figure 9- 21 and Figure 9- 20 show SEM images taken from the surface of IPA and corona discharged winged fiber materials (500x magnification). Images clearly show effect of corona discharge and increased particle collection on winged fibers.

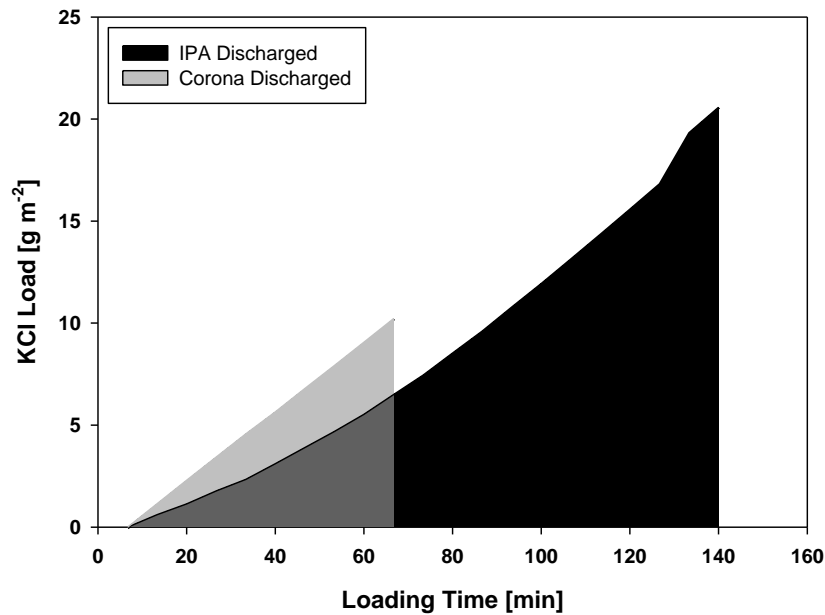


Figure 9- 17: Salt loading over time of unwashed/caustic-treated Corona discharged winged fiber materials

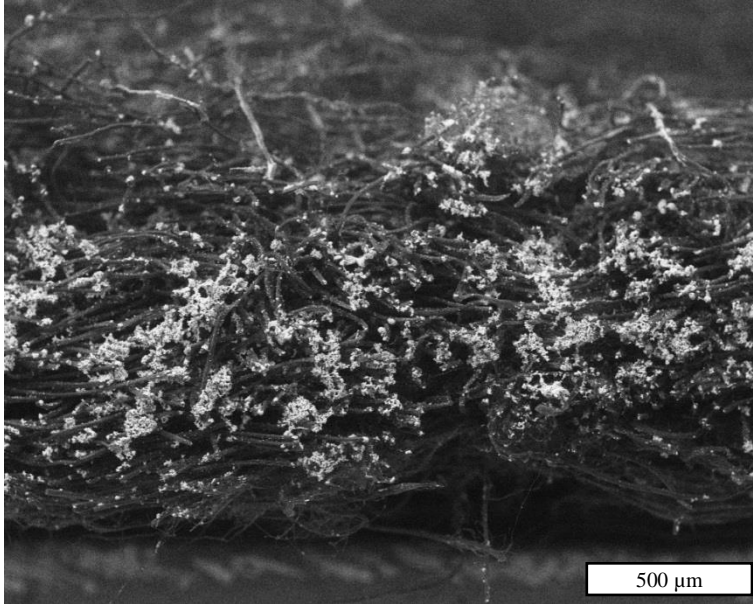


Figure 9- 18: SEM image taken from the cross-section of caustic-treated winged fiber nonwovens (IPA discharged)

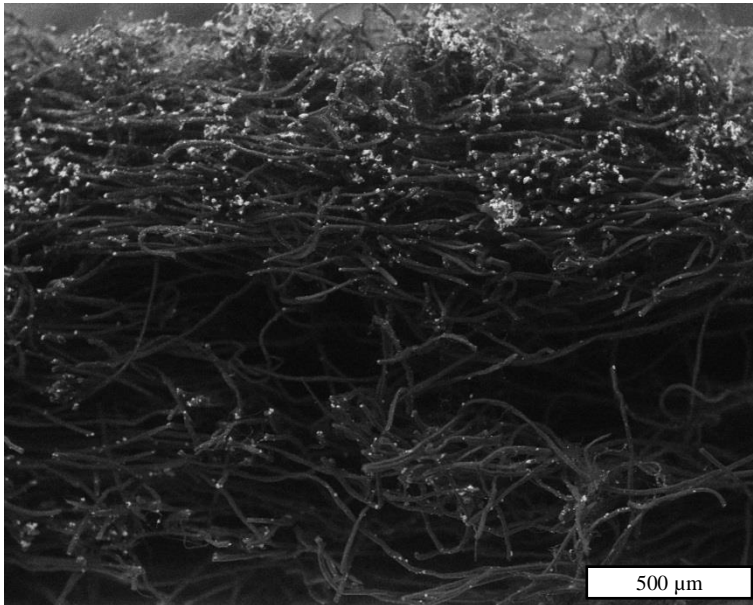


Figure 9- 19: SEM image taken from the cross-section of caustic-treated winged fiber nonwovens (corona discharged)

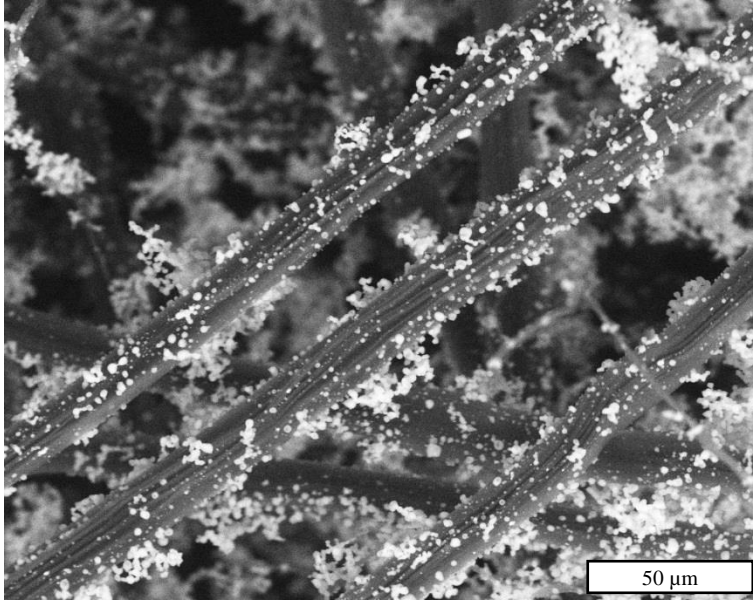


Figure 9- 20: SEM image taken from the surface of caustic-treated winged fiber nonwovens (IPA discharged)

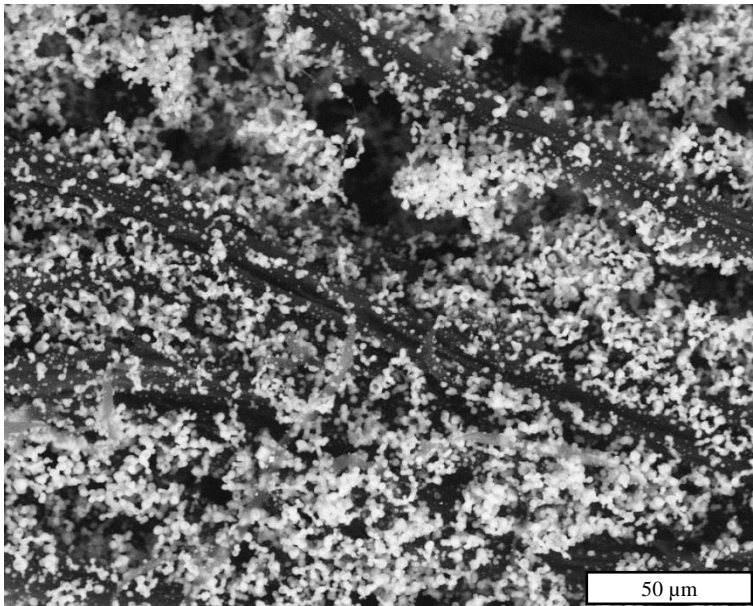


Figure 9- 21: SEM image taken from the surface of caustic-treated winged fiber nonwovens (corona discharged)

9.5 Conclusion

This study demonstrated winged fiber nonwovens to require much higher hydroentangling pressures compared to island-in-the-sea nonwovens. Also, webs bonded from just one side and with jet spacing larger than 600 μm fell apart during the caustic treatment. Thus, both required force and also energy ratio is different for winged fiber than island-in-the-sea bicomponent structures.

BET specific surface area of winged fibers was tested to be in the same range as 37 and 108 island-in-the-sea nonwovens. Gravimetical measurements and SEM images from the cross-section proved poly (lactic acid) to be completely removed from the material.

Study also demonstrated winged fiber nonwovens to have better charging potential compared to island-in-the-sea structures. Further experiments showed island-in-the-sea samples to have higher pressure drops after corona discharge, whereas pressure drop of winged fiber nonwovens did not change. Loading winged fiber structures with potassium chloride proved loading capacity of caustic-treated nonwovens to be higher compared to unwashed materials. However, corona discharged samples showed faster loading and cake formation but less loading capacity compared to IPA discharged materials.

9.6 References

Erdem, G. & Trinkaus, M. J. (2008). WO2008155691 A1.

Fan, J. & Hunter, L. (2009). *Engineering apparel fabrics and garments*: Elsevier.

Haggard, J., Wilkie, A., Brang, J. & Taylor, J. (2008). US Patent No. US7431869 B2.

Mohan, V. (2011). Acoustical Properties of Winged Fibers.

Pourdeyhimi, B. & Chappas, W. (2012a). US Patent No. US8129019 B2.

Pourdeyhimi, B. & Chappas, W. (2012b). US Patent No. US20120148841 A1.

Pourdeyhimi, B., Chappas, W. & Barnes, H. M. (2013). US Patent No. US20130133980 A1.

Yeom, B. Y. & Pourdeyhimi, B. (2011). Web fabrication and characterization of unique winged shaped, area-enhanced fibers via a bicomponent spunbond process. *Journal of materials science*, 46(10), 3252-3257.

CHAPTER 10

- Overall Conclusion -

- Jet spacing was found to be a crucial parameter greatly influencing the structure and properties of unwashed but also caustic-treated island-in-the-sea nonwoven materials. Even after treating the materials with a caustic solution influence of jet spacing was measurable. Hydroentangling with large jet spacing resulted in high- and low density regions showing lower solid volume fractions, higher air permeabilities and also a reduced resistance to flow. To our surprise filtration efficiency increased for jet spacing larger than 1800 μm . In other words, improved filtration media can be produced at significantly lower energy input.
- Hydroentangling pressure was reported to have a significant effect on the structure and properties of spunbond island-in-the-sea nonwoven materials. Reducing the manifolds pressure resulted in low density structures with reduced pressure drops and enhanced capture efficiencies. Study revealed not jet spacing but manifold pressure to be the all-important factor for producing improved filtration media.
- We demonstrated spunbond bicomponent spinning combined with subsequent caustic treatments to be capable to produce microfiber nonwovens with BET specific surface areas up to 3.5 g m^{-2} . Experiments indicated the caustic washing to work to remove sea compound from 37 and 108 island-in-the-sea structures but not from fabrics with island counts higher than that. In addition, ability to spread and randomly orientate fibers of structures with island counts higher than 37 was found to be critical. Structure collapsing was found when hydroentangling 108 island-in-the-sea webs with jet spacing larger than

1800 μm . Contrary to that, 37 island-in-the-sea structures showed improved filtration properties beyond that point.

- Study on mixed media alternating island-in-the-sea nonwoven materials demonstrated higher manifold peak pressures but not specific energy to be necessary for sufficient bonding. We attribute this to the implementation of larger fibers within the material resulting in an increased demand of force during hydroentangling. It was further shown that fiber spreading and reorientation is different from mixed media than conventional island-in-the-sea structures. Nevertheless, mixed media structures showed improved quality factors as pressure drop was significantly reduced.
- Research further proved specific energy to be not a sufficient measure for predicting and describing the influence of hydroentangling on nonwoven materials. We demonstrated that hydroentangling with more manifolds but less jet pressure results in different properties than hydroentangling with less manifolds and higher jet pressures at same specific energy. Investigation revealed higher manifold pressures to result in more oriented materials. Furthermore, hydroentangling with high manifold pressures and large jet spacing is preferred for the development of high- and low density regions.
- Hydroentangling with multiple manifolds with equal pressures was proven to influence the structure and properties of nonwoven materials. We demonstrated that even though

manifold pressure was not increased hydroentangling with multiple manifolds with same pressure led to structures with lower air permeabilities but higher mechanical properties.

- We showed winged fiber nonwoven webs to require much higher manifold pressures during hydroentangling than conventional island-in-the-sea webs and the energy ratio to be a crucial parameter. Only materials hydroentangled from both sides with high manifold pressures withstood the caustic treatment. BET specific surface area of winged fiber materials after sheath removal showed comparable values to island-in-the-sea nonwovens. Winged fiber nonwovens turned out better charging potential compared to island-in-the-sea materials. Interestingly, island-in-the-sea materials showed increased pressure drops after corona discharge, whereas winged fiber structures did not show any change. In addition, caustic-treated winged fiber nonwovens revealed to have higher salt loading capacity compared to unwashed materials. Corona discharged media showed rapid salt loading and cake formation, whereas IPA discharged materials the opposite.

CHAPTER 11

- Future Recommendations -

Following Topics are recommended for Future Work

- Using jet strips with more than one row of orifices to reduce displaced jet streaks because of fabric movement during hydroentangling. Furthermore, amount of necessary manifolds could be reduced by this.
- Spunbond nonwovens bonded via hydroentangling usually show a bias in MD but caustic-treatment is limited in changing the ODF back to a random orientation. However, a more random fiber orientation is desired as this would boost the filtration efficiency of the medium. For this reason it is recommended to consider other web formation processes being capable to produce webs with randomly oriented fibers. For subsequent hydroentangling it is recommended to use reduced manifold pressures to prevent reorientation towards MD direction.
- Mixed media structures with homo- to bicomponent ratios other than 50/50. As homocomponent fibers are assumed to be the reason for insufficient island separation and spreading it is highly recommended to lower the amount of large fibers within the mixed media structure. Island count is recommended to be 37 or higher provided that subsequent removal processes work adequately.
- Mixed media structures could be imitated by carding a combination of small and large denier fibers or mixing bicomponent and monocomponent staple fibers together.

- Mixed media structures with island-in-the-sea fibers and also side-by-side bicomponent fibers with different thermal properties. After removing the sea compound from the island-in-the-sea fibers subsequent thermal processes could cause side-by-side fibers to crimp and open the structure

(Listed Topics are not addressed in this Dissertation)

Appendix

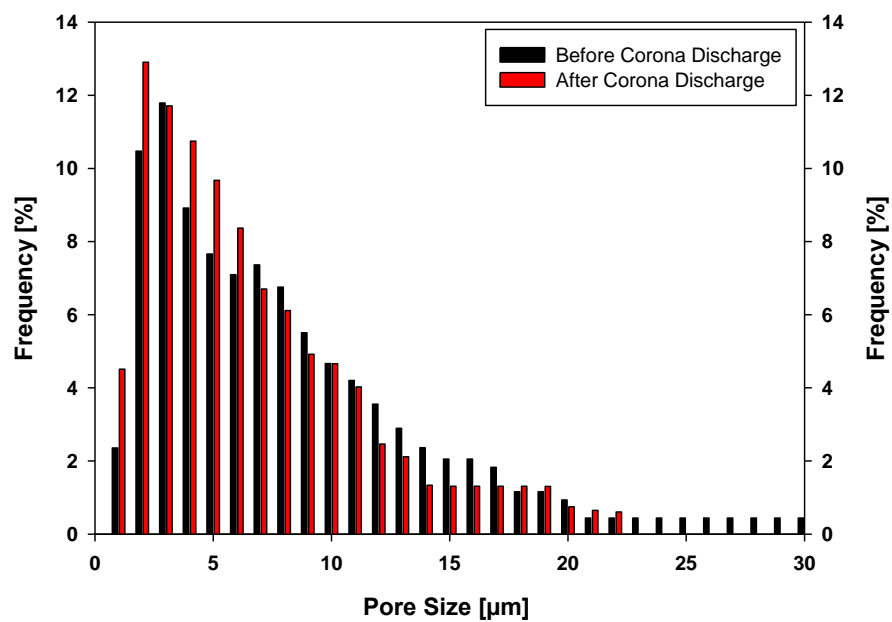


Figure 12- 2: Pore size distribution of 37 InS structure before/after corona discharge